

University of Alberta

An Evaluation of Polypyrrole Dodecylbenzene Sulfonate for Artificial Muscle

Applications

by

Sean Maw, B.A.Sc., M.A.Sc.



A thesis submitted to the Faculty of Graduate Studies and Research in partial fulfillment
of the requirements for the degree of Doctor of Philosophy.

Centre for Neuroscience

Edmonton, AB

Fall 2002



National Library
of Canada

Acquisitions and
Bibliographic Services

395 Wellington Street
Ottawa ON K1A 0N4
Canada

Bibliothèque nationale
du Canada

Acquisitions et
services bibliographiques

395, rue Wellington
Ottawa ON K1A 0N4
Canada

Your file *Votre référence*

Our file *Notre référence*

The author has granted a non-exclusive licence allowing the National Library of Canada to reproduce, loan, distribute or sell copies of this thesis in microform, paper or electronic formats.

The author retains ownership of the copyright in this thesis. Neither the thesis nor substantial extracts from it may be printed or otherwise reproduced without the author's permission.

L'auteur a accordé une licence non exclusive permettant à la Bibliothèque nationale du Canada de reproduire, prêter, distribuer ou vendre des copies de cette thèse sous la forme de microfiche/film, de reproduction sur papier ou sur format électronique.

L'auteur conserve la propriété du droit d'auteur qui protège cette thèse. Ni la thèse ni des extraits substantiels de celle-ci ne doivent être imprimés ou autrement reproduits sans son autorisation.

0-612-81237-5

Canada

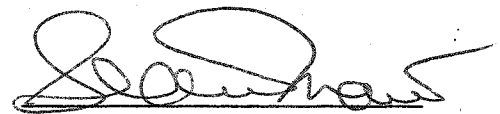
University of Alberta

Library Release Form

Name of Author: Sean Maw
Title of Thesis: An Evaluation of Polypyrrole Dodecylbenzene Sulfonate
for Artificial Muscle Applications
Degree: Doctor of Philosophy
Year this Degree Granted: 2002

Permission is hereby granted to the University of Alberta Library to reproduce single copies of this thesis and to lend or sell such copies for private, scholarly, or scientific research purposes only.

The author reserves all other publication and other rights in association with the copyright in the thesis, and except as herein before provided, neither the thesis nor any substantial portion thereof may be printed or otherwise reproduced in any material form whatever without the author's prior written permission.



36 Point McKay Cres NW

Calgary, AB T3B 5B4

Sept 4, 2002


University of Alberta

Faculty of Graduate Studies and Research


The undersigned certify that they have read, and recommend to the Faculty of Graduate Studies and Research for acceptance, a thesis entitled "An Evaluation of Polypyrrole Dodecylbenzene Sulfonate for Artificial Muscle Applications", submitted by Sean Maw in partial fulfillment of the requirements for the degree of Doctor of Philosophy.



supervisor Dr. Richard B. Stein



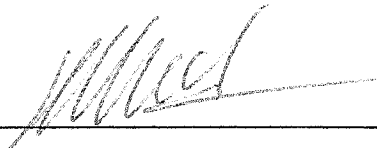
external examiner Dr. Don Leo



committee member Dr. Tessa Gordon



committee member Dr. Michael Williams



committee member Dr. Hasan Uludag

Abstract

Although it has shown some promise, the suitability of polypyrrole dodecylbenzene sulfonate, or PPy(DBS), in an artificial muscle fiber (AMF) actuation role has remained unclear. The purpose of this thesis was to evaluate and assess the material in terms of its suitability for that role. The criteria for comparing the performance of AMFs to natural muscle fibers are highlighted. Polypyrrole is also reviewed with respect to its general qualities, structure, production and handling.

In terms of the experimental content of the thesis, a bilayer bending beam model was adopted for the evaluation of PPy(DBS)'s actuation ability with respect to a number of production and activation variables. PPy(DBS) films change their electromechanical behaviour in response to changes in deposition current density, monomer and electrolyte concentration, cycling frequency, and cycling range. These dependencies were characterized and evaluated. SEM imagery was also collected, as were elemental analyses under different conditions. Endurance tests were performed, and power and efficiency levels were measured.

Overall, PPy(DBS) showed potential with respect to endurance ($> 10^5$ cycles), mass density ($\cong 1400 \text{ kg/m}^3$) and power density (up to 2.8 W/kg). It performed well with respect to frequency response ($\cong 1 \text{ Hz}$) and strain (up to 10%), and it performed very well with respect to stimulation modes, safety, noisiness, smell, active contractile stress (up to 2 MPa) and energy density (maximum of 4.9 kJ/m^3). These results led to the conclusion that PPy(DBS) should continue to be pursued for AMF applications. However, top efficiency levels were only $.02\%$ which is inadequate. Improved efficiency should be the main focus of future work, to ensure the general use of PPy(DBS) in AMF actuation.

Acknowledgements

It has been a long haul, and partly as a result, there are many people that I need to thank who helped me get to the finish. The person who helped me get to the start was Dr. Dejan Popovic. He encouraged me to pursue this topic, and I probably would not have, without that encouragement.

All along, from the start until the finish, I have been supported by my Committee, led by my supervisor Dr. Richard Stein. I have always appreciated his good nature, his patience and his willingness to let me do it “my way” (which was not always the best way!). Drs. Tessa Gordon and Michael Williams have always been there as well, right from the start, and I am indebted to them for it. Both contributed logistical support with lab equipment and the like.

The completion of the thesis would not have been possible without the assistance of at least two other individuals, those being Dr. Elisabeth Smela and Dr. Ken Yoshida. Ken designed the pivotal LabVIEW data acquisition software that I used for all of my experiments. Elisabeth was my inspiration for the particular focus of my thesis (PPy(DBS)), and she mentored me over several years and two trips to Scandinavia. She was my ever-present Committee member in absentia, and she was instrumental in ensuring that the quality of my work was high.

Other key supporting characters in my PhD drama included Rob Rolf for technical support in the lab, George Braybrook of Earth Sciences and Tina Barker of ChemMin Engineering for their help with the SEM work, Kelly James for the use of his video camera for months at a time, Dr. Nai-Hong Li for his help with the PVA/PAA work, Microlyne staff (formerly Alberta Microelectronics Center) for initial technical

support, Drs. J. Kentfield, Rod Fauvel and Doug Weber for assistance in the power calculation formulations, Dr. Keir Pearson for the use of his Nicolet oscilloscope, Drs. Jed Harrison, Christine McDermott and Michael Finot for electrochemistry assistance, Dr. Ruth Morey Sorrentino for help with siliconCOACH, and Dr. Peter Sommer-Larsen for resource support via the ARTMUS program of Denmark.

Over the many years that I spent in Edmonton, I was lucky enough to get to know many wonderful students and staff at the University of Alberta, many of whom made up the Division (and now Centre) for Neuroscience. I would especially like to thank Centre staff Toni Stringam, Carol Ann Johnson and Brenda Topliss for their support throughout.

In terms of financial support, I am indebted to the now-defunct federal Network Centre of Excellence (NCE) for Neuroscience, the Alberta Heritage Foundation for Medical Research (AHFMR) and the University of Alberta's Department of Biomedical Engineering. I would also like to note Jacques Thibault's support at the Calgary Olympic Oval for giving me the leave of absence that was necessary for me to finish.

Finally, I would like to thank my wife Cher, and my family, for their patience and indulgence. They have put up with a lot, over a long period of time, and I appreciate the sacrifice that they have made in so many ways.

Table of Contents

1. Introduction	
1.1 Motivation and Goals.....	1
1.2 Characteristics of Natural Muscle.....	9
1.3 A Polypyrrole Primer.....	25
1.4 References.....	45
2. The Effects of Varying Deposition Current Density on Bending Behaviour in PPy(DBS)-Actuated Bending Beams	
2.1 Introduction.....	51
2.2 Experimental.....	55
2.3 Results and Observations.....	60
2.3.1 Film Growth.....	60
2.3.2 Conditioning Cycles.....	60
2.3.3 Voltage Steps.....	68
2.3.4 Current Steps.....	71
2.3.5 Post-Step Cycles.....	74
2.3.6 Film Adhesion.....	75
2.4 Discussion.....	76
2.5 Conclusions.....	80
2.6 References.....	82
3. The Effects of Varying Monomer and Electrolyte Concentrations in Deposition and Stimulation Solutions on the Bending Behaviour in PPy(DBS)-Actuated Bending Beams	
3.1 Introduction.....	88
3.2 Experimental.....	95
3.3 Results and Observations.....	100
3.3.1 Film Growth.....	100
3.3.2 Conditioning Cycles.....	103
3.3.3 Voltage Steps.....	116
3.3.4 Current Steps.....	126
3.3.5 Post-Step Cycles.....	128
3.3.6 Beam Motion Analysis.....	131
3.3.7 Film Adhesion.....	132
3.4 Discussion.....	133
3.5 Conclusions.....	137
3.6 References.....	139
4. How Stimulation History Affects the Current Behaviour of PPy(DBS)-Actuated Bending Beams	
4.1 Introduction.....	149
4.2 Experimental.....	157

4.3 Results and Observations	161
4.3.1 Film Growth	161
4.3.2 Conditioning Cycles	161
4.3.3 Range Variations	169
4.3.4 History Variations	181
4.3.5 Post-Experimental Cycling	193
4.4 Discussion	199
4.5 Conclusions	203
4.6 References	207
5. The Frequency Response of PPy(DBS)-Actuated Bending Beams Under Various Conditions	
5.1 Introduction	212
5.2 Experimental	216
5.3 Results and Observations	221
5.3.1 Film Growth	221
5.3.2 Conditioning Cycles	224
5.3.3 SEM Data	224
5.3.4 Frequency Response Data	233
5.4 Discussion	250
5.5 Conclusions	258
5.6 References	261
6. Power, Efficiency, Endurance and Other Functional Characteristics of PPy(DBS)-Actuated Bending Beams	
6.1 Introduction	267
6.2 Experimental	270
6.3 Methods of Analysis	273
6.3.1 Mechanical Work	273
6.3.2 Electrical Work, Efficiency and Power	281
6.4 Results and Observations	287
6.4.1 Film Growth	287
6.4.2 Conditioning Cycles	287
6.4.3 Cycling Endurance	289
6.4.4 Power and Efficiency	291
6.5 Discussion	309
6.6 Conclusions	323
6.7 References	324
7. General Discussion	
7.1 A Model to Fit the Observations	330
7.2 Assessing PPy(DBS) Against the Performance Criteria	339
7.3 Significance of the Findings	343
7.4 Future Work	346
7.5 Conclusions and Recommendations	354
7.6 References	357

List of Tables

Table 1-1 AMF Performance Criteria. A list of functional performance standards for artificial muscle fibers, inspired by natural muscle fibers.

Table 2-1 Results of Conditioning Cycles (Reduction Half Cycles). The table shows the amount of backcurling, the extent of the redox peaks (both in I and V), and the charge transfers during the 1st and 15th reduction half-cycles for the 0.4, 4.0 and 40 mA deposition current density conditions.

Table 2-2 Results of Conditioning Cycles (Oxidation Half Cycles). The table shows the amount of curling, the extent of the redox peaks (both in I and V), and the charge transfers during the 1st and 15th oxidation half cycles for the 0.4, 4.0 and 40 mA deposition current density conditions.

Table 2-3 Results of Voltage Step Cycles (Reduction Half Cycles). The table shows the amount of backcurling, the extent of the peak redox currents, and the charge transfers (including as a percentage of deposition charge) during the 1st and 15th reduction half-cycles for the 0.4, 4.0 and 40 mA deposition current density conditions.

Table 3-1 Deposition/Stimulation Combinations. The various combinations of deposition NaDBS concentration, deposition pyrrole concentration, stimulation NaDBS concentration and stimulation intensity levels used in the concentration effects experiment.

Table 3-2 Conditioning Movement Per Unit Charge Ratios. Averages of the ratios of curling movement (mm) to charge exchange (mC) during the conditioning cycles, under all combinations of low, medium and high concentration levels of DN, DP and SN. An overall ratio for all of the data is also provided.

Table 3-3 Voltage Step Movement Per Unit Charge Ratios. Averages of the ratios of curling movement (mm) to charge exchange (mC) during the voltage steps, under all combinations of low, medium and high concentration levels of DN, DP and SN. An overall ratio for all of the data is also provided.

Table 3-4 Voltage Step Percentage Charge Exchanges by Condition. For the voltage steps, average calculations of the percentage of charge exchanges during the steps versus the amounts of charge put down during depositions, under all combinations of low, medium and high concentration levels of DN, DP and SN. An overall percentage for all of the data is also provided.

Table 3-5 Post-Step Movement Per Unit Charge Ratios. Averages of the ratios of curling movement (mm) to charge exchange (mC) during the post-step cycling, under all combinations of low, medium and high concentration levels of DN, DP and SN. An overall ratio for all of the data is also provided.

Table 4-1 Variable Round Conditions. A description of the experimental and control conditions carried out in the stimulation history experiment.

Table 4-2 Results of Conditioning Cycles (Reduction Half Cycles). The table shows the amount of backcurling, the extent of the redox peaks (both in I and V), and the charge transfers during the 1st and 15th reduction half-cycles for the 0.3, 0.6 and 2.4 mA deposition current density conditions.

Table 4-3 Results of Conditioning Cycles (Oxidation Half Cycles). The table shows the amount of curling, the extent of the redox peaks (both in I and V), and the charge transfers during the 1st and 15th oxidation half cycles for the 0.3, 0.6 and 2.4 mA deposition current density conditions.

Table 4-4 Movement Responsiveness (ROM/Q) for Modal Stimulation. Movement responsiveness in mm/mC, for samples of the two different DCD values, for the three different modes of stimulation (voltage step, ramp voltammetry, and current step).

Table 5-1 Frequency Response Experimental Conditions. A description of the 20 experimental conditions tested in the frequency response experiment.

Table 5-2 Stimulation Frequencies. The cycling frequencies, scan rates and cycling ranges for the 13 sets of 15 CVs in the frequency response experiment.

Table 5-3 SEM Sample Preparations. The various combinations of deposition NaDBS concentration, deposition pyrrole concentration, stimulation NaDBS concentration and stimulation intensity levels used in the SEM study.

Table 6-1 Power Sample Preparations. A description of the 8 experimental conditions carried out in the power and efficiency experiment.

Table 6-2 Video Analysis Time Steps versus Stimulation Frequency. An itemization of the stimulation frequencies, cycling periods, data analysis time intervals, and data analysis frequencies for the power and efficiency experiment.

Table 6-3 .20 Hz Power and Efficiency Data. A selection of mechanical and electrical work, power and efficiency measurements taken from the 14th cycle of the .20 Hz stimulation set for all 8 sample conditions.

Table 6-4 .40 Hz Power and Efficiency Data. A selection of mechanical and electrical work, power and efficiency measurements taken from the 14th cycle of the .40 Hz stimulation set for all 8 sample conditions.

List of Figures and Illustrations

Figure 1-1 *The oxidative polymerization process that converts pyrrole into polypyrrole.*

Figure 1-2 *A more complex version of the oxidative polymerization process that converts pyrrole into polypyrrole. The figure illustrates polypyrrole chain propagation (Imisides et al. 1996).*

Figure 1-3 *A representation of a standard deposition plot (current versus time). Characteristic features of this amperogram include the initial peak, the smooth drop-off to a plateau and the subsequent recovery to a higher plateau. These features likely correspond to double-layer charging, nucleation and polymer growth. The nature of the plot characteristics vary with deposition conditions.*

Figure 1-4 *Examples of electrolyte dopants used in polypyrrole synthesis.*

Figure 1-5 *The doping/dedoping process that converts oxidized PPy into reduced PPy, and vice versa.*

Figure 1-6 *A sample cyclic voltammogram (CV) for PPy(DBS) cycled between -1.1 V and +0.4 V. Characteristic features include the oxidation peak (upper right) and the reduction peak (lower left).*

Figure 1-7 *Top illustration shows a cross-section of a bending beam of the type used in this thesis. The PPy(DBS) layer is cycled through reduction and oxidation to expand and contract, respectively. This causes the beam to bend, as per the bottom illustration. During reduction the positive charges of the polymer are neutralized, leaving a net negative charge on the polymer due to the trapped DBS anions. Positive sodium cations move into the polymer to compensate, expanding the polymer. During oxidation the polymer is positively charged and it compensates for the anions itself. As a result, the mobile sodium cations leave the polymer matrix and the polymer contracts.*

Figure 1-8 *A frequency response plot for the curling behaviour of an early bending beam produced during training in Linköping, Sweden. PPy(DBS) was deposited on gold-coated Mylar[®]. Subsequent stimulation of the PPy(DBS) with NaDBS led to changes in volume in the PPy(DBS). That, in turn, led to curling of the beam. The amount of curl was measured in degrees by comparing tangents of the two ends of the beam.*

Figure 2-1 *The experimental apparatus for the electropolymerization of the pyrrole, as well as for the stimulation of the polypyrrole dodecylbenzene sulfonate. The HP Function Generator controlled deposition and stimulation signals via the PINE Bi-Potentiostat. The Nicolet Oscilloscope provided user feedback, while the PC collected data. The video camera recorded beam movement activity.*

Figure 2-2 Schematic illustrating how the range of movement of the tip of each beam was measured. Note that the measured distance is that of the actual curved path that the tip traveled i.e. not just a straight line from the oxidized position to the reduced position.

Figure 2-3 Deposition voltammograms sampled at 100 Hz and collected using LabVIEW software. The different plots correspond to samples of PPy(DBS) deposited at different deposition current densities (DCDs). Data analysis was performed using custom Matlab[®] routines.

Figure 2-4 Deposition current density versus the average deposition potential. The best-fit curve is a 3-parameter sigmoid function of the form $[39.8/(1 + e^{-(x-1.06)/.15})]$ such that $R^2 = .99$, $P < .0001$.

Figure 2-5 Movement of the beam tip during deposition, versus DCD (top) and versus time on a log scale (bottom). The same amount of charge was deposited for every data point (300 mC). The regression line in the top graph is a 2-parameter hyperbolic decay function of the form $[10.7/(11.3 + x)]$ such that $R^2 = .92$, $P < .0001$. The higher the DCD value, the lower the amount of curling that took place during deposition. The regression line in the bottom graph is a 2-parameter log function of the form $[-.42 + .17*\ln(x)]$ such that $R^2 = .92$, $P < .0001$. The shorter the deposition, the lower the amount of curling that took place during deposition.

Figure 2-6 The maximum half-cycle extent of beam tip movement versus DCD during the fifteen conditioning cycles. The regression line is linear ($R^2 = .92$, $P < .0001$). The higher the DCD, the lower the amount of beam curling.

Figure 2-7 Beam tip movements during the oxidative halves of the conditioning cycles, with respect to the specific conditioning cycle, as a function of DCD. Error bars represent ± 1 standard deviation of the average values shown. Low DCD samples curl more but take longer to reach their maximal curling extent.

Figure 2-8 Conditioning CVs sampled at 100 Hz and collected using LabVIEW software during the twelfth cycle.

Figure 2-9 The maximum extent of the beam tip movement during reduction in the 15th conditioning cycle versus the reductive charge transfer during that cycle, as a function of DCD. The regression line is linear ($R^2 = .75$, $P < .0001$), and the slope is 0.79 mm/mC. The extent of the beam tip movement was proportional to the amount of charge transferred, independent of DCD value. However, low DCD samples tended to transfer more charge (and therefore backcurl more) while high DCD samples tended to transfer less charge (and therefore backcurl less).

Figure 2-10 Anodic and cathodic (redox) voltage peaks with respect to conditioning cycle, as a function of DCD. Error bars represent ± 1 standard deviation of the average values shown. For high DCD samples, the anodic peaks are mostly stationary over time

while the cathodic peaks move in the anodic direction. For low DCD samples, the anodic peaks shift anodically while the cathodic peaks are mostly stationary.

Figure 2-11 A schematic representation of beam position versus time during one of the later conditioning oxidation half-cycles for two typical beams grown at 0.4 and 40 mA/cm² respectively. Low DCD samples start more backcurled and end more curled, moving both more extensively and more rapidly (i.e. the slope of the lines).

Figure 2-12 Voltage step responses (amperograms) sampled at 100 Hz and collected using LabVIEW software during the 4th voltage step cycle.

Figure 2-13 A schematic representation of beam position versus time during one of the later voltage step oxidation half-cycles, for two typical beams grown at 0.4 and 40 mA/cm². Low DCD samples start more backcurled and end more curled, moving both more extensively and more rapidly. Movements were largely completed in the first half of the cycles, following the current responses to the voltage stimulation.

Figure 2-14 A schematic representation of beam position versus time during one of the later current step oxidation half-cycles, for two typical beams grown at 0.4 and 40 mA/cm² and stimulated at a relatively high charge percentage-of-maximum value. Low DCD samples start more backcurled and end more curled, moving both more extensively and more rapidly without any pause at the two extremes.

Figure 2-15 The maximum half-cycle extent of the beam tip movement during the five current step cycles, versus DCD. The 10 mC samples are labeled with an equivalent charge percentage value. The 25% of maximum charge open circles show how DCD is important for a given percentage of charge stimulation. The 10 mC charge black circles show how DCD may not be very important for a given fixed amount of charge stimulation. The column of symbols above each DCD value that was tested show a rough proportionality between movement extent and percentage of charge stimulation except, possibly, at very high percentage levels i.e. $\geq 100\%$.

Figure 3-1 The experimental apparatus for the electropolymerization of the pyrrole, as well as for the stimulation of the polypyrrole dodecylbenzene sulfonate. The HP Function Generator controlled deposition and stimulation signals via the PINE Bi-Potentiostat. The Nicolet Oscilloscope provided user feedback, while the PC collected data. The video camera recorded beam movement activity. Lower photo shows details of the cell.

Figure 3-2 Deposition voltammograms sampled at 100 Hz and collected using LabVIEW software. The different plots correspond to samples of PPy(DBS) deposited at different pyrrole and NaDBS concentrations (.02 M, .08 M and .32 M). The top plot shows the effects of varying NaDBS concentration, while the bottom plot shows the effects of varying pyrrole concentration during deposition. Data analysis was performed using custom Matlab[®] routines.

Figure 3-3 Plots of average deposition potential versus deposition pyrrole (DP) and deposition NaDBS (DN) concentrations. Low levels are taken as .01-.02 M, medium levels as .04-.08 M and high levels are taken as .16-.32 M. Error bars are ± 1 standard deviation for a population of between 1 and 9 samples per condition (average of 5).

Figure 3-4 Curling versus conditioning cycle number, by SN concentration group (top). The low, medium and high SN concentration ranges are shown in the legend. Error bars are ± 1 standard deviation for a population of 11-23 samples per condition. Note the substantial differences despite variation among DN and DP values within SN groupings. The middle graph shows curling versus the scaled log of the product SN*DN. Error bars are ± 1 standard deviation for a population of 5-19 samples per product value. The bottom graph shows a scatter plot of curling versus the scaled log of the product SN*DN*DP. A total of 45 data points are plotted.

Figure 3-5 Conditioning cycle 15 oxidation curling versus deposition curling (top), by SN concentration level (values as shown in the legend). Conditioning cycle 15 oxidation curling versus deposition curling (bottom), by DCD level (values as shown in the legend). Data for the bottom graph was taken from Chapter 2.

Figure 3-6 Conditioning cycle 15 range of movement (x-axis) versus charge exchange during the reduction half cycle (mC). The top graph presents the data with respect to DP levels, the middle graph presents it with respect to DN levels, and the bottom graph presents it with respect to SN levels. Low levels are .01-.02 M, mid are .04-.08 M and high are .16-.32 M. The oxidation half cycle data points formed similar patterns.

Figure 3-7 Conditioning cycle 15 peak reduction currents (x-axis) versus peak voltage during the half cycle (V). Since current correlates well with exchanged charge, the Q vs. V graph looks very similar, and since range of movement correlates well with exchanged charge, it looks similar as well. Low levels = .01-.02M, mid = .04-.08M, high = .16-.32M.

Figure 3-8 Peak reduction current versus cycle number, by SN concentration group. The low, medium and high SN concentration ranges are shown in the legend. Error bars are ± 1 standard deviation for a population of 11-23 samples per condition. Note that within the SN groupings, there was variation among DN and DP values. The lower graph plots the peak currents from the 15th oxidative half cycles versus respective SN values.

Figure 3-9 15th conditioning cycle peak reduction current, by SN, DN and DP concentration groups. The DP concentration ranges form the rows, the DN concentration ranges form the columns, and the SN concentration ranges are represented within each graph. Where present, error bars are ± 1 standard deviation for a population of 2-3 samples per condition.

Figure 3-10 15th conditioning half-cycle oxidation charge transfer, by SN, DN and DP concentration groups. The DP concentration ranges form the rows, the DN

concentration ranges form the columns, and the SN concentration ranges are represented within each graph. Where present, error bars are ± 1 standard deviation for a population of 2-3 samples per condition.

Figure 3-11 Conditioning half cycle reductive charge exchanges versus cycle number, by SN concentration group. The low, medium and high SN concentration ranges are shown in the legend. Error bars are ± 1 standard deviation for a population of 11-23 samples per condition. Note that within the SN groupings, there was variation among DN and DP values. The lower graph plots the charge exchanges from the 15th oxidative half cycles versus respective SN values.

Figure 3-12 Curling movements during oxidative voltage steps, versus cycle number, by SN concentration group. The low, medium and high SN concentration ranges are shown in the legend. Error bars are ± 1 standard deviation for a population of 11-18 samples per condition. Note that within the SN groupings, there was variation among DN and DP values.

Figure 3-13 Voltage step peak reduction current versus cycle number, by SN concentration group. The low, medium and high SN concentration ranges are shown in the legend. Error bars are ± 1 standard deviation for a population of 11-18 samples per condition. Note that within the SN groupings, there was variation among DN and DP values. The lower graph plots the peak currents from the 5th reductive half cycles versus respective SN values.

Figure 3-14 Voltage step half cycle reductive charge exchanges versus cycle number, by SN concentration group. The low, medium and high SN concentration ranges are shown in the legend. Error bars are ± 1 standard deviation for a population of 11-23 samples per condition. Note that within the SN groupings, there was variation among DN and DP values.

Figure 3-15 Voltage step cycle 5 reductive range of movement (x-axis) versus charge exchange during the half cycle (mC). The top graph presents the data with respect to DP levels, the middle graph presents it with respect to DN levels, and the bottom graph presents it with respect to SN levels. Low levels are .01-.02 M, mid are .04-.08 M and high are .16-.32 M.

Figure 3-16 Voltage step cycle 5 reductive half cycle charge exchange (x-axis) versus peak current during the half cycle (mC). The top graph presents the data with respect to DP levels, the middle graph presents it with respect to DN levels, and the bottom graph presents it with respect to SN levels. Low levels are .01-.02 M, mid are .04-.08 M and high are .16-.32 M.

Figure 3-17 Voltage step amperograms sampled at 100 Hz and collected using LabVIEW software. The top plot helps show the effects of varying the stimulation NaDBS concentration, where .08 M DP and .08 M DN were used with the .02 M SN sample and where .04 M DP and .08 M DN were used with the .32 M sample. The bottom plot shows

the effects of varying pyrrole concentration during deposition. DN and SN are both .04 M for the two plots shown. Data analysis was performed using custom Matlab[®] routines.

Figure 3-18 Post-step cycle 15 reductive half cycle peak currents (x-axes) versus peak voltage during the half cycle (V). Both graphs present the data with respect to DP levels, with the top graph showing the oxidative data and the bottom graph showing the reductive data. Low levels are .01-.02 M, mid are .04-.08 M and high are .16-.32 M.

Figure 4-1 Differences in twitch and tetanus behaviour between slow and fast twitch muscle. Plots in A show twitches of motor units. Plots in B show 12 Hz stimulation tetanic tension. Plots in C show the force produced during tetanus over 330 seconds, where each second the muscle is activated by a brief burst of tetanic stimulation. Note the scales on the vertical axes (from Ghez 1991, and Burke et al. 1974).

Figure 4-2 Differences in twitch and tetanus behaviour depend on the precise stimulation pattern. Plot A shows an unfused tetanus at 12 Hz along with an extra impulse (the arrow) that creates a long-lasting increase in tension. Plot B shows an extra impulse inserted at the start of the stimulus train (a doublet). Plot C starts with the doublet again, but misses a pulse midway, causing a lasting decrease in tension (from Ghez 1991, and Burke et al. 1970).

Figure 4-3 Deposition voltammograms sampled at 100 Hz and collected using LabVIEW software. The different plots correspond to the first 125 seconds of the three representative depositions. The samples of PPy(DBS) were deposited at different deposition current densities (DCDs). The history samples were produced at 2 mA/cm² and 16 mA/cm², while the range samples were produced at 4 mA/cm². Data analysis was performed using custom Matlab[®] routines.

Figure 4-4 Conditioning CVs collected from the range samples using LabVIEW software during the 14th cycle. The three plots are representative of their classes of samples. Note that the data for the 50 mHz sample was collected at 100 Hz, the data for the 100 mHz sample was collected at 200 Hz and the data for the 200 mHz sample was collected at 400 Hz.

Figure 4-5 Average peak currents (x-axis) versus average charge exchange per half cycle for the 1st, 4th, 7th, 10th and 15th cycles of each conditioning set in the range experiment. Oxidative half cycle data are in the upper right quadrant while reductive half cycle data are in the lower left quadrant. Seven samples were averaged per data point.

Figure 4-6 Average range of movement (ROM) of the beam tips per oxidative half cycle for the 1st, 4th, 7th, 10th and 15th cycles of each conditioning set in the range experiment. The three plots correspond to the movement patterns related to the three cycling rates used. Error bars are ± 1 standard deviation (7 samples per data point).

Figure 4-7 Charge exchange versus peak voltage. Each data point represents the respective Q/V values for the 5th cycle of each of the 5 sets, where the cycling limits expanded in both directions by 0.1 V with each set. Note that in the top graph, cycling frequencies are held constant with the expanding cycling range (so scan rates increase), while in the bottom graph scan rate is kept constant (so cycling frequency decreases). There are subtle differences in the way the data behaves.

Figure 4-8 Drop-off in curling with cycling frequency. The data with respect to scan rate look very similar. Note the change in drop-off with cycling range.

Figure 4-9 Drop-off in charge exchange with scan rate (or cycling frequency). Note the similarity in drop-off with cycling range.

Figure 4-10 Change in peak voltages with respect to scan rate. Note the nature of the changes in rise/fall with cycling range. The changes in peak voltages with respect to cycling frequency are very similar, and differ mostly in the middle data points which are higher on the oxidation side and lower on the reduction side such that most of the lines joining the last two data points in each data set are essentially flat i.e. the peak voltages are at or beyond the cycling limits.

Figure 4-11 Charge exchange versus peak voltage. Each data point represents the respective Q/V values for the 5th cycle of each of the 5 sets, where the cycling limits expand in the reduction direction by 0.1 V with each set. Cycling frequencies are held constant with the expanding cycling range (so scan rates increase). See Figure 4-7 for comparison.

Figure 4-12 Change in charge exchange with respect to scan rate. Note the nature of the changes in rise/fall with cycling range.

Figure 4-13 Charge exchange versus peak voltage. Each data point represents the respective Q/V values for the 5th cycle of each of the 5 sets, where the cycling limits expand in the oxidation direction by 0.1 V with each set. Cycling frequencies are held constant with the expanding cycling range (so scan rates increase). See Figures 4-7 and 4-11 for comparison.

Figure 4-14 Representative CVs from reduction, oxidation and redox range expansion, where the cycling took place at 50 mHz on the left, and at 200 mHz on the right. CVs for the same at 150 mV/s and 600 mV/s are similar.

Figure 4-15 Amperograms from the stimulation mode variations collected using LabVIEW software. Current step, voltage step and cyclic voltammetry current signals for the 40th cycle for the samples grown at 2 mA/cm². The data was collected at 100 Hz.

Figure 4-16 Charge exchange levels, per cycle, for the stimulation frequency variations. The left graph shows the data from the low DCD samples. The right graph shows the data from the high DCD samples. Similar patterns, different relative magnitudes.

Figure 4-17 Cyclic voltammograms from the stimulation frequency variations collected using LabVIEW software. The 40th cycle for the .03 Hz, .30 Hz and 3.0 Hz samples grown at 16 mA/cm². The data was collected at 100 Hz.

Figure 4-18 Cyclic voltammograms from the stimulation NaDBS variations collected using LabVIEW software. The 40th cycle for the .02 M, .08 M and .32 M NaDBS samples grown at 16 mA/cm². The data was collected at 100 Hz.

Figure 4-19 Voltammograms from the current step variations collected using LabVIEW software. Voltage signals for the 40th cycle from the 50%, 100% and 150% samples grown at 2 mA/cm². The data was collected at 100 Hz.

Figure 5-1 Deposition curling (movement of the beam tip, in cm) under different conditions of current density, and Kapton[®] and PPy(DBS) thickness. Thin Kapton[®] film results are on the left (HN 50). Thick Kapton[®] film results are on the right (HN 100). Low DCD values (2 mA/cm²) are on the top. High DCD values (16 mA/cm²) are on the bottom. Each graph shows the amount of curling half way through the deposition (Half Dep) and at the end of the deposition (Full Dep), over a range of PPy(DBS) film thicknesses (where 300 mC is approximately equivalent to 10 μm).

Figure 5-2 Deposition curling (movement of the beam tip, in cm) under different conditions of beam length (1.0 and 1.5 cm) and deposition concentrations (DP and DN). Constant DN results are on the left (.08 M). Constant DP results are on the right (.08 M). Short beam values (1.0 cm) are on the top. The longer beam values (1.5 cm) are on the bottom. Each graph shows the degree of curling over the deposition. In all cases, the depositions lasted about 500 seconds. The amount of curling was measured at the half-way point of the deposition and at the end of the deposition. Error bars are ± 1 standard deviation for a population of 3 for the 1.0 cm samples and of 7 for the 1.5 cm samples.

Figure 5-3 Voltage step responses for the SEM samples stimulated in .02 M, .08 M and .32 M NaDBS. These amperograms have been sampled at 100 Hz and collected using LabVIEW software. Data analysis was performed using custom Matlab[®] routines. Note the stimulation artifacts both prior to and after the actual voltage step. They reflect the short time periods between the signal generator being on and not yet producing a signal and the signal generator power being turned on/off.

Figure 5-4 Normalized weight percentages of the three elements oxygen, sulfur and sodium in the PPy(DBS) films produced in different concentrations of pyrrole and NaDBS. Note that low refers to .02 M, mid refers to .08 M and hi refers to .32 M. Also note that the Na percentages have all been multiplied by 5 for illustrative clarity.

Figure 5-5 Normalized weight percentages of the three elements oxygen, sulfur and sodium in the PPy(DBS) films stimulated by reductive or oxidative voltage steps in different concentrations of stimulation NaDBS (SN). Note that low refers to .02 M, mid refers to .08 M and hi refers to .32 M NaDBS. Also note that the upper graph consists of

data taken from a 30.5 degree takeoff angle, while the lower graph consists of data from the same sample set, but collected at a 75.0 degree takeoff angle.

Figure 5-6 SEM images of PPy(DBS) films produced in different levels of pyrrole concentration. The top image (a) shows a film produced in .02 M pyrrole. The lower left image (b) shows a film produced in .08 M pyrrole, and the lower right image (c) shows a film produced in .32 M pyrrole. Scale bars are 10 μm . Magnification is X1000, at 5 KV.

Figure 5-7 SEM images of edges of PPy(DBS) films. The top left image (a) shows the central edge of a 10 μm thick film produced in .08 M pyrrole/.08 M NaDBS at 1 mA/cm^2 . Magnification is X750 at 5 KV. The top right image (b) shows a similar sample grown at 4 mA/cm^2 (X3500, 5 KV). The lower left image (c, X750, 15 KV) shows the lateral edge of the beam shown in a) when it was still bonded to Kapton[®], illustrating the distortions that occur at the edges of the beams. The last image, lower right (d), shows the results of a difficult deposition at 28 mA/cm^2 (X1000, 15 KV).

Figure 5-8 Representative cyclic voltammograms for samples cycled at .10 and .80 Hz. The top row is for thin PPy(DBS) films (2.5 μm), the middle row is for medium thickness films (10 μm) and the bottom row is for thick films (40 μm). Each plot shows samples produced at 2 mA/cm^2 and at 16 mA/cm^2 .

Figure 5-9 At top, curling on the 15th cycle versus stimulation cycling frequency for a sample produced at 2 mA/cm^2 , on HN 100 Kapton[®], to a projected thickness of 5 μm . Middle graph shows charge exchange on the 15th cycle versus stimulation cycling frequency, for the same sample. At bottom, peak currents for the same sample.

Figure 5-10 The ratio of charge exchange to peak current (top) and the ratio of curling movement to charge exchange or movement responsiveness (bottom) on the 15th cycle, versus stimulation cycling frequency, for a single sample produced at 2 mA/cm^2 , on HN 100 Kapton[®], to a projected thickness of 5 μm .

Figure 5-11 Curling with respect to PPy(DBS) film thickness (deposition charge density) where the data shown combines the HN 50 and HN 100 results. Left plots are for samples grown at 2 mA/cm^2 . Right plots are for samples grown at 16 mA/cm^2 . Plots, in descending order, are of samples stimulated at .05 Hz, .40 Hz, 3.2 Hz and then .05 Hz.

Figure 5-12 Charge exchange with respect to PPy(DBS) film thickness (deposition charge density) where the data shown combines the HN 50 and HN 100 results. Left plots are for samples grown at 2 mA/cm^2 . Right plots are for samples grown at 16 mA/cm^2 . Plots, in descending order, are of samples stimulated at .05 Hz, .40 Hz, 3.2 Hz and then .05 Hz.

Figure 5-13 Peak currents with respect to PPy(DBS) film thickness (deposition charge density) where the data shown combines the HN 50 and HN 100 results. Left plots are for samples grown at 2 mA/cm^2 . Right plots are for samples grown at 16 mA/cm^2 . Plots, in descending order, are of samples stimulated at .05 Hz, .40 Hz, 3.2 Hz and then .05 Hz.

Figure 5-14 Voltage peaks with respect to PPy(DBS) film thickness (deposition charge density) where the data shown combines the HN 50 and HN 100 results. Left plots are for samples grown at 2 mA/cm^2 . Right plots are for samples grown at 16 mA/cm^2 . Plots, in descending order, are of samples stimulated at .05 Hz, .40 Hz, 3.2 Hz and then .05 Hz.

Figure 5-15 Movement responsiveness with respect to PPy(DBS) film thickness (deposition charge density) where the data shown are the 16 mA/cm^2 results. The lesser plots on each graph are for HN 100 samples, while the more responsive plots are the HN 50 samples. Plots, in descending order, are of samples stimulated at .05 Hz, .40 Hz, 3.2 Hz and then .05 Hz again.

Figure 5-16 Cycling frequency versus curling range of motion (cm). Top left plot shows results for thin PPy(DBS) samples. Top right plots show results for mid-thickness PPy(DBS) samples. Bottom center plots show results for thick PPy(DBS) samples. Each plot shows results for thin and thick Kapton[®] film samples, combined with low and high DCD values.

Figure 5-17 Cycling frequency versus curling responsiveness (mm/mC). Top left plot shows results for thin PPy(DBS) samples. Top right plots show results for mid-thickness PPy(DBS) samples. Bottom center plots show results for thick PPy(DBS) samples. Each plot shows results for thin and thick Kapton[®] film samples, combined with low and high DCD values.

Figure 5-18 Cycling frequency versus peak redox currents (mA). Left plot shows results for thin PPy(DBS) samples. Right plots shows results for thick PPy(DBS) samples. Each plot shows results for thin and thick Kapton[®] film samples, combined with low and high DCD values.

Figure 5-19 Cycling frequency versus cycle by cycle charge exchange (mC). Left plot shows results for thin PPy(DBS) samples. Right plots shows results for thick PPy(DBS) samples. Each plot shows results for thin and thick Kapton[®] film samples, combined with low and high DCD values.

Figure 6-1 Plot of the equations used to relate Reynolds number to coefficient of drag (C_D). From .005 to .99, the equation used is $C_D = \text{EXP}(-(\ln Re) / (.55 \times (1 - Re - .2 \times (1 - Re^2)) + .6 \times (1 - Re^{(.17 \times (Re - .6) (Re - .6) + .06))})$. From 1.01 to 10, the equation is $C_D = 13.8 - 8.5 \times ((\log(10 \times Re)) - 1) - .13 \times Re$. These two equations covered the range of Reynolds numbers that arose during the analysis.

Figure 6-2 Instantaneous current, voltage and power for the 14th cycle of one of the power and efficiency samples, at .05 Hz and at .40 Hz. The driving ramp voltage signal is the same in both cases. However, the current response is quite different in quality and magnitude, resulting in a substantially different power signal between the two cases.

Figure 6-3 Simulated CVs illustrating issues of electrical work and efficiency. In both diagrams, the vertically striped areas represent the work accounted for within the CV. The darkly shaded areas represent electrical work that is also consumed during stimulation, but which does not contribute to electromechanical transduction directly. The lightly shaded quadrants represent those areas where the electrical work is actually negative since the IV product contains one negative term. Finally, note that the upper diagram shows a relatively slow cycling frequency while the bottom diagram shows a CV taken at a relatively higher cycling frequency.

Figure 6-4 Deposition curling (movement of the beam tip, in cm) under conditions of different Kapton[®] thicknesses (HN 50 = 12.7 μm and HN 100 = 25.4 μm), different PPy(DBS) thicknesses (5 μm and 20 μm), and different DCD values (2 mA/cm^2 and 16 mA/cm^2).

Figure 6-5 Curling (top) and oxidative half cycle charge exchange (bottom) in the power and efficiency experiment, under all 8 experimental conditions and all 4 stimulation frequencies. Note the relationships between corresponding PPy(DBS) film thicknesses (150 mC and 600 mC), Kapton[®] thicknesses (HN 50 and HN 100) and DCD values (2 mA/cm^2 and 16 mA/cm^2).

Figure 6-6 Reductive half cycle peak currents (top) and reductive half cycle peak voltages (bottom) in the power and efficiency experiment, under all 8 experimental conditions and all 4 stimulation frequencies. Note the relationships between corresponding PPy(DBS) film thicknesses (150 mC and 600 mC), Kapton[®] thicknesses (HN 50 and HN 100) and DCD values (2 mA/cm^2 and 16 mA/cm^2).

Figure 6-7 Movement responsiveness, or curling per unit charge exchange (top) and charge exchange capacities, or ratio of charge exchange during cycling to initial doping charge deposited during polymerization (bottom) in the power and efficiency experiment, under all 8 experimental conditions and all 4 stimulation frequencies. Note the relationships between corresponding PPy(DBS) film thicknesses (150 mC and 600 mC), Kapton[®] thicknesses (HN 50 and HN 100) and DCD values (2 mA/cm^2 and 16 mA/cm^2).

Figure 6-8 Power and efficiency experimental data, shown relative to cycling frequency. Top graph shows curling of thin Kapton[®] samples. Bottom graph shows curling of thick Kapton[®] samples. Each graph shows the samples varying in DCD (2 mA/cm^2 or 16 mA/cm^2) and PPy(DBS) film thickness (5 μm or 20 μm). Note the relationships between samples differing in one variable, as well as the interaction effects.

Figure 6-9 Power and efficiency experimental data, shown relative to cycling frequency. Top graph shows the peak currents of thin Kapton[®] samples. Bottom graph shows the peak currents of thick Kapton[®] samples. Each graph shows the samples varying in DCD (2 mA/cm^2 or 16 mA/cm^2) and PPy(DBS) film thickness (5 μm or 20 μm). Note the relationships between samples differing in one variable, as well as the interaction effects.

Figure 6-10 Power and efficiency experimental data, shown relative to cycling frequency. Top graph shows the peak voltages of thin Kapton® samples. Bottom graph shows the peak voltages of thick Kapton® samples. Each graph shows the samples varying in DCD (2 mA/cm² or 16 mA/cm²) and PPy(DBS) film thickness (5 µm or 20 µm). Note the relationships between samples differing in one variable, as well as the interaction effects.

Figure 6-11 Power and efficiency experimental data, shown relative to cycling frequency. Top graph shows the movement responsiveness of thin Kapton® samples, where the responsiveness measure is the ratio of beam curling to charge exchange bringing about the beam curling. Bottom graph shows the movement responsiveness of thick Kapton® samples. Each graph shows the samples varying in DCD (2 mA/cm² or 16 mA/cm²) and PPy(DBS) film thickness (5 µm or 20 µm). Note the relationships between samples differing in one variable, as well as the interaction effects.

Figure 6-12 Power and efficiency experimental data, shown relative to cycling frequency. Top graph shows the charge exchange capacities of thin Kapton® samples, where the exchange capacity measure is the ratio of charge exchange during cycling to the doping charge deposited on the beam during polymerization. Bottom graph shows the charge exchange capacities of thick Kapton® samples. Each graph shows the samples varying in DCD (2 mA/cm² or 16 mA/cm²) and PPy(DBS) film thickness (5 µm or 20 µm). Note the relationships between samples differing in one variable, as well as the interaction effects.

Figure 6-13 Plots used to visualize the power and efficiency calculations of the gravitational, drag and inertial work components of the first sample (2 mA/cm², HN 50, 5 µm PPy(DBS)). The two lines on each graph correspond to the position, velocity or work of the two beam elements that the beam was divided into for the analysis.

Figure 6-14 Plots used to visualize the power and efficiency calculations of the torque (elastic energy), total mechanical, and total electrical work of the first sample (2 mA/cm², HN 50, 5 µm PPy(DBS)). The “top” and “end” lines on the upper two graphs correspond to the work of the two beam elements that the beam was divided into for the analysis.

Figure 7-1 Proposed differences in the nature of the polymer growth in relatively favourable (top) and relatively poor (bottom) growing conditions. Better growth conditions would result in lower bulk density due to the reduced space filling of longer chains, and more electrostatic interactions pushing chains away from each other away due to improved polaron and dipolaron formation would create more deposition stresses leading to more deposition strain i.e. bending.

Figure 7-2 Schematics of various muscle biomechanics for insect flight (<http://hannover.park.org/Canada/Museum/insects/evolution>). AMFs could function in such an arrangement to facilitate the development of biorobotic insects for use in exploration, remote sensing, intelligence gathering, and entertainment.

List of Symbols, Nomenclature, and Abbreviations

a	acceleration, in m/s^2 unless otherwise specified
Å	angstrom, 10^{-10} m
AC	alternating current
ACN	acetonitrile, or CH_3CN
ADP	adenosine diphosphate
Ag	silver
AMF	artificial muscle fiber
amperogram	a plot of current versus time
aq	aqueous/in water
ATP	adenosine triphosphate
Au	gold
backcurl	beam strain as a result of reduction with PPy(DBS) in NaDBS
backside	that side of the Kapton [®] without the metal layer on it
bpm	beats per minute
BS	benzene sulfonate
C	coulomb, a unit of charge
cc	cubic centimeter
C_D	coefficient of drag
Cl	chlorine/chloride
ClO_4	perchlorate
curl	beam strain as a result of oxidation with PPy(DBS) in NaDBS
CV	cyclic voltammogram, a plot of current versus voltage
d	distance, in m unless otherwise specified
DBS	dodecylbenzene sulfonate
DCD	deposition current density, measured in mA/cm^2
DN	the concentration of NaDBS in the deposition solution
dopant	in PPy(DBS), it is the negative counterion (anion) DBS
DP	the concentration of pyrrole in the deposition solution
E	Young's Modulus, relating strain and stress for a given material
ERF	electrorheological fluid

erg	a cgs unit of work equal to 10^{-7} J
Excel	Microsoft® spreadsheet software package
F	force, measured in Newtons
FES	functional electrical stimulation
g	gravitational acceleration, 9.81 m/s^2
GPa	gigapascals, a measure of pressure or stress, 10^9 N/m^2
H	hydrogen
high	concentration range, .16-.32 M
HN	see Kapton®
Hz	hertz, base unit of frequency in s^{-1}
I	current, or moment of inertia
IPMC	ionic polymer-metal composite
J	Joule, unit of work or energy
K	potassium
Kapton® HN	tough, aromatic polyimide film from Dupont
KCl	potassium chloride
keV	kilo-electron volt, a unit of energy
kg	kilogram, 10^3 grams
kJ	kilojoule, 10^3 Joules
kPa	kilopascal, 10^3 N/m^2
kV	kilovolt, 10^3 V
KV	see keV
LabVIEW	data acquisition hardware and software toolset
Li	lithium
LiClO_4	lithium perchlorate
low	concentration range, .01-.02 M
LPF	low pass filter
m	mass, in kg unless otherwise specified
M	molarity - base unit of solution concentration, or moment
mA	milliamp, a measure of current, $1/1000^{\text{th}}$ of an amp

Matlab®	mathematical analysis software package
mC	millicoulomb, a measure of electrical charge, 1/1000 th of a coulomb
medium	concentration range, .04-.08 M
mHz	millihertz, 1/1000 th of a hertz
mid	see medium
mil	1/1000 th of an inch or 25.4 μm
MOI	moment of inertia, I
molarity	moles of solute per volume of solution
MPa	megapascals, a measure of pressure or stress, 10^6 N/m^2
ms	millisecond
mV	millivolt, a measure of electric potential, 1/1000 th of a volt
mW	milliwatt, a measure of power, 1/1000 th of a watt
Mylar®	polyester film from Dupont
n-doped	or n-type, negative charge carrier
Na	sodium
NA	neutral axis in an elastic beam
NaCl	sodium chloride
NaDBS	sodium dodecylbenzene sulfonate
NH ₄ Cl	ammonium chloride
NH ₄	ammonia
NO ₃	nitrate
Normal	a type of statistical distribution, symmetrical about the mean, one peak
O	oxygen
P	power, measured in watts unless otherwise specified
p-doped	or p-type, positive charge carrier
P _i	phosphate
peak	locations of maximum or minimum current in a CV
PGT	Princeton Gamma-Tech, manufacturer of SEM detector components
pH	a measure of acidity, concentration of hydrogen ions
Plexiglas	polymethyl methacrylate
PPy	polypyrrole

pTS	para-toluene sulfonate
PVA/PAA	polyvinyl alcohol/polyacrylic acid
PVDF	polyvinylidene fluoride
Q	electric charge
Re	Reynolds number, for fluid dynamics drag analyses
roc	radius of curvature
ROM	range of (curling) movement of the beam tips
S	sulfur, or Siemen (unit of conductivity)
SCE	saturated calomel electrode
SD	standard deviation
SEM	scanning electron microscope
SigmaPlot®	statistical plotting and analysis software package
siliconCOACH	video analysis software package
SMA	shape memory alloy
SN	the concentration of NaDBS in the stimulation solution
SpArCCS	Spinal Arm-Control Circuitry Simulator
takeoff angle	the angle between the specimen surface and the X-ray detector in SEM
U	internal elastic (strain) energy, in Joules
μm	micrometer, 10^{-6} m
V	voltage, or volt, a measure of electric potential
voltammogram	a plot of voltage (potential) versus time
W	work, or Watt, a measure of power
ZAF	software/algorithms used to correct raw x-ray intensity measurements for absorption, fluorescence and atomic number effects in SEM
Zn	zinc
ZnCl ₂	zinc chloride
ϵ	strain, measured in %
ν	kinematic viscosity, cm^2/s
ρ	fluid density, or radius of curvature
σ	stress, in N/m^2

1. Introduction

1.1 Motivation and Goals

For over 50 years, scientists and engineers have been trying to develop a useful artificial muscle fiber, or AMF (Kuhn 1949). Motivations have not always been clear, but the promise of an actuator that behaves like natural muscle has captivated many. Various approaches have achieved some measure of success but not so much so that they have come into common use. Nevertheless, in the last 5-10 years several notable advances have been realized, suggesting that the time is near for the production of an artificial muscle fiber with the right balance of qualities that would make it suitable for use in prosthetic, orthotic, biorobotic, or other neuromuscular modeling applications. Success would mean the development of a new form of linear, as opposed to rotary, actuator that could have extensive industrial applications, not to mention biomedical and pedagogical applications. But what specifically would constitute success?

Experience in laboratories around the world has shown that the key criterion is *balance*. For example, some recent technology demonstrations have featured impressive results (Kanatzidis 1990, Baughman et al. 1991, Hunter and Lafontaine 1992, Suzuki and Hirasaka 1993, Hirai et al. 1994, Smela et al. 1995a), and yet none have become widely applied. The reason is that each suffers from at least one significant shortcoming or design trade-off. Some have involved materials that depend on high voltage stimulation, while others vary considerably in their response time. Many require hydraulics as infrastructural support and others, such as shape memory alloys, exhibit great strength but depend upon relatively high levels of power input and heat dissipation (Hunter and Lafontaine 1992). Still more, such as the polypyrrole microactuators, are difficult to

work with because of their small size. To be fair, each approach has had slightly different objectives beyond the basic goal of producing a contractile actuator. It has been those differences in design tolerances that have hindered comparisons of different approaches. Is there not a basic set of qualities that indicate when one approach is better than another? Not really, as it depends on the application. However, we should be able to agree on a number of comparative measures even if their importance is different in different situations. A good source of those measures can come from examining, and from trying to mimic, the functional characteristics of natural muscle. This would include such measures as power consumption, operational device efficiency, heat dissipation densities, durability, strength and power densities, response time and frequency response. Doing well on one or two of these performance dimensions only to fall very short on others would not constitute success within the framework of emulating natural muscle. Therein lies the main challenge ... to do well against all of these criteria at once, thereby achieving a balance in performance. The guiding principle in the search for a feasible AMF, as outlined in this thesis, will be to replicate the functional characteristics of natural skeletal muscle fibers as closely as possible.

In an age when artificial hearts, bones, kidneys, lungs and even intelligence, are common, it may seem strange that artificial muscle fibers are not yet a commercial or even a clinical reality. Perhaps because there has not been a life-saving impetus for this technology, it has remained largely under-developed, at least until recently. In the last ten years or so there have been a number of attempts to create artificial muscles and artificial muscle fibers. As it was for artificial neural networks in the 1950s up until the late 1970s, today's activity in artificial muscle fiber research cuts thinly across many

disparate disciplines. As a result, even researchers who know about other work in the field cannot always help one other. The applications that are pursued can also be subtly, yet significantly, different. All of these factors have contributed to slow progress.

Nevertheless, AMF research has gone on, carried out by small and devoted groups of scientists and engineers spread around the world in countries as far flung as the United States, Australia, Japan, the United Kingdom, Spain, Sweden, Denmark, Canada and Italy. The main areas of activity are in polymers, micromachines and shape memory alloys. Funding for research has come from private industry, the military and from publicly funded scientific, engineering and medical research organizations.

For the purposes of this thesis, the technology that will be used to try and achieve the main goals will be based upon conducting polymers and specifically upon a contractile electroactive polymer called polypyrrole dodecylbenzene sulfonate, or PPy(DBS). PPy(DBS), in bilayer devices, has demonstrated several desirable qualities that are needed in the AMF application such as fast stimulation response time, adequate frequency response and potentially high strength and device efficiency (Smela et al. 1995a-b). The challenge in this project will be to achieve adequate performance levels across several different dimensions simultaneously.

Thus, while the underlying goal of this thesis is to produce an artificial muscle fiber (AMF) that can be used in prosthetics, biorobotics, motor control research and education, the specific goal of this thesis will be to evaluate PPy(DBS) for its suitability in the actuation role in an AMF application where the intent is to have the AMF possess qualities as similar to natural muscle as possible. Clearly this is a high-risk venture and

as the following pages will show, others who have tried to reach this goal have experienced only limited success.

As to why one might choose to pursue AMFs, my personal interest has stemmed from an early infatuation with artificial intelligence. That led to artificial neural networks, computational neuroscience and a Master's thesis centered on a software-based neuromuscular simulation tool called SpArCCS (Maw 1993, Maw et al. 1996). The logical extension to SpArCCS was to construct a physical simulation which could then be used for all the purposes that SpArCCS was designed for i.e. education, research, and biorobotics. In terms of education, live demonstrations of neuromuscular concepts could be presented to students using AMFs. As a man-made physical system, control of the artificial muscle fibers could be easily and rapidly reconfigured to answer *what if* types of questions. Such questions could be the basis for original motor control research that might otherwise be impossible or difficult to perform with biological or software systems. A good analogy would be the development of artificial neural networks. While gross simplifications of biological neural networks, they do allow researchers to explore some key issues relevant to the functioning of the biological world. AMF research could influence motor control research in similar ways. Finally, even if their similarities with natural muscle fibers were insufficient to be broadly applicable in education and research, AMFs could still find broad application in the areas of prosthetics and robotics as long as they met certain standards of power, efficiency, strength, durability and frequency response. Taken alone or in pairs, several of these criteria have already been met by a few different AMF technologies.

In any event, in wanting to construct a physical model of a neuromuscular system, an effective actuator was required. Even though a variety of such actuators are available, they all have significant shortcomings. I was looking to develop a better approach, and PPy(DBS) looked like it had potential. Success in this development would mean that AMFs could be used to create functional artificial neuromuscular systems and the applications of such systems would only be limited by the imagination. Biorobotics, orthotics and prosthetics would only be the starting point. An efficient, strong, silent and safe AMF would have great commercial, biomedical and pedagogical potential.

Beyond education, there are at least three main application areas for artificial muscle fiber technology. The groupings are not completely exclusive but they do stem from different design criteria and are therefore differentiated in what follows. In general terms, the groupings can be labeled biomedical, industrial and scientific.

In terms of biomedical applications, artificial muscle fibers offer the possibility of significant advances in biocompatible prosthetics and orthotics. In the field of prosthetic design, AMF actuators could open the door to more realistic artificial limb segments and digits. Enhanced realism would be apparent in appearance, performance and control. If the application was some form of muscle atrophy, AMFs could also have a role in orthotics development. Sleeves of artificial muscle could be fitted around the joints of paraplegics to create new types of orthotic devices. Better yet, truly bionic gloves could enhance grip. The AMFs could also be useful in controlling tremor in Parkinson's disease. The fact that they would operate silently would be another advantage.

In industrial applications, the criteria for the design of AMFs are significantly more relaxed. For instance, heat dissipation and power requirements are generally not as

stringent as in most biomedical situations. However, greater overall strength or higher frequency responses may be required. In comparison to the biomedical and scientific areas, industrial uses of AMF technology would likely be characterized by a greater variety of design specifications and less adherence to biologically imposed constraints. A look at some of the anticipated industrial uses should convince the reader of this fact.

First, artificial muscle fibers would constitute a significantly new and different type of actuation system for robots. The system would be able to be based on population-coded control strategies capable of controlling joint stiffness as well as load capacity. Adaptive control could be enhanced over present-day approaches, and weight, size, shape and noise criteria could also favour AMFs in certain situations. Already, North American companies are forming based on these prospects and ideas. It is anticipated that such AMF-actuated robots will find uses in such diverse fields as entertainment, space exploration, hazardous duties, and harsh environments. With behaviours resembling those of natural muscles, they could be used to construct the latest in special effects for the movie industry. Tailored appropriately, their unique characteristics of fidelity, control, low weight and low power input could be a boon to space robotics, telescience and haptic interfaces. For similar tasks, AMFs could also find a role in robotics as applied to remote hazardous duties here on Earth such as in waste disposal, mining, military duty, and undersea construction (Ayers et al. 2000, Wilbur et al. 2001).

The last area of application, scientific, has a great deal in common with the biomedical perspective. That is, while the success of AMFs in prosthetics will depend significantly on the fidelity of natural muscle emulation, the scientific benefits of AMFs will rely almost entirely on this factor. Imagine having an artificial muscle constructed of

artificial muscle fibers. If the AMFs behaved in a manner similar to their natural counterparts, and if the fibers were integrated together into a muscle in a manner congruent to real muscle, a researcher would have a truly exciting tool of scientific discovery at hand. At a time when molecular biology is the fashion, it is discouraging that we have not yet thoroughly defined how the brain controls muscle fibers within the context of functional movement. Comprehensive observations of necessary variables are difficult, if not impossible, in intact higher animals. Computer simulations are valuable but their validity is sometimes questionable due to their many degrees of freedom and the difficulty in verifying results. A physical simulation, based on AMFs in the context of a complete neuromusculoskeletal system, could bridge the gap. Researchers could experiment with different control strategies for coordination of muscle fiber recruitment and firing. They could use computers to generate stimulation patterns based on the simulated behaviour of hypothetical spinal circuits. A logical extension of this line of research would be artificial intelligence experiments. The neuromuscular test-bed could be used as the motor component of a fully integrated artificial central nervous system.

As a final comment on goals and motivations for AMF research, one could rightly question why the emphasis here is on AMFs as opposed to artificial muscles. It would seem, after all, that a singular muscle might be easier to develop than a muscle fiber. Indeed, a great deal of recent research has been directed towards this goal (Shiga et al. 1989, Suzuki and Hirasaka 1993, Hirai et al. 1994). Certainly making efficient artificial muscles out of AMFs will be another level of challenging research and development even if a suitable AMF can be produced. So why pursue the fiber in the first place? The various reasons can be summarized in one statement: artificial muscles and AMFs allow

researchers and educators to do different things and to answer different types of questions, and I am more interested in what the AMFs can do and answer. All issues concerning motor units, such as the different force vectors that they create, would be irrelevant with monolithic artificial muscles. From a biorobotics perspective, one could argue that monolithic muscles would be more likely to succeed but by applying some of the criteria already mentioned to research that has already been performed in this area, it appears that smaller and modular may be better (or at least more efficient and robust) than bigger and singular, even in industrial applications.

So if one assumes that AMFs are worth pursuing and that natural muscle fibers are worth emulating, at least at a functional level, one would reasonably ask questions such as, how do natural muscle fibers perform mechanical work? More specifically, what are their modes and mechanisms, what drives the processes, and how might they be synthetically replicated? The next section will provide some answers to these questions.

1.2 Characteristics of Natural Muscle

To evaluate the functional similarity of a given artificial muscle fiber to that of a natural muscle fiber, one must be familiar with the characteristics of the natural muscle fiber. This section therefore describes natural muscle fibers, referring most often to the characteristics of striated mammalian skeletal muscle. There are certainly other types of natural muscle fibers with other characteristics. However, here we will concentrate on factors most relevant to mammalian neuromuscular systems since they are most applicable to our potential applications. They are also among the best and most thoroughly studied.

Although not the only way in which living things produce movement, muscles are surprisingly ubiquitous. They come in many forms and differ in many ways, but they all share a few fundamental principles. Chemical energy stored in various molecules is released and transformed into mechanical energy and heat. This behaviour is brought about by electrical stimulation that causes cation concentration changes in the solution surrounding the contractile proteins. The outcome is an efficient electrochemomechanical transformation of energy resulting in force production.

Conceptually, natural muscle fibers can be thought of as short, contractile, elastic pieces of fine yarn. On average, they are approximately 50 micrometers in diameter while they vary from 2 to more than 100 millimeters in length (Hunter and Lafontaine 1992, Woledge et al. 1985). Larger fibers are distinguished from smaller ones by their greater diameter and by the fact that they contract, relax, and fatigue more quickly than their thinner counterparts (Rothwell 1994). Larger fibers are also stronger.

The essential way in which muscles operate is by changing the nature (charge and shape) of complex polymers and by changing how those polymers interact with each other in response to electrical stimulation. Action potentials travel down motor neuron axons to specialized synapses that facilitate the depolarization of the muscle membrane. This initiates an action potential that spreads within the fibers into the myofibrils and initiates a cascade of events which result in a change in conformation of myosin protein projections as they interact with actin proteins. This change in conformation produces tensile forces between the actin and myosin chains which are then transferred through the super-structure of the isolated muscle cell to produce macro-scale contractions of up to 50% in length. The contractile forces in an intact muscle can be summed and controlled by virtue of which fibers get recruited (some are stronger and faster than others), in what order they get recruited (the size principle, Henneman et al. 1965), and how frequently they get recruited (briefly up to 200 Hz in human muscle (Rothwell 1994)). The success of the general design and its many variations is evidenced by its ubiquity in nature. The efficiency of these systems is also remarkable. In human muscle, efficiency levels can exceed 35% (Hunter and Lafontaine 1992). As molecular-scale machines, muscle fibrils are further organized at the cellular (muscle fiber), multi-cellular (motor unit) and tissue (muscle) scales. Each of these organizational levels provides different abilities and perspectives in the control of the macro-scale actuation.

The potential similarities with artificial systems lie in the management of the electrochemistry. The electrochemical process begins when the muscle fiber is stimulated to contract via the excitation of the alpha motor neuron that innervates it. The motor neuron sends an action potential (AP) down its axon to the motor end plate which

abuts the muscle fiber. The arrival of the action potential at the neuromuscular junction initiates a release of the neurotransmitter acetylcholine which in turn produces a local depolarization of the muscle fiber's membrane. This initiates an AP which spreads over the fiber's membrane and into invaginations (T-tubules) that penetrate the volume of the fiber. This penetration allows the AP to access the internal mechanisms of the muscle fiber which include cisternae (sarcoplasmic reticulum) that store calcium ions. When depolarized, these cisternae release their calcium, increasing the concentration of the cation in the regions of the contractile proteins, actin and myosin, that make up the thin (1-2 μm diameter) contractile elements of the muscle fibers called myofibrils. Troponin, attached to the actin chains, changes conformation in response to the increased levels of calcium. As troponin changes its conformation, it removes the blockage set up by another regulatory protein (tropomyosin) to expose binding sites for the heads of the myosin molecules to bind to. From the energy released in the transformation of ATP to ADP and P_i , it is believed that the myosin heads then pivot much like a sculler moves their oars. This power stroke of debated length (between 8 and 100 nm, Warshaw 1996) slides the actin chains past the myosin chains, contracting the fiber. The total force produced (on the order of grams) is a function of the number of cross-bridge interactions.

After a fraction of a second, the calcium is pumped back into the cisternae, the tropomyosin resumes its blockage of the myosin heads, and the cycle is ready to be repeated. From the time the action potential reaches the neuromuscular junction, it takes about 10 ms (Mannard and Stein 1974, Bawa and Stein 1976) before the muscle fiber begins to exert force and possibly shorten.

This is certainly a simplified view, but it does capture the major aspects of the sliding filament theory and of our current understanding of muscular contraction (McComas 1996, Rothwell 1994, Ghez 1991). Today, the sliding filament theory is largely accepted as fact except for the actual power stroke process which is still debated in certain quarters (Pollack 1990).

At the cellular level we can talk about the behaviour of the muscle fibers in slightly different terms. The first concept that is relevant is the twitch. A muscle fiber twitch is a smoothly graded rise and fall in the level of tension exerted by a fiber over time. A twitch occurs in response to the stimulating impulse from a motor neuron. If a series of impulses stimulates the muscle fiber, a series of twitches is elicited. If the impulses are close enough together in time, the resulting twitches begin to summate non-linearly. For instance, stimulation rates of at least 15 Hz are required to cause fast twitching human muscle fibers to begin summing (Brooks 1986). However, the extent to which such summation takes place is limited. For instance, if the stimulation frequency is sufficiently high (anywhere from 25-40 Hz, depending on the type of muscle fiber), the fiber will go into a tetanic state. In tetanus, a muscle fiber exhibits a relatively constant level of tension anywhere from 2-10 times the maximum twitch strength. Between tetanus and single twitch stimulation frequencies lies a complex range of sub-tetanic behaviours. At these frequencies, twitches summate but not to the extent that a relatively constant level of tension is created, as in tetanus. In the sub-tetanic range especially, irregular trains of stimulation can create highly non-linear response characteristics in the fibers. For instance, an extra stimulating impulse inserted into an otherwise perfectly regular impulse train can create an increased level of tension that will

last much longer than the decay constant of the fiber. Furthermore, such irregular stimulation patterns are more common than isolated twitches or tetanus in behaving animals. In intact human muscles, for instance, stimulation rates of fibers generally range from a low of 6-8 Hz to a high of 20-35 Hz (Rothwell 1994).

What this view of muscle physiology has not conveyed thus far is the breadth of differences between different muscle fibers. Constructed of many different molecular elements, every muscle fiber is slightly different in form and function. For example, different fiber types have different isoforms of myosin and troponin, as well as different T-tubule systems and mitochondrial densities (the source of ATP). Stronger, faster acting “fast twitch” fibers employ glycolysis for energy production, and they fatigue quickly. In cats, for example, fast twitch tension peaks within 10-50 ms and relaxes again in less than 100 ms. These fibers can sustain a high level of force production for only about 30 seconds before their tension generating performance drops off dramatically. However, they can generate greater forces (up to 5-10 times as great) than those of “slow twitch” fibers. These weaker and slower acting slow twitch fibers employ an oxidative metabolism that is fatigue resistant. They take longer to twitch i.e. up to 50-150 ms to peak, and up to 400 ms to relax. However, they can maintain their force output for more than an hour at tetanus. In general, increases and decreases in tension in fast twitch fibers are 2-4 times faster than in slow twitch fibers, and this is a function of the more highly optimized calcium release and reuptake systems in fast twitch muscle (Hochachka 1994).

These sorts of parameter values do vary between species, but the proportional differences between fast and slow twitch fibers are well maintained. In general, the “fastness” of muscle fibers is greater in smaller animals.

Because slow twitch fibers have greater rise and decay time constants, they reach tetanus at a lower stimulation frequency than do fast twitch fibers. Slow fibers also have a greater tetanus to twitch strength ratio as compared to fast twitch fibers (Brooks 1986). It is also worth noting that fast twitch fibers have a larger diameter than slow twitch fibers and they are activated in larger sized groups (motor units). However, slow fibers are recruited first in most functional situations. The net effect is that each incremental set of muscle fibers recruited into action is slightly more powerful than its predecessors. This provides for a smoothly graded increase in muscle force output with increased levels of fiber recruitment, until one considers fatigue, at least.

The reader should also be aware that fast fatigue-resistant fibers do exist. These fibers exhibit a combination of features of fast and slow twitch fibers, but for our purposes they only underline the fact that there usually exists significant parametric variability within any given population of natural fibers.

Fatigue certainly does vary by fiber type. It is thought to be manifested centrally, systemically and/or within the myofibril itself. Fatigue due to failure in neuromuscular transmission, although a primary factor in some diseases such as myasthenia gravis, is also an important contributor to so-called "high frequency fatigue" i.e. fatigue when muscles are stimulated at high frequencies. At the systems level, the activation of large numbers of muscle fibers in a muscle can lead to increased intramuscular pressures which allow the interstitial potassium ion concentrations to increase as blood flow is reduced. This affects the dynamics of the membrane depolarization. Also, the pH can be affected by the build-up of H^+ ions produced by the glycolytic reactions. Within the myofibril, there can also be a failure in the excitation-contraction system as the cisternae lose the

ability to cycle significant quantities of calcium (McComas 1996). Recovery comes from re-establishing initial concentration levels of the various electrolytes, and that is facilitated by the capillarization of the muscles (a benefit of endurance training).

Fatigue is an adaptive response to ongoing stimulation at a rate that cannot be sustained metabolically. There are also other types of adaptive responses that can take place in muscle fibers. One of them is the training effect. As an example, low numbers of high intensity contractions can bring about an adaptive response that results in an increase in the number of myofilaments per muscle fiber, and a concomitant increase in strength. Endurance training, on the other hand, leads to adaptive responses that increase the energy stores of the muscle cells, reducing the chances that these cells will get into a fatigued state (McComas 1996).

Muscle fibers exhibit other non-linear qualities. For example, fast twitch and slow twitch fibers differ in their response to trains of action potentials although they both act as low pass filters to their motor neuronal stimulus trains. In both cases, they can be very sensitive to irregular stimulation patterns. An initial doublet of stimulation produces a non-linear enhancement of the contraction force. This “catch-like” non-linearity, better known in molluscs, has also been seen in cats (Zajac and Young 1975), and these are not the only non-linearities of the muscle fiber system. After a fiber has been held in tetanus, a subsequent twitch response within a few seconds is heightened. This is called post-tetanic potentiation and there are various theories as to its origin (Moore and Stull 1984, Allen et al. 1989). Likewise, one can observe a progressive increase in the isometric twitch response when a fiber is stimulated at low frequencies e.g. 2 Hz (Slomíc et al. 1968). In addition, twitch and tetanus contractions are sensitive to temperature and to the

length of the muscle fiber pre-stimulation (Rack and Westbury 1969, Stein et al. 1982). All of these examples show that stimulation history is important in natural muscle, and that we cannot fully characterize what will happen in the present without knowing what has occurred in the recent past. If we are trying to make AMFs that behave like natural muscle, then we need to appreciate these sorts of responses and account for them as best we can.

There are at least two other major non-linear factors in the active tension generation capabilities of natural muscle fibers. The first is a length dependent factor. That is, the amount of tension a fiber can produce varies with its current length. At the intact muscle level, over the physiological range of a muscle's length, tetanic tension levels can vary dramatically. They can be very low at the shortest length of the muscle i.e. less than 10% of the strength at a more ideal/stretched length. As muscle length increases, contractile force increases in a parabolic fashion. The peak of this curve is reached just before the maximum length of the muscle is reached. A slight dip in total tension is noted at the extreme (stretched) end of the muscle's length, even including what are by then significant levels of passive tension (Ghez 1991). Exactly how any single muscle fiber behaves in this context is undetermined, but like the muscle as a whole, the constituent contractile elements of a fiber (the sarcomeres) are known to have a certain length at which they begin to generate tension. Tension then increases with increasing sarcomere length to peak at a point corresponding to 100-120% of a resting sarcomere's length. After this point, as the fiber and sarcomere continue to lengthen, the tension falls gradually to zero.

The second major non-linear factor in active tension generation is a dependency on the rate of change of length of the fiber. This relationship was established by A.V. Hill in the late 1930s (Hill 1938). Essentially, he discovered that if a muscle is shortening when it is stimulated, the actively generated tension will be reduced on a roughly exponential curve that is graded by the rate of shortening. The curve is scaled in magnitude by the activation level of the muscle. Later work examined the other side of the graph. There, it was found that if a muscle is lengthening when it is stimulated, the strength of the response will be enhanced. This effect also varies with the rate of lengthening (Brooks 1986).

Other important features of muscle fibers include their frequency response characteristics. As a generalization, we can say that muscle fibers act as low pass filters (LPFs) to their neural input. The action potential and calcium release in the muscle fiber takes place over the space of a few milliseconds. The twitch tension response of the fiber, on the other hand, lasts anywhere from 50 to several hundred milliseconds, depending on the type of muscle involved. Once the stimulation frequency reaches a certain critical level (the cut-off frequency), the range of contraction will start to decrease rapidly as the fiber will not have had enough time to fully relax before the next stimulus is received. In 1976, Aaron et al. showed that the cut-off frequency for unloaded human biceps muscle was approximately 2.3 Hz under isometric conditions, and slightly less under load. Bawa et al. (1976) found similar values for plantaris muscle. Partridge (1966) first demonstrated the LPF qualities of muscle fibers when he sinusoidally modulated the frequency of a stimulus train to a muscle fiber. At low modulation frequencies (e.g. 16 Hz), the fibers faithfully varied tension in a sinusoidal fashion, albeit

with a slight phase lag. At higher modulations (e.g. 1.6 Hz), the fluctuations in tension were reduced, and by a frequency modulation of 4 Hz there was almost no variation in tension at all. He also showed that the fibers exhibit a phase lag which increases with stimulation rate.

The fact that fast and slow twitch fibers contract and fatigue at different speeds does affect their frequency response characteristics. However, so do the pre-stimulation fiber lengths in any frequency response evaluation (Mannard and Stein, 1973). Clearly, natural muscle fibers behave in complex ways. Therefore, it would be of great scientific and practical interest to create equivalent functional differences in AMFs. Such an accomplishment would open the door to using more naturally inspired motor control strategies in controlling AMFs, leading to a greater understanding of those strategies.

Hopefully this collection of behaviours that natural muscle exhibits has convinced the reader that muscle is a very complex system, and that there are good reasons why it has proven difficult to emulate. However, there is quite a bit more to it. If we look at some of the more mechanical qualities, including work, strain and force production, we can learn more about relevant qualities of muscle. For instance, isolated muscle fibers can contract by over 50% when stimulated, and by over 10% within the context of actual limb movements. Hunter and Lafontaine (1992) add that the maximum strain rate is approximately 300% per second. The mass density of muscle is almost exactly 1000 kg/m³ (Hunter and Lafontaine 1992, Woledge et al. 1985). The peak static tensile stress developed by vertebrate skeletal muscle is about 350 kPa, although the maximum sustainable stress level is closer to 100 kPa. Power density varies between 50 and 200 W/kg in humans. The high end of this range is reached only transiently, and only in

certain muscles. Overall energy efficiency levels can exceed 35% although values of 20-25% are more typical, in line with modern combustion engines. Such power and efficiency levels are one of the reasons that functional electrical stimulation (FES) is so attractive in comparison to most other orthotic technologies. It has been estimated that implanted FES power gains are on the order of 200,000 since they take advantage of the efficient “in-house” neuromuscular actuators (Kralj and Grobelnik 1973). In terms of cycling endurance, a useful high-end benchmark is the standard set by an average person’s heart. It will beat approximately 3×10^9 times during their life, equal to about 75 years at 75 bpm.

Hunter and Lafontaine (1992) discuss all of these findings, as well as others such as the importance of stiffness in natural muscle, in their comparative study of natural muscle versus various actuator technologies. Muscle stiffness varies with actively generated tension, increasing by a factor of five as tension increases from rest to the peak reached during a single twitch. Research also indicates that this variability in stiffness could be as high as a factor of 10 with respect to tetanus. Other related points include the fact that human muscle has an intrinsic stiffness on the order of 60 MN/m^2 , that stiffness varies inversely with temperature (Woledge et al. 1985), and that stiffness exhibits hysteresis with respect to muscle contraction and relaxation.

In addition to actively generated tension, muscle fibers also exhibit passive tensile characteristics. The strength of the passively produced tension can be as much as 15% of the actively generated tension within the physiological length range of a given muscle (Brooks 1986). Passive tension starts to make a contribution to overall muscle tension at about the half-way point in a muscle’s physiological length range. This contribution rises

in a roughly exponential manner up to the end of the physiological range (Ghez 1991). Note, however, that the level of passive elastic force is higher, per unit of cross-sectional area, in whole muscles than in single fibers due to the effects of connective tissue in muscle (Woledge et al. 1985).

Finally, while difficult to measure, there do exist some evaluations reflecting the thermal dissipative characteristics of muscle. In experiments with frog fibers stimulated at tetanus, thermal output has been found to range from a high of 40 down to a steady state of 14 W/kg. However, the range of thermal dissipation values gathered before, during and after various stimulation routines is broad, and the range between species is even broader. Values spanning a range of 0.35 W/kg for tortoises to 134 W/kg for rat fast twitch fibers have been collected. In general though, the slow twitch steady state levels tend to be approximately 1/6 of those of fast twitch fibers (Woledge et al. 1985).

Clearly, natural muscle fibers are amazing pieces of machinery. It is therefore not surprising that they have proliferated in life-forms over the past 500 million years here on Earth. Given the success of the design, it is also not terribly surprising that their artificial reproduction has proven to be so challenging. If our design goal is to produce AMFs as similar as possible in function to natural muscle fibers, then many suitable performance criteria should now be apparent. A list of such criteria is shown in Table 1-1.

These criteria and constraints include many of the important parameters of natural muscle fibers. Such key factors include fiber size and shape, mass density, durability, stimulation mode, stimulation response time, stiffness, twitch and tetanus strength, length and rate of change of length stress production dependencies, tensile strength, strain, parametric variation, fatigue, strain rate/frequency response, heat dissipation/endurance,

power output, power consumption and efficiency. However, they also include other factors such as cost, manufacturability, safety, sound, and smell that aren't generally important issues in nature, per se.

Table 1-1 AMF Performance Criteria

Shape	2 mm to 100 mm long fiber
Density	$\leq 1500 \text{ kg/m}^3$
Functional Durability	$\geq 10^5$ cycles
Stimulation Mode	electrical, pulsatile, low voltage, low current
Stimulation Reaction Time	$\leq 250 \text{ ms}$
Time to Twitch Peak Tension	scaleable 10-100 ms post-stimulation
Tetanus vs. Twitch Tension	greater force output in tetanus, ideally 2-10x
Shortening Behaviour	active tension decreases
Lengthening Behaviour	active tension increases
Maximum Contractile Stress	ideally scaleable, 50-400 kPa
Stiffness	ideally 60 MPa but variable wrt stimulation
Strain	ideally scaleable, 15-50%
Strain Rate	ideally scaleable, 100-300% per second
Functional Variability	scaleable slow/fast & strong/weak variations
Fatigue	some versions "tire" rapidly, others don't
Frequency Response	$\geq 2 \text{ Hz}$
Thermal Output	$\leq 135 \text{ W/kg}$
Thermal Endurance	functions in 0 to +35°C environments
Work Efficiency (output/input)	$\geq 25\%$
Cost	minimize
Safety	ideally biocompatible, no high V, I, toxins
Power Density	ideally scaleable, 50-200 W/kg
Energy Density	$\geq 0.8 \text{ kJ/m}^3$
Sound/Smell	quiet/odourless

The size and shape criteria help ensure that AMFs will be usable where natural muscle fibers are found, using similar control strategies and familiar structural arrangements. The mass density is also important since too heavy an actuator will require too much power and may cause problems at the interface between a prosthetic/orthotic and the user. It is not anticipated that excessive lightness will be a problem, however. Many polymers, for instance, are in the range of 1000-1500 kg/m³.

Durability is important in the sense that muscle fibers are not considered practically replaceable and yet they are called upon to be working almost continuously at varying rates of intensity. Cycling 10⁵ times would at least show credible potential for durability on the order of months. Another aspect of durability concerns damage resistance. If an AMF is very sensitive to touch, let alone impact, it will be of very limited use. This could be a question of packaging, but such protection would also increase weight and complexity and could complicate thermal control.

In and of itself, stimulation mode is not that important. However, it has strong interactions with other variables. In terms of exercising practical and rapid control with low overhead in terms of weight, complexity, volume and power, there are really no feasible alternatives to electric stimulation. As for stimulation reaction time, it is necessary that the reaction time be rapid if the muscles are to be of any functional use.

Concern over the time it takes to reach peak tension during a fiber twitch stems from the same source as the concern over stimulation reaction time. If the force producing response is not rapid enough then the actuator becomes behaviorally ineffective for anything but the slowest movements. This factor ties in tightly with frequency response as well as tetanus. One of the key features of natural muscle is the

tetanus response. Failure to replicate this at some level would change the nature of the artificial neuromuscular system entirely. Likewise for frequency response. Too slow a response and the muscles would be functionally unresponsive to the environment. As a final related consideration, the characteristic changes in force producing behaviour during muscle shortening and lengthening may also be quite important physiologically. These features might not be too important in industrial applications, but they would more likely be so for biomedical and educational applications.

Active tensile strength is, of course, a vital factor under both isotonic and isometric conditions. Without it, a fiber that is too weak will not be used. On the other hand, a fiber that is extremely strong will likely involve some tradeoffs in terms of energy input or heat dissipation. This again may be more acceptable in industrial applications but here we shall aim at the middle ground. A related factor is stiffness. At different levels of stimulation, an AMF should exhibit changing levels of stiffness as this may be one of the most important and yet under-appreciated aspects of muscle fiber physiology (Hunter and Lafontaine 1992). Also related to tensile strength (or more specifically tensile stress) through stiffness, is strain and strain rate. These factors are also vital to success. Without significant levels of strain and high supporting strain rates, either no significant movement will take place or movement will once again be too slow.

Functional variability is also important if AMFs are to replicate the range of natural behaviour. Variation in muscle fiber strength and endurance (fatigue) is part and parcel of how muscle control is exercised. The orderly recruitment of muscle fibers is based upon it. The variation also allows for optimization of control fidelity, and fatigue can clearly be considered adaptive. It automatically brings about a cessation of activity

that is increasingly damaging to the organism. Such an adaptive trait of AMFs, if it was necessary, would be highly desirable.

Thermal control is also included as both a specific safety factor and as a sink of wasted resources for cooling. Very hot materials and processes would be dangerous to users in many applications and would require active cooling systems of some sort. Given the natural need for such systems, it may not be totally avoidable in artificial systems but at some point it becomes counterproductive. In a related vein, power consumption also ranks up with strength as a variable determining success. Excessive power requirements eliminate portability and reduce efficiency. Efficiency is a bellwether indicator as it relates energy input and output, both important variables in their own right.

Another thermal consideration is the temperature range in which a given AMF can function. To be practical, a given prosthetic/orthotic system would have to be able to function over a range of 0°C to + 35°C, at a minimum. This could be ensured by enclosing the fibers within other structures and/or fluid media. However, extra thermal management could also be costly, complex and heavy.

Finally, there is the issue of cost. If a given approach is too expensive, it will not be used in practice. Similar non-natural concerns include basic safety where safety implies an absence of toxic substances, high voltages or currents, exposed hot surfaces, and/or uncontrolled behaviours. On more aesthetic grounds, AMFs feasible for use on or within humans would have to be relatively quiet and odourless, if not absolutely so.

If all of these performance criteria were met, we would have an artificial muscle fiber that would be potentially very useful. Our next step therefore, is to take a close look at the material that we will use to hopefully make such a device.

1.3 A Polypyrrole Primer

There are many ways in which an AMF can be potentially fabricated (see Hunter and Lafontaine 1992). Since similitude with natural muscle fibers is a key objective of the author, polymers were selected as the way in which to proceed. Hunter and Lafontaine's comparative study also suggested that they had good potential. In comparison, shape memory alloys (SMAs) had significant heat dissipation problems, piezoelectric actuators produced very small strains at high voltages, and electrostatic and electrostrictive devices also needed large voltages/voltage fields.

Narrowing the field to polymers did not restrict the choices that much, however. There are piezopolymers (Zentel and Brehmer 1995) and electrostrictive polymers (Pelrine et al 2000), for instance. In the end, several polymer systems were examined closely including PVA/PAA copolymers (e.g. Caldwell and Taylor 1990) and temperature sensitive proteins (Urry 1993). However, in the end, polypyrrole was adopted as the material of choice primarily on the basis of some exciting work reported by Smela et al. (1995a). Their self-folding micro-boxes provided a powerful example of the potential that PPy(DBS) has in the field of actuation. As a conducting polymer, polypyrrole (PPy) has the desirable feature of changing dimensions and therefore volume, under low voltage stimulation (e.g. Smela 1999). As such, it may be a suitable material for fabricating artificial muscle fibers (AMFs) and other types of soft, linear actuators.

PPy consists of 5-membered heterocyclic rings, and is one member of the growing family of conducting polymers. When polymerized in bulk through electrochemical deposition, it is an oxidized, doped, stable and amorphous thin film that

exhibits high levels of conductivity. Reducing the conductive PPy to a neutral conjugated form renders it significantly less conductive (semi-conductive or insulative).

Conductive polymers such as PPy undergo dimensional changes of 0.5-10% due to alternating reduction and oxidation, or doping and dedoping. Doping, in polypyrrole's case, can be defined as the introduction of positive mobile charge carriers due to oxidative processes (Reynolds 1988). Dedoping, achieved through reductive processes, results in the loss of such carriers. The application of such oxidative and reductive processes can be controlled using electric potentials. When such alternating doping and dedoping takes place, ions can be driven in and/or out of the polymer from the surrounding electrolyte solution as a result of electroneutrality constraints within the polymer. This is what brings about the volume changes. Whether doping corresponds to expansion or to contraction depends on the electrolytes used during polymerization and activation. In our case, with PPy(DBS), DBS was the anion and sodium was the cation. Since DBS is so large and bulky, it generally gets trapped in the polymer matrix during polymerization. That forces sodium to become the mobile charge compensating agent.

In any event, during doping and dedoping, removing and adding electrons from the conjugated chains changes the electron density of the chains as well as their carbon-carbon bond lengths. At low levels of doping, the charges on the PPy chains are stored in cationic polarons, or single unit charge entities. These paramagnetic polarons are radical ions delocalized over a region of the polymer backbone generally 3-4 rings long. They possess spin and a positive charge, and they can move along the polymer chain as carbon bonds reorganize themselves. At higher doping levels, charge can also be stored as a spinless, dicationic bipolaron if a polaron further oxidizes or if two polarons diffuse

together (Reynolds 1988). One of the most appealing characteristics of conducting polymers is the low voltage stimulation required to bring about these changes. One of the least appealing characteristics is that response times to stimulation can be slow. However, with thoughtful selection of monomer, dopant and deposition conditions, this problem can be substantially mitigated as it has been with PPy(DBS).

At first glance, a comparison between the ways in which PPy and natural muscle fibers contract may not seem instructive. The mechanisms appear to be quite different. With conducting polymers such as PPy, electric energy is not just used as a signal to initiate a process that ends in contraction. Rather, it drives the process by promoting charge transport in the active polymer layer, causing conformational and macroscopic volume change. However, in both PPy and natural muscle, a change in internal cation concentration is critical. With natural muscle fibers, the processes are more intricate. Thus, if work with conducting polymers makes anything clear, it is the miraculous nature of the machinery in natural muscles.

Like other conducting polymers, PPy is an extended π -conjugated polymer system, meaning that it possesses alternating single/double carbon bonds along the polymer chain. It is the conjugated nature of these polymers that allows electrons to move along the chain, facilitating high levels of electrical conductivity. As a consequence of being conjugated, these polymers are dopable and as the films are electrochemically oxidized and/or reduced to produce varying mechanical and electrical properties they take in or expel ions to balance the net charge in the polymer. For instance, since PPy is polymerized in an oxidized state with a shortage of electrons along the chain, it draws in negative anions such as DBS from the surrounding electrolyte

during polymerization. Thus the doped polymer is actually a salt with negatively charged ions interspersed throughout its structure. This incorporation of the anionic counterions into the polymer balances the net charge in the polymer without dramatically damaging conductivity characteristics by interfering with along-chain and/or band-hopping conduction. Indeed, aromatic anions actually enhance conductivity likely due to enhanced band-hopping. Oxidized polymers are often called p-type or p-doped conductors i.e. positive charge carriers, missing electrons. N-type or n-doped conductors are negative charge carriers. Most conjugated polymers are p-doped. In fact, PPy can only be a p-doped conductor or a neutral/insulating semi-conductor in reduced form.

PPy is also often referred to as a self-doped polymer, although technically this depends on the electrolyte used during deposition. Self-doping systems involve an electrochemically inert dopant anion which becomes covalently bound to the conjugated polymer chain during synthesis (Reynolds 1988). This can lead to ion-specific charge transport properties. The bound anion is the polymer's dopant ion and it can give the polymer certain ionic or polyelectrolytic properties. Whether the anion dopant is trapped by virtue of covalent bonding (self-doping) or by virtue of its large size, PPy can carry out charge transport during oxidation and reduction via the expulsion and/or insertion of cations. Since the anions are always bound/trapped in the PPy they will always be ready to be the counterions to the mobile cations. Since only the cations are mobile in this situation, ion specific transport can be achieved.

In terms of its other salient features, pyrrole exhibits a relatively low oxidation potential and as a result does not require strong oxidants or high potentials to polymerize. PPy can be manufactured to reach conductivity levels of 100-1000 S/cm or more. In

other words, PPy can exhibit conductivity levels similar to those of metals. It can also be heated to 200°C without significantly degrading its electrical characteristics. In terms of its appearance, doped PPy tends to have a dark and opaque blue/black colour while dedoped/undoped PPy film tends to have a yellow/green colour and is transparent. Thus, PPy has the potential to be used in electrochromic displays.

If one wants to use PPy as the active material in an AMF, the first question that might arise is “how does one produce polypyrrole?” The first step in working with polypyrrole is polymerizing the monomer, and this process is as much a black art as it is a science. Most of the physical properties of conducting polymers are established during their polymerization. In other words, the polymerization step is very important.

Many details of the electropolymerization process can influence the characteristics of the resulting PPy film. For instance, it can be electrodeposited/polymerized in aqueous or organic solvents in conjunction with a variety of electrolytes. It can be sensitive to temperature, electrode size, voltage and current, and it can be altered by certain processes both before and after the actual polymerization process.

The electropolymerization of heterocycles such as pyrrole takes place in an electrochemical cell containing two or three electrodes. Polymerization takes place at the working electrode/anode where oxidation occurs. Often, the resulting film can then be peeled off of the anode at the end of the deposition process. In situations such as ours, where bending beams are being produced using PPy, the goal is to not have the film delaminate off of the electrode.

In order for the electropolymerization to take place, there must be a suitable electrolyte present in the monomer/deposition solution before the oxidation can occur.

One must use a solvent in which the monomer is soluble but the oligomer is not (the polymer is not soluble in any solvent). Given these conditions, oligomers will precipitate out of solution onto the electrode/anode to form polymer. Therefore, the film will get thicker with deposition time.

Conducting polymers such as polypyrrole generally polymerize according to the following process: $4n \text{ C}_4\text{H}_4\text{NH} + n\text{A}^- \Rightarrow [(\text{C}_4\text{H}_2\text{NH})_4\cdot\text{A}^-]_n + 8n \text{ H}^+ + 9ne^-$. This is shown graphically in Figure 1-1. However, this is really too simple a representation for our purposes. The situation is better described by Figure 1-2. The polymerization is actually an E(CE)_n process where monomer oxidation is an electrochemical process (E), radical-radical coupling is a chemical process (C) and chain propagation is another electrochemical process (E) (John and Wallace 1991). The first step involves electrochemical oxidation of the monomer such that it becomes a delocalized radical cation. This cation has the highest spin density at the alpha position. In other words, the third resonance form shown in Figure 1-2 is the most stable. The second step is dimerization of the monomer radicals via radical-radical coupling at the alpha positions. This coupling is then followed by expulsion of two H⁺ ions, leaving a neutral dimer. The driving force for this step is the return to aromaticity. The last step, chain propagation, proceeds via oxidation of the neutral dimer to form a dimer radical which combines chemically with other monomeric, dimeric or oligomeric radicals to extend the chain. These last two processes are repeated indefinitely until chain growth is terminated by an "undesirable" reaction. Indeed, PPy is rarely an easy material to polymerize. As many as 30% of the CC links between rings are not of the desired 2,5 type that yield linear chains. Many form as 2,3 links, which are considered to be chain defects. They lower the bulk

Figure 1-1 The oxidative polymerization process that converts pyrrole into polypyrrole.

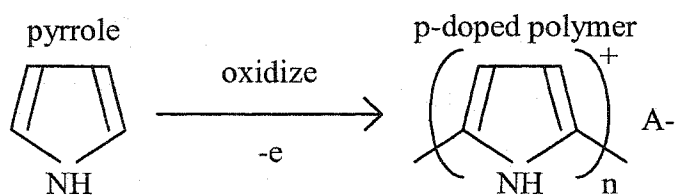
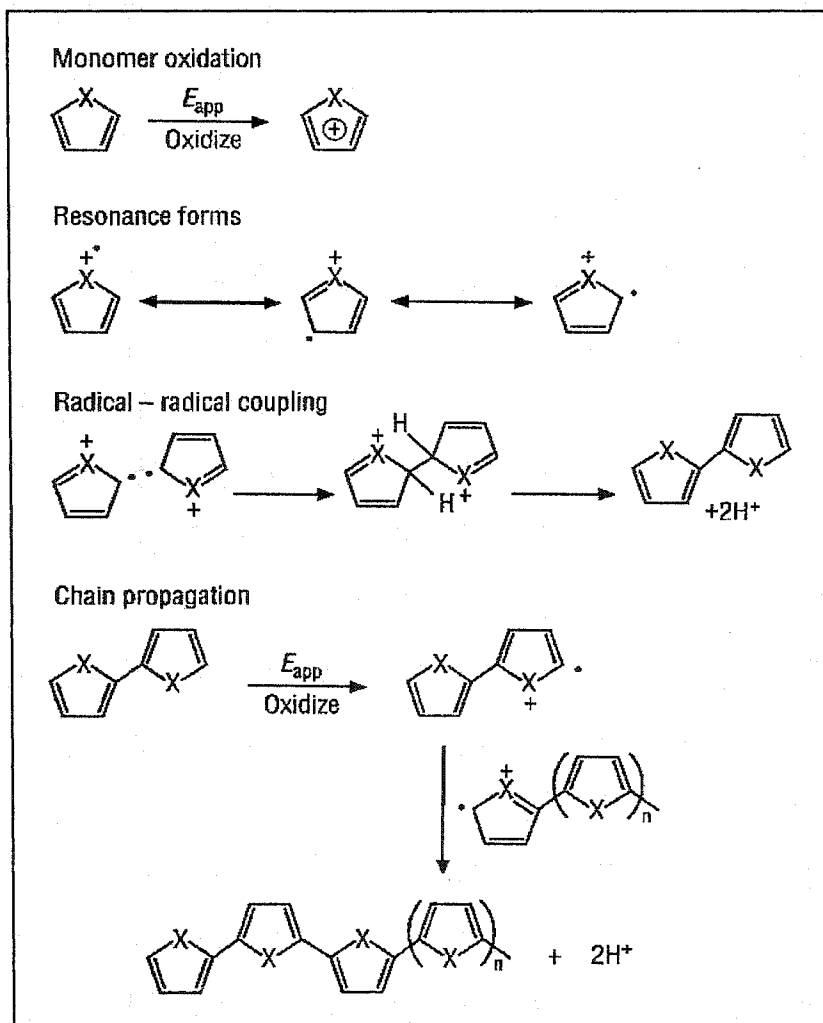


Figure 1-2 A more complex version of the oxidative polymerization process that converts pyrrole into polypyrrole. The figure illustrates polypyrrole chain propagation (Imisides et al. 1996).



conductivity of the PPy sample and they contribute to PPy's amorphous nature. Cross-linking between chains also influences film morphology.

It used to be believed that neutral monomers were adsorbed onto the electrode surface prior to oxidation. However, John and Wallace (1991) found that PPy growth was primarily the result of continual precipitation of oligomeric intermediates from solution rather than from the sequential addition of monomers onto the ends of existing polymer chains. Diffusive transport of these intermediates away from the electrode can explain coulombic inefficiencies during polymerization.

As such, the choice of solvent has been found to be important. According to Imisides et al. (1996), the nucleophilic nature of water as opposed to that of organic solvents such as acetonitrile (ACN), interferes with the radical-radical coupling step and slows the whole process down. John and Wallace (1991) found that minimum pyrrole concentrations required for growth on microelectrodes were always greater in aqueous solutions compared to ACN solutions. This was attributed to any or all of i) the diffusion rate of oligomers away from electrodes is greater in water, ii) the solubility of oligomers is greater in water thus requiring a greater chain length before precipitation, and iii) the nucleophilic nature of water may interfere with radical intermediates. The dependence on diffusion was confirmed by stirring deposition solutions. This inhibited deposition.

With regards to the three-dimensional growth of PPy, a characteristic deposition plot is shown in Figure 1-3. Typically, with a step in potential, an initial capacitive spike in current is noted (the double-layer charging effect) followed by a smooth and rapid drop-off. This is followed by a sigmoidal rise in current to a fairly stable plateau value. The sigmoid is shorter and steeper with higher potentials. It is likely that nucleation is

Figure 1-3 A representation of a standard deposition plot (current versus time). Characteristic features of this amperogram include the initial peak, the smooth drop-off to a plateau and the subsequent recovery to a higher plateau. These features likely correspond to double-layer charging, nucleation and polymer growth. The nature of the plot characteristics vary with deposition conditions.



taking place during the sigmoidal portion of the plot, since it appears that the size of the electroactive area is increasing (hence the increase in current). Higher potentials shorten/steepen the sigmoid i.e. they seem to accelerate the nucleation process. Once this nucleation process is complete, the current draw is fairly stable, suggesting one dimensional growth as if pyrrole oligomers were being added onto the ends of existing chains.

Two other general issues should also be noted at this point. The first is that as pyrrole polymerizes, hydrated counter/anions from solution are incorporated into the polymer to compensate for the positive charges on the polymer chains. The nature of this process plays a large part in determining the final electromechanical characteristics of the PPy. The second issue is crosslinking. During polymerization, crosslinking between PPy chains takes place, even at room temperature. As the temperature increases, the degree of crosslinking increases. This is generally an undesirable situation as it reduces overall conductivity and likely affects other physical characteristics as well.

Polypyrrole can be produced fairly easily in a modestly equipped chemical lab. However, as noted, the quality and physical properties of electrochemically deposited PPy films are strongly dependent upon deposition conditions such as the substrate, solvent, temperature, and nature of the electrolyte.

Standard equipment for PPy electrochemical depositions usually includes a potentiostat/galvanostat, a universal programmer/function generator, and an XY data recorder for dealing with cyclic voltammograms (CVs) and deposition plots. A digital coulomb meter is also often valuable and conductivity/resistivity is usually measured with a standard 4-point probe. The actual deposition process takes place inside an

electrochemical cell. Three electrodes are commonly used. The anode/working electrode is the electrode on which the pyrrole polymerizes, the counter electrode is the cathode, and there is usually a reference electrode, as there was in my work.

Counter electrodes (cathodes) are generally gold or platinum wire, plate or mesh, carbon rods, large copper foils or nickel. It is important that they be symmetrically aligned with the working electrode, inert, and of comparable or greater surface area. I used a piece of platinum foil without difficulty.

Working electrodes (anodes) come in many varieties. Examples in the literature include polished gold, gold-plated copper, stainless steel, platinum, indium tin oxide-coated glass, and vitreous carbon. I used metal-coated Mylar[®] and Kapton[®] strips for my working electrodes.

The most common reference electrodes used in PPy deposition cells are saturated calomel (SCE) and Ag/AgCl. Usually these are placed in the same cell as the working and counter electrodes using a standard 3-neck 100 ml electrochemical cell, for instance. I used an Ag/AgCl reference electrode in my experiments.

The concentrations of pyrrole monomer and electrolyte in the deposition solution play a crucial role in the qualities of resulting PPy films. In terms of the pyrrole monomer, as-received pyrrole is usually distilled before use, sometimes under nitrogen (Elliott et al. 1991), often twice freshly (John and Wallace 1991), and under reduced pressure or vacuum (Mitchell and Geri 1987, Otero et al. 1996). In addition, it is sometimes purged with nitrogen or argon just before use. For very sensitive and/or exacting experiments, it is used immediately after purification by distillation under reduced pressure (Nishizawa et al. 1991). For my application, this level of diligence was

not required. I did distill or otherwise purify the pyrrole, however. In terms of storing pyrrole and/or pyrrole solutions, it is important that the solutions be protected from light and oxygen as pyrrole is photoreactive and oligomerizes in light and warm conditions. In Edmonton, I aliquotted freshly distilled pyrrole and then froze it. The pyrrole was subsequently thawed and used immediately.

The use of freshly made pyrrole solution is important as well. Deionized water is always used in deposition solutions. I have noted, as have Warren and Anderson (1987), that aged aqueous solutions invariably produce poorer quality deposits. The oligomers tend to darken the solution from faintly yellow/clear to darker yellow/brown. Warren and Anderson suggest three hours as a useful lifetime for pyrrole solution used for thick film preparation, at room temperature. I certainly never exceeded this limit.

The two main choices for solvent in the deposition cell are acetonitrile (ACN, or CH_3CN) and water. Propylene and ethylene carbonate solutions are also used at times (Hasegawa et al. 1986, Slama and Tanguy 1989). While cheaper and easier to work with, water also has the attraction of solubilizing a greater variety of electrolytes such as inorganics, surfactants, and polymeric anions that come in water-soluble salts or free acids. However, the hydration of the films in water introduces asymmetries in the anodic and cathodic CV peaks whereas such significant asymmetries are not evident in ACN CVs (Warren and Anderson 1987). It is also worth noting that while PPy can be prepared in either ACN or in aqueous solutions, PPy is most often activated afterwards in aqueous solutions.

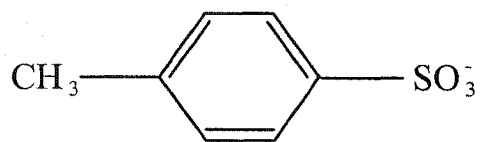
Choosing the appropriate electrolyte for the deposition solution is arguably one of the most important choices a researcher can make in polymerizing pyrrole, depending on

the objective of the polymerization. If mechanical activity is the goal, then the choice of electrolyte is very important. It affects range and velocity of movement, as well as film modulus and strength. Figure 1-4 shows some of the more common dopants, including the one that was used in this thesis work, dodecylbenzene sulfonate (DBS).

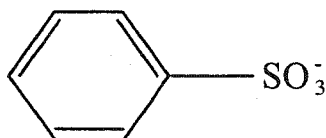
The temperature at which one deposits may also be a factor. Generally, most PPy is deposited at room temperature. However, some researchers deposit under other conditions. For instance, Hasegawa et al. (1986) and Ogasawara et al. (1986) deposited in propylene carbonate solutions at temperatures as low as -30°C . Ogasawara's group found that the lower the preparation temperature was, the higher the conductivity of the resulting film would be. Controlling temperature was not a feasible option for this work, but it is something that will be considered in future work (see Chapter 7). Among other things, the temperature likely affects the degree of cross-linking between polymer chains.

Yet another key factor in polymerization is the voltage and/or current setting. One commonly deposits either potentiostatically (constant controlled voltage) or galvanostatically (constant controlled current). Galvanostatic depositions generally make charge deposition calculations easier. Such depositions are described by stating a current level and/or current density, such as 1 mA/cm^2 . I found galvanostatic depositions to be more repeatable than potentiostatic, and they also allowed me to control film thickness more easily (as per Smela 1999). The interaction between deposition voltage (or current) and time is very predictable. The longer the deposition duration and the higher the current is, the thicker the film. Experimental deposition times range from a few seconds to hours. For a given experimental set-up, calibration tests using profilometers can be performed to ascertain relationships between deposition current density, deposition

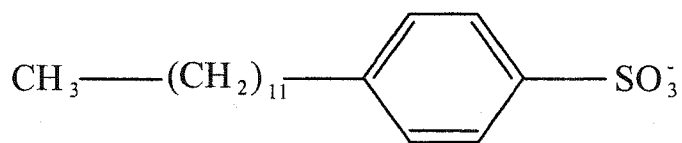
Figure 1-4 Examples of electrolyte dopants used in polypyrrole synthesis.



p-Toluenesulfonate



Benzenesulfonate



p-Dodecylbenzenesulfonate



Perchlorate

duration and film thickness. Monitoring deposited charge offers the easiest electrical measurement of deposition thickness.

Once polymerized, polypyrrole reacts in characteristic physical and chemical ways in response to moderate redox voltages in both ACN and aqueous solutions. With PPy(DBS), cations are expelled and inserted during oxidation and reduction, respectively. Figures 1-5 and 1-6 illustrate the process and the cyclic voltammogram, respectively, for a film being cycled (stimulated). In the thesis work, cycling took place over a range of approximately -1.1 V to +0.4 V. The peaks in the CV represent faradaic current, or the current resulting from the doping/dedoping and the movement of compensating cations.

When cations are the mobile component and anions are trapped in the polymer, then polarons and bipolarons are eliminated during reduction and simultaneously there are reduced repelling forces holding the chains apart. However, the negative anions are trapped in the polymer and since charge balance must be maintained, positive cations enter and the polymer expands. During oxidation when polarons and bipolarons are introduced, cations are expelled since the polarons/bipolarons are compensated by the trapped anions and the cations become excess mobile charges. They leave the matrix, and the polymer contracts. If this is all happening when the PPy(DBS) has been deposited on a beam of flexible substrate such as gold-coated Kapton[®], then the effect will be to bend the beam as happens in bimetal thermostats (Timoshenko 1925). Figure 1-7 illustrates both a cross-section of such a beam and how it bends and straightens.

In general, one uses the same electrochemical equipment during stimulation as one does during deposition. However, the electrical signals are often different and the electrolytic solutions can be somewhat more varied. As an example, Otero and

Figure 1-5 The doping/dedoping process that converts oxidized PPy into reduced PPy, and vice versa.

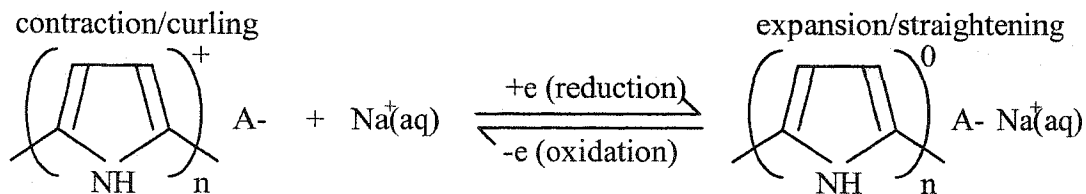


Figure 1-6 A sample cyclic voltammogram (CV) for PPy(DBS) cycled between -1.1 V and +0.4 V. Characteristic features include the oxidation peak (upper right) and the reduction peak (lower left).

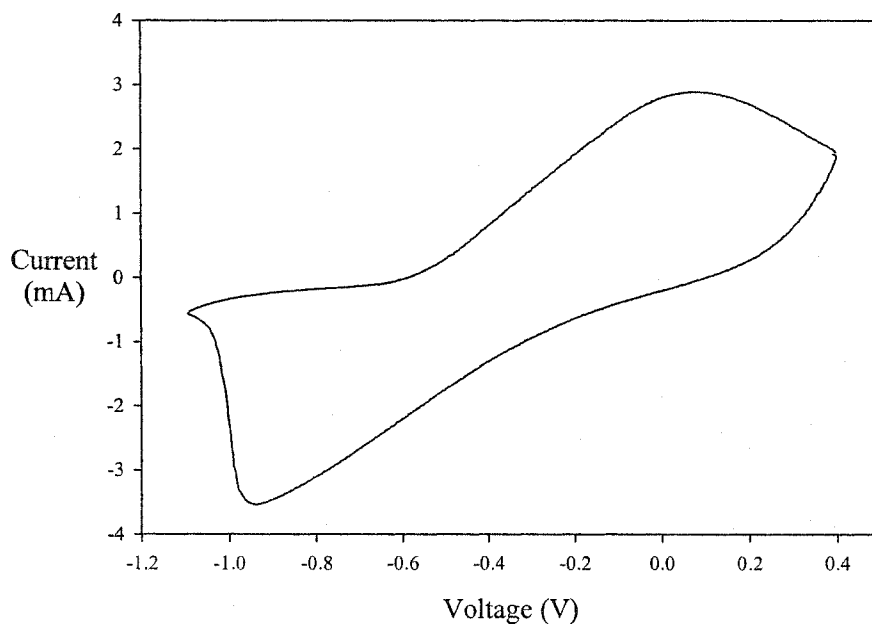
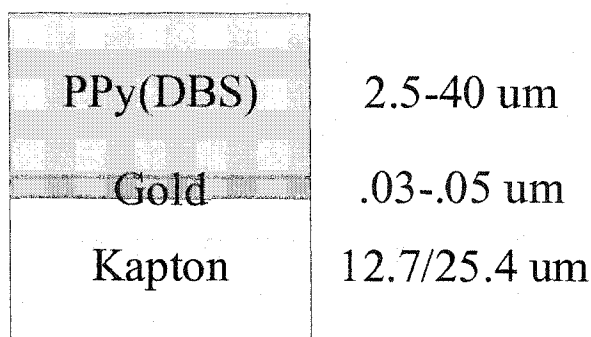
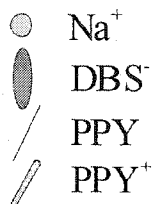
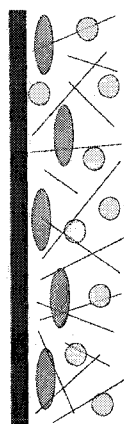


Figure 1-7 Top illustration shows a cross-section of a bending beam of the type used in this thesis. The PPy(DBS) layer is cycled through reduction and oxidation to expand and contract, respectively. This causes the beam to bend, as per the bottom illustration. During reduction the positive charges of the polymer are neutralized, leaving a net negative charge on the polymer due to the trapped DBS anions. Positive sodium cations move into the polymer to compensate, expanding the polymer. During oxidation the polymer is positively charged and it compensates for the anions itself. As a result, the mobile sodium cations leave the polymer matrix and the polymer contracts.

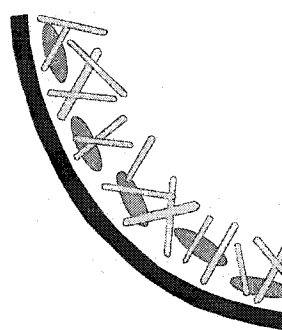
Beam Cross-section



Reduction



Oxidation



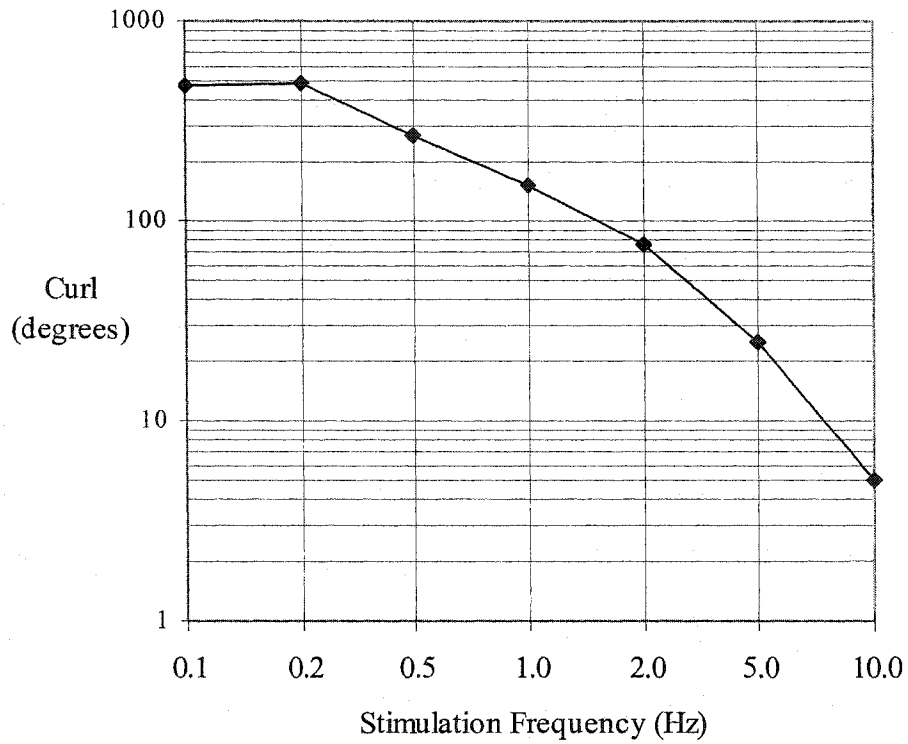
Rodríguez (1993) discuss using voltage sweeps and steps, current sweeps and steps, and combinations of these different stimulation modes. The most common method is the voltage sweep/scan. The parameters of this approach include the scan rate and the upper and lower scan limits. Essentially, the voltage applied to the PPy is ramped up and down at the set rate, between the set limits. To get true cyclic electromechanical activity in the PPy film it is necessary to “capture” the anodic and cathodic peaks when sweeping through the voltage range. The anodic/oxidation peak is in the upper right of a CV (see Figure 1-6, for example) while the cathodic/reduction peak is in the lower left of the CV. To capture the peaks one must set appropriate cycling limits, and they vary with cycling frequency, electrolyte concentration, temperature, etc.

One must also be careful to not use excessive voltages or currents, however, as at very high anodic potentials the excess driving force goes towards water oxidation and oxygen release. Indeed, the presence of oxygen bubbles on the working electrode indicates that the PPy is being destroyed. Water oxidation on a voltammogram appears as a rapid rise in current. Large cathodic potentials should be avoided as well, as hydrogen gas can be produced in those situations.

To conclude this section on polypyrrole, we finish with a figure that inspired hope for success early on in this thesis. In the early days of the thesis work, a bending beam was produced by the author when he was in training in Linköping, Sweden. PPy(DBS) was deposited on a backing of thick gold-coated Mylar[®]. When the PPy(DBS) was reduced and oxidized, it expanded and contracted causing the beam to straighten and curl, respectively. The beam was stimulated at a wide range of cycling frequencies and the range of movement of the beam (the curling angle) was subsequently analyzed. The

frequency response plot, shown in Figure 1-8, was one of the results. With a cut-off frequency of approximately 0.2 Hz, it offered inspiration to see the subsequent work through. In the following chapters, we will examine that work.

Figure 1-8 A frequency response plot for the curling behaviour of an early bending beam produced during training in Linköping, Sweden. PPy(DBS) was deposited on gold-coated Mylar[®]. Subsequent stimulation of the PPy(DBS) with NaDBS led to changes in volume in the PPy(DBS). That, in turn, led to curling of the beam. The amount of curl was measured in degrees by comparing tangents of the two ends of the beam.



1.4 References

Aaron, S.L. and Stein, R.B. (1976) "Comparison of an EMG-controlled prosthesis and the normal human biceps brachii muscle", *Am. J. Phys. Med.*, Vol. 55, #1, pg. 1-14

Allen, D.G., Lee, J.A., and Westerblad, H. (1989) "Intracellular calcium and tension during fatigue in isolated single muscle fibres from *Xenopus laevis*", *Journal of Physiology*, Vol. 415, pg. 433-58

Ayers, J., Witting, J., McGruer, N., Olcott, C., and Massa, D. (2000) "Lobster robots", In: **Proceedings of the International Symposium on Aqua Biomechanisms**, T. Wu and N. Kato [eds], Tokai University, Japan

Baughman, R.H., Shacklette, L.W., Elsenbaumer, R.L., Plichta, E.J., and Becht, C. (1991) "Micro electromechanical actuators based on conducting polymers", In: **Molecular Electronics**, P.I. Lazarev [ed], Kluwer Academic Publishers, pg 267-289

Bawa, P. and Stein, R.B. (1976) "The frequency response of human soleus muscle", *Journal of Neurophysiology*, Vol. 39, pg. 788-793

Bawa, P., Mannard, A., and Stein, R.B. (1976) "Effects of elastic loads on the contractions of cat muscles", *Biol. Cybernetics*, Vol. 22, pg. 129-137

Brooks, V.B. (1986) **The Neural Basis of Motor Control**, Oxford University Press

Caldwell, D.G. and Taylor, P.M. (1990) "Chemically stimulated pseudo-muscular actuation", *Int. J. Engng. Sci.*, Vol. 28, #8, pg. 797-808

Elliott, C.M., Kopelove, A.B., Albery, W.J., and Chen, Z. (1991) "Nonaqueous electrochemistry of polypyrrole/polystyrenesulfonate composite films: Voltammetric, coulometric, EPR and AC impedance studies", *J. Phys. Chem.*, Vol. 95, pg. 1743-1747

Ghez, C. (1991) "Chapter 36 - Muscles", In: **Principles of Neural Science, 3rd Ed.**, E.R. Kandel, J.H. Schwartz, and T.M. Jessell [eds], Appeltion & Lange, Norwalk, USA

Hasegawa, S., Kamiya, K., Tanaka, J., and Tanaka, M. (1986) "Far-infrared spectra and electronic structure of polypyrrole perchlorate", *Synthetic Metals*, Vol. 14, pg. 97-102

Henneman, E., Somjen, G., and Carpenter, D.O. (1965) "Functional significance of cell size in spinal motoneurons", *Journal of Neurophysiology*, Vol. 28, pg 560-80

Hill, A.V. (1938) "The heat of shortening and the dynamic constants of muscle", *Proc. Roy. Soc. (London)*, Vol. B126, pg. 136-195

Hirai, T., Nemoto, H., Hirai, N., and Hayashi, S. (1994) "Electrostriction of highly swollen polymer gel: possible application for gel actuator", *Journal of Applied Polymer Science*, Vol. 53, #1, July 5, pg. 79-84

Hochachka, Peter W. (1994) **Muscles as Molecular and Metabolic Machines**, CRC Press, USA

Hunter, I.W. and Lafontaine, S. (1992) "A comparison of muscle with artificial actuators", *IEEE Solid-State Sensors and Actuators Workshop Technical Digest*, June 21-25, Hilton Head Island, USA, pg. 178-85

Imisides, M.D., John, R., and Wallace, G.G. (1996) "Microsensors based on conducting polymers", *Chemtech*, May, pg. 19-25

John, R. and Wallace, G.G. (1991) "The use of microelectrodes to probe the electro-polymerization mechanism of heterocyclic conducting polymers", *Journal of Electroanalytical Chemistry*, Vol. 306, pg. 157-167

Kanatzidis, M.G. (1990) "Conductive Polymers", *C&EN*, December 3, pg. 36-54

Kralj, A. and Grobelnik, S. (1973) "Functional electrical stimulation - a new hope for paraplegic patients?", *Bulletin of Prosthetics Research*, Fall

Kuhn, W. (1949) "Artificial muscle model", *Experientia*, Vol. 5, #8, pg. 318-319

Mannard, A. and Stein, R.B. (1973) "Determination of the frequency response of isometric soleus muscle in the cat using random nerve stimulation", *J. Physiol. (London)*, Vol. 229, pg. 275-296

Mannard, A.C. and Stein, R.B. (1974) "Determination of the frequency response of isometric soleus muscle in the cat using random nerve stimulation", *Journal of Physiology*, Vol. 229, pg. 275-296

Maw, S. (1993) **A Spinal Arm-Control Circuitry Simulator (SpArCCS)**, M.A.Sc. Thesis, University of Waterloo, Canada

Maw, S., Frank, J., and Greig, G. (1996) "A spinal circuitry simulator as a teaching tool for neuromuscular physiology", *Advances in Physiology Education*, The American Physiological Society, Vol. 15, #1, June, pg. 50-68

McComas, A.J. (1996) **Skeletal Muscle: Form and Function**, Human Kinetics, USA

Mitchell, G.R. and Geri, A. (1987) "Molecular organisation of electrochemically prepared conducting polypyrrole films", *Journal of Physics D: Applied Physics*, Vol. 20, pg. 1346-1353

Moore, R.L. and Stull, J.T. (1984) "Myosin light chain phosphorylation in fast and slow skeletal muscles in situ", *American Journal of Physiology*, Vol. 247, pg. C462-471

- Nishizawa, M., Shibuya, M., Sawaguchi, T., Matsue, T., and Uchida, I. (1991) "Electrochemical preparation of ultrathin polypyrrole film at microarray electrodes", *Journal of Physical Chemistry*, Vol. 95, pg. 9042-9044
- Ogasawara, M., Funahashi, K., Demura, T., Hagiwara, T., and Iwata, K. (1986) "Enhancement of electrical conductivity of polypyrrole by stretching", *Synthetic Metals*, Vol. 14, pg. 61-69
- Otero, T.F. and Rodríguez, J. (1993) "Electrochemomechanical and electrochemo-positioning devices: artificial muscles", In: **Intrinsically Conducting Polymers: An Emerging Technology**, M. Aldissi [ed], Kluwer Academic Publishers, pg. 179-190
- Otero, T.F., Grande, H., and Rodríguez, J. (1996) "Reversible electrochemical reactions in conducting polymers: a molecular approach to artificial muscles", *Journal of Physical Organic Chemistry*, Vol. 9, pg. 381-386
- Partridge, L.D. (1966) "Signal-handling characteristics of load-moving skeletal muscle", *Am. J. Physiol.*, Vol. 210, pg. 1178-1191
- Pelrine, R.E., Kornbluh, R.D., and Joseph, J.P. (1998) "Electrostriction of polymer dielectrics with compliant electrodes as a means of actuation", *Sensors and Actuators - A Phys.*, Vol. 64, Issue 1, pg. 77-85
- Pollack, G.H. (1990) **Muscles and Molecules: Uncovering the Principles of Biological Motion**, Ebner and Sons, Seattle, WA, USA
- Rack, P.M.H. and Westbury, D.R. (1969) "The effects of length and stimulus rate on tension in the isometric cat soleus muscle", *J. Physiol.*, Vol. 204, pg. 443-460
- Reynolds, J.R. (1988) "Electrically conductive polymers", *Chemtech*, July, pg. 440-447

Rothwell, J. (1994) **Control of Human Voluntary Movement (2nd Ed.)**, Chapman & Hall, London

Shiga, T., Hirose, Y., Okada, A., and Kurauchi, T. (1989) "Bending of high strength polymer gel in an electric field", *Polymer Preprints*, Vol. 30, pg. 310-311

Slama, M. and Tanguy, J. (1989) "Influence of the electrolyte on the electrochemical doping process of polypyrrole", *Synthetic Metals*, Vol. 28, pg. C139-C144

Slomíc, A., Rosenfalck, A., and Buchthal, F. (1968) "Electrical and mechanical responses of normal and myasthenic muscle with particular reference to the staircase phenomenon", *Brain Research*, Vol. 10, pg. 1-78

Smela, E., Inganäs, O., and Lundström, I. (1995a) "Controlled folding of micrometer-size structures", *Science*, Vol. 268, June 23, pg. 1735-1738

Smela, E., Inganäs, O., and Lundström, I. (1995b) "Self-opening and closing boxes and other micromachined folding structures", *The 8th International Conference on Solid-State Sensors and Actuators, and Eurosensors IX*, Stockholm, Sweden, June, pg. 350-51

Smela, E. (1999) "Microfabrication of PPy microactuators and other conjugated polymer devices", *J. Micromech. Microeng.*, Vol. 9, pg. 1-18

Stein, R.B., Gordon, T., and Shriver, J. (1982) "Temperature dependence of mammalian muscle contractions and ATPase activities", *Biophys. J.*, November, pg. 97-107

Suzuki, M. and Hirasawa, O. (1993) "An approach to artificial muscle using polymer gels formed by micro-phase separation", In: **Vol 110 - Advances in Polymer Science (Responsive Gels: Volume Transitions II)**, pg. 241-261

Timoshenko, S. (1925) "Analysis of bi-metal thermostats", *J. Opt. Soc. Am.*, Vol. 11, pg. 233-256

Urry, D.W. (1993) "Molecular machines: how motion and other functions of living organisms can result from reversible chemical changes", *Angew. Chem. Int. Ed. Engl.*, Vol. 32, pg. 819-841

Warren, L.F. and Anderson, D.P. (1987) "Polypyrrole films from aqueous electrolytes", *Journal of the Electrochemical Society: Electrochemical Science and Technology*, Vol. 134, #1, January, pg. 101-105

Warshaw, D.M. (1996) "The in vitro motility assay: a window into the myosin molecular motor", *News Physiol. Sci.*, Vol. 11, February, pg. 1-7

Wilbur, C., Vorus, W., Cao, Y., and Currie, S. (2001) "A lamprey-based undulatory vehicle", In: **Neurotechnology for Biomimetic Robots**, J. Ayers, J. Davis and A. Rudolph [eds], MIT Press, in press

Woledge, R.C., Curtin, N.A., and Homsher, E. (1985) **Energetic Aspects of Muscle Contraction**, Academic Press, London

Zajac, F.E. and Young, J. (1975) "Motor unit discharge patterns during treadmill walking and trotting in the cat", *Abstract #255*, 5th Annual Meeting of the Society for Neuroscience, New York

Zentel, R. and Brehmer, M. (1995) "Create ferroelectric liquid crystal elastomers", *Chemtech*, May, pg. 41-48

2. The Effects of Varying Deposition Current Density on Bending Behaviour in PPy(DBS)-Actuated Bending Beams¹

2.1 Introduction

Polypyrrole dodecylbenzene sulfonate, or PPy(DBS), is an electrically conductive polymer that changes volume under low voltage electrochemical stimulation. As such, it may be a suitable material for fabricating artificial muscle fibers (AMFs). It is known that production parameters such as the deposition current density (DCD) significantly affect various properties of polypyrrole such as its conductivity (Hahn et al. 1986a, Satoh et al. 1986, Mitchell and Geri 1987, Yamaura et al. 1988, Stanković et al. 1994, Dyreklev et al. 1996). What is not yet clear is how such parameters affect the dynamic electromechanical characteristics of PPy(DBS). Since these characteristics are critical in the AMF application, this chapter examines the effects of varying deposition current density between 0.4 and 40 mA/cm² on bending beam behaviour.

In the last several years, various research efforts have been directed towards the development of artificial muscle fibers. Much of this activity has focused on polymers that change volume in response to various chemical or electrical stimuli (de Gennes et al. 1997, Caldwell and Taylor 1990, Kaneto et al. 1995, Bohon and Krause 1998, Della Santa et al. 1997, Baughman 1996, Wang and Shahinpoor 1997, Sansiñena et al. 1997, Wallace et al. 1997, Smela 1999). Within this body of work, some recent successes have been experienced with polypyrrole (Madden et al. 1999 and 2000, Pei and Inganäs 1993a, Smela et al. 1995, Smela and Gadegaard 1999). We therefore considered polypyrrole to be a promising candidate for use in the actuation of artificial muscle fibers.

¹ A version of this chapter has been published by Sean Maw, Elisabeth Smela, Ken Yoshida, Peter Sommer-

Any prospective AMF material must have certain qualities to be functionally effective. Its performance must fall within certain limits along a number of dimensions. Among these are contractile strength, maximal strain, strain rate, stiffness, durability/endurance, cost, stimulation mode, reaction time, power output, efficiency, and frequency response. Conducting polymers, such as polypyrrole, appear promising on the basis of observed and calculated contractile strength (Baughman et al. 1991, Hunter and Lafontaine 1992), strain rate (Baughman 1996, Madden et al. 2000), production cost, stimulation mode (Madden et al. 1999 and 2000, Pei and Inganäs 1993a, Smela et al. 1995, Smela and Gadegaard 1999, Baughman et al. 1991, Hunter and Lafontaine 1992), and reaction time (Madden et al. 2000). Issues that may present more of a challenge include maximal strain, frequency response, durability, power output, efficiency, and ease of manufacture. To properly evaluate polypyrrole in the AMF role, its performance with respect to these criteria needs to be better characterized.

This last point is not straightforward, since different polypyrroles are produced under different synthesis conditions. PPy is usually synthesized as a film in an electrochemical cell under oxidative conditions. Anions are incorporated into the polymer matrix during polymerization. The nature of the final material varies with the nature of the electrolyte (anion and solvent). Indeed, depending on the nature of the solvent, the anion and the electrolyte concentration, the electrical, structural and mechanical qualities may vary significantly (e.g. Beck et al. 1994, Stanković et al. 1994, Ko et al. 1990, Kiani and Mitchell 1992, Ohno et al. 1994, Kassim et al. 1994, Kupila and Kankare 1995, Kaplin and Qutubuddin 1995, Truong et al. 1995, Kaynak 1997, Murray et

Larsen, and Richard B. Stein in *Sensors and Actuators A*, pp. 175-184, 2001.

al. 1997). As these studies attest, polypyrrole films incorporating different anions are essentially different materials. While many electrochemical characteristics of PPy films incorporating various anions have been examined, the effects of polymerization and stimulation variables on the dynamic electromechanical characteristics of PPy(DBS) have not.

The work described in this study involved the anion dodecylbenzene sulfonate (DBS), a large surfactant, and water as the solvent. Because polypyrrole is formed in its oxidized state, DBS anions are incorporated into the polymer matrix during deposition. Because these anions are so bulky, they become trapped in the polymer matrix. Thus, during electrochemical stimulation, charge compensation is carried out by cations (Pei and Inganäs 1993b-c). In our case, the cation was sodium.

The independent variable in our study was deposition current density (DCD), which determines deposition rate. DCD can be defined as the current drawn during deposition divided by the area of the deposit. Closely related to DCD is deposition potential. Different DCD values are sustained by different deposition potentials, and vice versa. Deposition rate has a well-documented influence on PPy morphology (Stanković et al. 1994, Dyreklev et al. 1996, Scrosati 1988, Hahn et al. 1986b), film density (Satoh et al. 1986, Buckley et al. 1987), conductivity (Hahn et al. 1986a, Satoh et al. 1986, Mitchell and Geri 1987, Yamaura et al. 1988, Stanković et al. 1994, Dyreklev et al. 1996), and static mechanical qualities (Satoh et al. 1986, Yamaura et al. 1988, Buckley et al. 1987). We controlled deposition current density (DCD) rather than potential because we found it led to more controlled depositions. The changes in deposition voltage were less dramatic and more reproducible than the changes in current when voltage was controlled. The

work described in this study shows how DCD affects the strain-related behaviour of PPy(DBS)-actuated bending beams. This factor was investigated so that DCD can be accounted for in the performance of PPy(DBS)-based actuators.

2.2 Experimental

Kapton[®] HN 100 sheets from Dupont, 1 mil (25.4 μm) thick, were coated on one side with 300-400 Å of gold (Au) by vacuum evaporation. The sheets were then cut into strips 1 mm wide using a sharp blade mounted on an automated Karl Süss scribing machine.

PPy(DBS) was deposited galvanostatically on a 1.5 ± 0.1 cm long portion of the gold-coated surface of each strip in an aqueous .20 M NaDBS / .20 M pyrrole solution. In each case, 300.0 ± 2.5 mC of charge was exchanged. The resulting deposition charge densities were 2.00 ± 0.15 C/cm² which corresponds to a PPy(DBS) film thickness of approximately 10 μm (Smela 1999). This thickness of PPy(DBS) produced bending beams that exhibited measurable ranges of movement. Several beams were prepared at each of the following deposition current densities: 0.4, 1.0, 4.0, 16, 28 and 40 mA/cm². This range effectively spanned the breadth of deposition current density (DCD) values that permitted sustainable and successful depositions.

Electropolymerization of the pyrrole monomer took place in a rectangular Plexiglas[®] cell 2.5 cm x 5.0 cm x 7.5 cm in size. The current at the working electrode was stepped from 0 mA to the target value and was held there until 300 mC of charge had been consumed. A platinum counter electrode approximately 6 cm² in submerged surface area was used in conjunction with a Fisher 13-620-53 Ag/AgCl reference electrode. The reference electrode was checked both before and after the experiment versus an SCE reference in .20 M NaDBS solution. During depositions, the working electrode Kapton[®] strips were suspended freely from tin-coated copper alligator clips, midway between the counter and reference electrodes, approximately 2 cm away from each. The gold side of

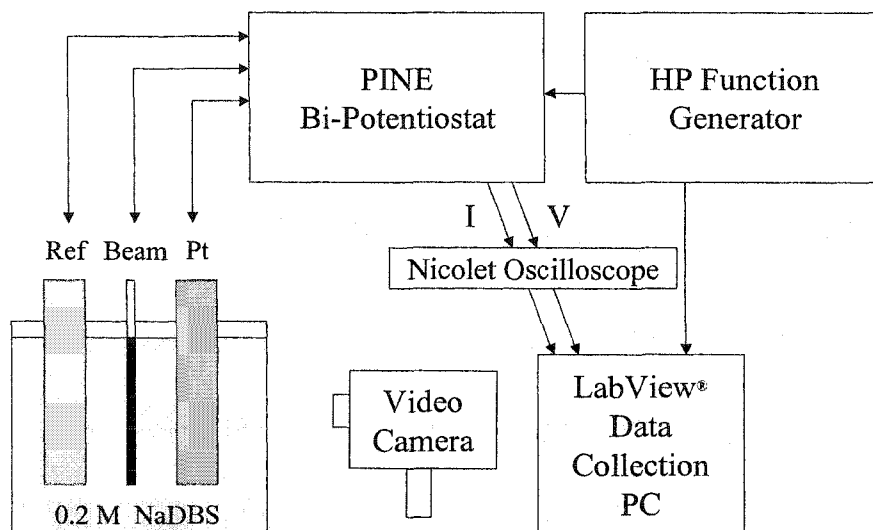
the beams faced the counter electrode. The three electrodes were suspended from a mount that was moved from the deposition cell to an identical rinse cell to an identical stimulation cell as the experiment proceeded.

The NaDBS and pyrrole were purchased from Aldrich (Canada), and MilliQ double-distilled and deionized water was used in all solutions. The solutions were not degassed. All deposition and stimulation experiments took place at room temperature and pressure. The pyrrole had been previously purified and was subsequently kept frozen in the dark at -70°C until needed. Deposition solutions were discarded after every use. Stimulation and rinse solutions were replaced after every three beams. The order in which beams were produced and then stimulated was randomized. After polypyrrole had been grown on a given Kapton[®] strip, the resulting beam was then rinsed in the rinsing cell. The sample was then transferred into a .20 M NaDBS aqueous solution for electrochemical stimulation.

An HP 8116A Pulse/Function Generator was used to control a PINE AFRDE5 Bi-Potentiostat, and a Nicolet 4094C Digital Oscilloscope provided real-time display of the data. Current and voltage levels were collected for off-line analysis using custom LabVIEW software sampling at 100 Hz. Further analysis was performed using custom Matlab[®] subroutines. Video footage of all beam movement activity was recorded. The overall experimental apparatus is shown in Figure 2-1.

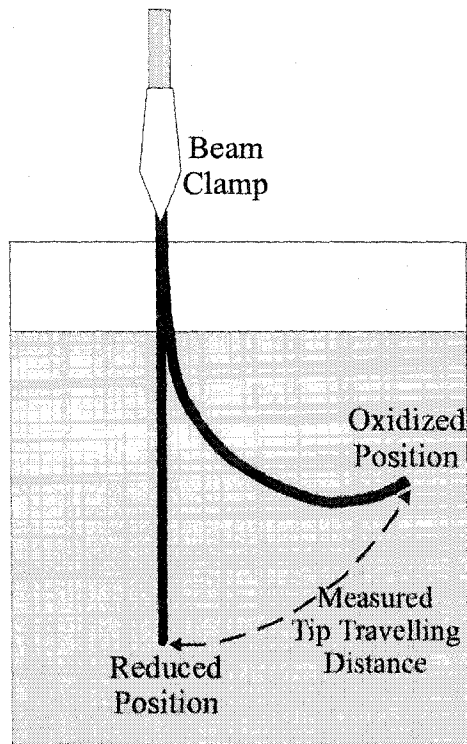
In all stimulation protocols, cycling began and ended at the oxidation limit. Each beam was subjected to 15 cycles of voltage ramp stimulation, 5 cycles of voltage step stimulation, 5 cycles of current step stimulation, and 15 cycles of voltage ramp stimulation to conclude. The range of beam tip movement was assessed every half-cycle

Figure 2-1 The experimental apparatus for the electropolymerization of the pyrrole, as well as for the stimulation of the polypyrrole dodecylbenzene sulfonate. The HP Function Generator controlled deposition and stimulation signals via the PINE Bi-Potentiostat. The Nicolet Oscilloscope provided user feedback, while the PC collected data. The video camera recorded beam movement activity.



by measuring the length of the path that the beam tip traveled during the half-cycle (Figure 2-2). This information was extracted from the videotape of each sample's deposition and stimulation. In general, we used the term *curling* to refer to the strain in the beams brought about by oxidation while *backcurling* refers to the strain brought about by reduction.

Figure 2-2 Schematic illustrating how the range of movement of the tip of each beam was measured. Note that the measured distance is that of the actual curved path that the tip traveled i.e. not just a straight line from the oxidized position to the reduced position. Also note that the length of the beam in solution is approximately 1.5 cm long.



2.3 Results and Observations

2.3.1 Film Growth

Deposition durations ranged from 50 to 5,000 seconds, depending on the DCD value. Figure 2-3 shows four representative deposition voltammograms. The average deposition potential versus DCD is shown in Figure 2-4. The most remarkable aspect of the depositions was the nature of the curling that the beams exhibited during the polymerization process. All of the beams slowly curled, with the PPy(DBS) surface on the outer side. Beams coated at lower DCD values curled more (Figure 2-5, top). However, there was also a relationship between curling extent and deposition duration. The data was approximately linear on a semi-log plot (Figure 2-5, bottom).

2.3.2 Conditioning Cycles

After film deposition was complete, each bending beam was cycled 15 times between -1.1 V and +0.4 V at 150 mV/s. In general, the beams curled film-side in during oxidation and straightened or backcurled with the film-side out during reduction. In other words, the PPy(DBS) contracted during oxidation and expanded during reduction as seen previously elsewhere (Smela 1999, Smela et al. 1995, Pei and Inganäs 1993a-c).

Figure 2-6 shows how the maximum half-cycle curling of the bending beams related to DCD while Figure 2-7 emphasizes oxidative beam tip movement as a function of cycle number. Both the maximum extent and the evolution of the bending behaviour over the 15 conditioning cycles were clearly affected by DCD. High DCD beams varied

Figure 2-3 Deposition voltammograms sampled at 100 Hz and collected using LabVIEW software. The different plots correspond to samples of PPy(DBS) deposited at different deposition current densities (DCDs). Data analysis was performed using custom Matlab[®] routines.

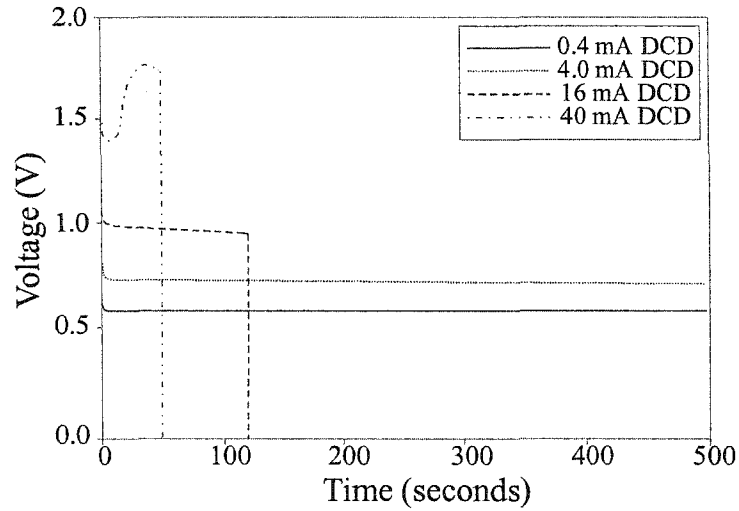


Figure 2-4 Deposition current density versus the average deposition potential. The best-fit curve is a 3-parameter sigmoid function of the form $[39.8/(1 + e^{-(x-1.06)/1.15})]$ such that $R^2 = .99$, $P < .0001$.

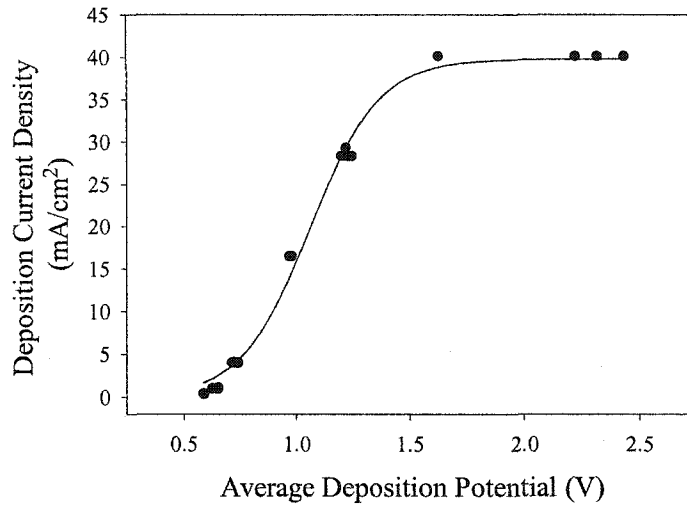


Figure 2-5 Movement of the beam tip during deposition, versus DCD (top) and versus time on a log scale (bottom). The same amount of charge was deposited for every data point (300 mC). The regression line in the top graph is a 2-parameter hyperbolic decay function of the form $[10.7/(11.3 + x)]$ such that $R^2 = .92$, $P < .0001$. The higher the DCD value, the lower the amount of curling that took place during deposition. The regression line in the bottom graph is a 2-parameter log function of the form $[-.42 + .17*\ln(x)]$ such that $R^2 = .92$, $P < .0001$. The shorter the deposition, the lower the amount of curling that took place during deposition.

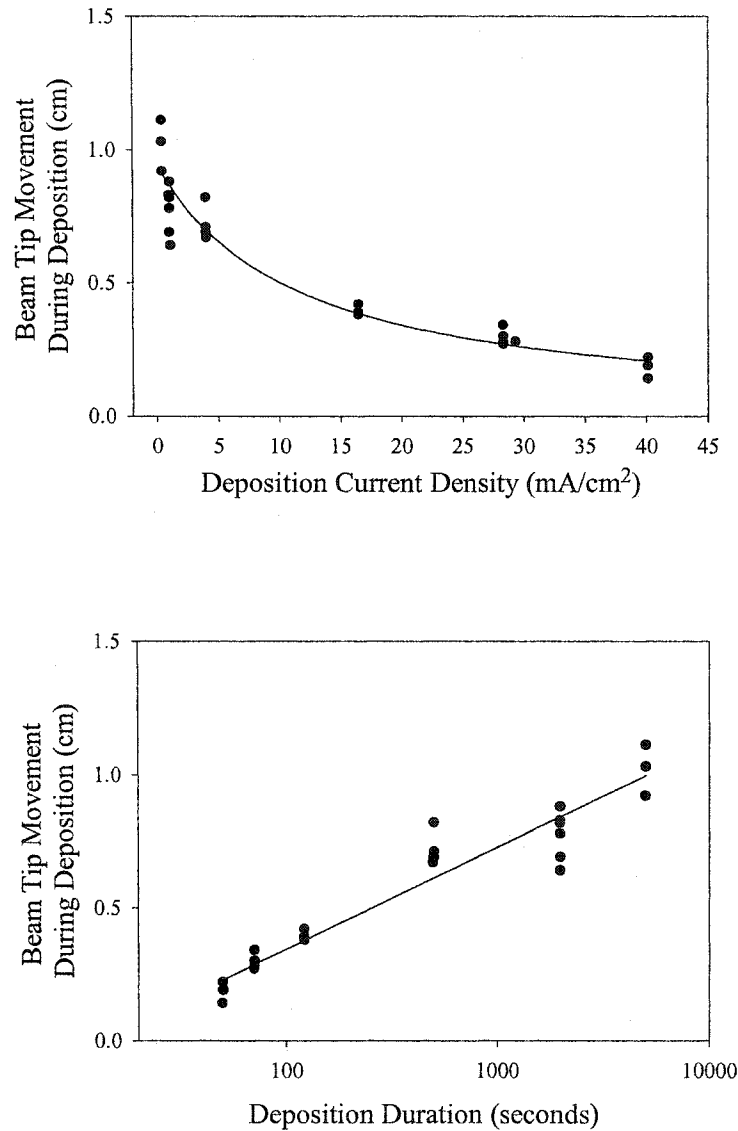


Figure 2-6 The maximum half-cycle extent of beam tip movement versus DCD during the fifteen conditioning cycles. The regression line is linear ($R^2 = .92$, $P < .0001$). The higher the DCD, the lower the amount of beam curling.

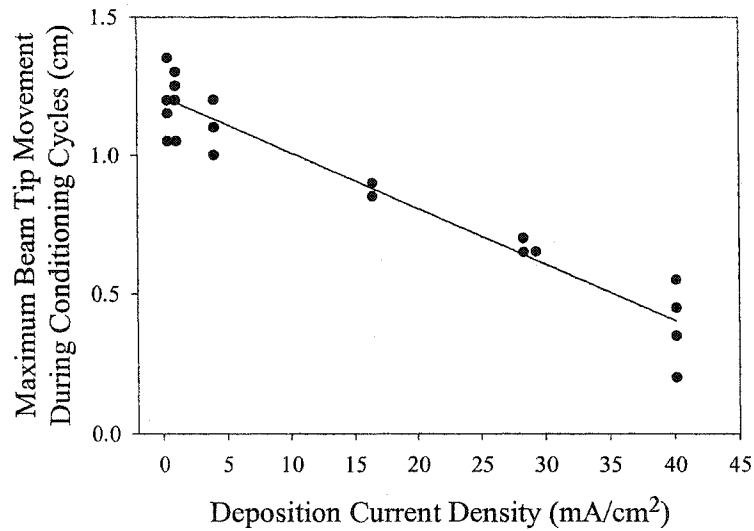
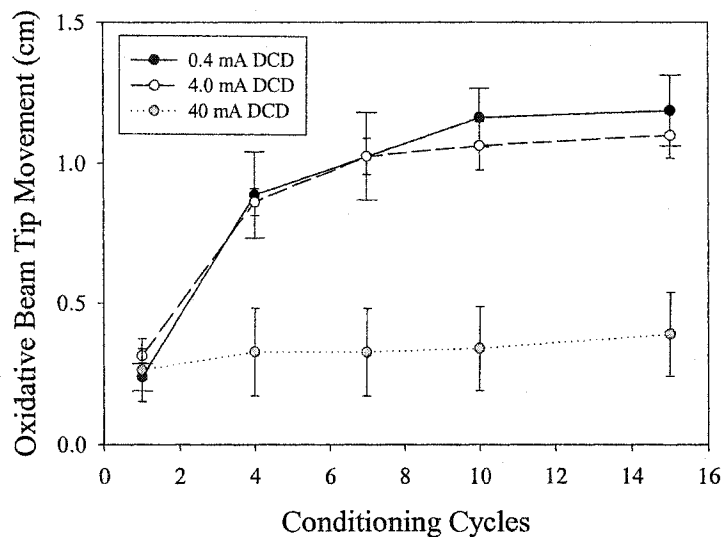


Figure 2-7 Beam tip movements during the oxidative halves of the conditioning cycles, with respect to the specific conditioning cycle, as a function of DCD. Error bars represent ± 1 standard deviation of the average values shown. Low DCD samples curl more but take longer to reach their maximal curling extent.



little in their curling activity from the 1st cycle to the 15th, with a maximum curl of about 4 mm. Low DCD beams, on the other hand, extended their range of movement by as much as 400% over the 15 cycles, to reach a final excursion of more than 12 mm.

Figure 2-8 shows four representative cyclic voltammograms that produced such bending activity. DCD played an important and predictable role in the electrochemical responses of the PPy(DBS). Films produced with higher DCDs exhibited weaker peak currents, reduced peak separation, and less charge transfer per cycle. The reduced peak separation resulted mainly from anodic shifts of the reduction peaks with increasing DCD (an average of 0.4 V over the tested DCD range). These results are consistent with the less extensive ranges of movement exhibited by high DCD samples.

Figure 2-9 shows how the extent of curling during the 15th reduction correlated with charge transfer. Charge transfer and peak current levels in the 15th cycle, for both oxidation and reduction, decreased linearly with respect to DCD. Values at 40 mA/cm² were, on average, less than half those at 0.4-1.0 mA/cm². For a given sample, curling extent was generally proportional to charge transfer and peak current values, except in the case of the first cycle or two. Indeed, during the first reduction, the charge transfer was quite large in spite of the fact that the beams did not curl very much. This phenomenon has been seen before (Shimoda and Smela 1998). However, for high DCD films, there was some initial backcurling. In the next few cycles, instead of curling significantly more to match the high level of charge exchange, the high DCD beams curled marginally more while exchanged reduction charge dropped more than 50%. For the low DCD films, the charge transfer changed minimally over the 15 cycles. However, the curling increased substantially. In so doing, the ratio of exchanged charge to curling extent that was

Figure 2-8 Conditioning CVs sampled at 100 Hz and collected using LabVIEW software during the twelfth cycle.

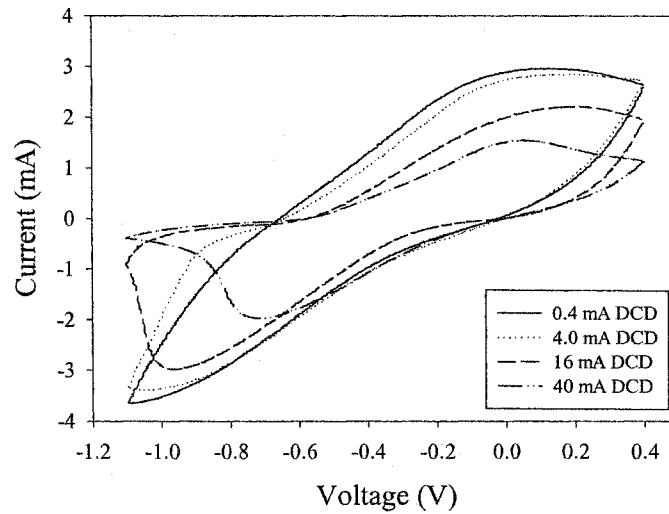
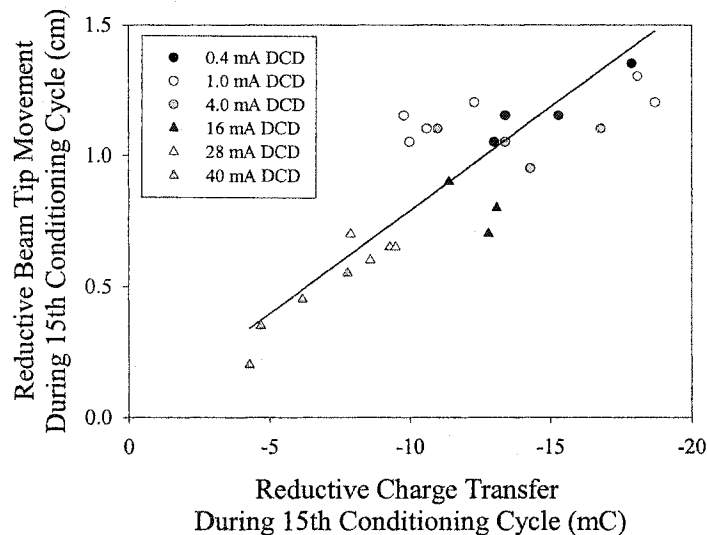


Figure 2-9 The maximum extent of the beam tip movement during reduction in the 15th conditioning cycle versus the reductive charge transfer during that cycle, as a function of DCD. The regression line is linear ($R^2 = .75$, $P < .0001$), and the slope is 0.79 mm/mC. The extent of the beam tip movement was proportional to the amount of charge transferred, independent of DCD value. However, low DCD samples tended to transfer more charge (and therefore backcurl more) while high DCD samples tended to transfer less charge (and therefore backcurl less).



common to almost all samples (as shown in Figure 2-9) was achieved by the 15th cycle.

The redox peaks also displayed a distinct pattern of behaviour based on DCD and cycle number (see Figure 2-10). The oxidation peaks of high DCD beams moved very little over the 15 cycles, while the oxidation peaks of low DCD beams initially appeared below 0V and then gradually moved in the anodic direction over time. Meanwhile, the reduction peaks all began at the lower limit (-1.1V) and then moved in the anodic direction over the 15 cycles, in proportion to their DCD value. As a result, for low DCD beams, the peaks separated during the 15 conditioning cycles while for high DCD beams, the peaks moved closer together. All of these results are summarized in Tables 2-1 and 2-2, suggesting that over time more of the PPy(DBS) in the low DCD beams became electrochemically and mechanically active.

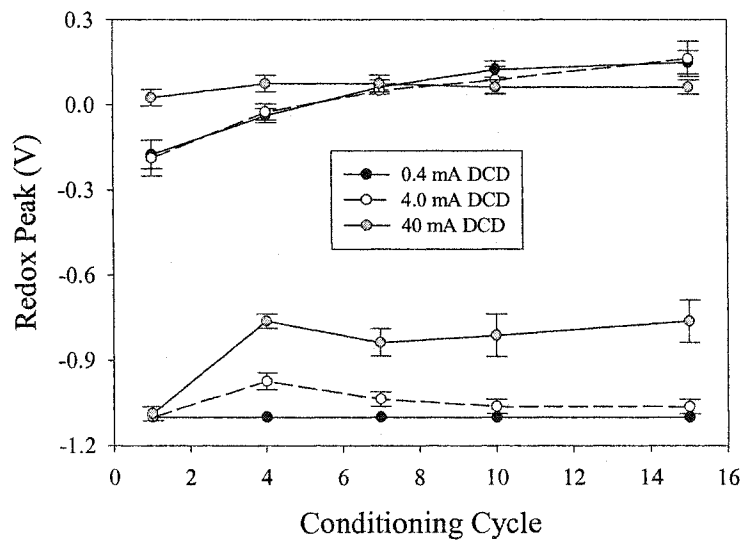
Table 2-1 Results of Conditioning Cycles (Reduction Half Cycles)

DCD (mA)	Backcurl 1 st cycle (cm)	Backcurl 15 th cycle (cm)	Peak V 1 st Cycle	Peak V 15 th Cycle	Charge Cycle1 (mC)	Charge Cycle15 (mC)	I _{pk} 1 st Cycle (mA)	I _{pk} 15 th Cycle (mA)
0.4	0.00	1.18	-1.10	-1.10	-14.73	-14.90	-3.95	-3.38
4.0	0.05	1.05	-1.10	-1.06	-14.93	-13.88	-3.90	-3.33
40	0.23	0.39	-1.09	-0.76	-13.85	-5.75	-3.10	-1.53

Table 2-2 Results of Conditioning Cycles (Oxidation Half Cycles)

DCD (mA)	Curl 1 st cycle (cm)	Curl 15 th cycle (cm)	Peak V 1 st Cycle	Peak V 15 th Cycle	Charge Cycle1 (mC)	Charge Cycle15 (mC)	I _{pk} 1 st Cycle (mA)	I _{pk} 15 th Cycle (mA)
0.4	0.24	1.19	-.18	.15	4.95	14.50	1.68	2.53
4.0	0.31	1.10	-.19	.16	4.35	13.55	1.55	2.50
40	0.26	0.39	.03	.06	3.48	5.55	1.10	1.15

Figure 2-10 Anodic and cathodic (redox) voltage peaks with respect to conditioning cycle, as a function of DCD. Error bars represent ± 1 standard deviation of the average values shown. For high DCD samples, the anodic peaks are mostly stationary over time while the cathodic peaks move in the anodic direction. For low DCD samples, the anodic peaks shift anodically while the cathodic peaks are mostly stationary.



An examination of the videotapes documenting the movements of the beams substantiated these numbers, but also revealed other information. After the first reduction, the expansion of the range of motion over the 15 cycles in all cases occurred in the oxidized/curled direction. The movement back and forth became increasingly pendular in the sense that movements started and ended slowly with a velocity peak midway (as illustrated in Figure 2-11). For low DCD values, the beams generally moved from a fairly backcurled position to a very curled position, whereas high DCD beams moved from a less backcurled position to an approximately straight position.

In summary, the conditioning cycles revealed that deposition current density plays an important role in determining contractile behaviour in PPy(DBS)-actuated bending beams. Low DCD values favour more extensive and more rapid curling. However, they also require a longer warm-up or break-in period (see Shimoda and Smela 1998). In all cases, movement extent was shown to be proportional to the amount of charge exchange.

2.3.3 Voltage Steps

After the conditioning cycles, each bending beam was stimulated with 5 cycles of voltage steps. The step levels were -1.1 V and +0.4 V and the cycling took place at .05 Hz i.e. each step lasted 10 seconds.

The maximum curling extent of the bending beams followed a pattern similar to Figure 2-6 except that the extent was about 50% greater across the full DCD range. Charge transfer values increased slightly more than proportionately. Figure 2-12 shows four representative examples of the resulting amperograms. Peak current levels were 200-

Figure 2-11 A schematic representation of beam position versus time during one of the later conditioning oxidation half-cycles for two typical beams grown at 0.4 and 40 mA/cm² respectively. Low DCD samples start more backcurled and end more curled, moving both more extensively and more rapidly (i.e. the slope of the lines).

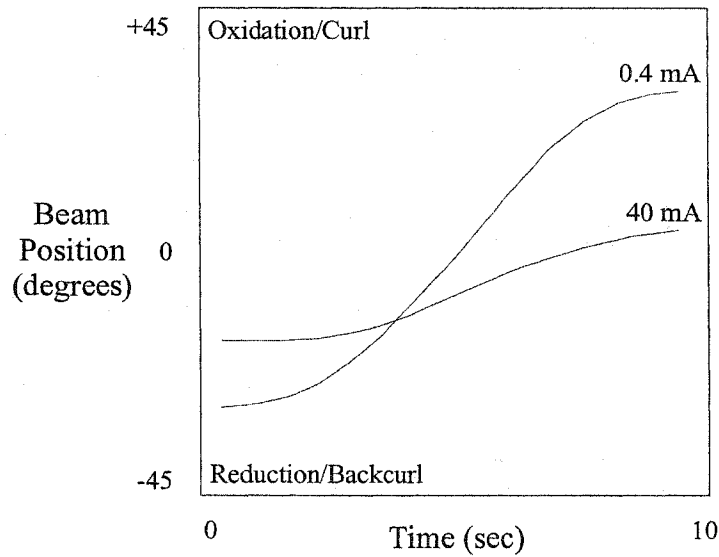
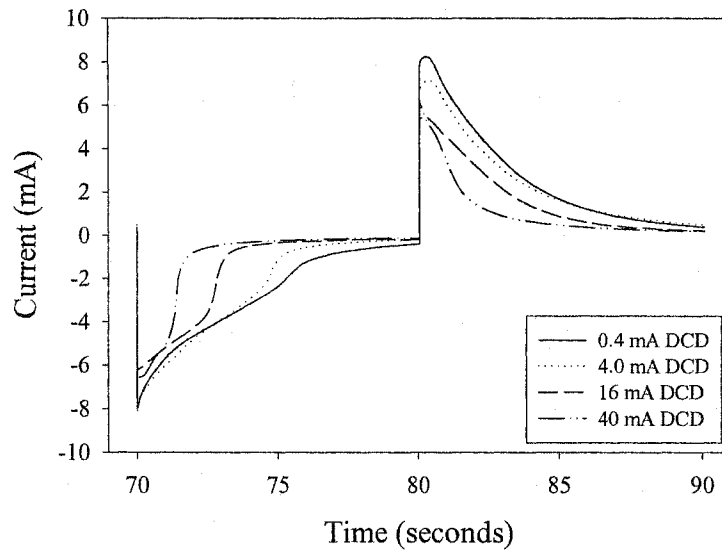


Figure 2-12 Voltage step responses (amperograms) sampled at 100 Hz and collected using LabVIEW software during the 4th voltage step cycle.



300% greater for the voltage steps than for the 15th conditioning cycle, with high DCD beams showing the greatest increases. Essentially, low DCD films exhibited higher and longer-lasting currents, resulting in more charge transfer and more extensive curling. The results from the voltage steps are summarized in Table 2-3.

Table 2-3 Results of Voltage Step Cycles (Reduction Half Cycles)

DCD (mA)	Backcurl 1 st cycle (cm)	Backcurl 5 th cycle (cm)	Charge 1 st Cycle (mC)	Charge 5 th Cycle (mC)	Charge as % of Deposition Charge	I _{pk} 1 st Cycle (mA)	I _{pk} 5 th Cycle (mA)
0.4	1.30	1.66	-19.93	-24.15	8.05	-5.15	-6.23
4.0	1.21	1.35	-17.28	-20.13	6.71	-5.23	-6.45
40	0.49	0.63	-7.58	-8.68	2.89	-3.85	-5.43

The amount of charge exchanged during the voltage step stimulation suggests what fraction of the PPy(DBS) film participated in the mechanical activity. Assuming a doping level of one charge for every 4 monomer units (Smela et al. 1995), on top of the two charges consumed per monomer during polymerization (Wallace et al. 1997), the charge exchanged should have been 11% of the polymerization charge in the ideal case. Our average value from these voltage step measurements for the low DCD films was just over 8%. For the high DCD films, the percentages ranged down to less than 2%, suggesting a very limited exchange of ions.

In terms of how the extent of beam bending evolved over the 5 voltage step cycles, the range of curling expanded by about 1 mm across all DCD values.

Video analysis further revealed that both reduction and oxidation movements could be characterized by a rapid initiation of movement followed by a gradual slowing

down to a stop, mirroring the currents drawn over each half cycle. The higher the currents were, the faster were the rapid movements (see Figure 2-13).

In summary, the voltage step data supported the earlier finding that low DCD beams transfer charge more easily, resulting in more curling for a given level of voltage stimulation.

2.3.4 Current Steps

After the voltage step cycles, each bending beam was stimulated with 5 cycles of current steps. The current steps were different for each beam. Current step levels were set at either 10 mC or at some pre-set percentage of the maximum charge transfer that took place during the voltage steps. The different percentages were 25%, 50%, 100% and 125%. In all, ten samples were stimulated at 10 mC, seven were stimulated at 25%, and 2 each were stimulated at 50%, 100% and 125%. Of course, the 10 mC steps could also be converted to equivalent percentages and this perspective was employed in the examination of the data where appropriate. In all cases, the stepping took place at .05 Hz and the step levels were symmetric (e.g. ± 1.0 mA).

Video analysis showed that the movements were slow and steady in both directions, with little or no stop time at each end of the curling/backcurling (see Figure 2-14). The degree of beam bending was generally proportional to the charge transfer for a given DCD value (see Figure 2-15). For instance, in the 0.4 to 4.0 mA/cm² range, the percentage of charge transfer generally increases as one moves up each column of symbols in the graph. Only the 125% samples were strong exceptions, suggesting that they may have been damaged by such stimulation. Nevertheless, this general result,

Figure 2-13 A schematic representation of beam position versus time during one of the later voltage step oxidation half-cycles, for two typical beams grown at 0.4 and 40 mA/cm². Low DCD samples start more backcurled and end more curled, moving both more extensively and more rapidly. Movements were largely completed in the first half of the cycles, following the current responses to the voltage stimulation.

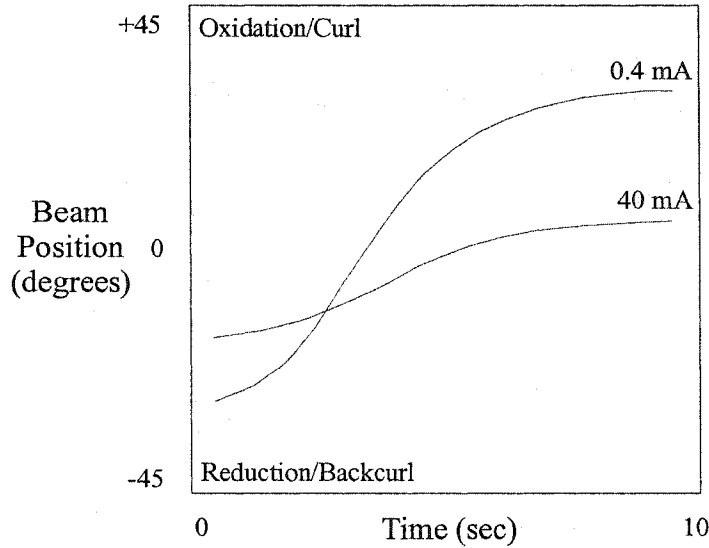


Figure 2-14 A schematic representation of beam position versus time during one of the later current step oxidation half-cycles, for two typical beams grown at 0.4 and 40 mA/cm² and stimulated at a relatively high charge percentage-of-maximum value. Low DCD samples start more backcurled and end more curled, moving both more extensively and more rapidly without any pause at the two extremes.

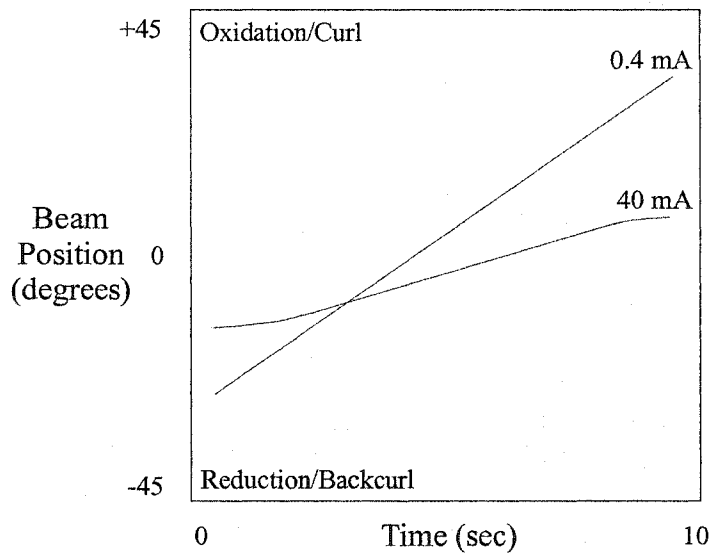
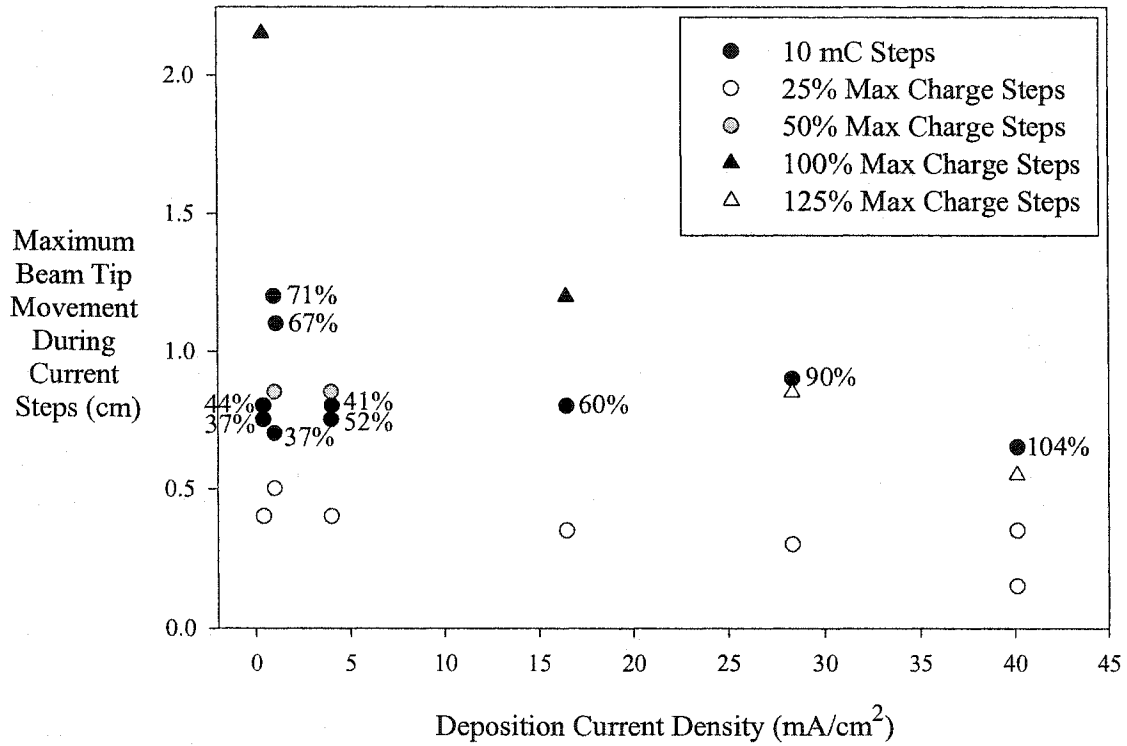


Figure 2-15 The maximum half-cycle extent of the beam tip movement during the five current step cycles, versus DCD. The 10 mC samples are labeled with an equivalent charge percentage value. The 25% of maximum charge open circles show how DCD is important for a given percentage of charge stimulation. The 10 mC charge black circles show how DCD may not be very important for a given fixed amount of charge stimulation. The column of symbols above each DCD value that was tested show a rough proportionality between movement extent and percentage of charge stimulation except, possibly, at very high percentage levels i.e. $\geq 100\%$.



combined with the data shown in Figure 2-9, does confirm Otero and Rodríguez' finding (1993a) that the extent of bilayer bending is determined by the amount of exchanged charge. Figure 2-15 also shows that the electromechanical (beam bending) effect of a given percentage of charge exchange does depend on DCD (see, for instance, the 25% data set). For a given amount (not percentage) of charge exchange, there was at most a slight effect across DCD values i.e. see the 10 mC data points. In other words, the charge exchange to strain proportionality was largely independent of DCD.

In summary, the current stepping showed that control over the extent and speed of curling can be well managed by controlling charge transfer and current levels. Beam bending is roughly proportional to the amount of charge transfer and this appears to be independent of DCD. However, the proportionality between beam bending and charge transfer does depend on DCD when percentage of charge transfer (compared to its natural maximum, found during voltage stimulation) is used.

2.3.5 Post-Step Cycles

After the current step cycles, each bending beam once again went through 15 cycles of CVs between -1.1 V and +0.4 V at 150 mV/s. In other words, the conditioning procedure was repeated. In conjunction with the current steps, this allowed for an examination of how stimulation history might interact with DCD. A clear effect was not noted given the limited data sets at 50%, 100% and 125%. Overall, the pattern was the same as in Figure 2-6 except for a general 10% increase in beam bending extent. In addition, beam movements were noticeably smoother.

2.3.6 Film Adhesion

At the end of the experiment, the beams were rinsed in deionized water and were stored in air for 1-2 hours before being subjected to a peel test. The peel test was meant to reveal how the current step stimulation may have affected the adhesion of the PPy(DBS) to the gold-coated Kapton[®]. The adhesion test consisted of firmly applying a piece of Scotch[®] 810D Magic Tape to the bottom half of each PPy(DBS)-coated beam. The beam was then smoothly peeled off of the tape, taking with it some, none or all of the PPy(DBS) as well as some, none or all of the metal layer.

In 19 of 22 cases the tape removed either most of or all of the PPy(DBS) and metal layer. Clearly, the adherence of the film to the metal layer was sound. It was the adherence of the metal to the Kapton[®] that was not. The 3 samples that did not peel were low DCD samples. This would be consistent with the findings of others who have noted that adhesion decreases with increasing deposition voltage (Kaplin and Qutubuddin 1995).

2.4 Discussion

Several investigators have described differences in polypyrrole electrochemical behaviour and morphology as a function of deposition potential and/or deposition current density (Sato et al. 1986, Stanković et al. 1994, Buckley et al. 1987, Bilger and Heinz 1993, Peres et al. 1989, Otero and Rodríguez 1993b). One of the ways in which these differences may be manifested is through dopant concentration in the film. Relating the dopant concentration to deposition potential, Sato et al. (1986) found that the concentration of dopants in PPy(pTS) did not change with deposition potential while Peres et al. (1989) contended that doping increased with increasing growth potential even though their data was less than convincing on this point. If anything, our circumstantial findings suggest that doping may decrease with increasing potential. Note, however, that the growth conditions in all of these other experiments were quite different, making comparisons dubious. For instance, the concentration of pyrrole monomer varied by a factor of 10, and the solvents and salts were also different.

Closer to the goals of this chapter, Bilger and Heinz (1993) studied the effects of growth voltage on subsequent electrochemical responses of PPy(LiClO₄) films. For films grown at low potentials, they noted that the reduction peaks shifted positively over time. At higher growth voltages they found the cyclic voltammograms to be more stable and symmetric, with reduced peak separation. We saw this last behaviour too. However, the significance of any differences or similarities is limited since both ions were mobile in their experiment. Kaplin and Qutubuddin (1995), on the other hand, worked with a relatively immobile anion in PPy(pTS). Peak redox currents decreased and reduction peak voltages moved anodically as growth voltage increased. We found this as well.

In high DCD films, the small amount of exchanged charge ($< 3\%$) that we found, as a percentage of deposition charge, suggested a very limited exchange of ions in these samples during potential stepping. This could be a function of either non-electroactive or inaccessible film regions. The higher voltages present during the formation of these films could have produced substantial amounts of poorly doped non-electroactive PPy(DBS) film. Alternatively, if the deeper layers of PPy(DBS) in the high DCD samples simply could not be accessed by the cations because the polymer lattice was too dense, then the charge transfer and mechanical deformation would also be limited. Our results do not tend to favour one explanation over the other as in almost all cases the post-current step cycles exchanged somewhat more charge and produced somewhat more extensive movements as compared to the conditioning cycles.

Indeed, it would be valuable if a polypyrrole film's capacity for strain was predictable on the basis of a simple production variable such as deposition current density. Fortunately, it would appear that this may be the case. One possible indicator of strain potential is the extent to which a given beam curls during deposition. This feature correlated well with a given beam's ensuing dynamic curling behaviour during stimulation. However, so did deposition duration. Future work will show which is the more influential indicator. Either way, the phenomenon begs the question, what is happening during deposition that causes the beam to bend? The bending itself makes it clear that the growing PPy(DBS) must be creating stresses that are strong enough to compress the Kapton[®] backing and cause backcurling. It may be that the polymer growth is arborous in nature and that the pressure (electrostatic or otherwise) of the growing

chains against each other pushes the system towards occupying more volume as the polymer chains grow away from the gold working electrode surface.

The subsequent curling behaviour that is a result of stimulation tells us more than just curling is proportional to charge exchange. It tells us that strain is. And it also tells us that strain rate is proportional to current. This was perhaps best illustrated by the voltage steps. The patterns of movement of the beams seemed to follow the traces of the amperograms quite closely.

As such, our data support Otero and Rodriguez' (1993a) findings that the extent of deformation is a function of exchanged charge and that the deformation rate can be controlled using applied current. There was the possibility that the coefficient relating charge transfer to strain might be different for films produced at different DCD values. In other words, a given amount of charge would cause beams grown at different DCD values to curl different amounts. However, we did not find convincing evidence to support this contention. Instead, we found that for a given level of voltage stimulation, the amount of charge exchanged depended on DCD, and the amount of curling followed suit at a proportion independent of DCD. In other words, DCD instilled a different propensity for a given film to exchange charge at a given level of voltage stimulation.

There are still several unexplained details though. For instance, what is going on in the first reduction where a relatively massive charge exchange takes place, but little curling occurs? Why, over the course of cycling, does most of the expansion of the curling range of motion occur on the oxidation side? Why does it increase at all? How does this happen with low DCD films where the charge exchange doesn't change very much? And what is the cause of the movement of the redox peaks, such as they are?

Over the course of the next few studies, we will keep these questions in mind so that by the end of the thesis a model can be put forward that explains all of these phenomena in a consistent and reasonable manner.

Examining the effects of deposition current density has provided us with an insight into how polypyrrole behaves, and why it behaves the way it does. However, many production parameters affect polypyrrole. Therefore, as we continue to explore how various factors influence the electromechanical behaviour of PPy(DBS), we will also need to be vigilant for interaction effects. For now, the next step will be to determine what role monomer and electrolyte concentration levels play in strain and strain rate capabilities.

2.5 Conclusions

The main finding with a bearing on artificial muscle fiber applications is that strain in PPy(DBS)-actuated bending beams can be controlled during both manufacture and use. Management of the deposition current density resulted in different qualities of PPy(DBS) as it relates to dynamic strain behaviour. Thus, deposition current density can and should be carefully considered in the design of PPy(DBS)-actuators.

Curling as a result of strain transverse to the plane of the film varied inversely with deposition current density under voltage stimulation. High DCD films exhibited less extensive movement, reduced peak separation and less charge transfer per cycle compared to low DCD films. Voltage stimulation showed that high DCD films were more "reluctant" to exchange a given amount of charge as evidenced by the more extreme voltage levels elicited by current step stimulation. Conversely, for a given level of voltage stimulation, they exchanged less charge and as a result, curled less extensively. High DCD films did, however, activate more rapidly with respect to the extent that they would ultimately perform as compared to the low DCD films that required longer "warm up" periods. On the other hand, using current step stimulation, the extent of curling was proportional to the amount of charge transferred, largely independent of DCD, and current steps provided the highest degree of control over curling extent and rate.

All results suggested that after the first few stimulation cycles, the extent of movement is proportional to exchanged charge, and that rate of movement is proportional to rate of charge exchange i.e. current. The movement responsiveness (curl per unit charge) appeared to be relatively constant with respect to DCD, although there was a weak tendency to be more responsive at lower DCD values. However, high DCD films

are simply not able to exchange high levels of charge and can be damaged if this is attempted. This is reflected in the decrease in charge exchange capacity (charge exchange per cycle as a percentage of deposited charge) with respect to increasing DCD.

From a practical standpoint, voltage steps produced faster and more extensive movements than ramp voltammetry, all other things being equal. Current steps provided more control over movement extent and speed. Low DCD samples, all else being equal, moved faster and more extensively under voltage stimulation and they had the ability to move over a great range when stimulated by current steps.

2.6 References

- Baughman, R.H., Shacklette, L.W., Elsenbaumer, R.L., Plichta, E.J., and Becht, C. (1991) "Micro electromechanical actuators based on conducting polymers", In: **Molecular Electronics**, P.I. Lazarev [ed], Kluwer Academic Publishers, pg. 267-89
- Baughman, R.H. (1996) "Conducting polymer artificial muscles", *Synthetic Metals*, Vol. 78, pg. 339-53
- Beck, F., Michaelis, R., Schloten, F., and Zinger, B. (1994) "Filmforming electropolymerization of pyrrole on iron in aqueous oxalic acid", *Electrochimica Acta*, Vol. 39, #2, pg. 229-234
- Bilger, R. and Heinz, J. (1993) "Role of the formation potential on the redox processes of polypyrrole studied by an electrochemical quartz microbalance", *Synthetic Metals*, Vol. 55-57, pg. 1424-1429
- Bohon, K. and Krause, S. (1998) "An electrorheological fluid and siloxane gel based electromechanical actuator: working toward an artificial muscle", *J. Poly. Sci. B. Polym. Phys.*, pg. 1091-94
- Buckley, L.J., Roylance, D.K., and Wnek, G.E. (1987) "Influence of dopant ion and synthesis variables on mechanical properties of polypyrrole films", *J. Poly. Sci: Part B: Poly. Phys.*, Vol. 25, pg. 2179-2188
- Caldwell, D.G. and Taylor, P.M. (1990) "Chemically stimulated pseudo-muscular actuation", *Int. J. Engng. Sci.*, Vol. 28, #8, pg. 797-808
- de Gennes, P-G., Hebert, M., and Kant, R. (1997) "Artificial muscles based on nematic gels", *Macromol. Symp.*, Vol. 113, pg. 39-49

Della Santa, A., De Rossi, D., and Mazzoldi, A. (1997) "Characterization and modeling of a conducting polymer muscle-like linear actuator", *Smart Mater. Struct.*, Vol. 6, pg. 23-24

Dyreklev, P., Granström, M., Inganäs, O., Gunaratne, L.M.W.K., Senadeera, G.K.R., Skaarup, S., and West, K. (1996) "The influence of polymerization rate on conductivity and crystallinity of electropolymerized polypyrrole", *Polymer*, Vol. 37, #13, pg. 2609-2613

Hahn, S.J., Gajda, W.J., Vogelhut, P.O., and Zeller, M.V. (1986a) "Auger and infrared study of polypyrrole films: evidence of chemical changes during electrochemical deposition and aging in air", *Synthetic Metals*, Vol. 14, pg. 89-96

Hahn, S.J., Stanchina, W.E., Gajda, W.J., and Vogelhut, P.O. (1986b) "The effect of growth rate variation on the conductivity and morphology of polypyrrole thin films", *J. Electron. Mater.*, Vol. 15, #3, pg. 145-49

Hunter, I.W. and Lafontaine, S. (1992) "A comparison of muscle with artificial actuators", *IEEE Solid-State Sensors and Actuators Workshop Technical Digest*, June 21-25, Hilton Head Island, USA, pg. 178-85

Kaneto, K., Kaneko, M., Min, Y., and MacDiarmid, A.G. (1995) "Artificial muscle: electromechanical actuators using polyaniline films", *Synthetic Metals*, Vol. 71, pg. 2211-12

Kaplin, D.A. and Qutubuddin, S. (1995) "Electrochemically synthesized polypyrrole films: effects of polymerization potential and electrolyte type", *Polymer*, Vol. 36, #6, pg. 1275-1286

Kassim, A., Davis, F.J., and Mitchell, G.R. (1994) "The role of the counter-ion during electropolymerization of polypyrrole-camphor sulfonate films", *Synthetic Metals*, Vol. 62, pg. 41-47

Kaynak, A. (1997) "Effect of synthesis parameters on the surface morphology of conducting polypyrrole films", *Mat. Research. Bull.*, Vol. 32, #3, pg. 271-85

Kiani, M.S. and Mitchell, G.R. (1992) "The role of the counter-ion in the preparation of polypyrrole films with enhanced properties using a pulsed electrochemical potential", *Synthetic Metals*, Vol. 48, pg. 203-18

Ko, J.M., Rhee, H.W., Park, S.-M., and Kim, C.Y. (1990) "Morphology and electrochemical properties of polypyrrole films prepared in aqueous and nonaqueous solvents", *J. Electrochem. Soc.*, Vol. 137, #3, March, pg. 905-909

Kupila, E.-L. and Kankare, J. (1995) "Influence of electrode pretreatment, counter anions and additives on the electropolymerization of pyrrole in aqueous solutions", *Synthetic Metals*, Vol. 74, pg. 241-249

Madden, J.D., Cush, R.A., Kanigan, T.S., and Hunter, I.W. (1999) "Encapsulated conducting polymer actuators", *Synthetic Metals*, Vol. 105, pg. 61-64

Madden, J.D., Cush, R.A., Kanigan, T.S., and Hunter, I.W. (2000) "Fast contracting polypyrrole actuators", *Synthetic Metals*, Vol. 113, pg. 185-92

Mitchell, G.R. and Geri, A. (1987) "Molecular organisation of electrochemically prepared conducting polypyrrole films", *J. Phys. D: Appl. Phys.*, Vol. 20, pg. 1346-1353

Murray, P., Spinks, G.M., Wallace, G.G., and Burford, R.P. (1997) "In-situ mechanical properties of tosylate doped (pTS) polypyrrole", *Synthetic Metals*, Vol. 84, pg. 847-48

Ohno, H., Yoshida, H., and Ohtsuka, Y. (1994) "Effect of salt species on the electrochemical p-doping of poly(pyrrole) films in poly(ethylene oxide) oligomers", *Solid State Ionics*, Vol. 68, pg. 125-131

Otero, T.F. and Rodríguez, J. (1993a) "Polypyrrole electrogeneration at different potentials in acetonitrile and acetonitrile/water solutions", *Synthetic Metals*, Vol. 55-57, pg. 1418-1423

Otero, T.F. and Rodríguez, J. (1993b) "Electrochemomechanical and electrochemopositioning devices: artificial muscles", In: **Intrinsically Conducting Polymers: An Emerging Technology**, M. Aldissi [ed], Kluwer Academic Publishers, pg. 179-90

Pei, Q. and Inganäs, O. (1993a) "Electrochemical muscles: bending strips built from conjugated polymers", *Synthetic Metals*, Vol. 55-57, pg. 3718-23

Pei, Q. and Inganäs, O. (1993b) "Electrochemical applications of the bending beam method; a novel way to study ion transport in electroactive polymers," *Sol. State Ion.*, Vol. 60, pg. 161-66

Pei, Q. and Inganäs, O. (1993c) "Electrochemical applications of the bending beam method. 2. Electroshrinking and slow relaxation in polypyrrole," *J. Phys. Chem.*, Vol. 97, pg. 6034-41

Peres, R.C.D., Pernaut, J.M., and DePaoli, M.A. (1989) "Properties of poly(pyrrole) films electrochemically synthesized in the presence of surfactants", *Synthetic Metals*, Vol. 28, pg. C59-C64

Sansiñena, J.M., Olazabal, V., Otero, T.F., Polo da Fonseca, C.N., and De Paoli, M.A. (1997) "A solid state artificial muscle based on polypyrrole and a solid polymeric electrolyte working in air", *Chem. Commun.*, pg. 2217-18

Satoh, M., Kaneto, K., and Yoshino, K. (1986) "Dependences of electrical and mechanical properties of conducting polypyrrole films on conditions of electrochemical polymerization in an aqueous medium", *Synthetic Metals*, Vol. 14, pg. 289-296

Scrosati, Bruno (1988) "Electrochemical properties of conducting polymers", *Prog. Solid St. Chem.*, Vol. 18, pg. 1-77

Shimoda, S. and Smela, E. (1998) "The effect of pH on polymerization and volume change in PPy(DBS)," *Electrochim. Acta*, Vol. 44, #2-3, pg. 219-38

Smela, E., Inganäs, O., and Lundström, I. (1995) "Controlled folding of micrometer-size structures", *Science*, Vol. 268, June 23, pg. 1735-38

Smela, E. (1999) "Microfabrication of PPy microactuators and other conjugated polymer devices", *J. Micromech. Microeng.*, Vol. 9, pg. 1-18

Smela, E. and Gadegaard, N. (1999) "Surprising volume change in PPy(DBS): an atomic force microscopy study", *Adv. Mat.*, Vol. 11, #11, pg. 953-57

Stanković, R., Pavlovic, O., Vojnovic, M., and Jovanovic, S. (1994) "The effects of preparation conditions on the properties of electrochemically synthesized thick films of polypyrrole", *Eur. Polym. J.*, Vol. 30, #3, pg. 385-393

Truong, V-T., Ennis, B.C., and Forsyth, M. (1995) "Ion exchange, anisotropic structure and thermal stability of polypyrrole films", *Synthetic Metals*, Vol. 69, pg. 479-80

Wallace, G.G., Spinks, G.M., and Teasdale, P.R. (1997) **Conductive Electroactive Polymers: Intelligent Materials Systems**, Technomic Publishing, USA, pg.1-106

Wang, G. and Shahinpoor, M. (1997) "Design for shape memory alloy rotatory joint actuators using shape memory effect and pseudoelastic effect", *SPIE*, Vol. 3040, pg. 23-30

Yamaura, M., Hagiwara, T., and Iwata, K. (1988) "Enhancement of electrical conductivity of polypyrrole film by stretching: counter ion effect", *Synthetic Metals*, Vol. 26, pg. 209-224

3. The Effects of Varying Monomer and Electrolyte Concentrations in Deposition and Stimulation Solutions on the Bending Behaviour in PPy(DBS)-Actuated Bending Beams

3.1 Introduction

Of all the major systems and organs in the human body, the one that has arguably withstood efforts at its physical simulation most successfully has been muscle. When complicated biological systems such as kidneys, lungs, hearts, bones, and even brains (vis-à-vis computers) have been functionally replicated with modern technology, why has muscle withstood all best efforts? One of the reasons must surely be the complexity of muscle's contractile and metabolic systems, combined with their small physical size. The diversity of the nature of the system's components is only matched by the number and interconnectedness of those same components at a micro-scale. Hochachka's exhaustive review of muscle as a machine (1994) provides an excellent illustration of this point.

If we are interested in trying to create artificial muscles, we can look at other attempts to emulate natural systems for lessons in how to proceed. For instance, mankind's efforts to fly have had to make use of the same principles of aerodynamics as those managed by birds. However, until recently, we have had to make do with different ways of working with these aerodynamic principles e.g. combustion engines for propulsion and fixed wings for lift. Likewise, to create functional artificial muscle fibers, we could try to use the same principles that skeletal muscle fibers employ, albeit in different ways.

The essential way in which muscles operate is by changing the nature (charge and shape) of complex polymers and by changing how those polymers interact with each other in response to electrical stimulation. Action potentials (APs) travel down motor

neuron axons to specialized synapses that facilitate the depolarization of the muscle membrane. This produces an AP which spreads over the muscle membrane into the myofibrils and initiates a cascade of events which result in the change in conformation of myosin protein projections as they interact with actin proteins. This change in conformation produces tensile forces between the actin and myosin chains which are then transferred through the super-structure of the isolated muscle cell to produce macro-scale contractions of up to 50% in length. The contractile forces can be summed and controlled by virtue of which fibres get recruited (some are stronger and faster than others), in what order they get recruited (the size principle, Henneman et al. 1965), and how frequently they get recruited (briefly up to 200 Hz in human muscle (Rothwell 1987)). The success of the general design and its many variations is evidenced by its ubiquity in nature. The efficiency of these systems is also remarkable. In human muscle, efficiency levels can exceed 35% (Hunter and Lafontaine 1992). As molecular scale machines, muscle fibrils are further organized into cellular (muscle fiber), multi-cellular (motor unit) and organic (muscle) units. Each organizational level provides different abilities and perspectives on control of the macro-scale actuation.

Mankind's concerted efforts at replicating this machinery began about 50 years ago (Katchalsky 1949, Kuhn 1949, Kuhn et al. 1950, Kuhn and Hargitay 1951, Kuhn et al. 1960). This early work focused on polyvalent alcohol/polyacrylic acid copolymer gels, as well as on proteins such as collagen and β -keratose (Pautard and Speakman 1960). These copolymers and proteins would contract and expand in response to stimulation with different solvents. Some impressive results and demonstrations were eventually achieved (Steinberg et al. 1966, Sussman and Katchalsky 1970, Caldwell and

Taylor 1990). The polymers would take in or expel the solvents in response to changes in the charge on ionizable groups along the polymer chains in the gels. These changes in the ionizable groups resulted in changes in attraction and repulsion between chains in the polymer, opening or closing the gel to allow for the movement of solvents in or out of the gel. By cycling solvents, temperature and/or pH, these researchers were able to produce polymers that contracted and expanded under controlled stimulation conditions. However, problems with efficiency, speed, power and durability that were often a function of the solvent manipulation prevented these systems from ever seeing common use.

More recently, a variety of research efforts have been directed towards the development of artificial muscle fibers that depend upon electrical stimulation (e.g. Kaneto et al. 1995, Bohon and Krause 1998, Della Santa et al. 1997, Baughman 1996, Wang and Shahinpoor 1997, Sansiñena et al. 1997, Wallace et al. 1997, Smela 1999, Maw et al. 2001, Pelrine et al. 1998). Even though they all operate under electrical stimulation, their specific mechanisms and principles of operation are still quite different. For example, Pelrine's electrostrictives work on the principle of electrostatic attraction between free charges on polymer electrodes, while Bohon and Krause work with electrorheological fluids (ERFs) that change from a fluid to a viscoelastic solid and back again upon exposure to an electric field. The polypyrrole that Della Santa, Smela and Maw work with and the polyaniline that Kaneto works with rely on the mass transport of (hydrated) ions in and out of the polymer films due to charge imbalances brought about by running current through the actuators. Meanwhile, the shape memory alloys (SMAs)

of Wang and Shahinpoor rely on the metallic phase transition brought about by temperature changes resulting from running a current through a metallic actuator.

The experimental work that is described in this study deals with the conductive polymer polypyrrole dodecylbenzene sulfonate (PPy(DBS)) that changes volume under electrical stimulation (e.g. Pei and Inganäs 1992, 1993a-c, Smela et al. 1995, Smela 1999, Smela and Gadegaard 1999, Madden et al. 1999 and 2000, Maw et al. 2001). The polypyrrole is synthesized as a film in an electrochemical cell by incorporating compensating anions into its polymer matrix during anodic polymerization. As such, the nature of the final material varies with the nature of the electrolyte solution (anion, cation and solvent). Indeed, depending on the nature of these ions and solvents as well as their concentrations, electrical and mechanical qualities will vary significantly (e.g. Beck et al. 1994, Naoi et al. 1995, Ko et al. 1990, Kiani and Mitchell 1992, Stanković et al. 1994, Ohno et al. 1994, Kassim et al. 1994, Kupila and Kankare 1995, Satoh et al. 1986, Kaplin and Qutubuddin 1995, Kaynak 1997, Murray et al. 1997). The work discussed in this chapter uses water as a solvent and dodecylbenzene sulfonate (DBS), a large surfactant, as the dopant/anion. As the polymerization of pyrrole is an anodic process, the DBS anions are incorporated into the polymer matrix during deposition to balance charge. After deposition, when the PPy(DBS) film is stimulated electrically, most of the large DBS anions remain trapped in the material, necessitating the movement of smaller cations (such as sodium) and their associated hydration shells, in and out of the polypyrrole matrix (McCormac et al. 1995). This activity plays a key role in the volume-changing nature of the polypyrrole.

If PPy(DBS), or any other material, is ever going to be used commonly in an artificial muscle fiber (AMF) application, it must perform well with respect to certain performance criteria, such as those outlined in Maw et al. (2001). To evaluate the materials against these criteria fairly, we need to understand how the materials work so that production and operational parameters can be optimized. Polypyrroles are, above all else, quite sensitive to a wide variety of fabrication parameters such as deposition current density and potential (Beck et al. 1994, Peres et al. 1989, Bilger and Heinze 1993, Wood and Iroh 1996, An et al. 1994, Mitchell and Geri 1987, Satoh et al. 1986, Hahn et al. 1986, Buckley et al. 1987, Dyreklev et al. 1996, Kaplin and Qutubuddin 1995, Kiani and Mitchell 1992, Stanković et al. 1994, Maw et al. 2001), deposition and stimulation electrolytes and/or dopants (Beck et al. 1994, Bobacka et al. 1994, John et al. 1992, Barisci et al. 1996, Matencio et al. 1994 and 1995, Kupila and Kankare 1993, Mitchell et al. 1988, Warren and Anderson 1987, Warren et al. 1989, Li and Qian 1989, Naoi et al. 1995, Yamaura et al. 1988, Kaynak 1997, Satoh et al. 1986, Kaplin and Qutubuddin 1995, Kupila and Kankare 1995, Buckley et al. 1987, Stanković et al. 1994, Ohno et al. 1994, Kiani and Mitchell 1992, Kassim et al. 1994), polymerization temperature (Otero and Rodríguez 1994, Kiani and Mitchell 1992, Stanković et al. 1994, Yamaura et al. 1988, Mitchell and Geri 1987, Satoh et al. 1986, Ohno et al. 1994, Ogasawara et al. 1986), polymerization and stimulation solvent (Stanković et al. 1994, Ko et al. 1990), monomer concentration (Beck et al. 1994, Stanković et al. 1994, Qian et al. 1986, Wood and Iroh 1996), electrode type or pretreatment (Smela et al. 1993, Cheung et al. 1988, Kupila and Kankare 1995), oxygen exposure (Bobacka et al. 1994) and pH (Kupila and Kankare 1993, Shimoda and Smela 1998, Li and Qian 1993, Wood and Iroh 1996, Li and

Qian 1989). Indeed, polypyrroles that incorporate different anions into their polymer matrix through different solvents can be considered to be distinctly different materials (albeit within a family) by virtue of their different electromechanical natures.

What I examine in this study are PPy(DBS)'s changing electromechanical responses to various levels of pyrrole monomer and NaDBS electrolyte concentrations in both the deposition solution and in the stimulation solution. Electrolyte/dopant concentration, for example, has been implicated for its influence on PPy morphology, conductivity and static mechanical qualities (Naoi et al. 1995, Bobacka et al. 1994, Otero and Sansiñena 1996, John et al. 1992, Iseki et al. 1991, Li and Qian 1989, Satoh et al. 1986, Ohno et al. 1994, Kassim et al. 1994). The effects of changes in monomer concentration have also been studied (Beck et al. 1994, Otero and Rodríguez 1994, Stanković et al. 1994, Qian et al. 1986, Wood and Iroh 1996). The model I use for studying the electromechanical behaviour of the PPy(DBS) film is that of the bending beam made popular by Pei and Inganäs (1992, 1993a-c) and originally by Timoshenko (1925), as it is sensitive to small changes in the volume of the PPy(DBS) film. The beams I used were all produced under the same conditions except for the deposition concentration levels of the monomer and electrolyte/dopant. Subsequent behavioural differences were assessed with respect to the different concentration levels that brought them about. As well, I employed three different modes of stimulation to see if the concentration differences brought about different effects in different stimulation scenarios. While the literature is replete with a variety of concentration levels of all three of these variables in different electrolyte and solvent systems, this is the first

comprehensive examination of the interaction of these variables in one system, especially as it pertains to electromechanical actuation.

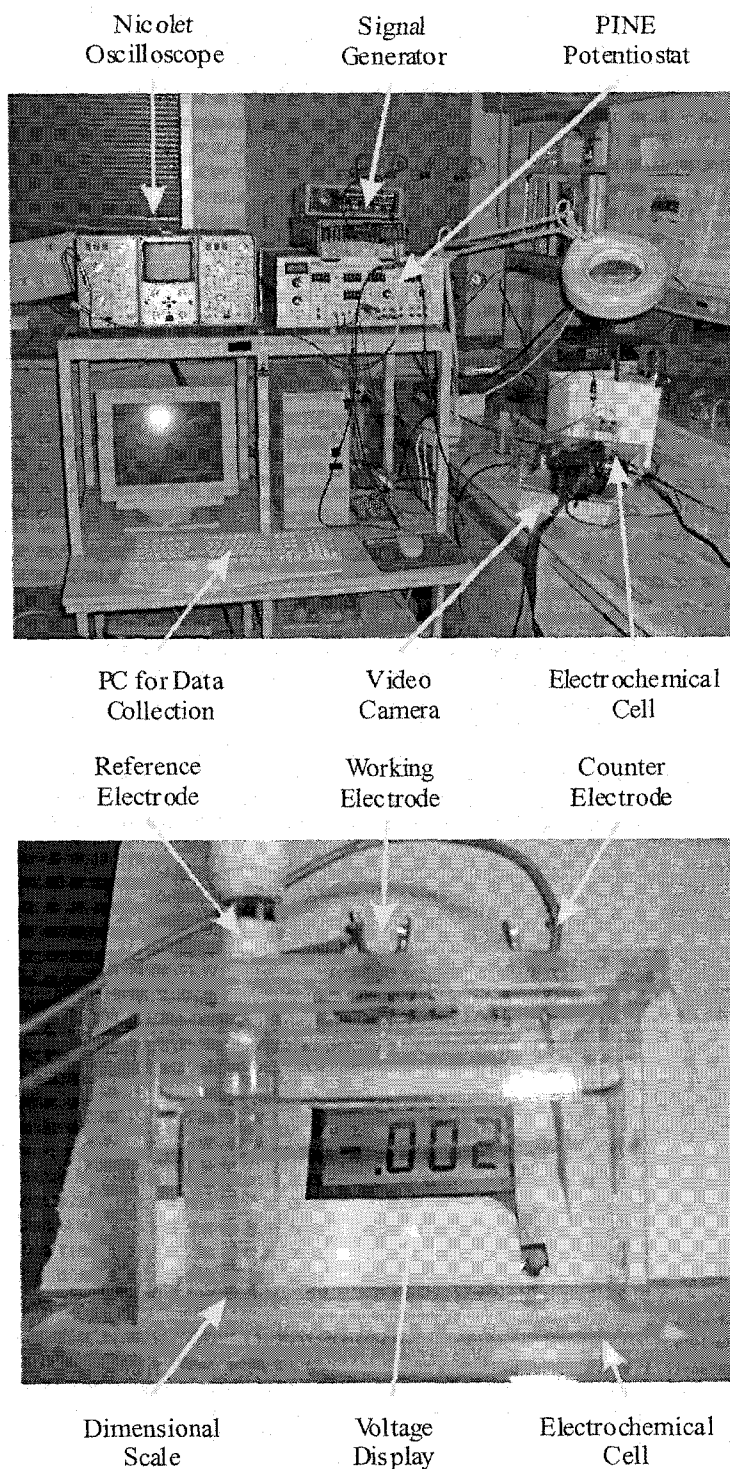
3.2 Experimental

The materials and apparatus used in this experiment were identical to those described in Chapter 2. Figure 3-1 shows the experimental set-up. This experiment's protocols differed from the earlier work however, and are therefore described below.

PPy(DBS) was deposited galvanostatically on a 1.5 cm long portion of a gold-coated Kapton[®] surface in an aqueous NaDBS solution containing pyrrole monomer. In each case, 225 mC of charge was exchanged. The resulting deposition charge density of 1.5 C/cm² corresponded to a PPy(DBS) film thickness of about 7.5 μm (Smela 1999). This thickness of PPy(DBS) produced bending beams that exhibited measurable ranges of movement. The PPy(DBS) film was deposited at a current density of 2 mA/cm².

After the polypyrrole had been grown on the Kapton[®] strip, the resulting beam was rinsed in a rinsing cell. The sample was then transferred into an aqueous NaDBS solution where it was subjected to 15 cycles of ramp voltammetry at 150 mV/s between -1.1 V and +0.4 V i.e. the cycling frequency was .05 Hz. This conditioning phase allowed for an assessment of the integrity of the beams and prepared them for further non-destructive testing. The given parameters were sufficient to capture redox peaks of the PPy(DBS) films. After the ramp voltammetry, the fibres were then stimulated with 5 cycles of voltage steps (again between -1.1 V and +0.4 V, at .05 Hz). This was followed by 5 cycles of current step stimulation, again at .05 Hz. For the fourth and final phase, each beam was stimulated with 15 cycles of ramp voltammetry, mirroring the first conditioning phase. This last phase of the procedure was carried out to assess how and if the voltage and current steps had affected the PPy(DBS). At this stage, the beam was then rinsed and stored in air for 24-48 hours before being subjected to a peel test. The

Figure 3-1 The experimental apparatus for the electropolymerization of the pyrrole, as well as for the stimulation of the polypyrrole dodecylbenzene sulfonate. The HP Function Generator controlled deposition and stimulation signals via the PINE Bi-Potentiostat. The Nicolet Oscilloscope provided user feedback, while the PC collected data. The video camera recorded beam movement activity. Lower photo shows details of the cell.



peel test was meant to reveal how the cycling may have affected the adhesion of the PPy(DBS) to the gold-coated Kapton[®]. As in Chapter 2, it involved applying tape to the beams and peeling the tape back. This could take all of the PPy(DBS) with it, some, or none at all, as well as any amount of the metallic interlayer.

The main variables that were manipulated in this experiment were the concentrations of the monomer (pyrrole) and of the electrolyte (NaDBS) in both the deposition solution and in the stimulation solution. All 36 combinations of .01, .02, .04, .08, .16 and .32 M pyrrole versus .01, .02, .04, .08, .16 and .32 M NaDBS were used to deposit PPy(DBS). These samples were then stimulated using one of the six noted NaDBS concentrations. For the current steps, the stimulation was performed at either 5 mC or at 100% of a given beam's maximum single-step reductive charge transfer that took place during the voltage step phase. Table 3-1 summarizes the experimental conditions for the samples, where *5mC* represents the 5 mC stimulation, *100%* represents stimulation using the maximum single-step reduction charge transfer during the voltage steps, and the concentrations represent the NaDBS concentration level at which the given sample was stimulated. The reduction charge transfer for every cycle was always recorded, and the *100%* figure simply represents the maximum value from the voltage steps. In the end, 60 samples were produced. More than one sample was produced for some conditions, and in some cases, no useful samples were produced at all as some growth and stimulation procedures failed or were outside of quality control specifications.

Quality control was manifested in several ways. In some cases, beams would fail (delaminate) at some point during the test procedures. Generally, the data from those samples was not used (at least not in the cycling set where the delamination took place).

In other cases, unusual voltage levels were produced, such as during “difficult” depositions. Those samples were discarded unless the unusual voltage levels proved to be quite persistent upon repeating the procedure. Low concentration combinations had a tendency to deposit poorly, for example. As a result, pyrrole concentrations of .015 M were used in place of .01 M on a few occasions, to facilitate successful depositions. Finally, if there were several samples made for a given condition, individual results were compared against group means and standard deviations. Generally, outliers in the stimulation data were retained. However, outliers in deposition data were usually discarded on the rationale that they represented a different deposition condition than the one all of the other samples in the group experienced.

In any event, when the various concentration levels were categorized into low (.01-.02), medium (.04-.08) and high (.16-.32), all 27 permutations of the various pyrrole deposition, NaDBS deposition, and NaDBS stimulation concentration levels were successfully produced.

Table 3-1 Deposition/Stimulation Combinations

		NaDBS					
		.01 M	.02 M	.04 M	.08 M	.16 M	.32 M
Pyrrole	.01 M	5mC,.01	100%,.01	5mC,.01	100%,.01	5mC,.01	100%,.01
	.02 M	5mC,.08	100%,.32	5mC,.08	100%,.32	5mC,.08	100%,.32
	.04 M	5mC,.04	100%,.04	5mC,.04	100%,.04	5mC,.04	100%,.04
	.08 M	5mC,.02	100%,.32	5mC,.02	100%,.32	5mC,.02	100%,.32
	.16 M	5mC,.16	100%,.16	5mC,.16	100%,.16	5mC,.16	100%,.16
	.32 M	5mC,.02	100%,.08	5mC,.02	100%,.08	5mC,.02	100%,.08

In all stimulation modes, redox currents and voltage levels were recorded, as well as the already mentioned charge transfers per cycle. Also in every case, cycling began and ended at the oxidation limit. The range of beam tip movement (curling) in all of the stimulation modes was assessed every half-cycle by measuring the length of the path that the beam tip traveled during the half-cycle. This information was extracted from videotape footage of the experiment. As in Chapter 2, *curling* refers to the movement of the bending beam from strain brought about due to oxidation. *Backcurling* refers to the strain brought about by reduction (although, in context, all beam bending behaviour will often be referred to as curling in this chapter). Also, for brevity, "low" concentrations will refer to the .01-.02 M range, "mid" or "medium" will refer to the .04-.08 M range and "high" will refer to the .16-.32 M range. Deposition pyrrole values will be referred to as "DP", deposition NaDBS concentrations will be referenced as "DN", and stimulation NaDBS concentration levels will be noted as "SN".

Where appropriate, sample means and population standard deviations were calculated using standard Microsoft Excel formulae.

Some qualitatively similar experiments were carried out in preliminary work. The PPy(DBS) films in these cases were grown on Au/Cr-coated silicon wafers and on 1 mm x 2 cm x 7.5 μm thick Kapton[®] strips. Concentrations of .05, .10, .20, .30 and .40 M were used for both the pyrrole and for the NaDBS. Where comparisons of data sets are both possible and reasonable, they are mentioned.

3.3 Results and Observations

3.3.1 Film Growth

In all, 46 usable samples were produced and activated. The depositions lasted 739.2 seconds \pm 3.2 seconds (1 standard deviation). Figure 3-2 shows some representative deposition voltammograms.

While the deposition current was the same in all cases ($.306 \pm .04$ mA), characteristics of the growth potential plots varied depending on the DP and DN concentration levels. Specifically, the height of the initial capacitance spike was influenced by both concentrations. The greater the DP and/or DN concentration, the shorter the height of the spike. This effect was most notable in the low-mid DN range and in the mid-high DP range. The DP concentration levels also influenced the average and final growth potential values substantially (see Figure 3-3). The greater the pyrrole concentration, the lower the average and final growth potential values were. Changes in DN had similar effects, though smaller. Preliminary data supported these findings. In addition, DP and DN both seemed to influence the amount of beam curling that occurred during deposition, albeit selectively. Their effects were only evident over certain ranges of concentration. For instance, at mid-high DP levels, from low-mid DN, curling increased noticeably. Also, at mid-high DN levels, from low-mid DP, curling increased noticeably. Overall, the distribution of curling values was almost perfectly Normal, centered on 0.5 cm, with most of the variation encompassed within ± 0.1 cm. However, there was a tendency towards less curling with respect to extreme mismatches of the two concentrations (e.g. .01/.32). It also sometimes happened that PPy(DBS) would grow around the beam onto the

Figure 3-2 Deposition voltammograms sampled at 100 Hz and collected using LabVIEW software. The different plots correspond to samples of PPy(DBS) deposited at different pyrrole and NaDBS concentrations (.02 M, .08 M and .32 M). The top plot shows the effects of varying NaDBS concentration, while the bottom plot shows the effects of varying pyrrole concentration during deposition. Data analysis was performed using custom Matlab[®] routines.

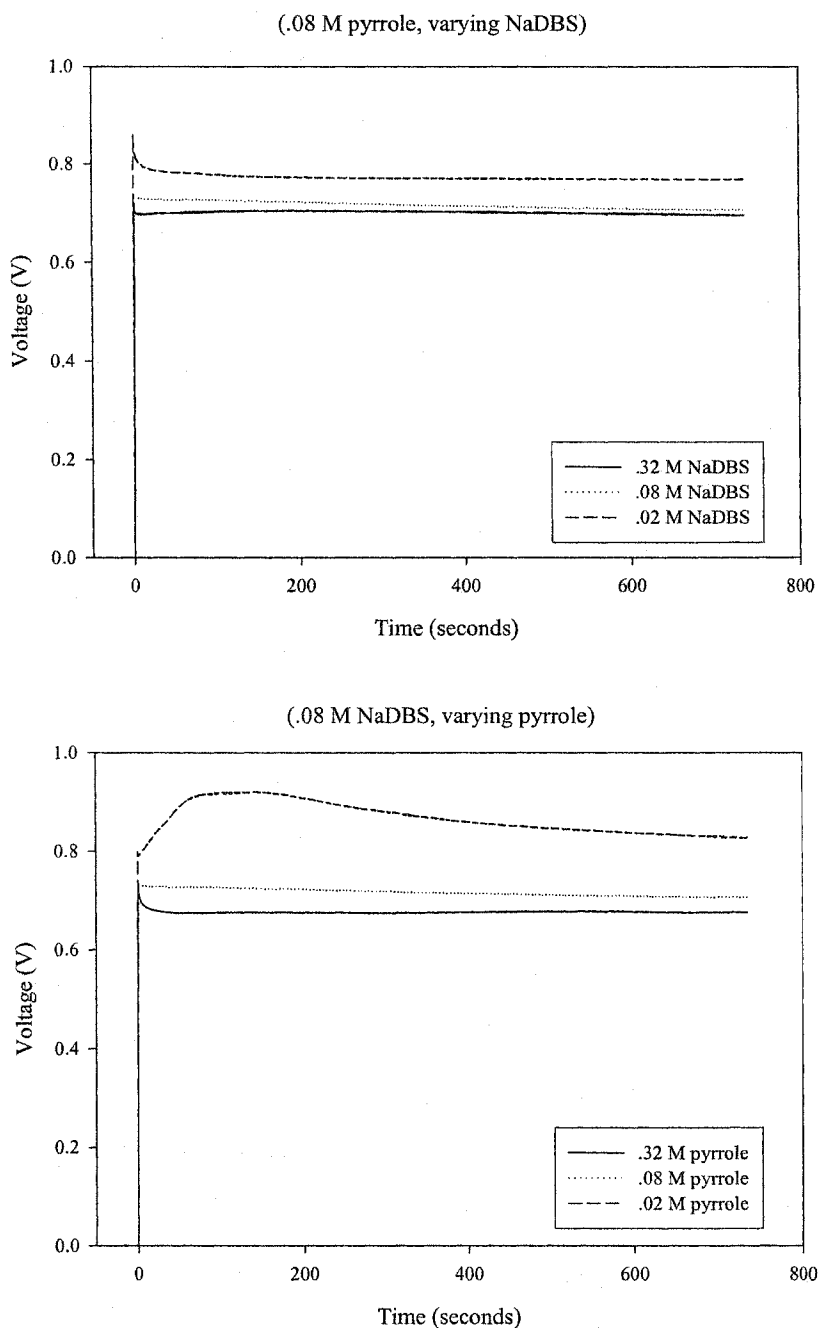
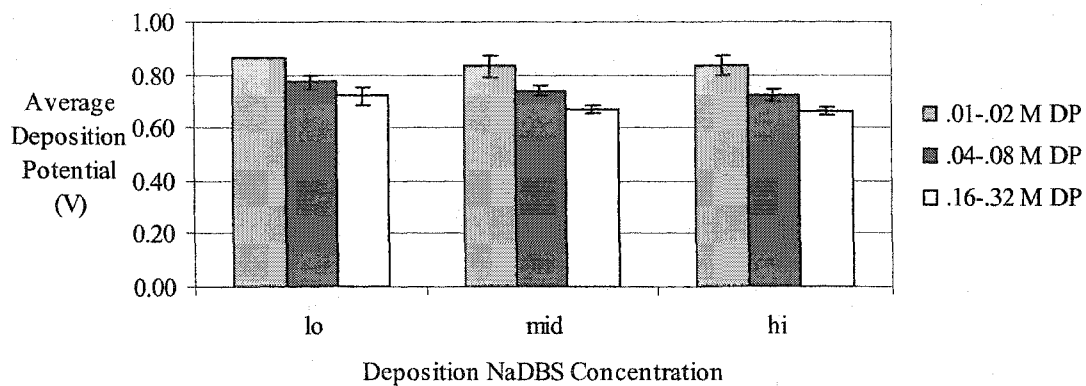


Figure 3-3 Plots of average deposition potential versus deposition pyrrole (DP) and deposition NaDBS (DN) concentrations. Low levels are taken as .01-.02 M, medium levels as .04-.08 M and high levels are taken as .16-.32 M. Error bars are ± 1 standard deviation for a population of between 1 and 9 samples per condition (average of 5).



backside of the Kapton[®]. Microscopic examinations showed that PPy(DBS) growth around the back of the beams was more prevalent at low total concentration levels. Any beams with substantial backside growth were not used for further study as their later curling performance could have been compromised by the backside PPy(DBS) build-up. Nevertheless, no correlation between deposition curling and backside growth was found.

3.3.2 Conditioning Cycles

The conditioning cycles were a pivotal part of this study, allowing me to focus clearly on the effects of changing concentrations on charge exchange, peak currents, peak voltages, and ranges of beam tip movement, before introducing other variables such as stimulation mode.

It is worth reviewing at this point the significance of these various measures, as there will be many results dealing with each of them. The peak currents tell us what kinds of power and energy requirements would be required by the PPy(DBS) films under different circumstances. Likewise, the peak voltages tell us similar things about what stimulation voltages are required under different conditions of stimulation. This would affect power source choices for any potential AMF system, and these sorts of results would also indicate whether variable voltage (or current) draws would be needed. Natural muscle operates on an all-or-nothing basis for contraction and does not depend on the size of the incoming action potential (which does not vary substantially, in any event), only on the arrangement of incoming action potentials with respect to time (see Introduction). Information regarding charge exchange is reflective of the capacity of the film to do work/contract, since strain is proportional to charge exchange (e.g. Maw et al.

2001). This is obviously quite important, and it is also important in how it relates to movement. Thus, calculations of how much movement (curl) occurs per unit charge exchanged (mC) are also common, reflecting the responsiveness of the films to strain under a given charge exchange. The measurement of the curling reflects strain levels and this is fundamental to the whole thesis. At times, I will also make reference to the shape of the voltammograms and amperograms. This is because the features of these plots show different qualities of the films in different ways. With the amperograms, for instance, we can get an excellent sense of how relatively fast the beam is moving with time, as this is well reflected in the instantaneous current levels. Finally, there will be several occasions where I will plot one set of values versus another (e.g. peak currents versus peak voltages). The purpose in doing this will be to show how these interacting variables relate to each other in different situations. That may provide a way of controlling the level of one variable via another, for example.

As in Chapter 2, the beams curled film-side in during oxidation and straightened or backcurled with the film-side out during reduction. In other words, the PPy(DBS) contracted during oxidation and expanded during reduction. Each beam went through 15 cycles of voltage ramp stimulation during the conditioning cycles.

In examining the cyclic voltammetry data, it is clear that variations in all three of the concentrations (DP, DN and SN) had measurable effects and that there were some interactions among the variables in certain situations. For instance, increasing DP levels leads to more negative reduction peaks and rounder redox peaks. Increases in SN lead to higher peak current levels and decreased peak separation. Also, at high SN levels, the electrochemical behaviour during the first few reductions is very different than during the

rest of the reduction cycles. The first reductions feature substantially greater currents and more negative peaks than those later on.

While all three concentrations were found to be important, there is no doubt that the variation in SN has the greatest effect within the concentration ranges that I studied (.02 to .32 M). Curling, for example, was primarily affected by SN levels, although there were some interaction effects with DP and DN. Also, high DN levels tended towards greater ranges of movement. Some of these details are shown in the graphs of Figure 3-4, including data suggestive of an interdependence of the concentration variables.

Over the 15 conditioning cycles, curling increased in every experimental condition. The biggest increases took place over the first few cycles. Low DP, DN and SN beams would increase their extent of curling the least over the 15 cycles while high concentration levels produced the greatest absolute increases in curling except with DP where the situation was not clear. The amount of net (oxidative) curling over the 15 cycles increased with SN.

As was noted in section 3.3.1, DN and DP seem to affect curling during deposition. However, they may produce more dramatic effects afterwards during various stimulation procedures. To investigate this, curling during the 15th conditioning cycle was plotted against curling during deposition, grouped by levels of DN, DP and SN. There were no apparent patterns in the data for DN and DP. However, given Figure 3-4, it was not surprising that a pattern was found with the SN data. This is shown in Figure 3-5 (top). It was not a correlation with the deposition curling though. It was simply a reflection of the relationship shown in Figure 3-4. When the same analysis was performed on the DCD data from Maw et al. (2001), however, a strong correlation was

Figure 3-4 Curling versus conditioning cycle number, by SN concentration group (top). The low, medium and high SN concentration ranges are shown in the legend. Error bars are ± 1 standard deviation for a population of 11-23 samples per condition. Note the substantial differences despite variation among DN and DP values within SN groupings. The middle graph shows curling versus the scaled log of the product SN*DN. Error bars are ± 1 standard deviation for a population of 5-19 samples per product value. The bottom graph shows a scatter plot of curling versus the scaled log of the product SN*DN*DP. A total of 45 data points are plotted.

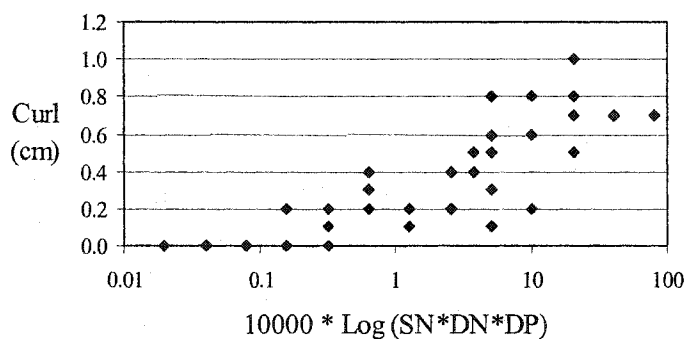
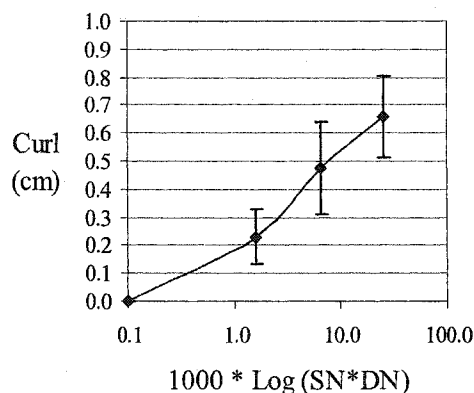
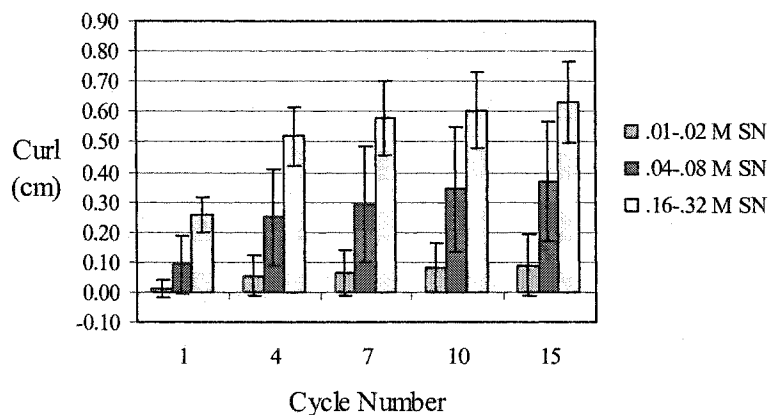
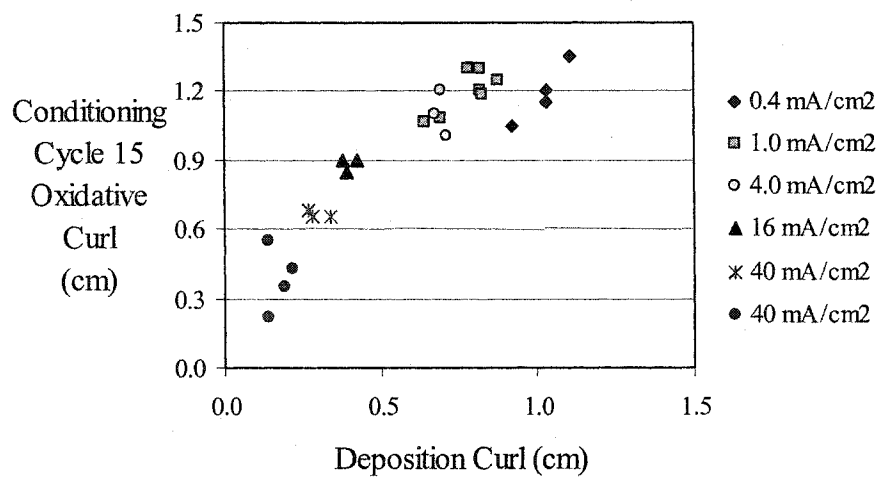
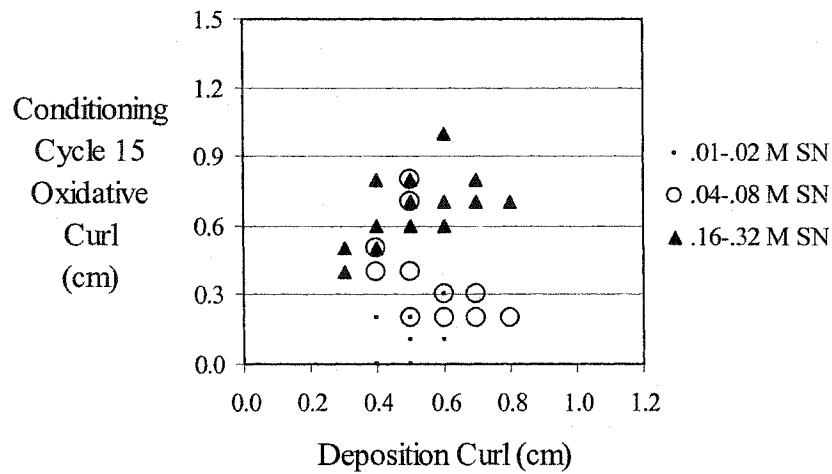


Figure 3-5 Conditioning cycle 15 oxidation curling versus deposition curling (top), by SN concentration level (values as shown in the legend). Conditioning cycle 15 oxidation curling versus deposition curling (bottom), by DCD level (values as shown in the legend). Data for the bottom graph was taken from Chapter 2.



found (see Figure 3-5, bottom).

Another point of interest is whether the changes in concentrations affect the range of movement to charge exchange ratio, or movement responsiveness. Chapter 2's findings suggested that DCD does not noticeably affect this measure. However, Figure 3-6 suggests that DN, DP and SN may. Table 3-2 summarizes the averages of the ratios of ROM to charge exchange for the points in Figure 3-6, showing that low DP, high DN and high SN values may produce more responsive films in terms of mechanical activity per unit charge exchanged. For example, the average of the ratios for all samples in the "low DP, hi DN, hi SN" condition was 0.872 mm/mC while that of the "hi DP, low-mid DN, low-mid SN" condition was 0.411 mm/mC.

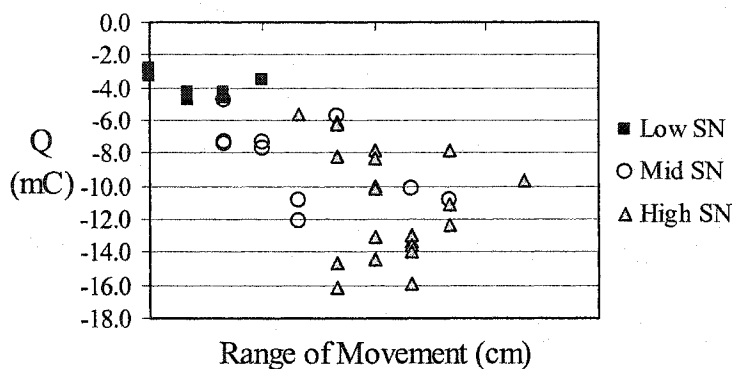
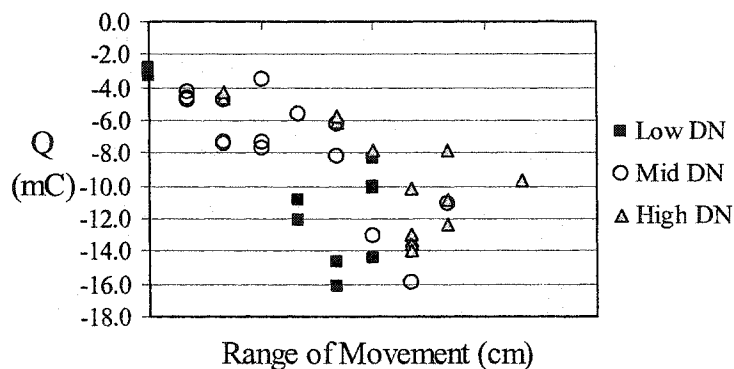
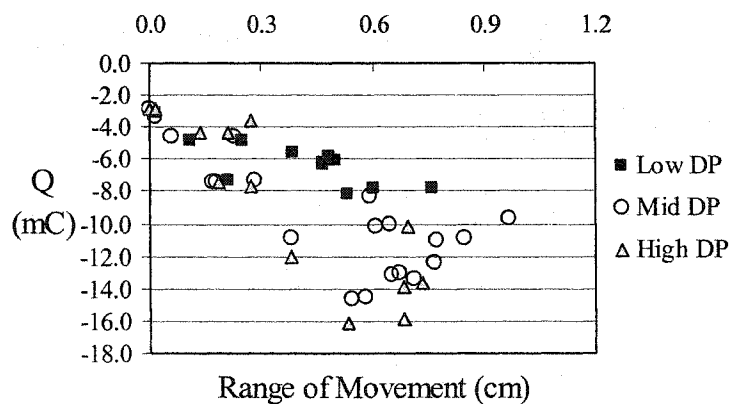
Table 3-2 Conditioning Movement Per Unit Charge Ratios

Overall 0.479 mm/mC	DP	DN	SN
Low (.01-.02 M)	0.664	0.459	0.399
Mid (.04-.08 M)	0.516	0.463	0.440
High (.16-.32 M)	0.452	0.682	0.631

The redox peaks of the CVs highlighted other effects of the concentration variations. Redox peaks have two major characteristics, peak magnitude (current) and peak position (voltage). One may also consider their shape and how sharp the peaks are. The DP, DN and SN levels affected all of these features.

Regarding the positions of the redox peaks with respect to SN, 15th cycle peaks would move towards 0 V with increasing SN concentration, especially at mid-high SN levels. Indeed, there was a clear decrease in peak separation with increasing SN levels. For a given SN level, over cycling time, the oxidation peak would become slightly more

Figure 3-6 Conditioning cycle 15 range of movement (x-axis) versus charge exchange during the reduction half cycle (mC). The top graph presents the data with respect to DP levels, the middle graph presents it with respect to DN levels, and the bottom graph presents it with respect to SN levels. Low levels are .01-.02 M, mid are .04-.08 M and high are .16-.32 M. The oxidation half cycle data points formed similar patterns.



positive while the reduction peak would become much more positive over the first few cycles before stabilizing. At low DP levels, the final reduction peaks were more anodic (positive). As DP levels increased, the peaks separated. The oxidation peaks became more positive while the reduction peaks became more negative. These findings were present in preliminary data as well. The effects of changes in concentration over the 15 cycles varied. Generally, from cycles 1 to 4, the reduction peaks moved the most, but higher levels of DP and/or lower levels of SN reduced this effect. In all cases, oxidation peaks became more positive with cycling, with high DP and low SN oxidation peaks moving most. High SN peaks moved least. Increasing DN levels led to more positive oxidation peaks. Figure 3-7 shows how DP affects the relationship between peak reduction voltages and peak reduction currents.

Regarding peak magnitudes, currents increased substantially with SN. Preliminary data again reinforced this finding. Over the 15 cycles at a given SN value, peak reduction currents dropped in magnitude over the first 4 cycles under all conditions. With DP and DN there were no clear patterns. However, at high SN levels higher DP and/or lower DN values would tend towards higher current levels. In general, the first cycle would feature the biggest reduction currents, the 4th would have the smallest, and then the currents would be fairly stable after that. The peak oxidation currents behaved a bit differently. They increased over all 15 cycles. At low SN levels, the increases were small (.44 mA). At mid SN levels, the increases were larger (.81 mA). The biggest increases in all cases took place in the early cycles. The DP and DN effects were similar (see Figures 3-8, 3-9).

Figure 3-7 Conditioning cycle 15 peak reduction currents (x-axis) versus peak voltage during the half cycle (V). Since current correlates well with exchanged charge, the Q vs. V graph looks very similar, and since range of movement correlates well with exchanged charge, it looks similar as well. Low levels =.01-.02M, mid =.04-.08M, high =.16-.32M.

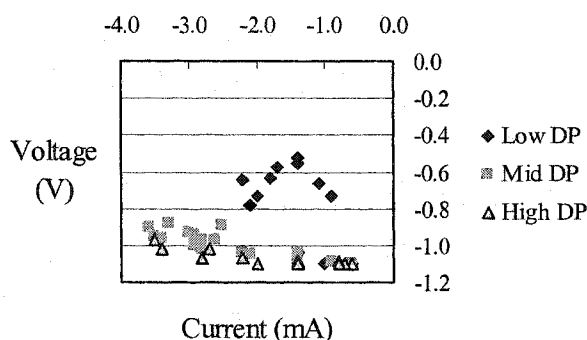


Figure 3-8 Peak reduction current versus cycle number, by SN concentration group. The low, medium and high SN concentration ranges are shown in the legend. Error bars are ± 1 standard deviation for a population of 11-23 samples per condition. Note that within the SN groupings, there was variation among DN and DP values. The lower graph plots the peak currents from the 15th oxidative half cycles versus respective SN values.

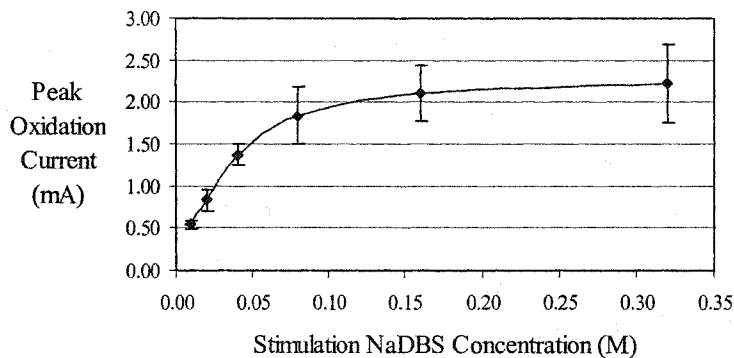
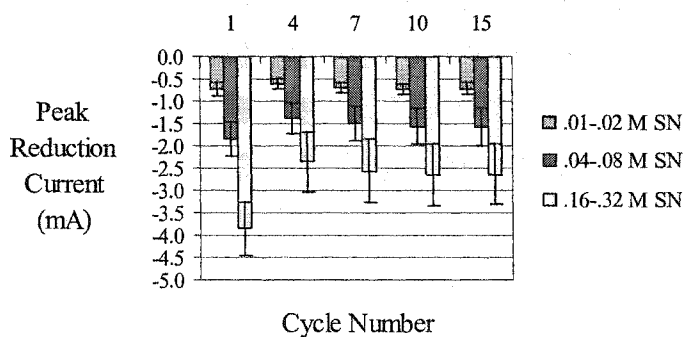
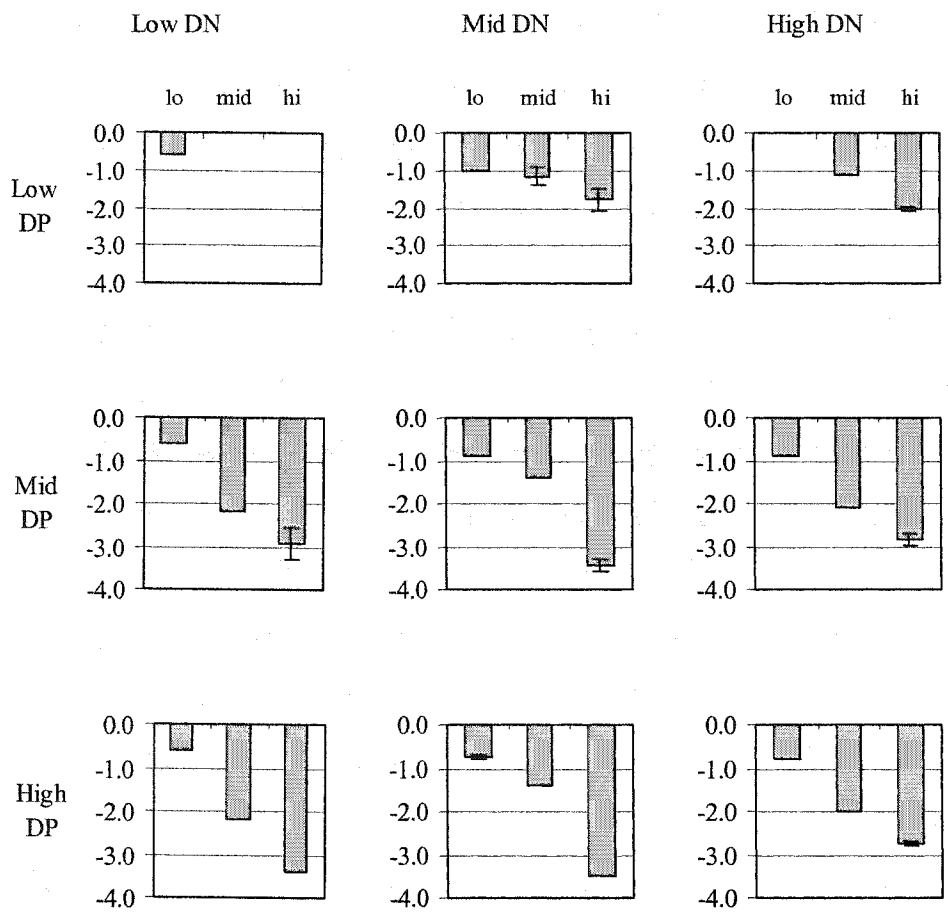


Figure 3-9 15th conditioning cycle peak reduction current, by SN, DN and DP concentration groups. The DP concentration ranges form the rows, the DN concentration ranges form the columns, and the SN concentration ranges are represented within each graph. Where present, error bars are ± 1 standard deviation for a population of 2-3 samples per condition.



Charge transfer levels were also modulated with respect to the various concentration levels (see Figure 3-10). Greater levels of charge transfer per unit peak current, with increasing DP, reflected the broader redox peaks produced at higher DP values. The sharper peaks reflective of higher SN levels were also reflected in the respective charge transfer to peak current ratios. The first reductions in all conditions involved a large reductive charge transfer followed by a much smaller one. Then the reductive charge transfer would increase slowly with time (cycles). Low DP levels produced the biggest initial drop-offs in reduction charge transfer, and the magnitude then stayed relatively low. Increasing DP (but more so SN) had the effect of increasing charge transfer, especially in the low-mid concentration range (see Figure 3-11). Preliminary data again supported these observations. For oxidative charge transfer, the biggest jumps once again occurred between cycles 1-4. However, these were jumps up and then the charge transfer increased slowly after that under all conditions over the remainder of the 15 cycles. Low DP and low SN samples increased the least though. Charge accumulation over the 15 cycles scaled up with SN to a plateau in the mid-range of SN concentration.

Most curious of all was the observation that during the first reduction, some beams would curl while others would backcurl. This has been noted by others in the past (Maw et al. 2001, Shimoda and Smela 1998) but its origin has remained a mystery. I was at least able to note some further conditions under which this phenomenon occurs. There was a clear pattern to the conditions under which the first reduction led to curling (otherwise associated with oxidation, not reduction). Mid-levels of DP combined with low levels of DN and high levels of SN concentration elicited the behaviour quite

Figure 3-10 15th conditioning half-cycle oxidation charge transfer, by SN, DN and DP concentration groups. The DP concentration ranges form the rows, the DN concentration ranges form the columns, and the SN concentration ranges are represented within each graph. Where present, error bars are ± 1 standard deviation for a population of 2-3 samples per condition.

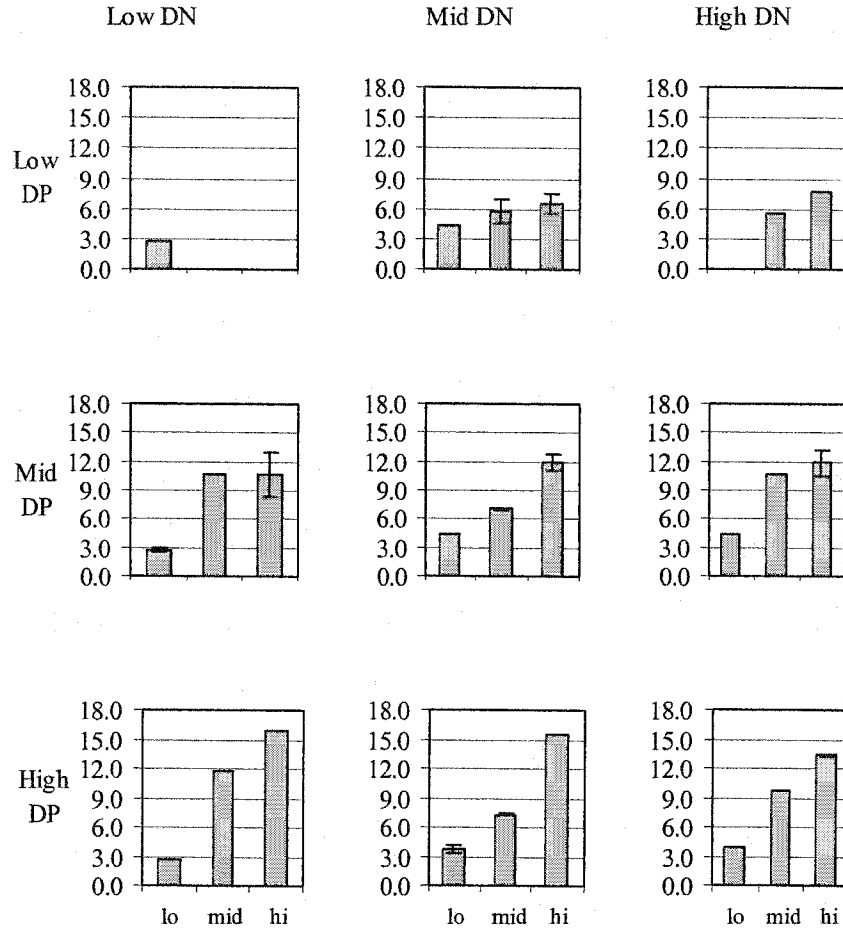
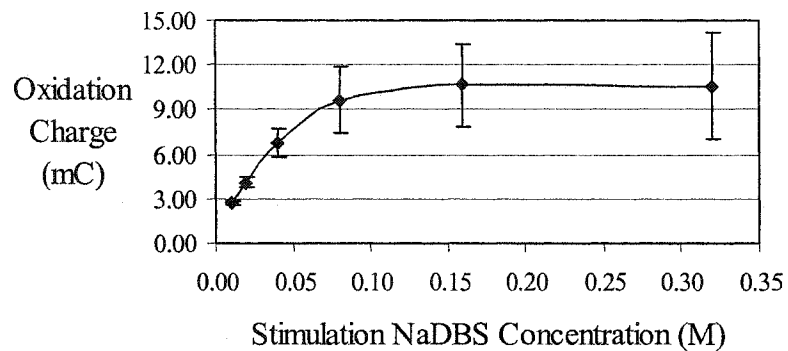
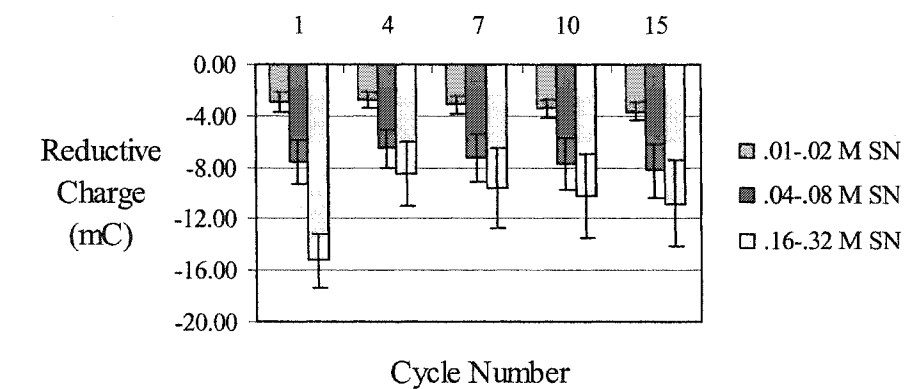


Figure 3-11 Conditioning half cycle reductive charge exchanges versus cycle number, by SN concentration group. The low, medium and high SN concentration ranges are shown in the legend. Error bars are ± 1 standard deviation for a population of 11-23 samples per condition. Note that within the SN groupings, there was variation among DN and DP values. The lower graph plots the charge exchanges from the 15th oxidative half cycles versus respective SN values.



consistently. Low levels of DP in conjunction with high levels of DN and SN produced strong initial backcurling.

In summary, all of the concentration levels played a role in the behaviour of the beams. Increases in the DP concentration levels led to increases in peak separation and to a lesser extent, increases in movement per unit charge transfer. Also, the redox peaks were broader. At high DP levels, over 15 cycles, the reduction peaks moved less while the oxidation peaks moved more. Increases in the DN concentration levels led to slightly increased curling. Also, oxidative peaks were more positive. SN, however, had the greatest influence. Increases in SN concentration led to increased peak current values, curling, net oxidative curling over 15 cycles, charge accumulation, sharper peaks, and decreased peak separation as both peaks moved towards 0 V. At low SN levels, over 15 cycles, reduction peaks moved less while oxidation peaks moved more. Interaction effects were shown to be potentially influential, as evidenced by the anomalous first reduction curling behaviour.

3.3.3 Voltage Steps

After the conditioning cycles, each bending beam was stimulated with 5 cycles of voltage steps. The step levels were -1.1 and +0.4 V and the cycling took place at .05 Hz i.e. each step lasted 10 seconds.

Charge accumulation over the 5 steps was affected by the SN concentration levels. At low SN levels, the accumulation was negative (-2.5 mC) while at mid-high levels, the accumulation was positive (1.5 to 3.0 mC). The amount of curling that took place during the 5th cycle was not substantially affected by either of the deposition concentrations

alone, although increases in DN from the mid-high concentration range did tend to increase the curling. It was the SN concentration that once again had the greatest effect (see Figure 3-12). Higher levels of SN concentration produced higher levels of curling except at high levels of DN and DP. Interaction effects were suggested by a very linear relationship between curling and the log of the scaled product of the NaDBS concentrations, as well as by a scatter plot of curling versus the log of the product of all three concentrations. The amount of curling during voltage step stimulation versus the conditioning cycles was increased by 25-50%. Charge transfers also increased, slightly more. Lower valued increases were associated with higher SN levels.

In terms of the peak currents produced by the voltage steps, the times of the oxidation peaks were only sensitive to the SN concentration. High SN levels decreased the time to peak for oxidation. There were no clear influences on the times of the reduction peaks. The magnitude of the peaks did not appear to be influenced by DP or DN levels. SN exercised the only clear influence and that effect was pronounced. Once again, higher SN levels led to higher current levels (see Figure 3-13). Preliminary data showed the same effect. Overall, in comparison to the conditioning cyclic voltammetry, there were substantial increases in peak current magnitudes. This time the increases were 200-300%, with the higher values being associated with higher SN levels.

The most interesting findings, however, arose from the analysis of charge transfer per cycle, and how that related to current levels, curling, and the concentration levels. SN was still influential, with greater concentrations correlating with greater charge transfers especially in the low-medium SN range (see Figure 3-14). However, the DP levels had a similar influence, and more so in conjunction with medium-high levels of SN.

Figure 3-12 Curling movements during oxidative voltage steps, versus cycle number, by SN concentration group. The low, medium and high SN concentration ranges are shown in the legend. Error bars are ± 1 standard deviation for a population of 11-18 samples per condition. Note that within the SN groupings, there was variation among DN and DP values.

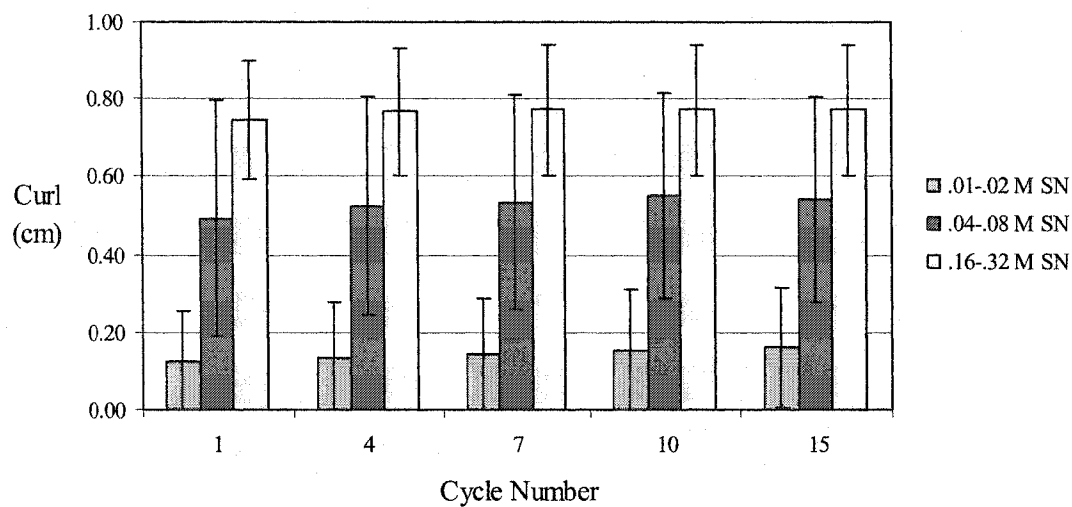


Figure 3-13 Voltage step peak reduction current versus cycle number, by SN concentration group. The low, medium and high SN concentration ranges are shown in the legend. Error bars are ± 1 standard deviation for a population of 11-18 samples per condition. Note that within the SN groupings, there was variation among DN and DP values. The lower graph plots the peak currents from the 5th reductive half cycles versus respective SN values.

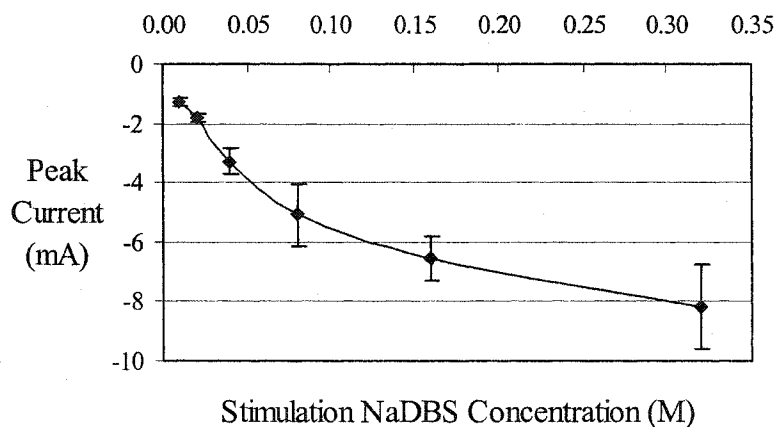
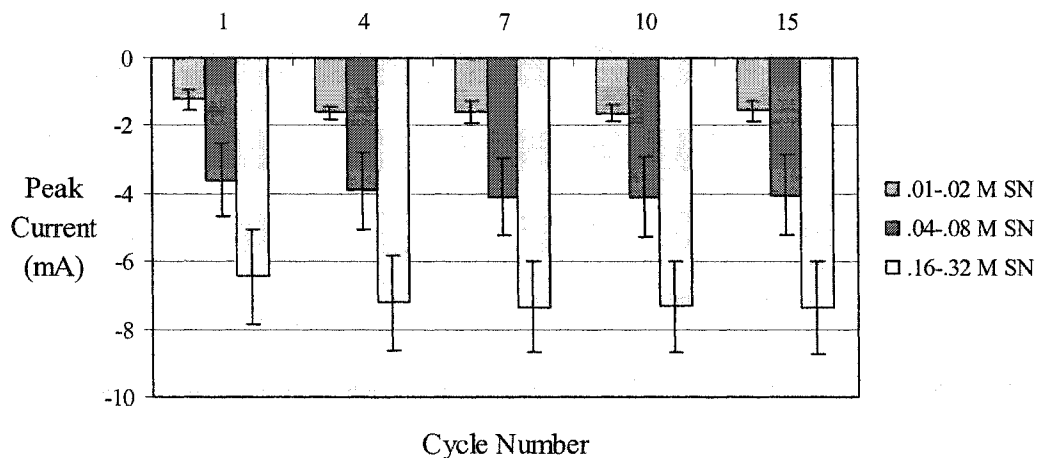
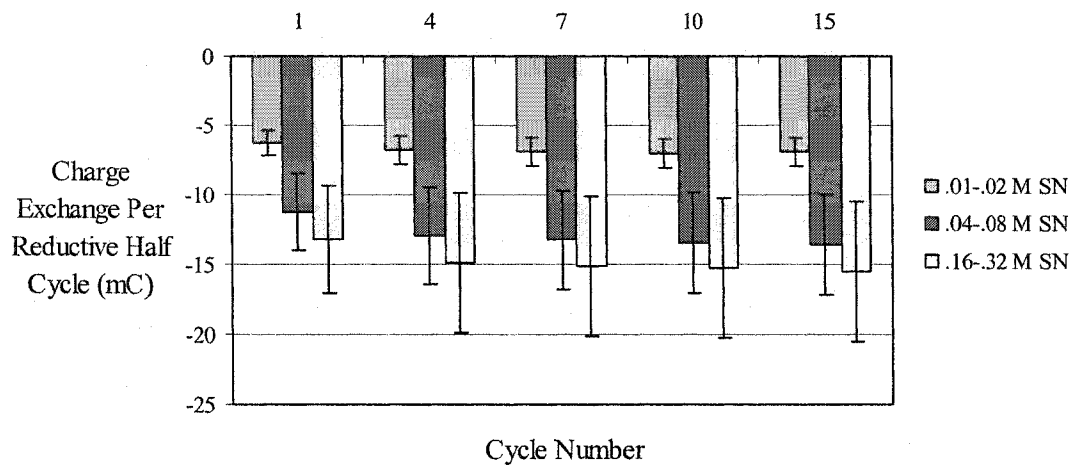


Figure 3-14 Voltage step half cycle reductive charge exchanges versus cycle number, by SN concentration group. The low, medium and high SN concentration ranges are shown in the legend. Error bars are ± 1 standard deviation for a population of 11-23 samples per condition. Note that within the SN groupings, there was variation among DN and DP values.



In addition, there was a notable effect of higher pyrrole levels producing films that would exhibit higher charge transfer values for a given amount of curl. DN produced the opposite effect. Higher DN levels created films that curled more for a given charge transfer. These and the effects from SN concentration changes are shown in Table 3-3. On a sample by sample basis, Figure 3-15 illustrates the patterns.

Table 3-3 Voltage Step Movement Per Unit Charge Ratios

Overall 0.412 mm/mC	DP	DN	SN
Low (.01-.02 M)	0.531	0.200	0.199
Mid (.04-.08 M)	0.403	0.374	0.417
High (.16-.32 M)	0.331	0.621	0.538

The pyrrole and SN levels had opposite effects on the relationship between peak current levels and charge transfer (reflecting how well the peak currents were maintained over the half cycle). Increasing pyrrole levels would increase the ratio of charge transfer to peak current while high SN levels often decreased the ratio (see Figure 3-16). Comparisons of the amperograms clearly show that as SN increases, the currents increase in magnitude but shorten in duration. That is, the current levels rise higher and fall faster at higher SN concentrations. The effects of DP and SN can most easily be seen in the amperograms of Figure 3-17.

The values of the variables generally did not change very much over the 5 voltage steps. A slight jump up in the magnitude of peak currents was observed from the 1st to the 2nd cycle during reduction. However, those values remained largely constant after that.

Figure 3-15 Voltage step cycle 5 reductive range of movement (x-axis) versus charge exchange during the half cycle (mC). The top graph presents the data with respect to DP levels, the middle graph presents it with respect to DN levels, and the bottom graph presents it with respect to SN levels. Low levels are .01-.02 M, mid are .04-.08 M and high are .16-.32 M.

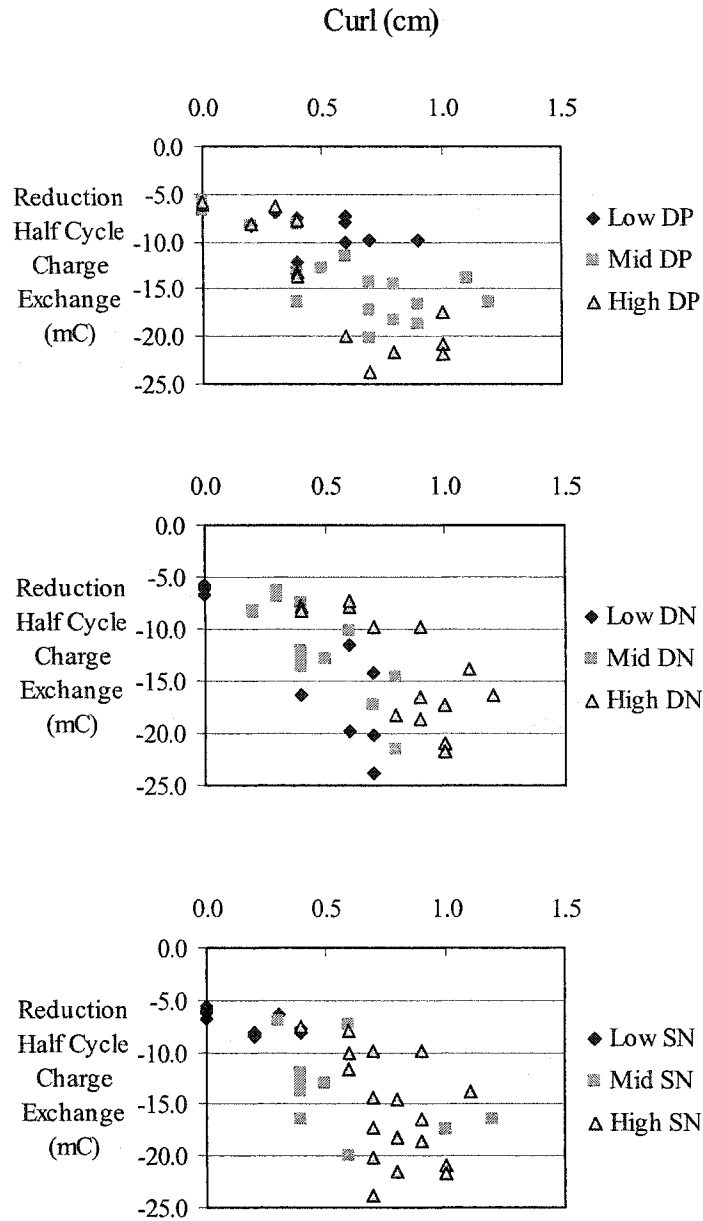


Figure 3-16 Voltage step cycle 5 reductive half cycle charge exchange (x-axis) versus peak current during the half cycle (mC). The top graph presents the data with respect to DP levels, the middle graph presents it with respect to DN levels, and the bottom graph presents it with respect to SN levels. Low levels are .01-.02 M, mid are .04-.08 M and high are .16-.32 M.

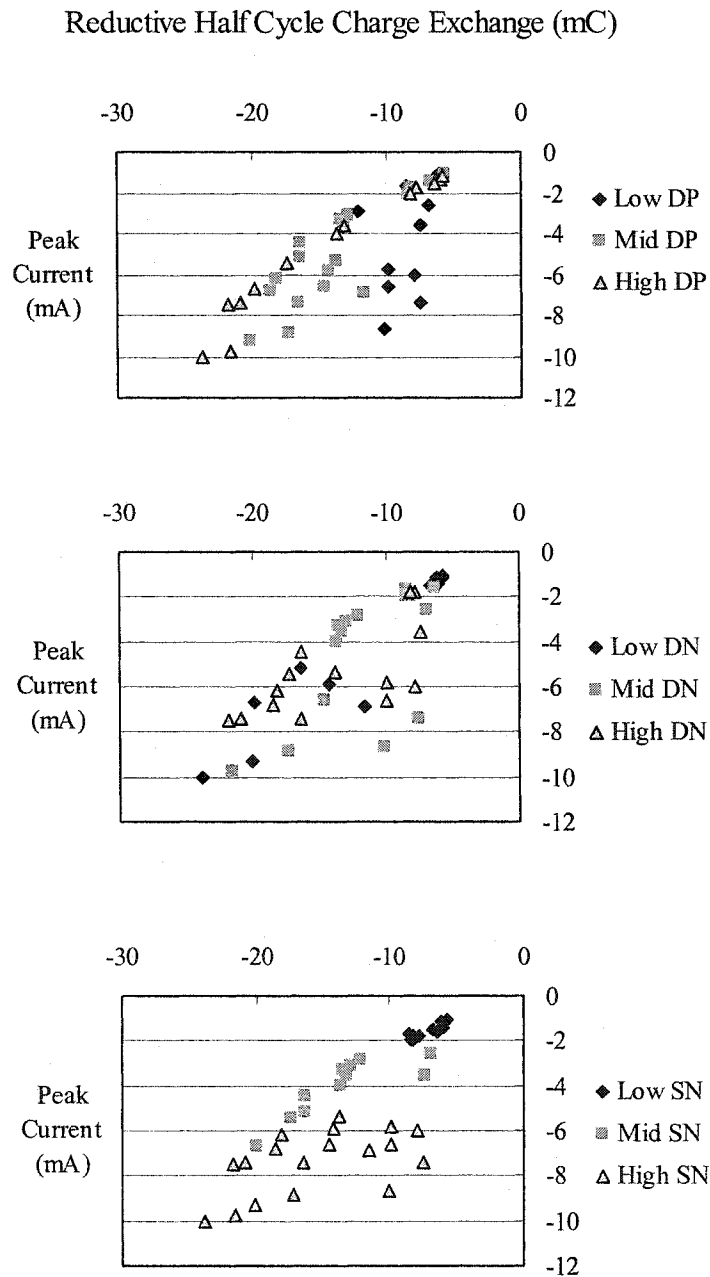
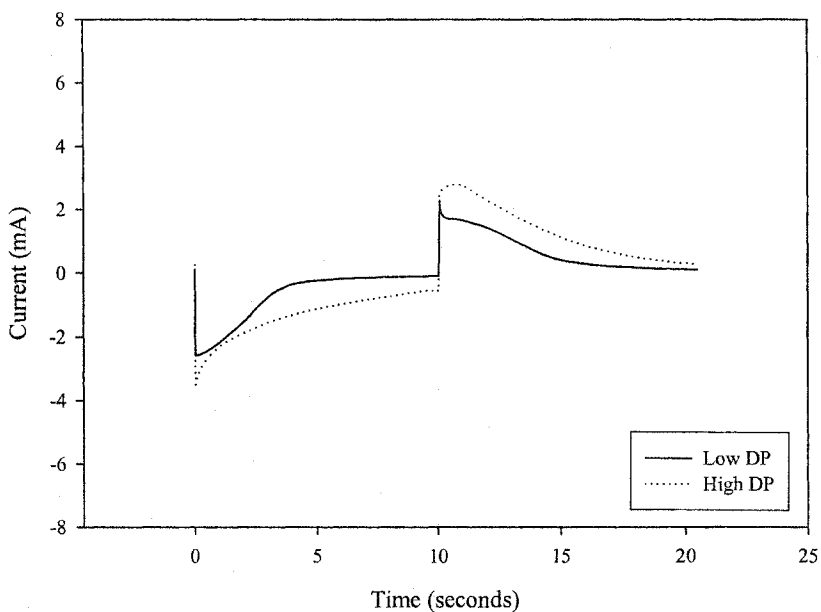
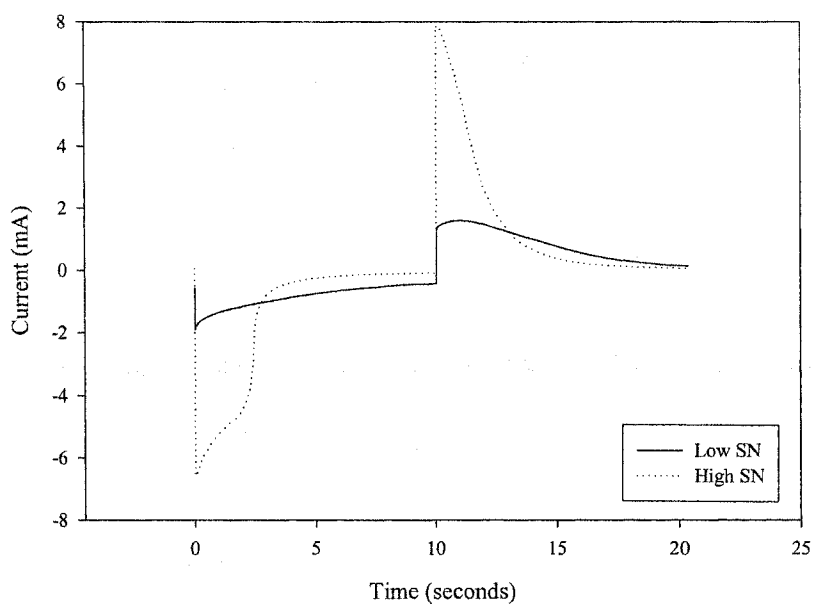


Figure 3-17 Voltage step amperograms sampled at 100 Hz and collected using LabVIEW software. The top plot helps show the effects of varying the stimulation NaDBS concentration, where .08 M DP and .08 M DN were used with the .02 M SN sample and where .04 M DP and .08 M DN were used with the .32 M sample. The bottom plot shows the effects of varying pyrrole concentration during deposition. DN and SN are both .04 M for the two plots shown. Data analysis was performed using custom Matlab[®] routines.



As discussed previously (Maw et al. 2001), the amount of charge exchanged during these cycles under ideal conditions should have been 11% of the deposition charge (24.75 mC in this experiment). Individual samples ranged from 2.4% to 10.6%. The three concentrations had differing effects on these values. DN had no apparent effect. SN and DP had noteworthy effects, however, and their interaction produced even clearer results. Table 3-4 provides the details. The 10.6% result arose from a .02 M DN, .32 M DP and .32 M SN combination and all high DP*SN products had high scores.

Table 3-4 Voltage Step Percentage Charge Exchanges by Condition

Overall 5.60 %	DP	DN	SN
Low (.01-.02 M)	3.83	5.48	3.06
Mid (.04-.08 M)	6.07	5.22	6.03
High (.16-.32 M)	6.33	6.14	6.87

Aside from the weak interaction effects influencing curling extent, the voltage step cycling reinforced the view that SN concentrations are most influential in determining the dynamic contractile activity of PPy(DBS) films. Increases in SN levels led to increases in curling, charge transfer, and current peaks. They decreased the time to reach (and fall from) those peaks and they also decreased the ratio of charge transfer to peak current. Pyrrole levels were also found to be important, but in more isolated ways. Higher pyrrole levels produced greater charge transfers per unit curl. They also produced a greater charge transfer to peak current ratio. DN concentrations were shown to interact with the others, and were shown to be important to the extent that they produced the opposite effect of pyrrole on charge transfer per unit curl. DP and SN were both found to be important in affecting the charge exchange capacity of the beams. Higher

concentration levels produced beams that operated at higher levels of theoretical efficiency.

3.3.4 Current Steps

After the voltage step cycles, each bending beam was stimulated with 5 cycles of current steps. The current steps were not the same for every beam. Current step levels were set at either 5 mC or at 100% of the maximum charge transfer that took place during the voltage steps. In all, 17 samples were stimulated at 5 mC, and 19 were stimulated at 100%. The 5 mC samples could also be converted to equivalent percentages and this perspective was employed in the examination of the data where appropriate. In all cases, the step levels were symmetric (e.g. ± 1.5 mA) and the cycling took place at .05 Hz.

In most cases, the 5 mC samples were stimulated at less than 100% of their maximum charge transfer during the voltage steps. Those stimulated at greater than 100% all failed. With regards to their curling extent, only SN had a strong influence. Increasing SN levels led to an increase in curling extent over most of the SN concentration range, although at high SN levels there may have been a slight decrease. The actual percentage of maximum that 5 mC represented varied with DP concentration. The percentages were somewhat lower at mid-high pyrrole values. The behaviour of the peak redox voltage levels was influenced primarily by SN. As SN increased, the peak redox voltage levels decreased in magnitude. This produced a surprising situation whereby lower voltage levels actually correlated with greater curling, keeping in mind that 5 mC was being exchanged each current step. However, DN also played a role. High DN films curled more for a given stimulation voltage. Equivalently, high DN films

required a higher stimulation voltage to produce a given amount of curl (since the slope was negative in the oxidative peak voltage/curling relationship).

The behaviour of the 100% samples was somewhat different. Keeping in mind that during the voltage steps higher SN levels brought on higher charge transfer values, it was not surprising then that increases in SN values correlated with increases in curling extent, at least in the low-medium DN range. At high DN levels, increases in SN (from mid-high levels) led to decreased curling activity. As SN levels increased, peak oxidation voltages decreased in magnitude, except at high DN levels where the situation was unclear. While the peak oxidation voltages decreased, the peak reduction voltages became slightly greater in magnitude under the same circumstances. To a lesser extent, increasing DN levels also seemed to increase the magnitude of the peak reduction voltages. Tying together these findings, increased charge transfer (and curling) was produced when peak oxidative voltages were low in magnitude, and when peak reductive voltages were high. It was also noted for the 100% samples (especially those at mid-high SN values), the reduction voltage would slowly increase in magnitude over the course of the 10 second step, only to increase dramatically and suddenly to a new level towards the end of the 10 second step. If this rapid increase in voltage took place earlier in the cycle then it became clear that the fiber was in the process of failing (electrochemically and/or through delamination).

In all cases of the 5 mC and 100% stimulation, increases in charge transfer correlated with increases in curling activity. However, the correlation was not nearly as strong as in my first experiment that varied deposition current density (Maw et al. 2001).

Given the variation in peak voltage values, I analyzed the variation in the difference between the peak values. The results were quite different between the 5 mC samples and the 100% samples. With the 5 mC samples, the peak to peak difference decreased with increasing SN over the low-medium concentration range and then stayed constant. Also, curling extent varied inversely with peak difference. With the 100% samples, the peak to peak differences did not change with respect to SN or curling extent.

Changes in curling extent and/or voltage peak values over the 5 current step cycles were generally small or non-existent.

In summary, the picture that the current steps presented was quite complex. SN again played an important role. For stimulation with a given charge transfer (i.e. 5 mC), higher SN levels produced more curl and the curl came about at lower magnitude voltages. DP seemed to establish the overall charge transfer (and therefore curling) capacity of the film, while DN played a role in determining how responsive a given film was to voltage stimulation. For stimulation at maximum charge capacity, higher SN levels had the effect of shifting the peaks negatively, in parallel. That is, the degree of peak difference did not change. If a film was pushed beyond this "maximum capacity", clear indicators of this situation were observed in the reduction voltage behaviour.

3.3.5 Post-Step Cycles

After the current step cycles, each bending beam was once again cycled 15 times between -1.1 and +0.4 V at 150 mV/s with a ramp function. In other words, the conditioning procedure was repeated.

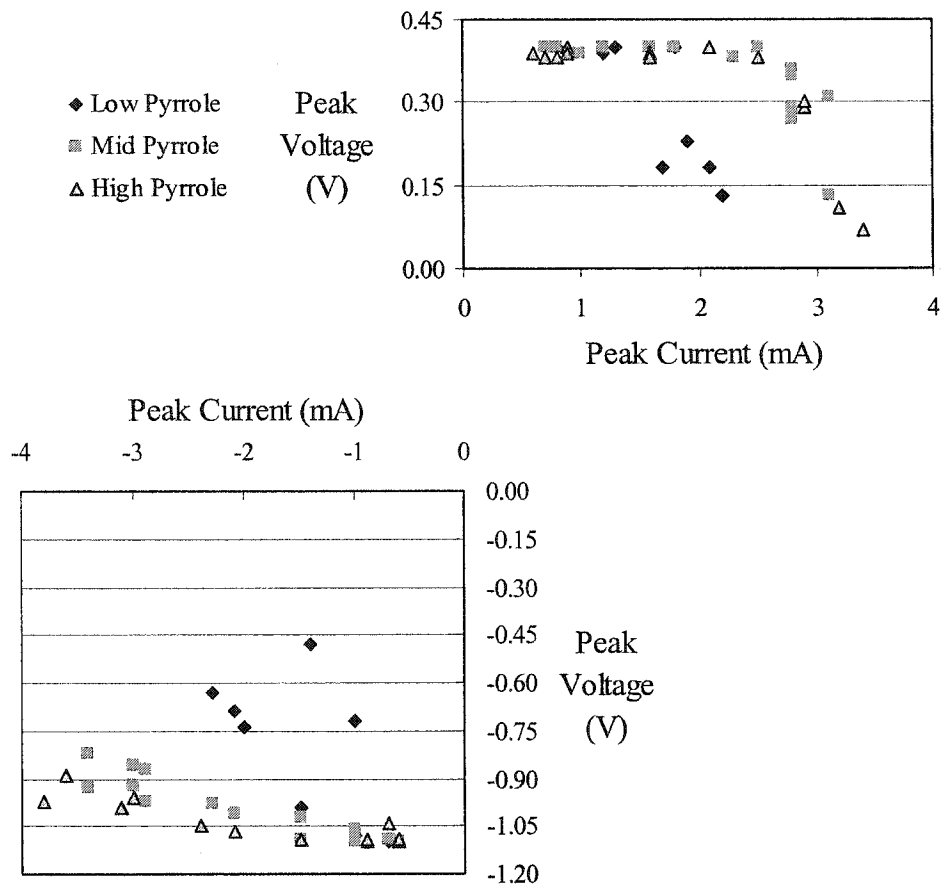
In general, the behaviour of the beams at this stage was reflective of how they behaved at the end of the conditioning phase. There were only four noteworthy discrepancies from this general characterization. The first is that most of the peak current levels, charge transfers, and curling extents were slightly greater in magnitude. The second is that the first cycle was different than the other cycles in the way that the early conditioning cycles had also been different from later cycles. However, with the post-step cycling, this effect was less pronounced. The third major difference was apparent in the peak voltages. In all but the high SN conditions, the 15th cycle oxidation peaks were at or beyond the cycling limit. The high SN oxidation peaks also moved away from 0 V with cycling, but not as much as in the low-mid SN conditions. Meanwhile, the low SN reduction peaks were also at or beyond the cycling limit while the mid-high SN reduction peaks actually moved slightly towards 0 V with cycling. Indeed, over the 15 cycles, peak separation increased in all cases. However, looking just at the last cycles, at high SN levels there was relatively less peak separation, and the peaks were really only captured at high SN levels. The interactions between the peak voltages and the charges exchanged and peak currents produced is illustrated in Figure 3-18.

The fourth and final main difference between the conditioning and post-step data was reflected in the movement responsiveness ratios (curling range of motion over charge exchanged, per half cycle). In the conditioning cycles, there were some trends (see Table 3-2) but none of them were very clear. This was not the case for the post-step cycles. Here again the DP levels were not very influential. However, both DN and DP levels were (Table 3-5 below), with substantial differences between the low and high conditions.

Table 3-5 Post-Step Movement Per Unit Charge Ratios

Overall 0.432 mm/mC	DP	DN	SN
Low (.01-.02 M)	0.493	0.227	0.272
Mid (.04-.08 M)	0.409	0.446	0.451
High (.16-.32 M)	0.421	0.614	0.542

Figure 3-18 Post-step cycle 15 reductive half cycle peak currents (x-axes) versus peak voltage during the half cycle (V). Both graphs present the data with respect to DP levels, with the top graph showing the oxidative data and the bottom graph showing the reductive data. Low levels are .01-.02 M, mid are .04-.08 M and high are .16-.32 M.



It should also be noted that there were no clear differences in the various post-step measured values between samples stimulated at 5 mC and those stimulated at 100% during the current steps.

3.3.6 Beam Motion Analysis

As in previous work (Maw et al. 2001), video footage of the beam curling was studied for patterns of behaviour. In general, these patterns were similar to those of the earlier work. However, more detail was revealed with the current work, including some very consistent and interesting patterns. First of all, during the conditioning cycles, the beams generally started in a backcurled position (from the deposition) and gradually moved into a more curled position. This was generally continued during the voltage steps. However, during the current stimulation and post-step cycling, the range of curling either shifted or expanded in the reductive direction. More specifically, there was an average net curling effect of +0.184 cm during the conditioning cycles, and of +0.071 cm during the voltage steps. Conversely, there was an average net backcurling of -0.053 cm during the current steps and of -0.036 cm during the post-step cycling.

There were also very characteristic "types" of movements exhibited by the beams. Many movements were pendular (starting and ending at low velocity, very smooth overall). Others showed characteristic pauses at the end of reduction and/or oxidation. Others started moving very rapidly and then slowed. All of these phenomena were a function of the current levels reflected in the CVs and amperograms. Low current levels were associated with either no movement or very slow movement. High current levels produced fast movements. In fact, one could very accurately predict the nature of a

beam's movement pattern by simply examining the beam's CV or amperogram under any particular stimulation scheme.

3.3.7 Film Adhesion

After the post-step cycles were complete, the beams were rinsed in deionized water and then stored in air for 17.5 to 74 hours (most were approximately 24 hours). They were then subjected to a peel test. The peel test was meant to reveal how all of the cycling may have affected the adhesion of the PPy(DBS) to the gold-coated Kapton[®]. In 3 of 60 cases there was no peeling at all. Another 2 experienced partial peeling and another 4 were mostly peeled. The rest peeled off completely, with varying levels of effort required. A qualitative scale was applied to this "effort", and the results were surprisingly clear. The tape removed either most of or all of the PPy(DBS)/metal bilayer. Clearly, the adherence of the film to the metal layer was quite sound. It was the adherence of the metal to the Kapton[®] that was less strong. An analysis of the data showed that higher deposition voltages led to the production of films that peeled off more easily. This stemmed from the fact that the higher the pyrrole monomer concentration, the more adherent the film to the Kapton[®]. Furthermore, of those 10 samples that delaminated at some point during the stimulation procedures, 5 had low DP values and 4 had mid-range DP values. Also interestingly, 7 of these 10 samples had a low/medium/high molar combination of some sort. Almost all samples that had some variation of this molar mix had poor adhesion.

3.4 Discussion

Several investigators have described differences in relevant polypyrrole electrochemical behaviour as a function of monomer and/or electrolyte and dopant concentration levels (Beck et al. 1994, Naoi et al. 1995, Otero and Sansiñena 1996, Iseki et al. 1991, Li and Qian 1989, Ohno et al. 1994, Otero and Rodríguez 1994, Qian et al. 1986). Like me, they have looked at what happens to redox peaks and currents, and to charge exchange when these variables are altered. For example, Naoi et al. (1995) found that increases in DN from my low to mid ranges resulted in higher peak currents during cyclic voltammetry. I saw a weak version of this effect. Otero and Sansiñena (1996) found that during current steps, increases in SN led to decreases in peak voltages and that during voltage steps, increases in SN led to increases in peak currents. I found this too. With Rodríguez (1994), Otero worked with PPy's polymer relative polythiophene and noted that the lower the monomer concentration, the lower the charge exchange capacity on voltage steps. However, increases in DP would increase DCD at constant deposition voltage. I found the same on the first point, and my data would suggest that the same would be true on the second.

Iseki et al. (1991) found that the response speed to a voltage step increased with KCl_{aq} . In my study, time to peak was reduced with high SN levels. They also stated that the ion-capturing capacity of a PPy film is constant. I would say "relatively constant", as I did see a slight increase in charge exchange in the films over cycling time. The subtle changes that I observed could grow even more with time, but further tests are needed.

Li and Qian (1989) worked with $\text{PPy}(\text{NO}_3)$ and found that higher stimulation electrolyte levels rounded their redox peaks and moved them slightly cathodically. That

differed from my findings on both counts but then again, their anions were more mobile. With PPy(SO₄), Qian et al. (1986) found that redox currents increased with monomer concentration in CV depositions. At best, I saw the currents rise and then fall with monomer concentration, but only weakly. Similarly, Ohno et al. (1994) saw peak oxidative currents increase and then decrease with electrolyte (LiClO₄) concentration (although the decrease was beyond 1 M). I certainly saw an increase, but I did not probe far enough along in the concentration range to see the decrease. In any event, the more mobile perchlorate anion would again make direct comparisons with PPy(DBS) difficult.

One of the most remarkable findings in the present work was the range of charge exchange capacities in the films. This underlined the importance of these concentration variables in PPy(DBS) mediated actuation. The charge exchange capacity reflects the charge carrying and therefore charge exchange capacity of the films. Since that is so intimately related to strain, it significantly restricts the capabilities of the films to do useful work when it is low.

As in my previous work (Maw et al. 2001), the beams curled during the deposition process with the PPy(DBS)-coated surface facing outwards. In that work, I had found that the amount of deposition curling had been a good predictor of later performance (curling extent). As well, the deposition curling extent seemed to vary with respect to deposition time, deposition current density (DCD) or some combination of the two. The present experiment held both of these variables constant. As a result, the amount of deposition curling was fairly constant across samples. Also, as predicted, the performance remained fairly constant at each of the different levels of stimulation NaDBS.

Whereas in my DCD study (Maw et al. 2001) I did not find any clear results to indicate that DCD affected movement responsiveness substantially, I did find that the DP, DN and SN variables influenced it noticeably in this study. As such, my data continue to support Otero and Rodríguez' (1993) findings that the extent of movement is proportional to charge, and that rate of movement is proportional to current. However, I clearly showed that the proportionality constant depends on the three concentrations and that it can be optimized.

Moreover, the fact that movement responsiveness was optimized by a particular combination of the three concentrations underlines the fact that these variables interact and that it is not enough to simply focus on any one of them. The effect of changing one variable while holding the other two constant is entirely dependent on the values that are held constant. Generalizations based on a fixed value for any of the concentrations are therefore not advised. Figures 3-9 gives a sense of this even for one of the most consistent patterns that I found (increases in SN lead to increases in charge exchange). When DP is low and DN is moderate, the increases due to SN are muted. When DN is low, the increases from low to mid SN values are large, but increases from mid to high SN values are almost non-existent.

So where does all of this leave us with respect to my goal of emulating natural muscle? In other words, are there any parallels in terms of form or function? There are some very basic similarities. With the beams, the initiating signal or "action potential" travels down the working electrode and initiates a change in how the PPy chains interact with each other. Cations go in and out of the polymer matrix with cycling, but more importantly, the process is diffusion rate limited, just as the distribution of calcium ions is

in real muscle. However, natural muscle is optimized for cation cycling so as to minimize the impact of the diffusion rate limited processes (Hochachka 1994). I have not yet begun to work on this problem, other than to now realize that increasing the levels of SN can help us in terms of producing higher strains and strain rates in PPy(DBS). The major differences are that PPy(DBS) is a relatively disorganized tangle of polymer chains in comparison to the finely interwoven network of machinery found in natural muscle and in PPy(DBS), the cations produce the stresses directly while they only act as a control signal in real muscle.

I have, at least, begun to explore the more functional aspects of the PPy(DBS) film in an actuation role. A logical next step will be to examine how the films cope with cycling speed and range, and to see whether they are at all sensitive to “history” i.e. past cycling activities. If they are, it will have a significant impact on how they are stimulated and controlled.

3.5 Conclusions

For the PPy(DBS)-actuated bending beams described in this chapter, curling as a result of strains transverse to the plane of the film is influenced most by stimulation NaDBS electrolyte levels, although deposition monomer and electrolyte levels also play significant roles in specific situations. These concentration variables are essential to consider when designing the performance of any PPy(DBS)-actuated mechanism.

More specifically, if growing PPy(DBS) galvanostatically, higher levels of DN and more importantly DP, will result in lower deposition potentials. Adhesion between the beam layers was optimized by using higher DP levels, presumably as a result of the relatively low deposition voltage levels.

During cyclic voltammetry, increasing SN levels will increase peak currents, charge exchange, curling, and charge accumulation. It will also reduce peak separation and sharpen the redox peaks. Increases in DN levels will produce films that curl more during cyclic voltammetry, and whose oxidation peaks migrate anodically with time. Increases in DP increase peak separation and broaden the peaks.

Voltage steps, all other things being equal, produce more curling than cyclic voltammetry as was found previously (Maw et al. 2001). Increases in SN sharpen the current peaks, while increases in DP widen them. High SN levels produce higher peak currents, but also shorter duration currents, whereas low SN values result in long low currents. Mid to high DP and SN levels combine to create films that maximize their potential charge carrying capacity, while films stimulated with more charge (higher currents) than they can take in are quickly damaged and fail.

Clearly, DP sets the capacity of PPy(DBS) films to carry and exchange charge. SN can then be manipulated to make best use of that capacity. On the other hand, movement responsiveness or the amount of strain per unit charge, is optimized by using low DP in combination with high DN and SN levels in any stimulation mode.

The dynamics of the beam movements are determined by the stimulation currents. Their magnitude at any given time is a reflection of the strain rate at that time. Furthermore, since we have the ability to create different shapes of CVs, voltammograms and amperograms by altering the three concentration levels (DP, DN, and SN), we have the ability to create the shapes of these plots that reflect the functionality that we may want. For example, if one wants a fast moving beam, then one wants high, short lasting peak currents, and these can be achieved with high SN levels. If, on the other hand, movement responsiveness is more important, then one would also want high DN and low DP levels. These examples illustrate the point that these concentration values are absolutely critical in determining everything from endurance to strain to strain rate in PPy(DBS)-actuated mechanisms. They should be carefully considered at all times.

3.6 References

- An, H., Haga, Y., Yuguchi, T., and Yosomiya, R. (1994) "Synthesis of polypyrrole by electrochemical polymerization using organic anion electrolytes and its application", *Die Angewandte Makromolekulare Chemie*, Vol. 218, #3814, pg. 137-151
- Barisci, J.N., Murray, P., Small, C.J., and Wallace, G.G. (1996) "Studies of the preparation and analytical application of polypyrrole-coated microelectrodes for determination of aluminum", *Electroanalysis*, Vol. 8, #4, pg. 330-335
- Baughman, R.H. (1996) "Conducting polymer artificial muscles", *Synthetic Metals*, Vol. 78, pg. 339-53
- Beck, F., Michaelis, R., Schloten, F., and Zinger, B. (1994) "Filmforming electropolymerization of pyrrole on iron in aqueous oxalic acid", *Electrochimica Acta*, Vol. 39, #2, pg. 229-234
- Bilger, R. and Heinze, J. (1993) "Role of the formation potential on the redox processes of polypyrrole studied by an electrochemical quartz microbalance", *Synthetic Metals*, Vol. 55-57, pg. 1424-1429
- Bobacka, J., Gao, Z., Ivaska, A., and Lewenstam, A. (1994) "Mechanism of ionic and redox sensitivity of p-type conducting polymers Part 2. Experimental study of polypyrrole", *J. Electroanal. Chem.*, Vol. 368, pg. 33-41
- Bohon, K. and Krause, S. (1998) "An electrorheological fluid and siloxane gel based electromechanical actuator: working toward an artificial muscle", *J. Poly. Sci. B. Polym. Phys.*, pg. 1091-94

Buckley, L.J., Roylance, D.K., and Wnek, G.E. (1987) "Influence of dopant ion and synthesis variables on mechanical properties of polypyrrole films", *Journal of Polymer Science: Part B: Polymer Physics*, Vol. 25, pg. 2179-2188

Caldwell, D.G. and Taylor, P.M. (1990) "Chemically stimulated pseudo-muscular actuation", *Int. J. Engng. Sci.*, Vol. 28, #8, pg. 797-808

Cheung, K.M., Bloor, D., and Stevens, G.C. (1988) "Characterization of polypyrrole electropolymerized on different electrodes", *Polymer*, Vol. 29, September, pg. 1709-17

Della Santa, A., De Rossi, D., and Mazzoldi, A. (1997) "Characterization and modeling of a conducting polymer muscle-like linear actuator", *Smart Mater. Struct.*, Vol. 6, pg. 23-24

Dyreklev, P., Granström, M., Inganäs, O., Gunaratne, L.M.W.K., Senadeera, G.K.R., Skaarup, S., and West, K. (1996) "The influence of polymerization rate on conductivity and crystallinity of electropolymerized polypyrrole", *Polymer*, Vol. 37, #13, pg. 2609-13

Hahn, S.J., Gajda, W.J., Vogelhut, P.O., and Zeller, M.V. (1986) "Auger and infrared study of polypyrrole films: evidence of chemical changes during electrochemical deposition and aging in air", *Synthetic Metals*, Vol. 14, pg. 89-96

Henneman, E., Somjen, G., and Carpenter, D.O. (1965) "Functional significance of cell size in spinal motoneurons", *Journal of Neurophysiology*, Vol. 28, pg 560-80

Hochachka, Peter W. (1994) **Muscles as Molecular and Metabolic Machines**, CRC Press, USA

Hunter, I.W. and Lafontaine, S. (1992) "A comparison of muscle with artificial actuators", *Proceedings of the IEEE Sensors and Actuators Workshop*, Hilton Head Island, June 21-25

Iseki, M., Kuhara, K., and Mizukami, A. (1991) "Study on electrically plastic devices made with electropolymerized films", *Jap. J. App. Phys.*, Vol. 30, #5, May, pg. 1117-121

John, R., John, M.J., Wallace, G.G., and Zhao, H. (1992) "Use of surfactants in the oxidative synthesis of conductive electroactive polymers", In: **Electrochemistry in Colloids and Dispersions**, R.A. Mackay and J. Texter [eds], VCH Publishers Inc., NY

Kaneto, K., Kaneko, M., Min, Y., and MacDiarmid, A.G. (1995) "Artificial muscle: electromechanical actuators using polyaniline films", *Synthetic Metals*, Vol. 71, pg. 2211-2212

Kaplin, D.A. and Qutubuddin, S. (1995) "Electrochemically synthesized polypyrrole films: effects of polymerization potential and electrolyte type", *Polymer*, Vol. 36, #6, pg. 1275-1286

Kassim, A., Davis, F.J., and Mitchell, G.R. (1994) "The role of the counter-ion during electropolymerization of polypyrrole-camphor sulfonate films", *Synthetic Metals*, Vol. 62, pg. 41-47

Katchalsky, A. (1949) "Rapid swelling and deswelling of reversible gels of polymeric acids by ionization", *Experientia*, Vol. 5, #8, pg. 319-20

Kaynak, A. (1997) "Effect of synthesis parameters on the surface morphology of conducting polypyrrole films", *Mat. Research. Bull.*, Vol. 32, #3, pg. 271-85

Kiani, M.S. and Mitchell, G.R. (1992) "The role of the counter-ion in the preparation of polypyrrole films with enhanced properties using a pulsed electrochemical potential", *Synthetic Metals*, Vol. 48, pg. 203-18

Ko, J.M., Rhee, H.W., Park, S.-M., and Kim, C.Y. (1990) "Morphology and electrochemical properties of polypyrrole films prepared in aqueous and nonaqueous solvents", *J. Electrochem. Soc.*, Vol. 137, #3, March, pg. 905-909

Kuhn, W. (1949) "Artificial muscle model", *Experientia*, Vol. 5, #8, pg. 318-319

Kuhn, W., Hargitay, B., Katchalsky, A., and Eisenberg, H. (1950) "Reversible dilation and contraction by changing the state of ionization of high-polymer acid networks", *Nature*, Vol. 165, #4196, April 1, pg. 514-16

Kuhn, W. and Hargitay, B. (1951) "Muskelähnliche kontraktion und dehnung von netzwerken polyvalenter fadenmolekulionen", *Experientia*, Vol VII - Fasc 1, pg. 1-11

Kuhn, W., Ramel, A., and Walters, D.H. (1960) "Conversion of chemical into mechanical energy by homogenous and cross-striated polymeric systems", In: **Size and Shape Changes of Contractile Polymers**, A. Wassermann [ed], Pergamon Press, pg. 41-77

Kupila, E.-L. and Kankare, J. (1993) "Electropolymerization of pyrrole: effects of pH and anions on the conductivity and growth kinetics of polypyrrole", *Synthetic Metals*, Vol. 55-57, pg. 1402-1405

Kupila, E.-L. and Kankare, J. (1995) "Influence of electrode pretreatment, counter anions and additives on the electropolymerization of pyrrole in aqueous solutions", *Synthetic Metals*, Vol. 74, pg 241-249

Li, Y. and Qian, R. (1989) "Effect of anion and solution pH on the electrochemical behavior of polypyrrole in aqueous solution", *Synthetic Metals*, Vol. 28, pg. C127-132

Li, Y. and Qian, R. (1993) "On the nature of redox processes in the cyclic voltammetry of polypyrrole nitrate in aqueous solutions", *J. Electroanalytical Chem.*, Vol. 362, pg. 267-272

Madden, J.D., Cush, R.A., Kanigan, T.S., Brenan, C.J., and Hunter, I.W. (1999) "Encapsulated polypyrrole actuators", *Synthetic Metals*, Vol. 105, pg. 61-64

Madden, J.D., Cush, R.A., Kanigan, T.S., and Hunter, I.W. (2000) "Fast contracting polypyrrole actuators", *Synthetic Metals*, Vol. 113, pg. 185-92

Matencio, T., De Paoli, M.-A., Peres, R.C.D., Torresi, R., and Cordoba de Torresi, S.I. (1994) "Ionic diffusion processes in polypyrrole", *J. Braz. Chem. Soc.*, Vol. 5, #3, pg. 191-96

Matencio, T., De Paoli, M.-A., Peres, R.C.D., Torresi, R.M., and Cordoba de Torresi, S.I. (1995) "Ionic exchanges in dodecylbenzenesulfonate doped polypyrrole Part 1: Optical beam deflection studies", *Synthetic Metals*, Vol. 72, pg. 59-64

Maw, S., Smela, E., Yoshida, K., Sommer-Larsen, P., and Stein, R.B. (2001) "The effects of varying deposition current density on bending behaviour in PPy(DBS)-actuated bending beams", *Sensors and Actuators A*, Vol. 89, pg. 175-184

McCormac, T., Breen, W., McGee, A., Cassidy, J.F., and Lyons, M.E.G. (1995) "Cyclic voltammetry of polypyrrole dodecylbenzene sulfonate layers", *Electroanalysis*, Vol. 7, #3, pg. 287-289

Mitchell, G.R. and Geri, A. (1987) "Molecular organisation of electrochemically prepared conducting polypyrrole films", *J. Phys. D: Appl. Phys.*, Vol. 20, pg. 1346-1353

Mitchell, G.R., Davis, F.J., and Legge, C.H. (1988) "The effect of dopant molecules on the molecular order of electrically-conducting films of polypyrrole", *Synthetic Metals*, Vol. 26, pg. 247-257

Murray, P., Spinks, G.M., Wallace, G.G., and Burford, R.P. (1997) "In-situ mechanical properties of tosylate doped (pTS) polypyrrole", *Synthetic Metals*, Vol. 84, pg 847-48

Naoi, K., Oura, Y., Maeda, M., and Nakamura, S. (1995) "Electrochemistry of surfactant-doped polypyrrole film (I): Formation of columnar structure by electropolymerization", *J. Electrochem. Soc.*, Vol. 142, #2, February, pg. 417-422

Ogasawara, M., Funahashi, K., Demura, T., Hagiwara, T., and Iwata, K. (1986) "Enhancement of electrical conductivity of polypyrrole by stretching", *Synthetic Metals*, Vol. 14, pg. 61-69

Ohno, H., Yoshida, H., and Ohtsuka, Y. (1994) "Effect of salt species on the electrochemical p-doping of poly(pyrrole) films in poly(ethylene oxide) oligomers", *Solid State Ionics*, Vol. 68, pg. 125-131

Otero, T.F. and Rodríguez, J. (1993) "Polypyrrole electrogeneration at different potentials in acetonitrile and acetonitrile/water solutions", *Synthetic Metals*, Vol. 55-57, pg. 1418-23

Otero, T.F. and Rodríguez, J. (1994) "Parallel kinetic studies of the electrogeneration of conducting polymers: mixed materials, composition and properties control", *Electrochimica Acta*, Vol. 39, #2, pg. 245-53

Otero, T.F. and Sansiñena, J.M. (1996) "Artificial muscles: influence of electrolyte concentration on bilayer movement", *3rd ICIM/ECSSM '96 Proceedings*, pg. 365-370

Pautard, F.G.E. and Speakman, P.T. (1960) "Reversible supercontraction of β -keratose", *Nature*, Vol. 185, #4707, January 16, pg. 176-177

Pei, Q. and Inganäs, O. (1992) "Electrochemical applications of the bending beam method. 1. Mass transport and volume changes in polypyrrole during redox", *J. Phys. Chem.*, Vol. 96, #25, pg. 10507-514

Pei, Q. and Inganäs, O. (1993a) "Electrochemical muscles: bending strips built from conjugated polymers", *Synthetic Metals*, Vol. 55-57, pg. 3718-23

Pei, Q. and Inganäs, O. (1993b) "Electrochemical applications of the bending beam method; a novel way to study ion transport in electroactive polymers," *Sol. State Ion.*, Vol. 60, pg. 161-66

Pei, Q. and Inganäs, O. (1993c) "Electrochemical applications of the bending beam method. 2. Electroshrinking and slow relaxation in polypyrrole," *J. Phys. Chem.*, Vol. 97, pg. 6034-41

Pelrine, R.E., Kornbluh, R.D., and Joseph, J.P. (1998) "Electrostriction of polymer dielectrics with compliant electrodes as a means of actuation", *Sensors and Actuators - A Phys.*, Vol. 64, Issue 1, pg. 77-85

Peres, R.C.D., Pernaut, J.M., and DePaoli, M.A. (1989) "Properties of poly(pyrrole) films electrochemically synthesized in the presence of surfactants", *Synthetic Metals*, Vol. 28, pg. C59-C64

Qian, R., Qiu, J., and Yan, B. (1986) "Electrochemical behaviour of oxidized polypyrrole in aqueous solutions", *Synthetic Metals*, Vol. 14, pg. 81-87

Rothwell, John C. (1987) **Control of Human Voluntary Movement**, Aspen Publishers Inc, USA

Sansañena, J.M., Olazabal, V., Otero, T.F., Polo da Fonseca, C.N., and De Paoli, M.A. (1997) "A solid state artificial muscle based on polypyrrole and a solid polymeric electrolyte working in air", *Chem. Commun.*, pg. 2217-18

Satoh, M., Kaneto, K., and Yoshino, K. (1986) "Dependences of electrical and mechanical properties of conducting polypyrrole films on conditions of electrochemical polymerization in an aqueous medium", *Synthetic Metals*, Vol. 14, pg. 289-296

Shimoda, S. and Smela, E. (1998) "The effect of pH on polymerization and volume change in PPy(DBS)," *Electrochim. Acta*, Vol. 44, #2-3, pg. 219-38

Smela, E., Inganäs, O., and Lundström, I. (1993) "Conducting polymers as artificial muscles: challenges and possibilities", *J. Micromech. Microeng.*, Vol. 3, pg. 203-205

Smela, E., Inganäs, O., and Lundström, I. (1995) "Controlled folding of micrometer-size structures", *Science*, Vol. 268, June 23, pg. 1735-1738

Smela, E. (1999) "Microfabrication of PPy microactuators and other conjugated polymer devices", *J. Micromech. Microeng.*, Vol. 9, pg. 1-18

Smela, E. and Gadegaard, N. (1999) "Surprising volume change in PPy(DBS): an atomic force microscopy study", *Advanced Materials*, Vol. 11, pg. 953-57

Stanković, R., Pavlovic, O., Vojnovic, M., and Jovanovic, S. (1994) "The effects of preparation conditions on the properties of electrochemically synthesized thick films of polypyrrole", *Eur. Polym. J.*, Vol. 30, #3, pg. 385-393

Steinberg, I.Z., Oplatka, A., and Katchalsky, A. (1966) "Mechanochemical engines", *Nature*, Vol. 210, #5036, May 7, pg. 568-71

Sussman, M.V. and Katchalsky, A. (1970) "Mechanochemical turbine: a new power cycle", *Science*, Vol. 167, January 2, pg. 45-47

Timoshenko, S. (1925) "Analysis of bi-metal thermostats", *J. Opt. Soc. Am.*, Vol. 11, pg. 233-256

Wallace, G.G., Spinks, G.M., and Teasdale, P.R. (1997) **Conductive Electroactive Polymers: Intelligent Materials Systems**, Technomic Publishing, USA

Wang, G. and Shahinpoor, M. (1997) "Design for shape memory alloy rotatory joint actuators using shape memory effect and pseudoelastic effect", *SPIE*, Vol. 3040, pg. 23-30

Warren, L.F. and Anderson, D.P. (1987) "Polypyrrole films from aqueous electrolytes", *Journal of the Electrochemical Society: Electrochemical Science and Technology*, Vol. 134, #1, January, pg. 101-105

Warren, L.F., Walker, J.A., Anderson, D.P., and Rhodes, C.G. (1989) "A study of the conducting polymer morphology", *Journal of the Electrochemical Society: Electrochemical Science and Technology*, Vol. 136, #8, August, pg. 2286-2295

Wood, G.A. and Iroh, J.O. (1996) "Efficiency of electropolymerization of pyrrole onto carbon fibers", *Synthetic Metals*, Vol. 80, pg. 73-82

Yamaura, M., Hagiwara, T., and Iwata, K. (1988) "Enhancement of electrical conductivity of polypyrrole film by stretching: counter ion effect", *Synthetic Metals*, Vol. 26, pg. 209-224

4. How Stimulation History Affects the Current Behaviour of PPy(DBS)-Actuated Bending Beams

4.1 Introduction

One of the things that makes natural muscle a non-linear system is the significance of “history”. That is, at any given time, a muscle’s past is relevant to its current state. We can most easily relate to this through the idea of muscle fatigue. Tired muscles are less able and willing to produce forces that they may well have produced just seconds before. On the other hand, history can also serve to build the capabilities of muscle, as can happen through physical training. For skeletal muscle, the past influences the present in these two fundamental ways, through fatigue and through adaptive change. To try and understand how these processes work, we first need to appreciate the current understanding of how muscle contraction happens.

The process begins when a muscle fiber is stimulated to contract via the excitation of the alpha motor neuron that innervates it. The motor neuron sends an action potential down its axon to the motor end plate which abuts the muscle fiber. The arrival of the action potential (AP) at the neuromuscular junction initiates a release of the neurotransmitter acetylcholine which in turn produces a local depolarization of the muscle fiber’s membrane. This produces an AP which spreads over the muscle fiber’s membrane and into invaginations (T-tubules) that penetrate the volume of the fiber. This penetration allows internal mechanisms of the muscle fiber to become depolarized which include cisternae (sarcoplasmic reticulum) that store calcium ions. When depolarized, these cisternae release the calcium, increasing the concentration of the cation in the regions of the contractile proteins, actin and myosin, that make up the thin (1-2 μm diameter) contractile elements of the muscle fibers called myofibrils. Troponin, attached

to the actin chains, changes conformation in response to the increased levels of calcium. As troponin changes its conformation, it removes the blockage set up by another regulatory protein (tropomyosin) to expose binding sites for the heads of the myosin molecules to bind to. From the energy released in the transformation of ATP to ADP and P_i , it is believed that the myosin heads then pivot much like a sculler moves their oars. This power stroke of debated length (between 8 and 100 nm, Warshaw 1996) slides the actin chains past the myosin chains, contracting the fiber. The total force produced is a function of the number of cross-bridge interactions. After a fraction of a second, the calcium is pumped back into the cisternae, the tropomyosin resumes its blockage of the myosin heads, and the cycle is ready to be repeated. The reader should note that this is a simplified view, but it does capture the major aspects of the sliding filament theory and of our current understanding of muscular contraction (McComas 1996, Rothwell 1987, Ghez 1991). Today, the sliding filament theory is largely accepted as fact except for the actual power stroke process which is still debated (Pollack 1990).

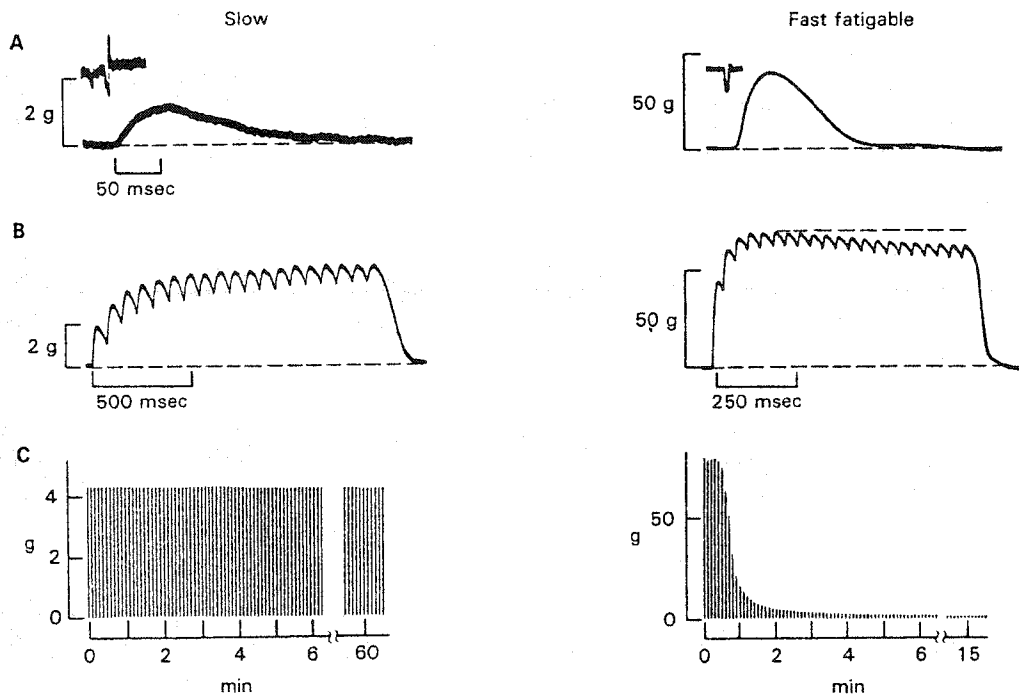
What this simplified view does not convey is the breadth of differences between different muscle fibers. Constructed of many different molecular elements, every muscle fiber is slightly different in form and function. For example, different fiber types have different isoforms of myosin and troponin, as well as different T-tubule systems and mitochondrial densities (the source of ATP). Stronger, faster acting “fast twitch” fibers employ glycolysis for energy production, and they fatigue quickly. Weaker and slower acting “slow twitch” fibers employ oxidative metabolism that is fatigue resistant. Hunter and Lafontaine (1992) report that overall, the maximum sustainable force output is about 30% of peak, which in vertebrate muscle corresponds to a stress of about 100 kPa.

“Fatigue” is thought to be manifested centrally, systemically and/or within the myofibril itself. Fatigue due to failure in neuromuscular transmission, although a primary factor in some diseases such as myasthenia gravis, is also an important contributor to so-called “high frequency fatigue” i.e. fatigue when muscles are stimulated at high frequencies. At a collective level, the activation of large numbers of muscle fibers in a muscle can lead to increased intramuscular pressures which allow the interstitial potassium ion concentrations to increase as blood flow is reduced. This affects the dynamics of the membrane depolarization. Also, the pH can be affected by the build-up of H^+ ions produced by the glycolytic reactions. Within the myofibril, there can also be a failure in the excitation-contraction system as the cisternae lose the ability to release significant quantities of calcium and to take it up again. Recovery comes from re-establishing initial concentration levels of the various electrolytes, and that is facilitated by the capillarization of the muscles (a benefit of endurance training).

On the training side, low numbers of high intensity contractions can bring about an adaptive response in muscle fibers that sees an increase in the number of myofilaments per muscle fiber, and a concomitant increase in strength. Endurance training, on the other hand, leads to adaptive responses that increase the energy stores of the muscle cells, reducing the chances that these cells will get into a fatigued state in the first place.

Finally, on a more short term basis, we can talk about how the twitch response of a muscle fiber summates to produce tetanus, a steady level of force production that is the result of a muscle fiber’s low pass filter response to high frequency stimulation. Figure 4-1 shows how fast twitch (FT) and slow twitch (ST) fibers differ in their responses to trains of action potentials. However, in both cases, they can be very sensitive to irregular

Figure 4-1 Differences in twitch and tetanus behaviour between slow and fast twitch muscle. Plots in A show twitches of motor units. Plots in B show 12 Hz stimulation tetanic tension. Plots in C show the force produced during tetanus over 330 seconds, where each second the muscle is activated by a brief burst of tetanic stimulation. Note the scales on the vertical axes (from Ghez 1991, and Burke et al. 1974).

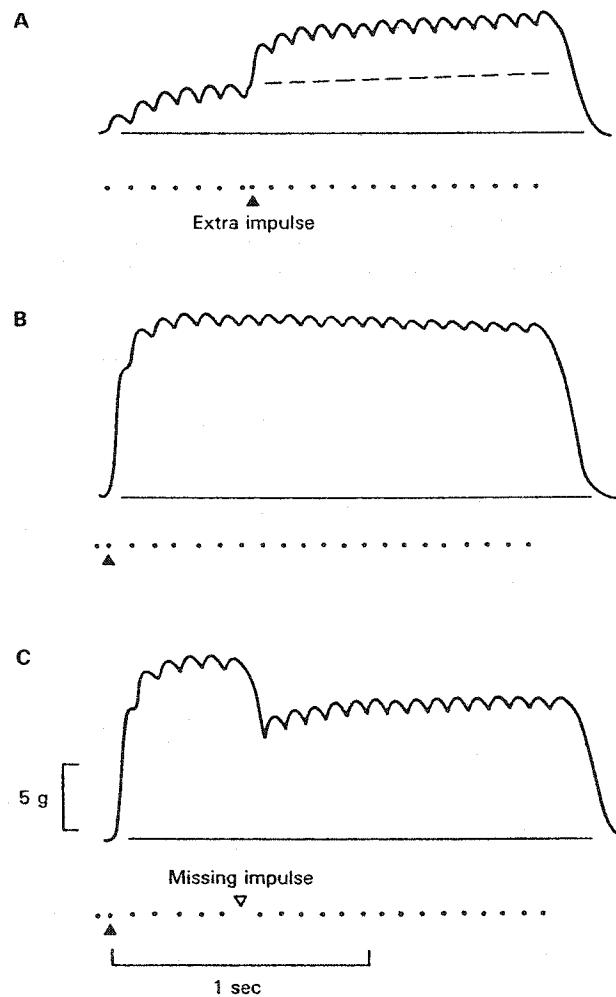


stimulation patterns, as is shown in Figure 4-2. The initial doublet creates a “catch-like” non-linearity that has been seen in cats (Zajac and Young 1975), and there are other noteworthy non-linearities. After a fiber has been held in tetanus, a subsequent twitch response within a few seconds is heightened. This is called post-tetanic potentiation and there are various theories as to its origin (Moore and Stull 1984, Allen et al. 1989). Likewise, one can observe a progressive increase in isometric twitch responses when a fiber is stimulated at low frequencies e.g. 2 Hz (Slomíc et al. 1968). In addition, twitch and tetanus contractions are sensitive to temperature and to the length of the muscle fiber pre-stimulation (Rack and Westbury 1969, Stein et al. 1982).

All of these natural processes, well explained or not, ensure that the past influences the present in muscle fiber behaviour. If we are interested in creating a physical simulation of muscle, and if we want it to be realistic in how it behaves, then we need to account for this influence of past activity. If this is not something that we desire in our physical model, then it would still be important in terms of knowing how the artificial muscles could best be controlled. After all, while we may not like muscle fatigue, it does serve an adaptive function as it prevents the host organism from over-utilizing a given muscle to the point where permanent damage may be incurred.

The study described in this chapter details the effects of various types of stimulation on the bending behaviour of PPy(DBS)-actuated bending beams as per Maw et al. (2001) and Pei and Inganäs (1992, 1993a-c). The intent is to determine if, and then how, history affects the contractile behaviour of PPy(DBS). To do this, the bending beams are taken through a series of cycles of stimulation of various types, after a set of conditioning cycles that act as the basis for later comparison. Any variance in behaviour

Figure 4-2 Differences in twitch and tetanus behaviour depend on the precise stimulation pattern. Plot A shows an unfused tetanus at 12 Hz along with an extra impulse (the arrow) that creates a long-lasting increase in tension. Plot B shows an extra impulse inserted at the start of the stimulus train (a doublet). Plot C starts with the doublet again, but misses a pulse midway, causing a lasting decrease in tension (from Ghez 1991, and Burke et al. 1970).



after the stimulus variations (in comparison to controls and to the conditioning cycles) is analyzed.

In these terms then, “history” is more than just endurance. It is more concerned with how functionality develops over time rather than the fact that the fiber still functions after a given time. As such, we could look at the evolution of peak currents, charge exchanges per cycle, and curling behaviour, over a series of ramp voltammetry or step cycles. This has been done, for instance, in the studies described in Chapters 2 and 3, and I will look at it here as well. However, it is not the primary issue that I will emphasize in this study since I have noted such effects previously. Here, I will concentrate on how the beams behave after having performed a certain task at a given intensity. I will look at how different beams behave the same or differently afterwards, having experienced those different tasks. These “tasks”, or stimulation conditions, include changes in stimulation mode (current steps, voltage steps, and ramp voltammetry), stimulation electrolyte concentration, cycling range, and stimulation frequency (although a more comprehensive stimulation frequency study will follow in Chapter 5).

By distinguishing the various aspects of “history” as I have, it does narrow the relevance of the literature considerably. There are relatively few precedents for this sort of study in the polypyrrole literature, and most are incidental. However, there are some. On the topic of “degradation with time”, one can look at studies on the thermal and environmental decay of polypyrrole’s conductivity (Hahn et al. 1986, Thiéblemont et al. 1994, Truong et al. 1995, Chen et al. 1994). Similarly, one can look at how the curvature, doping, volume changes and peak currents of bending beams like ours change with holding time at a given stimulation voltage (Pei and Inganäs 1992, 1993b-d) or over

cycling (Pei and Inganäs 1993a, Pei et al. 1993). Chiarelli et al. (1995), Della Santa et al. (1997) and Bobacka et al. (1994) have all shown concern for the initial “conditioning” of polypyrrole films, to get them “warmed up” to steady state behaviour. Indeed, much like these research teams, several other researchers have reported on the changes in peak currents, peak voltages, charge exchange, conductivity, actuator length, force production, and modulus with cycling and/or step holds (Gandhi et al. 1995, Kupila et al. 1995, Wegner et al. 1987, Ko et al. 1994, Kuwabata et al. 1984, Iseki et al. 1991, Li and Qian 1993, Maw et al. 2001, Otero and De Larreta 1988). Somewhat closer to what I will emphasize in this study, Pei and Inganäs (1993c) have looked specifically at cyclic voltammetry features after various voltage step holds. As well, Ko et al. (1994) and De Paoli et al. (1992) have looked at how their CVs change as a result of alterations in the cycling range. I will refer back to some of these results when I discuss the findings of this study later.

4.2 Experimental

The general methods and equipment used in this study were again identical to those described in Chapter 2. However, the protocols differed from the earlier work and these are reviewed below.

In this set of experiments, Kapton[®] HN 100 sheets from Dupont, 1 mil (25.4 μm) thick, were coated on one side with $400 \pm 50 \text{ \AA}$ of gold (Au) by vacuum evaporation. The sheets were cut into strips 1 mm wide using a sharp blade mounted on an automated Karl Süss scribing machine.

PPy was deposited galvanostatically on a 1.5 cm long portion of the gold-coated surface of each strip in an aqueous .16 M NaDBS / .16 M pyrrole solution. In each case, 300 mC of charge was exchanged. The resulting deposition charge density of 2 C/cm^2 corresponded to a PPy(DBS) film thickness of approximately $10 \mu\text{m}$ (Smela 1999). This thickness of PPy(DBS) produced bending beams that exhibited measurable ranges of movement.

Three sets of beams were produced. One set was deposited at 2 mA/cm^2 , another was deposited at 16 mA/cm^2 , and a third was deposited at 4 mA/cm^2 . Past work (Maw et al. 2001) has shown that these values produce some variance in mechanical behaviour as a function of the DCD. After deposition, each beam was run through one of two experiments.

In the first experiment (the “history” experiment), the beams were run through three rounds of stimulation. The first round was common to all. Every beam went through 21 conditioning cycles of ramp voltammetry stimulation between -1.1 V and $+0.4 \text{ V}$, at 150 mV/s or $.05 \text{ Hz}$. This took place in a .16 M NaDBS aqueous solution.

The second round was the variable round. Every beam went through 41 cycles of one of the stimulation conditions listed in Table 4-1, such that for each of the two DCD values, every condition was tested. Altogether, per DCD value, this provided 3 samples at different current stimulation levels, 4 samples at different stimulation frequencies, 4 samples at different stimulation NaDBS concentrations, and 3 samples in different stimulation modes (voltage step, current step, and cyclic voltammetry).

Table 4-1 Variable Round Conditions

Condition	Varied Stimulation Parameter	Stimulation Specifications
1	Mode	Voltage steps -1.1/+0.4 V, .16 M, .05 Hz
2	Mode	Current steps - ± 100%, .16 M, .05 Hz
3	NaDBS []	-1.1/+0.4 V, .02 M, .05 Hz
4	NaDBS []	-1.1/+0.4 V, .08 M, .05 Hz
5	NaDBS []	-1.1/+0.4 V, .32 M, .05 Hz
6	Cycling Frequency	-1.1/+0.4 V, .16 M, .03 Hz
7	Cycling Frequency	-1.1/+0.4 V, .16 M, .30 Hz
8	Cycling Frequency	-1.1/+0.4 V, .16 M, 3.0 Hz
9	Current Intensity	Current step - ± 50%, .16 M, .05 Hz
10	Current Intensity	Current step - ± 150%, .16 M, .05 Hz
-	Control	Cyclic Voltammetry -1.1/+0.4V, .16M, .05Hz

The third and final round of stimulation was identical to the first. If the variable round had indeed affected the beams differentially, then it was hoped that this would appear as differences in mechanical behaviour in the third and final round.

In the second experiment, which I will refer to as the “range” experiment, the arrangement was similar and the beams were prepared in the same way as in the history experiment. Each beam went through an initial 15 conditioning cycles of ramp voltammetry stimulation between -1.1 V and +0.4 V, at 150, 300 or 600 mV/s (50, 100 or 200 mHz, respectively), in a .32 M NaDBS aqueous solution. In the third and final phase

of the experiment, this conditioning procedure was repeated with the intent, once again, of detecting differences in behaviour resulting from the middle portion of the experiment. During that second (middle) phase of the experiment each beam went through one of 24 different conditions. These conditions consisted of various changes in the cycling limits. There were four general classes of conditions: oxidative range expansion, reductive range expansion, redox range expansion, and no range expansion at all (the control condition). Each beam went through 5 sets of 5 cycles, where the range was expanded set by set (except in the case of the controls). Altering the cycling range begged the question of whether the cycling frequency or the scanning rate was more important in determining resultant behaviour. As a result, I looked at both variables.

Three cycling frequencies and three scan rates were used: 50, 100 and 200 mHz and 150, 300 and 600 mV/s, corresponding to the conditioning stimulation conditions. One sample for each of these frequencies and/or scan rates for each of the 4 conditions described above was prepared. However, in effect, I looked at a larger number of scan rates and cycling frequencies since these two variables are so intimately related. For instance, if a sample was having its oxidation limit increased over the 5 sets of cycles while the cycling was being produced at a constant frequency, that would inherently mean that the scanning rate was increasing from set to set. Conversely, cycling at a constant scanning rate would imply a decrease in cycling frequency over the five sets. The net result was a large volume of data corresponding to a wide array of parameter values, comparable between samples. Fixing the scanning rate or cycling frequency for a given sample while expanding the range provided for behavioural comparisons within samples.

As noted, each beam went through 5 sets of 5 cycles. The cycles were ramp voltammetry and the stimulation solution was .32 M NaDBS. In the case of the oxidative range expansion, the range expanded by +0.1 V each set. For instance, in the first set the cycling range spanned from -1.1 to +0.5 V while in the fifth set the range spanned -1.1 to +0.9 V. Likewise, in the case of the reductive range expansion, the reduction limit went from -1.2 to -1.6 V over the 5 sets. The expansion at both limits simply combined these patterns (e.g. -1.2 to +0.5 V in the first set), while the controls went through 5 sets of cycling between -1.1 and +0.4 V.

In all cases, deposition and stimulation solutions were discarded after every two or three uses. The order in which beams were produced and then stimulated was randomized. In all, 37 samples were produced, tested and evaluated for the history experiment, while 28 went through the range experiment. In all stimulation conditions, cycling started and ended at the oxidation limit. Range of movement of the beam tip, charge transfer per half cycle, maximum currents, and voltages at those redox peaks, were all recorded for every cycle. Where appropriate, results from past work (Chapters 2 and 3) were also incorporated.

4.3 Results and Observations

4.3.1 Film Growth

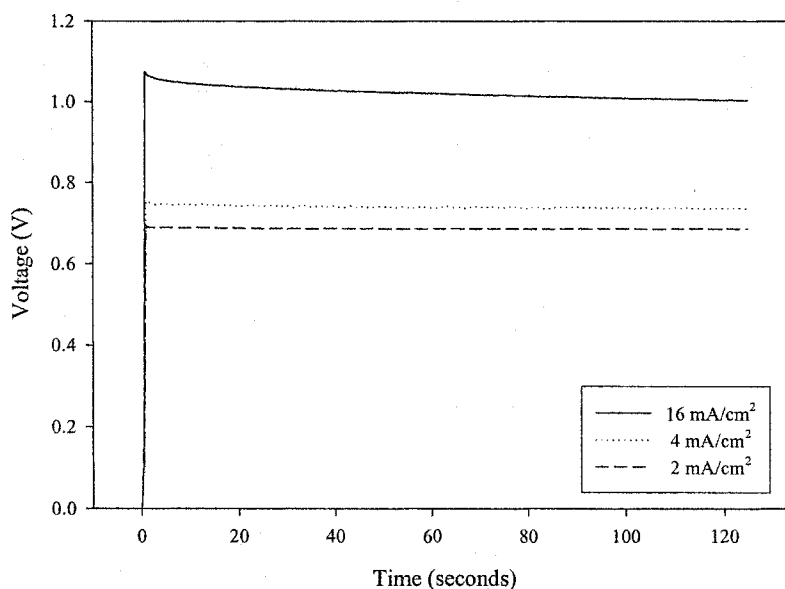
For the history and range experiments, all of the samples were prepared under one of three conditions. These conditions were identical except for the deposition current density. The three densities used were $.297 \pm .001$ mA (2 mA/cm²), $.594 \pm .001$ mA (4 mA/cm²) and $2.383 \pm .001$ mA (16 mA/cm²). Over all 65 samples, the deposited charge varied from 299.9 to 301.7 mC. Deposition durations averaged 1008.6, 504.7 and 126.1 seconds respective to the deposition current densities. Backside growth was minimal and constant among the history samples, and was low and constant among the range samples.

As per the findings of Chapter 2, higher DCD values (and therefore shorter deposition durations) generally correlated with decreased deposition curling, although differences between 4 and 16 mA/cm² were small. Capacitance spikes increased in magnitude with DCD, as did average and final deposition potentials in correspondence with the DCD experimental data of Chapter 2. Figure 4-3 shows some representative deposition voltammograms.

4.3.2 Conditioning Cycles

As in Chapter 3, it is worth reviewing at this point the significance of the various measures that are noted in all of the Results sub-sections. The large volume of results regarding a relative few measures can create confusion if one does not keep in mind why these findings are relevant. The peak currents, for instance, tell us what kinds of power and energy requirements would be required by the PPy(DBS) films under different circumstances. Likewise, the peak voltages tell us similar things about what stimulation

Figure 4-3 Deposition voltammograms sampled at 100 Hz and collected using LabVIEW software. The different plots correspond to the first 125 seconds of the three representative depositions. The samples of PPy(DBS) were deposited at different deposition current densities (DCDs). The history samples were produced at 2 mA/cm² and 16 mA/cm², while the range samples were produced at 4 mA/cm². Data analysis was performed using custom Matlab[®] routines.



voltages are required under different conditions of stimulation. This would also affect power source choices for any potential AMF system, and these sorts of results would also indicate whether variable voltage (or current) draws would be needed. Natural muscle operates on an all-or-nothing basis for contraction and does not depend on the size of the incoming action potential (which does not vary substantially, in any event), only on the arrangement of incoming action potentials with respect to time (see Introduction). Information regarding charge exchange is reflective of the capacity of the film to do work/contract, since strain is proportional to charge exchange (e.g. Maw et al. 2001). This is obviously quite important, and it is also important in how it relates to movement. Thus, calculations of how much movement (curl) occurs per unit charge exchanged (mC) will also be common, reflecting the responsiveness of strains in the films to charge exchanges. The amount of charge exchange relative to the amount originally deposited during polymerization is also important in that it reflects the charge exchange capacity of the film. While the movement responsiveness indicates how efficient a film may be at creating movement for a given charge, the charge exchange capacity reflects the amount of strain that the film can possibly produce. The actual measurement of the curling reflects strain levels and this is fundamental to the whole thesis. At times, I will also make reference to the shape of the voltammograms and amperograms. This is because the features of these plots show different qualities of the films, in different ways. With the amperograms, for instance, we can get an excellent sense of how fast the beam is moving with time, as this is well reflected in the instantaneous current levels. Finally, there will be several occasions where I compare one set of values to another (e.g. peak currents versus peak voltages). The purpose in doing this will be to show how these

interacting variables relate to each other in different situations. This may show a dependency of one variable upon another, for instance.

Starting with the range samples, there were some clear patterns especially as they related to cycling rate. The general CV patterns (of the 14th cycle in each set) are shown in Figure 4-4. Representative of all of the other CVs collected for their classes, they show that peak currents increase with sweep rate and/or cycling frequency, and that the peaks separate. Figure 4-5 shows how the amount of charge exchange per cycle decreases as currents increase. This appears as a clockwise rotation of data around the graph with increasing cycling rate. Note the first oxidative half cycle data points with the low current and charge exchange values, and that over the course of the cycles the data points move outward radially.

Figure 4-6 shows the range of movement over the 15 oxidative half cycles for the three classes of samples. Clearly, movement extent decreases with increasing cycling rate. However, the ratio of range of movement to charge exchange (movement responsiveness) is relatively insensitive to cycling rate in the range tested, at least by the end of the sets. It varied between .501 and .595 mm/mC with an average of .535 mm/mC. Charge exchange capacity, however, did decrease substantially with cycling frequency, going from 6.0% to 4.2% to 2.6%.

The conditioning data collected for the history samples mirrored the findings of Chapter 2. In this experiment there were two sets of data, corresponding to low and high DCD values (2 mA/cm² and 16 mA/cm²). As in Chapter 2, range of movement of the beam tips decreased with DCD as did charge exchange. In terms of the CVs, the pattern for increasing DCD value mirrored that of decreasing cycling rate as seen with the range

Figure 4-4 Conditioning CVs collected from the range samples using LabVIEW software during the 14th cycle. The three plots are representative of their classes of samples. Note that the data for the 50 mHz sample was collected at 100 Hz, the data for the 100 mHz sample was collected at 200 Hz and the data for the 200 mHz sample was collected at 400 Hz.

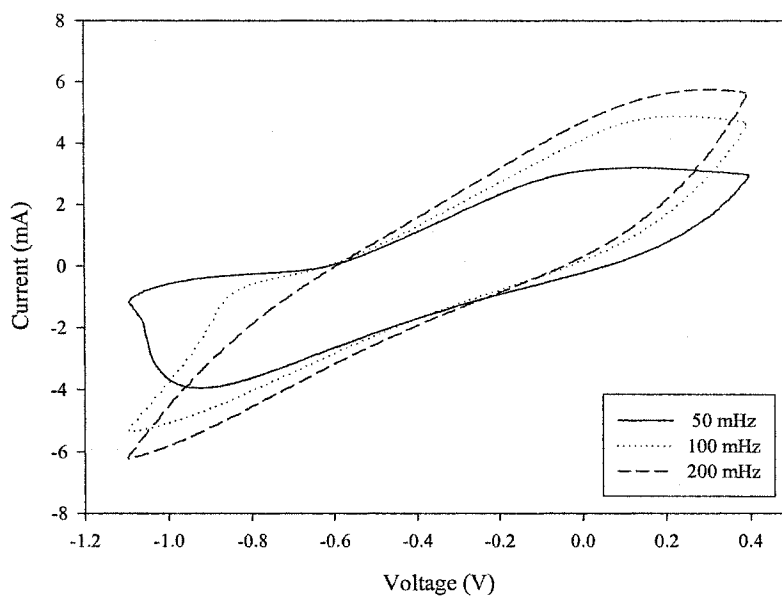


Figure 4-5 Average peak currents (x-axis) versus average charge exchange per half cycle for the 1st, 4th, 7th, 10th and 15th cycles of each conditioning set in the range experiment. Oxidative half cycle data are in the upper right quadrant while reductive half cycle data are in the lower left quadrant. Seven samples were averaged per data point.

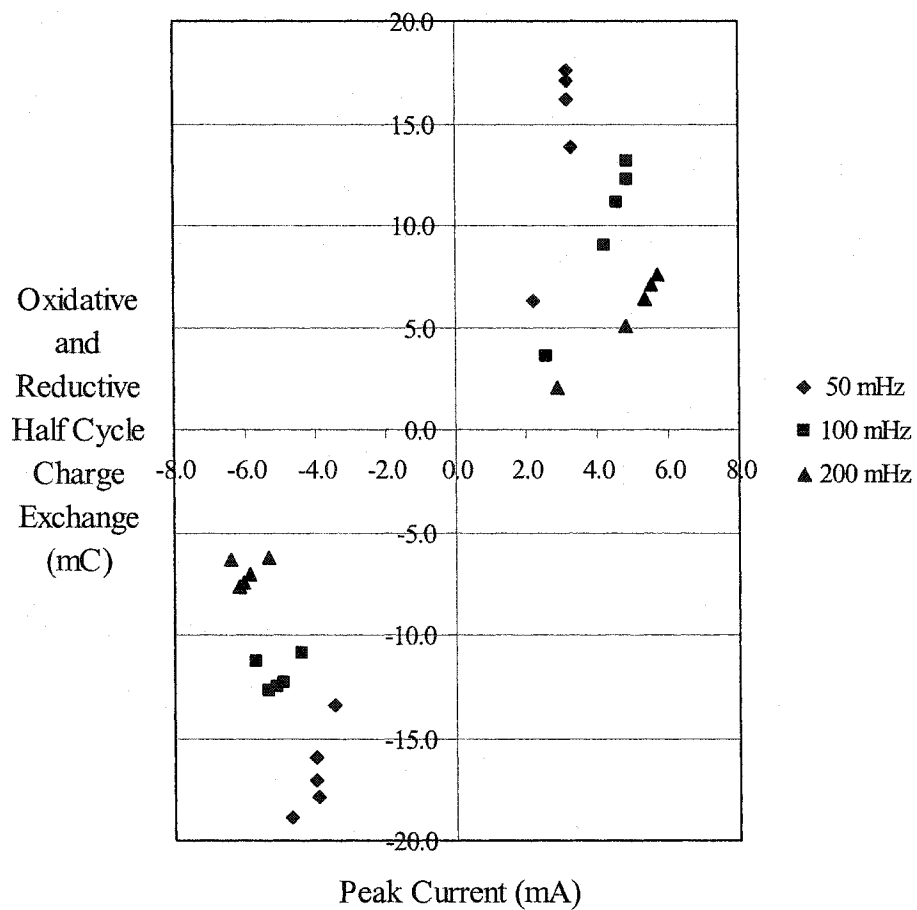
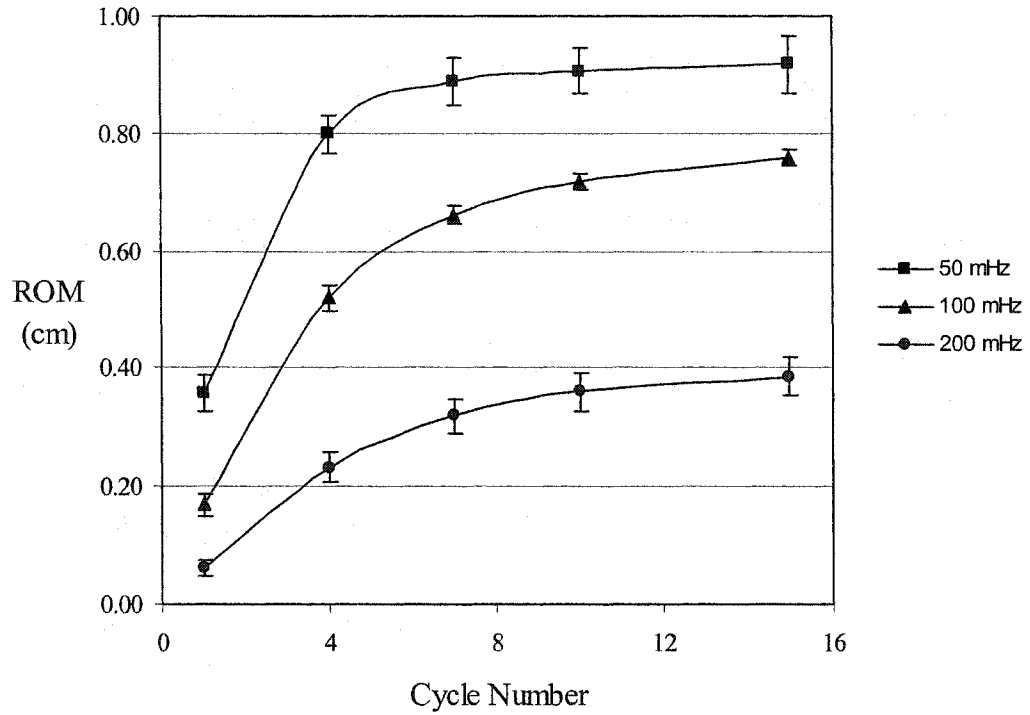


Figure 4-6 Average range of movement (ROM) of the beam tips per oxidative half cycle for the 1st, 4th, 7th, 10th and 15th cycles of each conditioning set in the range experiment. The three plots correspond to the movement patterns related to the three cycling rates used. Error bars are ± 1 standard deviation (7 samples per data point).



samples. In other words, with increasing DCD the peak currents decreased and the peak separation was reduced (mostly due to anodic shifts of the reduction peaks). The ratio of range of movement to charge exchange was also found to be slightly higher for high DCD in this experiment. For both reduction and oxidation, it increased from zero to a plateau value of approximately .55 mm/mC at about the 6th cycle. Charge exchange capacity, on the other hand, was better at the low DCD level (5.4% vs. 4.1% on the 21st cycle). Also, at the high DCD level, there was a clear drop from 4.7% to 3.5% from the 1st cycle to the 6th, whereas with the low DCD samples there was no change at 4.5%.

Finally, in comparison to Figure 4-5, the current/charge data points of the history conditioning data fell along one radial line. The lower DCD data points lay more to the outside along the radial line, reflecting higher currents and charge exchanges.

Tables 4-2 and 4-3 show summary information from the various sets of conditioning data. The 0.3 mA and 2.4 mA data come from the history samples, while the 0.6 mA data comes from the range experiment. Keep in mind that the 0.6 mA data was gathered under slightly different conditions e.g. stimulation NaDBS concentration of .32 M versus .16 M for the 0.3 mA and 2.4 mA data. Also, the gold layer of the range samples was about 5 nm thinner, on average.

Table 4-2 Results of Conditioning Cycles (Reduction Half Cycles)

DCD (mA)	Backcurl 1 st cyc (cm)	Backcurl 15 th cyc (cm)	Pk V 1 st cyc (V)	Pk V 15 th cyc (V)	ΔQ 1 st cyc (mC)	ΔQ 15 th cyc (mC)	Pk I 1 st cyc (mA)	Pk I 15 th cyc (mA)
0.3	0.00	0.85	-1.10	-1.07	-13.5	-15.7	-3.4	-3.1
0.6	0.00	0.91	-1.09	-0.92	-18.9	-17.8	-4.7	-3.9
2.4	0.04	0.66	-1.10	-0.98	-14.2	-11.9	-3.5	-2.8

Table 4-3 Results of Conditioning Cycles (Oxidation Half Cycles)

DCD (mA)	Curl 1 st cyc (cm)	Curl 15 th cyc (cm)	Pk V 1 st cyc (V)	Pk V 15 th cyc (V)	ΔQ 1 st cyc (mC)	ΔQ 15 th cyc (mC)	Pk I 1 st cyc (mA)	Pk I 15 th cyc (mA)
0.3	0.16	0.86	-0.11	0.25	4.3	15.6	1.6	2.8
0.6	0.36	0.91	-0.13	0.13	6.3	17.5	2.3	3.2
2.4	0.14	0.67	-0.08	0.22	4.1	11.8	1.5	2.4

4.3.3 Range Variations

For the middle part of the range experiment where the cycling range was varied, the samples either experienced an expansion in the oxidation limit, an expansion in the reduction limit, an expansion in both limits, or an expansion in neither limit (the control).

Over the 5 sets of 5 cycles, the controls (50 mHz or 150 mV/s, 100 mHz or 300 mV/s, and 200 mHz or 600 mHz samples) experienced the same stimulation each time. Their behaviour did not change very much over the 5 sets of stimulation. The patterns of behaviour that were observed mirrored those of the conditioning cycles, except that the curling performance of the 50 mHz control gradually fell between the 100 and 200 mHz samples. Charge exchange increased about 8-10% for the 100 and 200 mHz samples (300 and 600 mV/s), but only marginally for the 50 mHz sample (150 mV/s). The same trends were found for peak oxidative currents and oxidative peak voltages. The reductive peaks did not change much at all. In terms of curling movements, the 100 mHz and 200 mHz samples (300 and 600 mV/s) both increased their range of movement while the 50 mHz (150 mV/s) sample's movements decreased marginally. The movement responsiveness ratio ranged from .39 to .62 mm/mC, decreasing slightly with time for the 50 mHz (150 mV/s) sample, increasing slightly with time for the 200 mHz (600 mV/s) sample, and staying fairly constant with the 100 mHz (300 mV/s) sample.

For the samples that saw both of their limits expand, there were several differences compared to the controls. With each set of cycles, the currents and charge exchanges would increase such that the data points would move out in a radial direction as per Figure 4-5. Both cycling limits expanded by 0.1 V with each of the 5 sets. If the scan rate was being kept constant, the cycling frequency would decrease with each set. If the cycling frequency was being kept constant, the scan rate would increase with each set. Currents and charge exchanges increased in both cases. However, the charge exchange increases were greater with respect to scan rate, while the current increases were greater with respect to cycling frequency, at least at 50-100 mHz. The relationship between charge exchange and peak voltage, shown in Figure 4-7, provides another example of how variations in scan rate and cycling frequency are manifested differently.

In terms of curling for the range expansion at both limits, there were increases in curling as the cycling range was expanded at each of the three control frequencies, and the rate of increase increased with frequency (see Figure 4-8). The situation was similar for scan rates, although somewhat different. There were no changes in ROM at 150 mV/s over the 5 sets of range expansion. Another key finding having to do with ROM was that for a given cycling range, increasing cycling frequency or scan rate would decrease the ROM. However, the amount of decrease scaled with the cycling range. The larger the range, the shallower the drop-off in curling extent would be.

With charge exchange, the situation was very clear. Charge exchange decreased in a linear fashion with cycling frequency and scan rate. However, it also increased in a linear fashion with cycling range (see Figure 4-9). The peak currents and voltages increased with frequency/scan rate, and linearly with cycling range. The peak voltages

Figure 4-7 Charge exchange versus peak voltage. Each data point represents the respective Q/V values for the 5th cycle of each of the 5 sets, where the cycling limits expanded in both directions by 0.1 V with each set. Note that in the top graph, cycling frequencies are held constant with the expanding cycling range (so scan rates increase), while in the bottom graph scan rate is kept constant (so cycling frequency decreases). There are subtle differences in the way the data behaves.

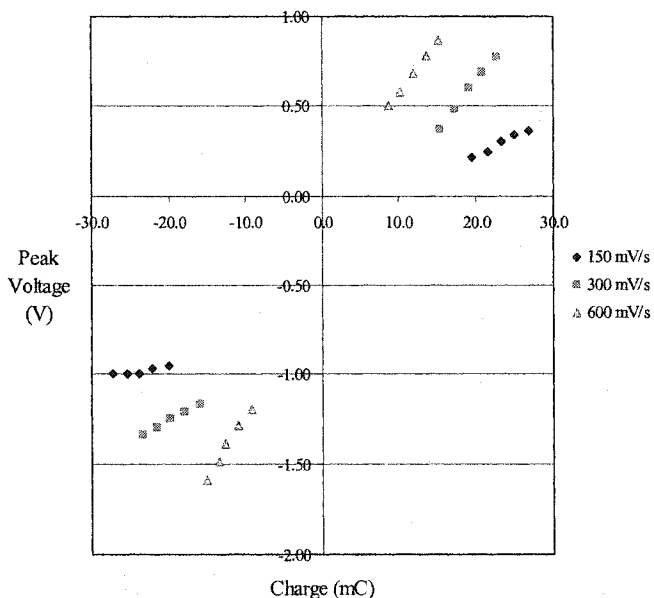
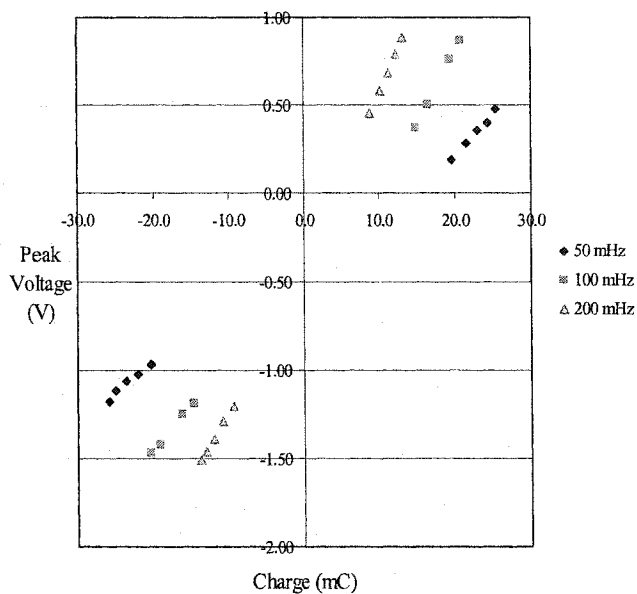


Figure 4-8 Drop-off in curling with cycling frequency. The data with respect to scan rate look very similar. Note the change in drop-off with cycling range.

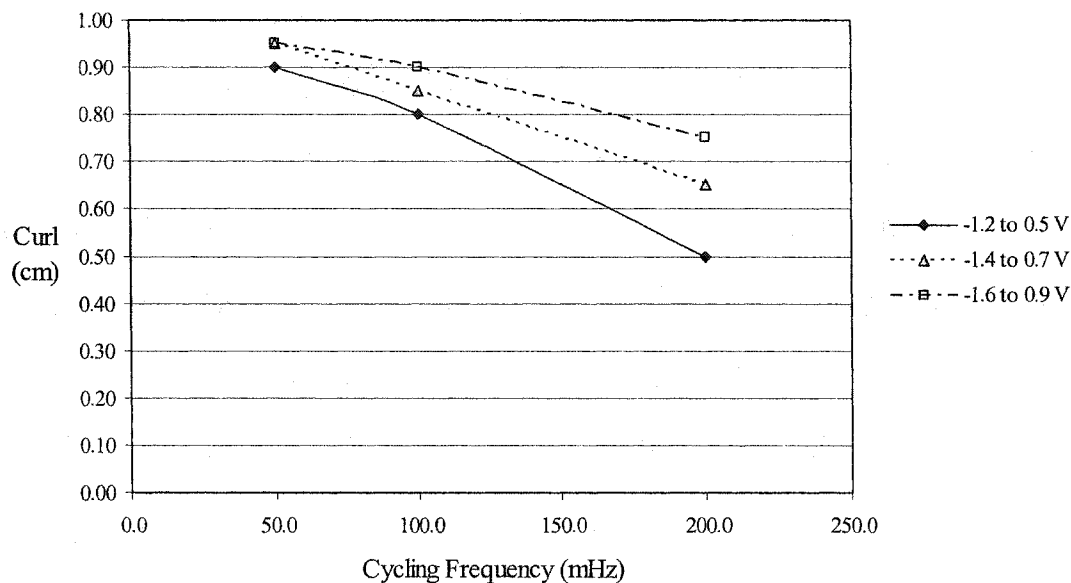
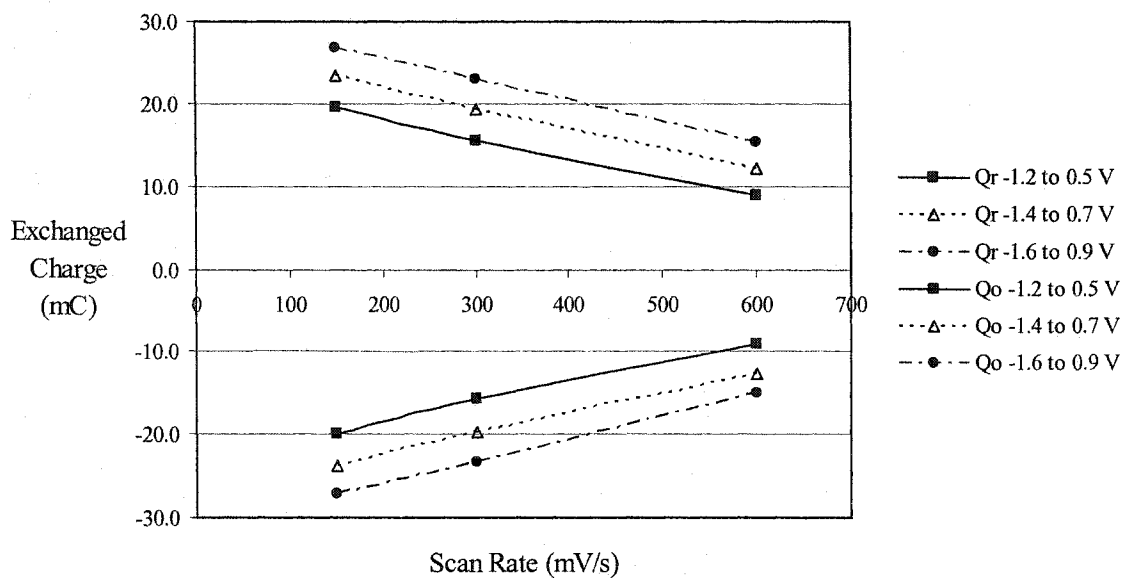


Figure 4-9 Drop-off in charge exchange with scan rate (or cycling frequency). Note the similarity in drop-off with cycling range.

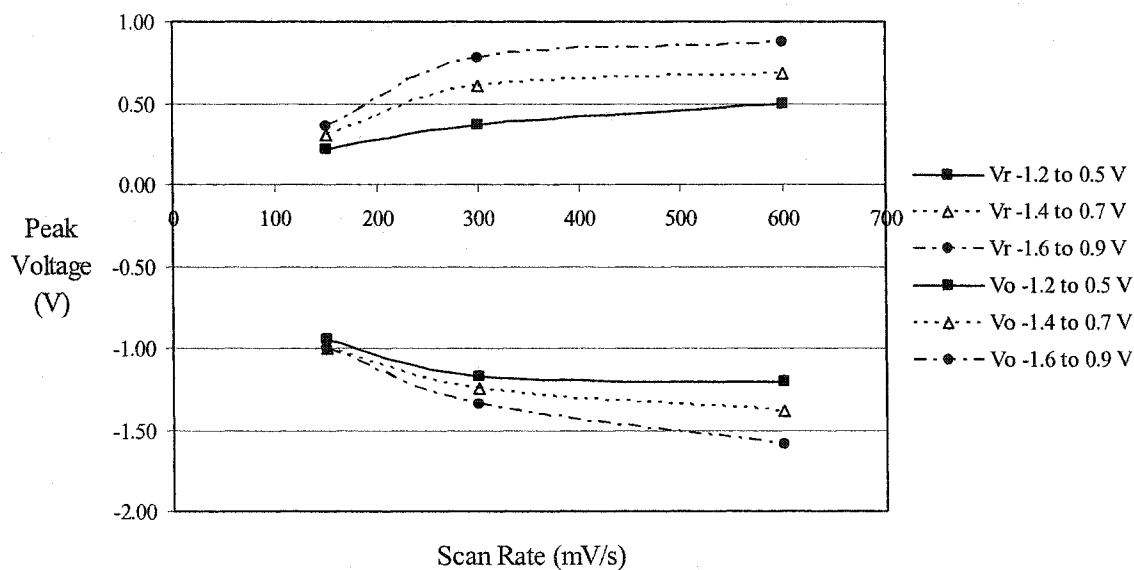


showed some subtle differences though (see Figure 4-10). At every cycling frequency and scan rate, expanding the cycling range led to expansion in the peak separation, with both peaks moving away from 0 V. With respect to just cycling frequency, the slope of this relationship (peak voltage versus cycling range) was the same for each frequency. However, the increase in peak voltage with frequency did not scale with frequency, as the 100 and 200 mHz peaks were usually almost identical i.e. at or beyond the limits. With scan rate, the situation was a bit different. The slope of peak voltage versus cycling range did scale with scan rate in 5 of 6 cases. In other words, the peak locations at higher scan rates were more sensitive to changes in cycling range (see Figure 4-10). Similar to the cycling frequency data, the 300 and 600 mV/s data were certainly closer to each other than the 150 and 300 mV/s data were, but they were nevertheless distinctly different.

In terms of movement responsiveness (curl per unit charge transfer), the data for cycling frequency and scan rate were very similar. As the cycling range expanded, the movement responsiveness decreased about 20% over the expansion range except in the case of the fastest cycling/scanning levels where it either remained fairly constant or it increased slightly. The worst to best levels spanned .35-.55 mm/mC. The charge exchange to peak current ratio increased with cycling range and increased at the same rate for each of the cycling frequencies and scan rates. The ratio scaled with cycling frequency and scan rate, with the lower the frequency/scan rate, the higher the ratio.

The data from the reduction range expansion and oxidation range expansion groups offered an interesting contrast to the data from the control and redox expansion groups. Looking at the data from the reduction range expansion first, we can see some noteworthy differences from the range expansion in both directions. As the reduction

Figure 4-10 Change in peak voltages with respect to scan rate. Note the nature of the changes in rise/fall with cycling range. The changes in peak voltages with respect to cycling frequency are very similar, and differ mostly in the middle data points which are higher on the oxidation side and lower on the reduction side such that most of the lines joining the last two data points in each data set are essentially flat i.e. the peak voltages are at or beyond the cycling limits.



range expands, the low frequency/scan rate curling decreases, the high frequency/scan rate curling increases and the middle frequency/rate curling remains largely unchanged, decreasing only slightly in the last 1-2 sets of range expansion. In contrast with the dual limit expansion, the charge exchange is reduced as the range is expanded in the reduction direction, especially in the last 2-3 sets (range expansions). Likewise, with respect to peak currents, there are weak increases with oxidation currents over the increases in reduction range, but the reduction currents actually shrink with range at the lower two frequency/scan rate levels. They rise at the highest frequency/scanning levels.

With regard to the peak voltages involved, the oxidation peaks were beyond the oxidation limit for the two higher cycling frequencies/scan rates at all ranges, as well as for the last 2-3 range expansions for the lowest cycling frequencies/scan rates. The reduction peaks behaved quite differently, however. For the lowest two cycling frequencies/scan rates, the reduction peaks moved anodically with increasing range whereas for the highest cycling frequencies/scan rates, the peaks moved slightly cathodically. Thus, peak separation did not change noticeably at the lowest and highest frequencies/scan rates, but it did decrease somewhat at the middle frequency/scan rate levels.

The movement responsiveness levels increased with cycling range at the highest cycling frequencies/scan rates, increased slightly at the middle frequencies/scan rates and decreased slightly with the lowest frequencies/scan rates. The charge exchange to peak oxidative current ratio went down with cycling range, inversely proportional to cycling frequency/scan rate. On the reductive side, the ratio decreased slightly with cycling range for the two highest frequencies/scan rates. The situation was less clear for the

lowest frequency/scan rate. Figure 4-11 shows a graph similar to Figure 4-7 for purposes of comparison regarding how charge exchange and peak voltage related to each other.

That leaves the range expansion in the oxidative direction. The behaviour in this situation was surprisingly different compared to that of the reductive expansion. For instance, with regards to curling, there was no clear change in curling with range expansion at any cycling frequency/scan rate. In general, there were no obvious differences in sensitivity to changes in cycling frequency as opposed to scan rate. In terms of charge exchange, at high frequencies/scan rates, again there was little/no change over the oxidative range expansion. However, as the cycling frequency/scan rate decreased, the charge exchange increased more and more with range expansion (see Figure 4-12). In terms of peak currents, peak reductive currents increased in magnitude with oxidative range expansion and the rate of increase was roughly equal at all cycling frequencies/scan rates. For the oxidative peak currents, however, the situation was not quite as clear. It appeared that the high frequency/scan rate data decreased slightly with oxidative range expansion, while the low frequency/scan rate data increased slightly. The middle data remained largely unchanged.

Looking at the movement of the peak voltages with respect to oxidative range expansion, there were some differences between the cycling frequency and the scan rate sensitivities. In all cases, the oxidative peaks moved anodically with oxidative range expansion. However, the low scan rate oxidation peaks were substantially more cathodic than the peaks at other scan rates, whereas with cycling frequency they were not as distinguishable. Likewise, for the reduction peaks, they were never actually reached at mid-high scan rates and frequencies. But at low frequencies/scan rates, they were

Figure 4-11 Charge exchange versus peak voltage. Each data point represents the respective Q/V values for the 5th cycle of each of the 5 sets, where the cycling limits expand in the reduction direction by 0.1 V with each set. Cycling frequencies are held constant with the expanding cycling range (so scan rates increase). See Figure 4-7 for comparison.

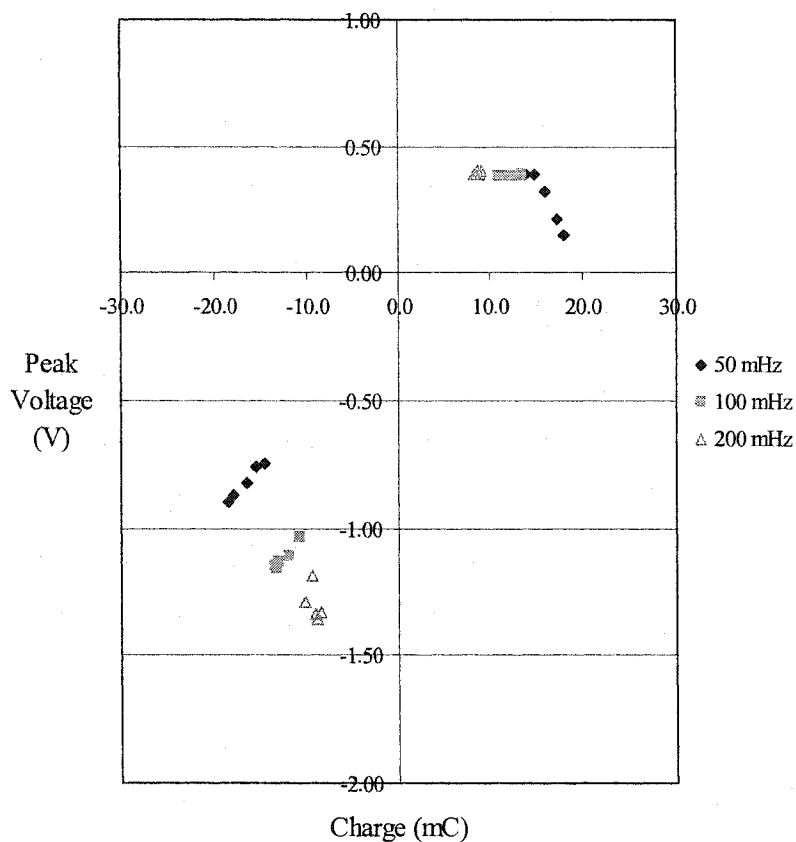
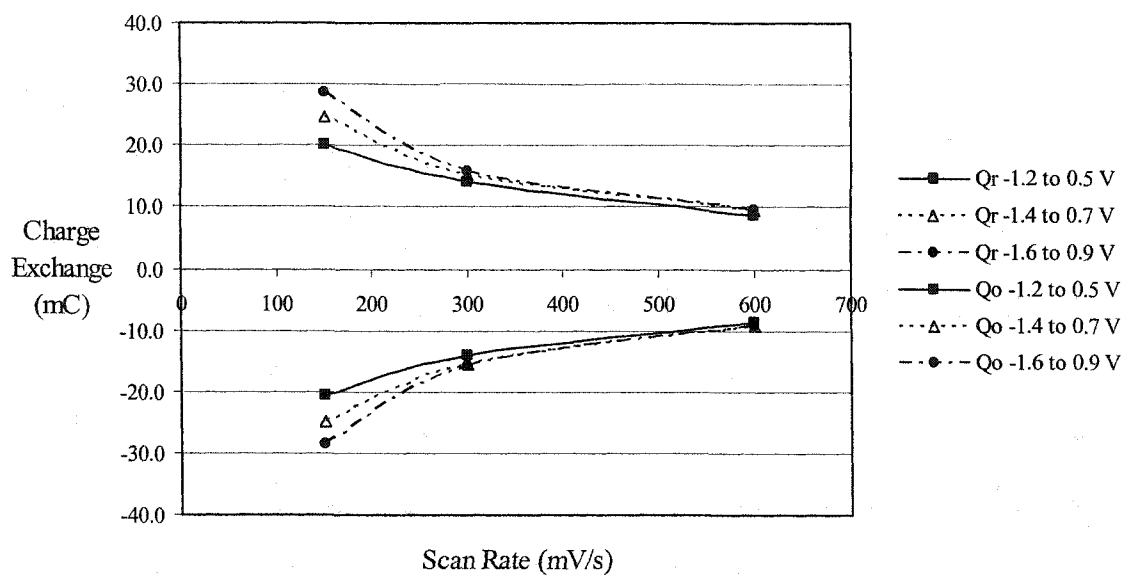


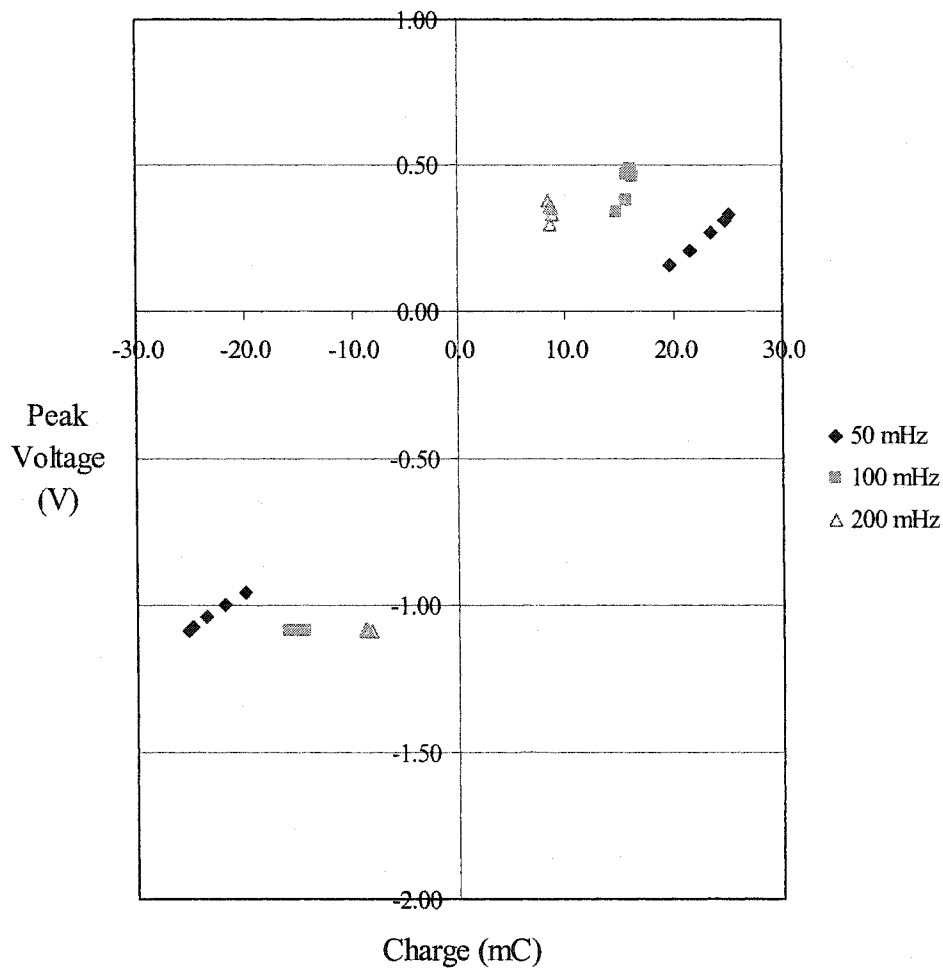
Figure 4-12 Change in charge exchange with respect to scan rate. Note the nature of the changes in rise/fall with cycling range.



reached when the cycling range was relatively short. Overall, peak separation increased with oxidative range expansion, scaling inversely with cycling frequency/scan rate. The lower the frequency/scan rate, the more the peaks would separate with increases in oxidative range.

In all cases with the oxidative range expansion data, movement responsiveness decreased with respect to range expansion, although the effect was slight at high frequency/scan rate. The lower the frequency/scan rate, the greater the rate at which it would decrease with range. However, it was the middle frequency/scan rate values that were the highest in all cases. Looking at all of the oxidation range expansion data, values varied from .30 to .60 mm/mC. Ratios of charge exchange to peak current were also moderately sensitive to increases in oxidation range. On the reduction side, ratios for low cycling frequencies/scan rates would increase in magnitude with oxidation range while the low-mid frequency/scan rate data did not vary with oxidation range. On the oxidation side, the ratios increased with oxidation range in all cases, at a rate inversely proportional to cycling frequency/scan rate. In all cases, the absolute values of the ratios were inversely proportional to cycling frequency/scan rate i.e. the low cycling frequency/scan rate samples exhibited the greatest ratios while the high cycling frequency/scan rate samples exhibited the smallest ratios. Figure 4-13 shows a graph similar to Figures 4-7 and 4-11, for purposes of comparison regarding how charge exchange and peak voltage related to each other during the oxidative expansion.

Figure 4-13 Charge exchange versus peak voltage. Each data point represents the respective Q/V values for the 5th cycle of each of the 5 sets, where the cycling limits expand in the oxidation direction by 0.1 V with each set. Cycling frequencies are held constant with the expanding cycling range (so scan rates increase). See Figures 4-7 and 4-11 for comparison.



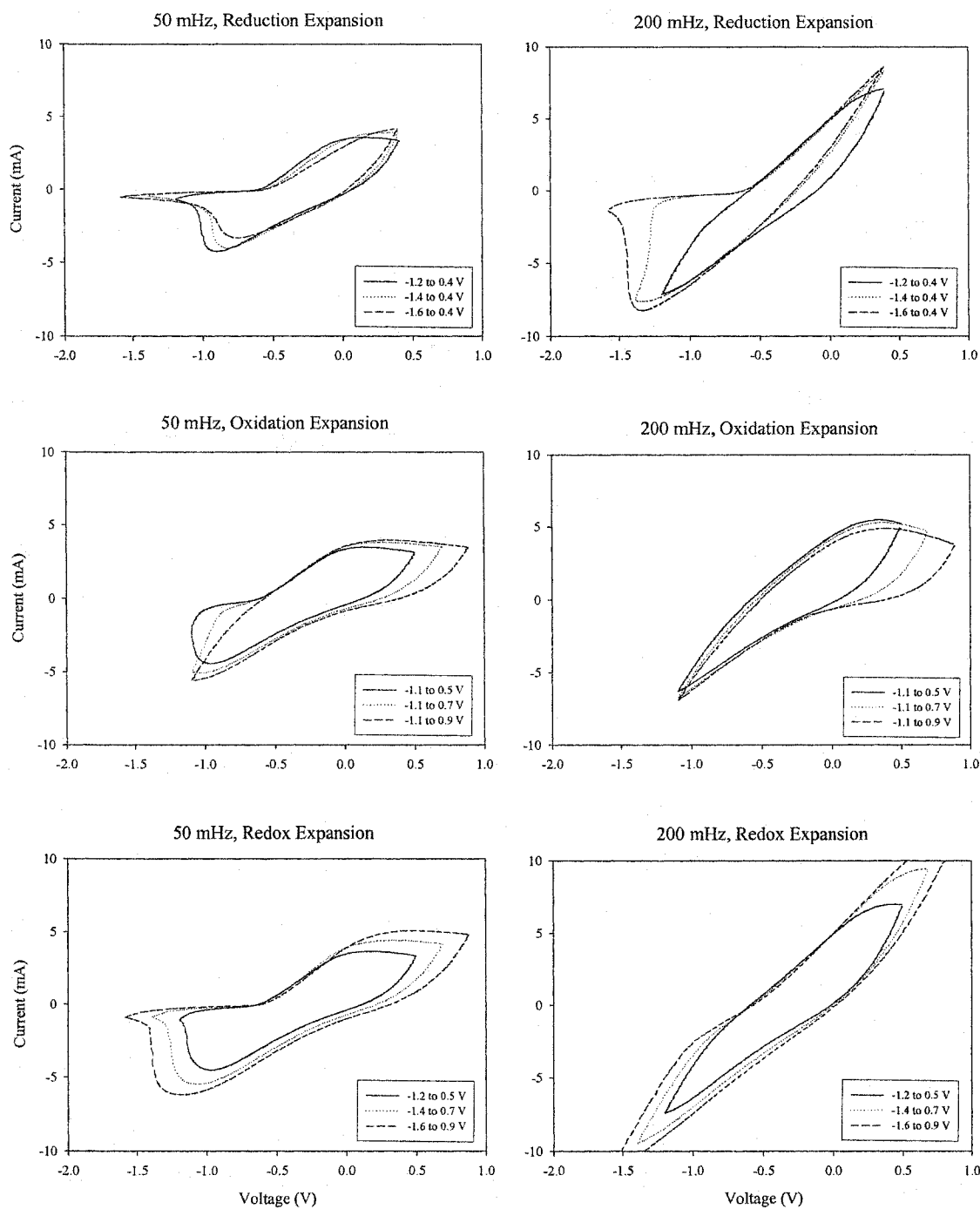
To conclude this section, we finish with a series of figures that show examples of CVs from the various range expansion conditions, and cycling frequencies. Figure 4-14 shows reduction, oxidation and redox range expansion CVs, at a cycling frequency of 50 mHz on the left, and the same at 200 mHz on the right.

4.3.4 History Variations

For the history experiment, the middle “variation” phase of the stimulation protocol looked at stimulation mode (voltage steps, ramp voltammetry, and current steps), stimulation NaDBS concentration (.02, .08 and .32 M), stimulation frequency (.03, .30 and 3.0 Hz) and stimulation current intensity (50%, 100% and 150%). There were two complete sets of all of this data, one for each of the DCD values that was employed (2 mA/cm² and 16 mA/cm²). Every sample went through 41 cycles of stimulation, and data was gathered every 10 cycles on charge, current, etc.

Regarding the three modes, the voltage steps were made to the same limits as the ramp voltammetry, and the current steps were set to a level that allowed for charge exchange equal to the greatest amount of charge exchange that took place during any of the conditioning cycles. Looking first at curling ROM, for both DCD values, voltage steps produced 15-20% more curl than the current steps and ramps, which were roughly equal. In general, the curling movements were 20-30% more extensive though, at low DCD. The patterns were almost identical with respect to charge exchange. The only differences were in the magnitude of the differences. For instance, charge exchange for the ramp voltammetry was about 10-15% greater than that of the current steps, and the voltage steps exchanged 15-35% more charge than the CVs. Low DCD charge exchange

Figure 4-14 Representative CVs from reduction, oxidation and redox range expansion, where the cycling took place at 50 mHz on the left, and at 200 mHz on the right. CVs for the same at 150 mV/s and 600 mV/s are similar.



was greater than high DCD charge exchange by 15-30%. Also, at high DCD, the charge exchange grew with time whereas at low DCD it did not after the first 10-20 cycles.

Charge accumulation over the 41 cycles was positive for voltage steps, while negative for CVs and current steps. Peak currents were highest for the voltage steps. Low DCD currents were 15-30% greater than high DCD currents. With regards to peak reduction voltages, they stayed essentially constant at low DCD, with the voltage steps holding at -1.09 V, the CVs settling at -1.04 V and the current steps settling at -.84 V. The high DCD reduction peaks were slightly more anodic. On the oxidation side, the current step peaks started very positive and moved towards 0 V with time. The CVs did the opposite. At low DCD, they all ended up at or beyond .40 V. At high DCD, the current step oxidation peaks were lowest at .23 V followed by the CVs at .35 V. Thus, peak separation did not change very much for the voltage step and CV modes, but did decrease with time for the current steps.

The patterns in movement responsiveness were quite interesting. For both DCD values, current steps were best and voltage steps were worst, and low DCD samples outperformed high DCD samples. Also, the responsiveness appeared to decrease with time for the high DCD samples. Table 4-4 shows some of these results.

Table 4-4 Movement Responsiveness (ROM/Q) for Modal Stimulation

Stimulation Mode	2 mA/cm ²	16 mA/cm ²
Voltage Step	0.425 mm/mC	0.402 mm/mC
CV	0.492 mm/mC	0.479 mm/mC
Current Step	0.594 mm/mC	0.533 mm/mC

With regard to the charge exchange to peak current ratio, CV measures were consistently about 100% greater than the voltage step measures, reflecting the difference in peak currents and how the current levels are maintained. Also, the low DCD ratios were 10-20% greater than their high DCD counterparts. All of this is best illustrated through a comparison of the amperograms for the 3 stimulation modes (see Figure 4-15).

The variations in stimulation frequency provided a wider look at how this variable affects charge exchange, peak movement and the like. Indeed, with the addition of the control samples, there were 4 stimulation frequencies to examine (.03, .05, .30 and 3.0 Hz). All of the measured parameters reacted to the changes in this variable.

Regarding range of curling movement, there was a very clear pattern with respect to cycling frequency. Higher stimulating frequencies produce less curling. This was true at both DCD levels, but there was an interesting difference. At the high frequency, the high DCD beam showed more movement than the low DCD beam. At the lowest frequency, the high DCD beam showed less movement than the low DCD beam. In other words, the curling showed less variation with cycling frequency with increasing DCD. In all cases, the amount of curling stayed fairly constant over the 41 cycles.

The charge exchange patterns were similar, as is shown in Figure 4-16. The only obvious difference between these plots and those of the curling movements was the proportionally larger gap between the .05 Hz and .30 Hz lines. The currents showed similar, though inverted, patterns. The higher the cycling frequency, the greater the peak currents were. And the high DCD currents were 10-15% smaller than the low DCD currents. The higher the frequency, the longer it took for the peak current value to settle. However, in all cases, the peak currents were relatively constant by the 41st cycle.

Figure 4-15 Amperograms from the stimulation mode variations collected using LabVIEW software. Current step, voltage step and cyclic voltammetry current signals for the 40th cycle for the samples grown at 2 mA/cm². The data was collected at 100 Hz.

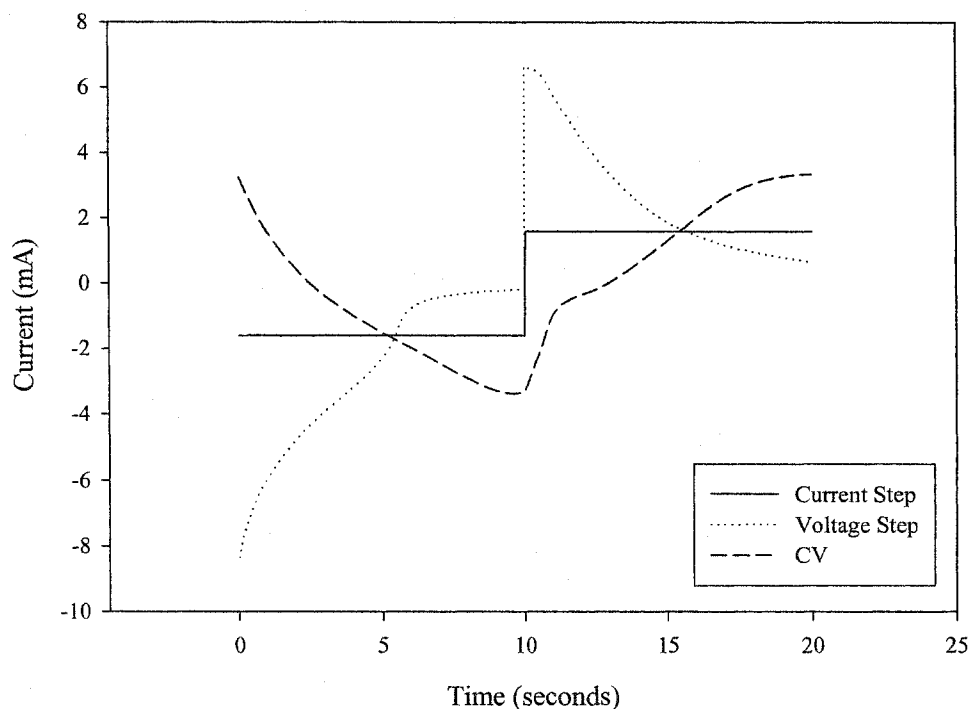
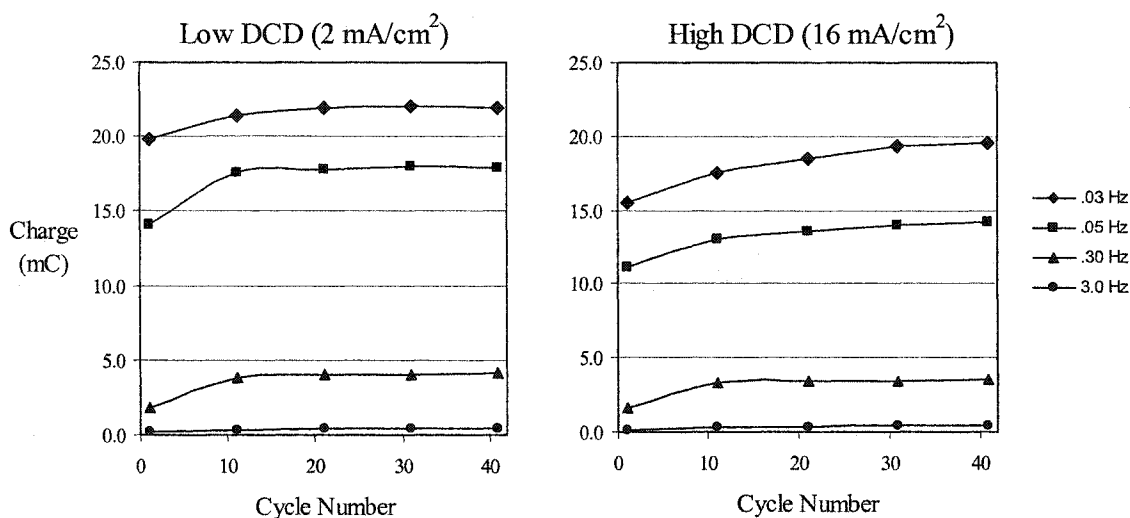


Figure 4-16 Charge exchange levels, per cycle, for the stimulation frequency variations. The left graph shows the data from the low DCD samples. The right graph shows the data from the high DCD samples. Similar patterns, different relative magnitudes.

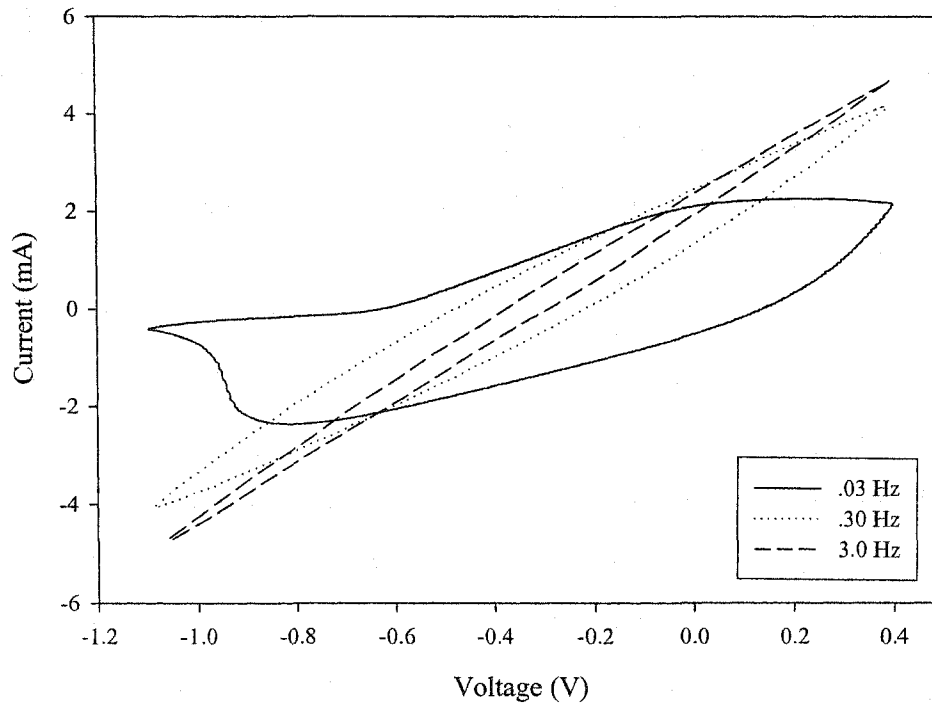


With respect to the voltage peaks, the peak separations showed a similar pattern for the two DCD values. Peak separation increased with cycling frequency to a peak and then it started to decrease. For the low DCD, it rose from 1.13 V to 1.49 V and then went back to 1.46 V. For the high DCD, it rose from 1.04 V to 1.49 V and then fell back to 1.32 V. This pattern was present every set and the values did not change very much with time. The peak separation pattern arose from the movement of both peaks. In general, both were closer to 0 V at low cycling frequencies, moved away from 0 V with increasing frequency and then started back towards 0 V at high frequencies (3.0 Hz). This apparent situation at 3.0 Hz was likely just a data collection artifact though, as the peaks were never fully captured in the CVs at .30 Hz. Many of these details regarding the cycling frequency CV features are best illustrated through a comparison of the CVs (see Figure 4-17).

On the topic of movement responsiveness, there was also a clear trend. It improved with cycling frequency at both DCD values, although the levels were slightly better for the low DCD. The responsiveness values for the .03, .05 and .30 Hz samples were 0.446, 0.492, and 0.854 mm/mC, and 0.398, 0.479 and 0.714 mm/mC for the low and high DCD samples at cycle 41, respectively. The magnitudes of the responsiveness values for the 3.0 Hz samples were not reliable. The movements were so small that combined with the accuracy of the curling measurements, the accuracies of the responsiveness values were suspect even though they did seem to continue the trend e.g. 1.250 mm/mC for the high DCD sample.

The ratio of charge exchange to peak current fell in almost exact inverse proportion to cycling frequency. For example, with low DCD samples at .03 Hz, the

Figure 4-17 Cyclic voltammograms from the stimulation frequency variations collected using LabVIEW software. The 40th cycle for the .03 Hz, .30 Hz and 3.0 Hz samples grown at 16 mA/cm². The data was collected at 100 Hz.



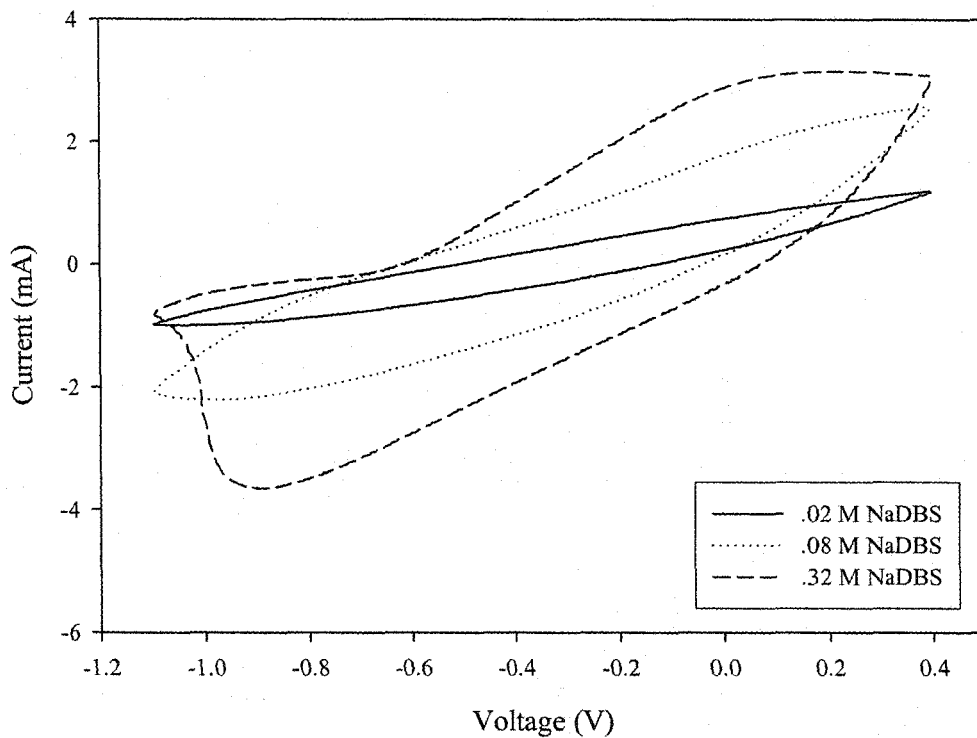
ratio was 8.6. It was .83 at .30 Hz, and .08 at 3.0 Hz. While the ratios were slightly smaller for high DCD samples, the proportions were the same.

The variations in stimulation NaDBS concentration (SN) produced results that generally mirrored the results of Chapter 3, and including the controls, there were 4 concentrations to work with here (.02, .08, .16 and .32 M).

Curling increased with SN, although there were no clear differences at the highest SN levels. High DCD samples moved 25-35% less than the low DCD samples. Curling levels were fairly steady overall, over the 41 cycles. Charge exchange followed a similar pattern, although the rate at which charge exchange increased with SN differed by DCD value. At low DCD, the rise would plateau out at a lower SN value. There were more noticeable differences between SN levels with the charge exchange at 16 mA/cm². The patterns with the peak currents were very similar to those of the charge exchanges.

With regard to the peak voltages, at low DCD, the reduction peaks did the same thing under all SN conditions. They started at the limit and slowly moved about .06 V anodically over the 41 cycles. The lower SN oxidation peaks were at or beyond the oxidation limit for the full 41 cycles. The higher SN peaks, however, started at about .25 V, rose to the limit by around the 30th cycle and then started back towards 0 V by the 40th cycle, in the case of .32 SN. Patterns for the high DCD were similar, but the peak separation was reduced in all but the lowest SN case. Indeed, peak separation decreased with increases in SN as both peaks moved towards 0 V. Nevertheless, both peaks slowly moved anodically over the 41 cycles. Many of these details regarding the SN concentration CV features are best illustrated through a comparison of the CVs (see Figure 4-18).

Figure 4-18 Cyclic voltammograms from the stimulation NaDBS variations collected using LabVIEW software. The 40th cycle for the .02 M, .08 M and .32 M NaDBS samples grown at 16 mA/cm². The data was collected at 100 Hz.



As in Chapter 3, the movement responsiveness data was not entirely clear. At low DCD, the trend was clean enough. The responsiveness went down with increases in SN (0.603 to 0.526 to 0.492 to 0.443 mm/mC). However, at high DCD, this pattern was not present. Indeed, all of the values were similar (0.424, 0.465, 0.479, 0.407 mm/mC). To add more confusion, these results could be interpreted as being at odds with the findings of Chapter 3, although I never varied SN with respect to fixed DP and DN values, and it may be the case that movement responsiveness is very sensitive to interaction effects.

The situation with the charge exchange to peak current ratio was equally complex and unclear. On the reduction side, the ratio falls off precipitously at high SN levels (and especially at high DCD levels) but is fairly stable at lower SN and DCD levels. Indeed, at the high DCD level, the ratio started off higher and finished lower over the SN concentration range. Interestingly, the opposite was true on the oxidation side. The range of values was narrower for the high DCD samples and the trend overall was a rise in the ratio with SN concentration.

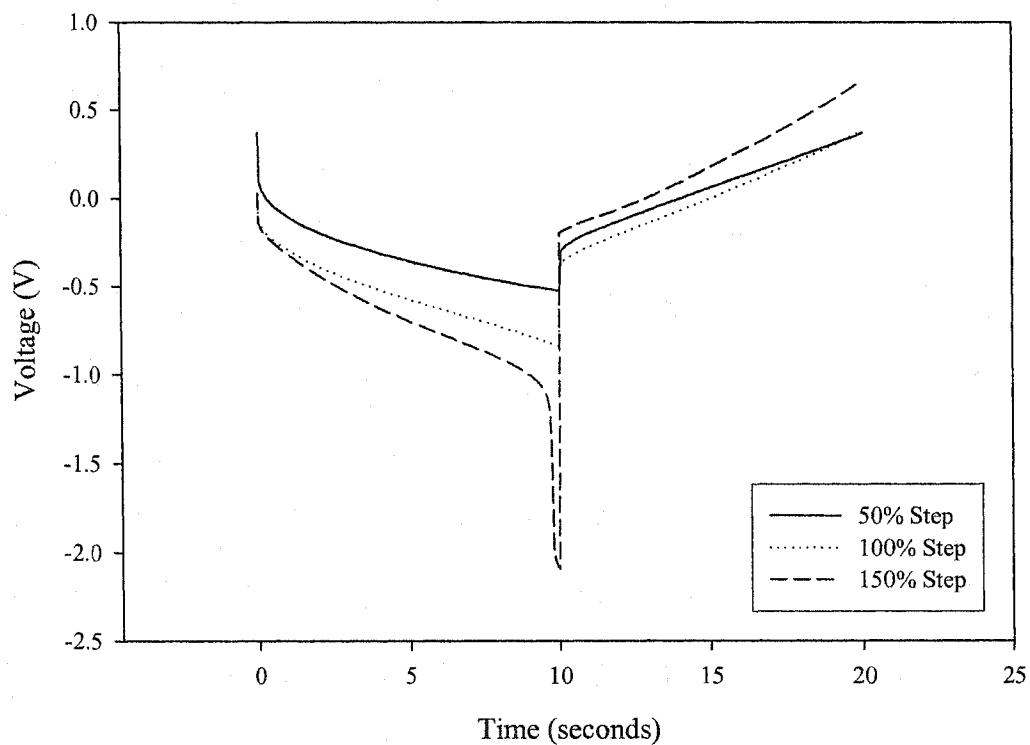
The last set of parametric variations was the current step variations. The current steps scaled relative to the charge exchange of the conditioning cycle where the most charge was exchanged. The curling patterns were fairly straightforward. The greater the step, the more curling that was produced. In all cases, the low DCD curling exceeded the high DCD curling, even accounting for the fact that the low DCD samples were being stimulated with about 1/3rd more charge. However, at 150% with the high DCD sample, the stimulation destroyed the integrity of the fiber, causing it to behave erratically.

For the current steps, the peak voltages did not represent the same thing as they did in the case of the CVs. However, it was worth looking at the differences between

conditions. The peak voltages in these cases were the maximum voltages attained during reduction and oxidation, independent of when they occurred during the current step. In general, the higher the percentage step, the greater the peak voltage. However, the exact nature of this relationship varied with DCD value and with reduction versus oxidation. On the reduction side, the peaks went from -0.5 to -0.8 to -2.2 V for both DCD values. They were fairly stable over the last 20 cycles or so. On the oxidation side there was more movement over the 41 cycles and less in common between DCD values. Both 50% samples started at the lowest peak voltage. However, the peak magnitude increased over time. The 100% samples both started in the middle, and went down slightly with time. The low DCD 150% sample stayed fairly high/constant over time, while the high DCD sample started high and went higher with time (to +2.2 V). Many of these details regarding the current level stimulation features are best illustrated through a comparison of the voltammograms (see Figure 4-19).

With movement responsiveness, the low DCD samples were again superior. However, the relationship with current level was not monotonic. The 50% samples performed best (0.774 and 0.645 mm/mC for the low and high DCD values, respectively), with the 150% samples next (0.646 mm/mC for the low DCD value). The 100% samples finished last at 0.594 and 0.533 mm/mC. The high DCD values were more stable over the 41 cycles.

Figure 4-19 Voltammograms from the current step variations collected using LabVIEW software. Voltage signals for the 40th cycle from the 50%, 100% and 150% samples grown at 2 mA/cm². The data was collected at 100 Hz.



4.3.5 Post-Experimental Cycling

For both experiments, one of the key steps was the last step. This involved repeating the conditioning protocol to see if the different stimulation conditions of the variable protocol would affect the curling of the beams afterwards.

We'll look first at the results of the range experiment. There were two main issues to examine here. One was to see whether and how the post-experimental data differed from the conditioning data by cycling frequency/scan rate. As well, and not necessarily dependently, one could also look at how the data may have been different with respect to the particular type of range expansion that it experienced.

Regarding the comparison to the conditioning data by cycling frequency/scan rate, the patterns found in the conditioning data were largely found in the post-experimental data as well, although many of the magnitudes were different. For instance, the charge exchange data were very similar to the data at the end of the conditioning phase in all ways. On the other hand, while the nature of the peak current relationships was also the same, the magnitudes of all the plots had changed. Most of the 200 mHz (600 mV/s) samples had increased 15-18%. The peak currents of the 100 mHz (300 mV/s) samples had also increased marginally (8-10%), and the peak currents of the 50 mHz (150 mV/s) samples either increased slightly (oxidation) or decreased (reduction). Oxidative peak voltages were now out of cycling range for the 100 and 200 mHz samples, and the peaks were approaching the cycling limits for the 50 mHz samples. Conversely, the reduction peaks were now more positive. At 200 mHz, they were still out of range, but for the 100 and 50 mHz samples, the reduction peaks had become .07

and .14 V more anodic compared to the conditioning cycles. In all cases, the peak separation had increased slightly since the conditioning cycles.

In terms of curling, there were some changes relative to the conditioning cycles. The 200 mHz samples still performed worst, but they had improved from .38 to .58 cm curl. Meanwhile, the 100 mHz samples had held steady and the 50 mHz samples had started to perform less well, falling from .92 to .74 cm. While the picture regarding movement responsiveness was not at all clear during the conditioning cycles, a very consistent pattern did appear at this stage. The higher the cycling frequency/scan rate, the better the responsiveness was. For the 50, 100 and 200 mHz cases respectively, the average values were .418, .535 and .641 mm/mC. Regarding the charge exchange to peak current ratio, it was essentially unchanged for the 100 and 200 mHz samples, but fell on the oxidation side and increased on the reduction side for the 50 mHz samples.

Equally interesting were the changes, or lack thereof, resulting from the various range expansions. Even without considering the different cycling frequencies/scan rates, the progression with respect to range expansion was quite clear. Values for charge accumulation, curling ROM, charge exchange, peak currents and peak locations/voltages all increased monotonically in the order of oxidation expansion, redox expansion and reduction expansion. Along this progression, peak voltages all became more anodic. The movement responsiveness increased and the ratio of charge exchange to peak current levels decreased. In general, the control samples were roughly equivalent to the redox expansion case and they always fell within the oxidation and reduction range expansion values except, notably, in the case of movement responsiveness, where the controls were the worst performer. Keep in mind that all of these trends were not terribly clear, by

range expansion group. The variations due to within-group cycling frequency differences masked any clarity. However, when the data was separated out by different cycling frequencies/scan rates, most of these trends became very obvious. The few exceptions were due to the fact that the groups still mixed the constant cycling frequency and constant scan rate data, which while similar, were sometimes slightly different (as seen previously in this section). For instance, the constant scan rate accumulation data was always greater than the constant cycling frequency data, and the mid-high cycling frequency peak reduction current data was always greater than the data corresponding to constant scan rates.

There was also an interesting interaction between cycling frequency/scan rate and the type of range expansion, with respect to curling ROM. We have seen that ROM decreased, in order, from oxidation, to redox, to reduction expansion, to controls, and from mid, to low, to high cycling frequency. The interactions explain these otherwise unclear patterns. From low to high cycling frequency, the oxidation range expansion curling went from best of all to worst of all while the reduction range expansion curling went from worst to best. The redox and control data points were always in the middle.

For the history experiment, just as with the range experiment, there were a few ways to look at the post-experimental data. The first was to look at it in the same way as the conditioning data, by DCD value. The second was to look at it by experimental condition (mode, SN, current, frequency) versus conditioning data, and controls.

Comparing with the conditioning data by DCD value, the low DCD curls remained approximately 20% more extensive and all curling had increased by 3-5%. Low DCD samples still produced greater charge exchange but the margin was reduced.

The low DCD charge exchanges had grown by about 15% while the high DCD average exchanges had grown by about 30%. With peak currents, the reduction currents grew in all cases by about 10%. On the oxidation side, the low DCD peak currents increased by 15% while the high DCD data increased by about 30%. With the peak voltages, the reduction peaks were slightly more anodic for both DCD values. However, all of the oxidation peaks were now either at or beyond the oxidation limits. Overall, peak separation increased from the conditioning to the post-experimental cycles.

With respect to movement responsiveness, there was a marked decline for the high DCD samples (from an average 0.548 to an average 0.447 mm/mC) as well as a marginal decline for the low DCD samples (from an average 0.539 to 0.503 mm/mC). Charge exchange to peak current ratios remained largely unchanged from the end of the conditioning cycles.

With regards to stimulation mode, there were not many differences in the behaviour of the beams during the post-experimental cycling. While all of the samples of a given DCD value had accumulated very similar amounts of charge during the conditioning cycles, in the post-experimental cycles the voltage step samples accumulated much more negative charge than did the others. Curling, charge exchange and peak currents were relatively unchanged. There were some slight differences on the voltage peaks, however. The reduction peaks for the CV samples both moved slightly in the anodic direction, as did the reduction peak of the high DCD current step sample. Movement responsiveness was reduced by 11-12% for the low DCD samples, and by 16-24% for the high DCD samples.

Looking at the samples of the stimulation frequency variations, again there were changes in charge accumulation that seemed to correlate with the varied factor. For both DCD values, the charge accumulation during post-variation cycling decreased with frequency until 3.0 Hz when it increased again. There were no clear effects on curling extent, charge exchange, peak currents or peak voltages though. Movement responsiveness was again reduced, by 5-20% for the low DCD samples and by 9-25% for the high samples. At both DCD values, the lowest frequency samples lost the most and the .30 Hz samples lost the least in terms of responsiveness.

With the variations in SN concentration, charge accumulation during the post-experimental cycles again provided the only hint of different pasts for the fibers. In all but 1 of 8 cases, they increased in magnitude with SN concentration. The only other remarkable point was that for the low DCD and low SN sample, the curling movement, charge exchange and peak current levels all increased substantially from the conditioning to the post-experimental cycles. Movement responsiveness was generally reduced with these samples but not in all cases, and there were clear differences between the two DCD values. The low DCD values saw a 9.5% gain at .02 M and losses of up to 11% on the others, while in general, the high DCD values saw losses of 17-21%.

Finally, with respect to the current step variations, there were some differences in performance based on stimulation history, keeping in mind that the 150% high DCD sample did not make it to the post-experimental round. This time, while charge accumulation did not show any pattern, some of the other measurements did. The surviving 150% sample expanded its curling ROM considerably (30%) while its charge exchange and peak currents shrank, relatively. Responsiveness losses (gains) were

similar to those of the SN concentrations. There was an 18% increase at 150% (for the low DCD sample) and losses in all other conditions, although greater losses at high DCD.

4.4 Discussion

Several investigators have described changes in relevant polypyrrole electrochemical behaviour as a function of stimulation activity (Chiarelli et al. 1995, Della Santa et al. 1997, Gandhi et al. 1995, Kupila et al. 1995, Wegner et al. 1987, Ko et al. 1994, Kuwabata et al. 1984, Iseki et al. 1991, Li and Qian 1993, Maw et al. 2001, Pei and Inganäs 1993a-d, Pei et al. 1993, De Paoli et al. 1992, Otero and De Larreta 1988). As such, they provide us with some indication of what may be expected when we examine the effects of stimulation history on current activity in PPy(DBS)-actuated bending beams. However, the broad spectrum of different electrolytes, dopants and solvents used in these various studies will limit how well their findings can be generalized.

For example, Kuwabata et al. (1984) completed 10,000 cycles of CVs with PPy(ClO₄) in KCl. Peak magnitudes decreased with time and both peaks shifted anodically. Otero and De Larreta (1988) saw their peak currents rise and then fall over 90 polymerization voltage step cycles with PPy(ClO₄). Chiarelli et al. (1995) also saw peak currents decrease with time over 15 hours with PPy(BS) in NaBS. The extent of strain cycling stayed quite steady over this time, but the rest length of the fiber did change slowly. Gandhi et al. (1995) saw the same mechanical creep effect in their tensile cycling tests. I also saw evidence of these effects in my work.

Ko et al. (1994) expanded the anodic cycling range with PPy(DS) in NH₄Cl and ZnCl₂. Both peaks grew. I found evidence of the same at my lowest cycling frequencies, and indeed, Ko's group was cycling at less than 100 mV/s. They also looked at charge exchange per cycle over time, and it decreased by about 30% over 100 cycles. My results

were steadier but some did degrade slightly with time. De Paoli et al. (1992), with PPy(DBS) in KCl, found that the reduction peaks grew significantly with time. They scanned much more slowly, however, and with very thin film.

Li and Qian (1993), Pei and Inganäs (1993c), and Kupila et al. (1995) all took note of the anomalous first reduction followed by much smaller reduction current levels. Della Santa et al. (1997), working with PPy(BS) in NaBS, observed that the early reductions settled to a steady state within 20 cycles and that peaks shifted anodically with time. They also contended that the first reduction reflected the film's dopant anion loss.

Pei and Inganäs' work (Pei et al. 1993, Pei and Inganäs 1992, 1993a-d) with polypyrrole and polyaniline bending beams showed that behaviour over time varied considerably with dopant and electrolyte, but that there were some trends. The range of bending tended to decrease initially but steadied in most cases after 40-60 cycles. Often, as in my studies (see Chapter 3), the average bend would increase or decrease slowly with time. They also held their PPy(Cl) films at negative potentials for varying periods of time (Pei and Inganäs 1993c) and then cycled them. The longer the hold, the greater and more anodic the first oxidation peak would be. Oxidation holds had much smaller effects and had to be very long (>1000 seconds) to produce any effect at all. When they did the same with PPy(DBS) films in NaDBS there were almost no effects at all for holds at the reduction limit. For holds at the oxidation limit, however, the reduction peak became deeper and more cathodic with increasing hold time.

Once again (see Maw et al. 2001), it was clearly observed that the beams that curled more during deposition, curled more during the conditioning cycles. Those beams that curled more were the low DCD beams, in comparison to the high DCD beams. I also

looked at how the charge exchange capacity varied over cycling time during the conditioning cycles. For low DCD films, they started out at about 4.5% and increased with time. For the high DCD films, they started out at 4.7% on average, quickly dropped to 3.5% and then gradually rose slowly with further cycling, always staying at values less than those of the low DCD beams.

During the current steps, the beams that were stimulated at more than the 100% charge level showed an extra feature in their voltammogram (see Figure 4-19). The late increase in voltage appeared to correlate with the fact that the film had expended its charge capacity. These overpotentials may have also been responsible for the poor subsequent performance of these fibers. Anecdotally, this second level of voltage produced delamination effects and destruction of the electrochemical activity in the films. Aside from these few “over-stimulation” situations, the activity of the beams held up well in terms of endurance, lasting more than 80 cycles in all cases.

In the introduction to this chapter, I discussed some of the ways in which natural muscle fibers behave, given past activity. Fatigue is a major influence, and the positive adaptations resulting from training can be as well. With the PPy(DBS) beams I saw several examples of fatigue and creep as curling extent dropped off with cycling and the angle of the beam at the redox limits changed with time. The literature provides several other examples. None of my various “training regimens” provided any notable positive benefits later on, except for range expansion. Such effects may be dependent on factors such as the NaDBS concentration in the stimulation solution, however, so more work is indicated. As well, range expansion may very well provide an effective training regime

for PPy(DBS) as it seems to create lasting effects in behaviour. More work in this area is also justified and required.

More than anything else, my current study showed that with PPy(DBS)-actuated devices, management of the cycling limits is important and so is cycling frequency. While changes in cycling frequency were introduced in this study, and while some very clear trends regarding how cycling frequency affects the beams were revealed, this topic deserves more attention. A broader range of frequencies in conjunction with different values of other variables will help to elucidate further qualities of the PPy(DBS) films. This will be the subject of the next study in Chapter 5.

4.5 Conclusions

For the PPy(DBS)-actuated bending beams described in this chapter, curling at any given time as a result of strains transverse to the plane of the film and with respect to past cycling activity, was shown to be influenced most by changes in cycling range in combination with cycling frequency.

Expansion of the cycling range at both limits led to a linear increase in charge exchange, peak currents, and peak voltage levels, as well as to an increase in curling. The increase in curling with range expansion increased with cycling frequency. Also, wider cycling ranges reduced the drop-off in curling with cycling frequency. Movement responsiveness decreased with cycling range, except at high frequencies. CVs showing redox range expansion uniformly scale up in size with cycling range. Increasing the cycling frequency decreases the hysteresis in the CVs.

Range expansion strictly on the reduction side had different effects. At low cycling frequencies, curling was reduced and the CVs would just develop a tail. At high frequencies, curling was enhanced and a true reduction peak developed as well as a thicker oxidation lobe. Movement responsiveness increased at high frequencies, increased slightly at mid-level frequencies and decreased slightly at low frequencies.

Range expansion strictly on the oxidation side produced other effects, including no changes in curling over the range of range expansion studied. Movement responsiveness went down, and charge exchange did not vary at high cycling frequencies although charge exchange did increase with increasing range at low-mid frequencies. At all frequencies studied, the oxidation lobe on the CV would grow with oxidation range expansion and the reduction peak would disappear (beyond the reduction limit).

As part of the history study, stimulation mode was examined. Voltage steps produced more curl than CVs. However, the amount of movement per unit charge exchange was worst for voltage steps and was best for current steps.

Cycling frequency was also controlled and varied. It had a strong effect which, among other things, decreased the curling as frequency increased from .03 to 3.0 Hz. It was found that increasing frequency or scan rate increases peak currents and peak voltage separation while decreasing charge exchange and therefore strain (curling). Movement responsiveness did not appear to be sensitive to cycling frequency at first (.05 to .20 Hz). However, later on, in the range of .03-3.0 Hz, it did increase with frequency while charge exchange capacity as a percentage of deposition charge decreased.

Increases in stimulation NaDBS levels had the same effects as those described in Chapter 3. However, since deposition pyrrole and NaDBS were fixed at .16 M here, there were some new subtleties that were not noticed previously. Specifically, curling did increase with SN, but to a limit where it plateaued (as did charge exchange).

For current step stimulation, curling increased with the size of the step, as did peak voltages. Movement responsiveness was better at lower and higher current levels.

In terms of how the bending beams behaved after the range expansion conditions in comparison to the earlier conditioning cycles, the higher the frequency of stimulation the more the peak currents had increased and the more the curling had improved. At low frequencies, curling had degraded. There was now a very clear pattern of movement responsiveness increasing with cycling frequency. At lower cycling frequencies, in the order of oxidation, redox/controls, and reduction range expansion, curling, charge exchange and peak currents all decreased while charge accumulation became more

positive and voltage peaks became more anodic. Movement responsiveness increased and charge per unit (peak) current decreased. For movement responsiveness, the controls actually performed worst. There were also interactions between type of range expansion and cycling frequency. At higher frequencies, the order of the range expansions reversed in terms of their effects on the various measures. For instance, at low frequencies oxidation expansion produced the best curling, while at high frequencies it produced the worst (and vice versa for reduction expansion).

In terms of how the “history” variations affected final performance, they did not have a dramatic effect in terms of curling, peak currents etc. This includes the cycling frequency variations, which would suggest that it was the range expansion that caused the frequency variations in the range experiment to become prominent.

Finally, lower and higher valued DCD samples went through all of the “history” variation conditions. There were consistent differences between samples of the two DCD values. These were mostly consistent with previous work (Maw et al. 2001). However, in the current work, low DCD films had greater movement responsiveness and charge exchange per peak current. Also, when cycling frequency was varied, low DCD beams had a greater range of movement values. For instance, at high cycling frequencies, they moved less than the high DCD samples. At low frequencies, they moved more. The charge exchanges and peak currents of high DCD beams did not plateau as early as those of low DCD beams, at higher SN levels. While movement responsiveness generally decreased during the post-step cycling versus the conditioning, low DCD samples had the smallest decreases.

We know that DCD, stimulation mode and stimulation NaDBS concentration are important in determining the performance of PPy(DBS)-actuated devices. We can now also say that stimulation frequency is critical. Regarding stimulation history, there did not appear to be an effect unless the cycling range was being manipulated. In that case, it can be quite important and it would appear that cycling frequency has an interactive effect as well. In fact, depending on the frequency that one is cycling at, one would probably want to alter one limit or the other to get the kind of strain characteristics that may be desired. Conversely, by changing cycling limits, one changes the frequency response of the beams as well as peak voltages, currents etc. We also now know that DCD interacts with frequency response characteristics, and that increasing stimulation NaDBS has its limits in terms of benefits. These findings, in combination with those of Chapters 2 and 3, provide makers of PPy(DBS)-actuators with an increasingly large arsenal of tools to design their actuators to particular functional specifications.

4.6 References

- Allen, D.G., Lee, J.A., and Westerblad, H. (1989) "Intracellular calcium and tension during fatigue in isolated single muscle fibres from *Xenopus laevis*", *Journal of Physiology*, Vol. 415, pg. 433-58
- Bobacka, J., Gao, Z., Ivaska, A., and Lewenstam, A. (1994) "Mechanism of ionic and redox sensitivity of p-type conducting polymers Part 2. Experimental study of polypyrrole", *J. Electroanal. Chem.*, Vol. 368, pg. 33-41
- Burke, R.E., Rudomin, P., and Zajac, F.E. III (1970) "Catch property in single mammalian motor units", *Science*, Vol. 168, pg. 122-124
- Burke, R.E., Levine, D.N., Salzman, M., and Tsairis, P. (1974) "Motor units in cat soleus muscle: Physiological, histochemical and morphological characteristics", *Journal of Physiology (London)*, Vol. 238, pg. 503-514
- Chen, X.B., Devaux, J., Issi, J.-P., and Billaud, D. (1994) "The stability of polypyrrole electrical conductivity", *Eur. Polym. J.*, Vol. 30, #7, pg. 809-11
- Chiarelli, P., Della Santa, A., De Rossi, D., and Mazzoldi, A. (1995) "Actuation properties of electrochemically driven polypyrrole free-standing films", *J. Intell. Mater. Struct. Syst.*, Vol. 6, pg. 32-37
- De Paoli, M.-A., Peres, R.C.D., Panero, S., and Scrosati, B. (1992) "Properties of electrochemically synthesized polymer electrodes – X. Study of polypyrrole/dodecylbenzene sulfonate", *Electrochimica Acta*, Vol. 37, pg. 1173-82
- Della Santa, A., De Rossi, D., and Mazzoldi, A. (1997) "Characterization and modeling of a conducting polymer muscle-like linear actuator", *Smart Mater. Struct.*, Vol. 6, pg. 23-24

Gandhi, M.R., Murray, P., Spinks, G.M., and Wallace, G.G. (1995) "Mechanism of electromechanical actuation in polypyrrole", *Synthetic Metals*, Vol. 73, pg. 247-256

Ghez, C. (1991) "Chapter 36 - Muscles", In: **Principles of Neural Science, 3rd Ed.**, E.R. Kandel, J.H. Schwartz, and T.M. Jessell [eds], Appelton & Lange, Norwalk, USA

Hahn, S.J., Gajda, W.J., Vogelhut, P.O., and Zeller, M.V. (1986) "Auger and infrared study of polypyrrole films: evidence of chemical changes during electrochemical deposition and aging in air", *Synthetic Metals*, Vol. 14, pg. 89-96

Hunter, I.W. and Lafontaine, S. (1992) "A comparison of muscle with artificial actuators", *Proceedings of the IEEE Sensors and Actuators Workshop*, Hilton Head Island, June 21-25

Iseki, M., Kuhara, K., and Mizukami, A. (1991) "Study on electrically plastic devices made with electropolymerized films", *Jap. J. App. Phys.*, Vol. 30, #5, May, pg. 1117-121

Ko, J.M., Kim, S., Kim, K.M., and Chung, I.J. (1994) "Electrochemical properties of dodecylsulfate-doped polypyrrole films in aqueous solution containing NH_4Cl and ZnCl_2 ", *Synthetic Metals*, Vol. 64, pg. 9-15

Kupila, E.-L., Lukkari, J., and Kankare, J. (1995) "Redox processes in thick films of polypyrrole/dodecylsulfate in the presence of alkali and tetramethylammonium chlorides", *Synthetic Metals*, Vol. 74, pg. 207-215

Kuwabata, S., Yoneyama, H., and Tamura, H. (1984) "Redox behavior and electrochromic properties of polypyrrole films in aqueous solutions", *Bulletin of the Chemical Society of Japan*, Vol. 57, pg. 2247-2253

Li, Y. and Qian, R. (1993) "On the nature of redox processes in the cyclic voltammetry of polypyrrole nitrate in aqueous solutions", *J. Electroanalytical Chem.*, Vol. 362, pg. 267-272

Maw, S., Smela, E., Yoshida, K., Sommer-Larsen, P., and Stein, R.B. (2001) "The effects of varying deposition current density on bending behaviour in PPy(DBS)-actuated bending beams", *Sensors and Actuators A*, Vol. 89, pg. 175-184

McComas, A.J. (1996) **Skeletal Muscle: Form and Function**, Human Kinetics, USA

Moore, R.L. and Stull, J.T. (1984) "Myosin light chain phosphorylation in fast and slow skeletal muscles in situ", *American Journal of Physiology*, Vol. 247, pg. C462-471

Otero, T.F. and De Larreta, E. (1988) "Electrochemical control of the morphology, adherence, appearance and growth of polypyrrole films", *Synthetic Metals*, Vol. 26, pg. 79-88

Pei, Q. and Inganäs, O. (1992) "Electrochemical applications of the bending beam method. 1. Mass transport and volume changes in polypyrrole during redox", *J. Phys. Chem.*, Vol. 96, #25, pg. 10507-514

Pei, Q. and Inganäs, O. (1993a) "Electrochemical muscles: bending strips built from conjugated polymers", *Synthetic Metals*, Vol. 55-57, pg. 3718-23

Pei, Q. and Inganäs, O. (1993b) "Electrochemical applications of the bending beam method; a novel way to study ion transport in electroactive polymers," *Sol. State Ion.*, Vol. 60, pg. 161-66

Pei, Q. and Inganäs, O. (1993c) "Electrochemical applications of the bending beam method. 2. Electroshrinking and slow relaxation in polypyrrole," *J. Phys. Chem.*, Vol. 97, pg. 6034-41

Pei, Q. and Inganäs, O. (1993d) "Electroelastomers: conjugated poly(3-octylthiophene) gels with controlled crosslinking", *Synthetic Metals*, Vol. 55-57, pg. 3724-3729

Pei, Q., Inganäs, O., and Lundström, I. (1993) "Bending bilayer strips built from polyaniline for artificial electrochemical muscles", *Smart Mater. Struct.*, Vol. 2, pg. 1-6

Pollack, G.H. (1990) **Muscles and Molecules: Uncovering the Principles of Biological Motion**, Ebner and Sons, Seattle, WA, USA

Rack, P.M.H. and Westbury, D.R. (1969) "The effects of length and stimulus rate on tension in the isometric cat soleus muscle", *J. Physiol.*, Vol. 204, pg. 443-460

Rothwell, John C. (1987) **Control of Human Voluntary Movement**, Aspen Publishers Inc, USA

Slomíc, A., Rosenfalck, A., and Buchthal, F. (1968) "Electrical and mechanical responses of normal and myasthenic muscle with particular reference to the staircase phenomenon", *Brain Research*, Vol. 10, pg. 1-78

Smela, E. (1999) "Microfabrication of PPy microactuators and other conjugated polymer devices", *J. Micromech. Microeng.*, Vol. 9, pg. 1-18

Stein, R.B., Gordon, T., and Shriver, J. (1982) "Temperature dependence of mammalian muscle contractions and ATPase activities", *Biophys. J.*, November, pg. 97-107

Thiéblemont, J.C., Planche, M.F., Pétrescu, C., Bouvier, J.M., and Bidan, G. (1994) "Kinetics of degradation of the electrical conductivity of polypyrrole under thermal aging", *Polymer Degradation and Stability*, Vol. 43, pg. 293-298

Truong, V-T., Ennis, B.C., and Forsyth, M. (1995) "Ion exchange, anisotropic structure and thermal stability of polypyrrole films", *Synthetic Metals*, Vol. 69, pg. 479-80

Warshaw, D.M. (1996) "The in vitro motility assay: a window into the myosin molecular motor", *News Physiol. Sci.*, Vol. 11, February, pg. 1-7

Wegner, G., Wernet, W., Glatzhofer, D.T., Ulanski, J., Kröhnke, C.H., and Mohammadi, M. (1987) "Chemistry and conductivity of some salts of polypyrrole", *Synthetic Metals*, Vol. 18, pg. 1-6

Zajac, F.E. and Young, J. (1975) "Motor unit discharge patterns during treadmill walking and trotting in the cat", *Abstract #255*, 5th Annual Meeting of the Society for Neuroscience, New York

5. The Frequency Response of PPy(DBS)-Actuated Bending Beams Under Various Conditions

5.1 Introduction

One of the fundamental functional properties of a muscle fiber is its frequency response. That is, how well does it follow a train of stimulation signals, both in terms of phase lag and magnitude of response, as the frequency of the stimulation signal is varied? For those interested in creating artificial muscle fibers (AMFs), the question is equally relevant. Indeed, it is one of the major challenges in creating an AMF since so many of the polymer approaches depend on diffusion rate limited processes. Still, that should not dissuade us from pursuing such approaches, since natural muscle employs an optimized diffusion rate limited process in handling the calcium ions that are pivotal to its excitation-contraction coupling, and natural muscle does quite well by it.

If we are trying to make AMFs that behave like natural muscle, then we need to know what the frequency response characteristics of natural muscle fibers are first. As a generalization, we can say that they act as low pass filters (LPFs) to their neural input. The action potential and calcium release in the muscle fiber takes place over the space of a few milliseconds. The twitch tension response of the fiber, on the other hand, lasts anywhere from 50 to several hundred milliseconds, depending on the type of muscle involved. As such, once the stimulation frequency reaches a certain critical level (the cut-off frequency), the range of contraction will start to decrease rapidly as the fiber will not have had time to fully relax before the next stimulus is received. In 1976, Aaron et al. showed that the cut-off frequency for unloaded human biceps muscle was approximately 2.3 Hz under isometric conditions, and slightly less under load. Bawa et al. (1976) found similar values for plantaris muscle. Partridge (1966) first demonstrated

the LPF qualities of muscle fibers when he sinusoidally modulated the frequency of a stimulus train to a muscle fiber. At low modulation frequencies (e.g. .16 Hz), the fibers faithfully varied tension in a sinusoidal fashion, albeit with a slight phase lag. At higher modulations (e.g. 1.6 Hz), the fluctuations in tension were reduced, and by a frequency modulation of 4 Hz there was almost no variation in tension at all. He also showed that the fibers exhibit a phase lag which increases with stimulation rate.

As noted previously (Chapter 4), there are different kinds of muscle fibers that contract and fatigue at different speeds. Not only do these factors affect the frequency response, but so do the pre-stimulation fiber lengths in any frequency response evaluation (Mannard and Stein, 1973). Clearly, natural muscle fibers behave in complex ways. Therefore, it would be of great scientific and practical interest to create equivalent functional differences in AMFs. Such an accomplishment would open the door to using more naturally inspired motor control strategies in controlling AMFs.

Since we also know that the various structural differences in the machinery of the natural muscle fiber are responsible for the functional differences between fast and slow twitch muscle, it would be prudent to look for such differences in AMF polymer formulations that would make them behave differently. We can do this with the volume-changing PPy(DBS) films (Maw et al. 2001, Smela 1999, Smela et al. 1995, Smela and Gadegaard 1999). Scanning electron microscopy (SEM) has been the method of choice for studying polypyrrole of late.

In the present study a wide variety of PPy(DBS)-actuated bending beams (Pei and Inganäs 1992, 1993a-c) are taken through several sets of ramp voltammetry cycles. Each set involves cycling at a different cycling frequency. The intent was to see how the

beams reacted to this sort of stimulation and to see if there were any patterns of differences between thin and thick beams and/or films made at different deposition current densities. A parallel SEM study looked for structural reasons as to why any behavioural differences may have been present.

Over the last 20 years, there have been many SEM images taken of the surfaces of polypyrrole films. There have been studies of polypyrrole with different deposition dopant concentrations (Kaynak 1997, John et al. 1992, Naoi et al. 1995), SEM images of stretched PPy(CF₃SO₃) films (Ogasawara et al. 1986, Yamaura et al. 1988) as well as some SEM images of PPy(DBS) (An et al. 1994, Peres et al. 1989), our primary interest here. Other SEM images have been taken of polypyrrole grown in different solvents (Otero and De Larreta 1988, Ko et al. 1990, Diaz and Hall 1983) and of polypyrrole grown with different electrolytes/dopants, most commonly para toluene sulfonate (Beck et al. 1994, Kaplin and Qutubuddin 1995, Gardner and Bartlett 1995, Gandhi et al. 1995, Wallace et al. 1997, Nishizawa et al. 1991, Salmon et al. 1982). Of closest interest to my current study are the few SEM images taken of polypyrrole films produced at different deposition current densities (Mitchell and Geri 1987, Scrosati 1988, Stanković et al. 1994, De Paoli et al. 1992).

Studies that have looked at the CVs (and related features such as peak currents) resulting from cyclic voltammetry performed at different scan rates/frequencies include Kaplin and Qutubuddin (1995), Ko et al. (1990), Scrosati (1988), Cheung et al. (1988), Diaz and Bargon (1986), Ko et al. (1994), Kuwabata et al. (1984), West et al. (1992), and Doblhofer and Rajeshwar (1998). Actual frequency response studies for polypyrrole are more limited (Madden et al. 2000 and 2001). However, these studies have been well

focused and sophisticated. Since they have had some of the same goals as ours, they provide a good reference point. I will look at how my results compare with theirs later in the Discussion.

5.2 Experimental

The general methods and equipment used in this study were once again identical to those described in Chapter 2. However, as in Chapters 3 and 4, the protocols differed from the earlier work and these are reviewed below.

In this set of experiments, Kapton[®] HN 50 and Kapton[®] HN 100 sheets from Dupont, .5 mil (12.7 μm) and 1 mil (25.4 μm) thick respectively, were coated on one side with $450 \pm 50 \text{ \AA}$ and $500 \pm 50 \text{ \AA}$ of gold (Au) respectively, both by vacuum evaporation. The sheets were cut into strips 1 mm wide using a sharp blade mounted on an automated Karl Süss scribing machine.

PPy was deposited galvanostatically on a 1.5 cm long portion of the gold-coated surface of each strip in an aqueous .16 M NaDBS / .16 M pyrrole solution. For each thickness of Kapton[®], there were two sets of 5 experimental conditions. The two sets corresponded to DCD values of 2 and 16 mA/cm². The five conditions pertained to the specific PPy(DBS) thickness that was deposited on any given beam. I deposited 75, 150, 300, 600 or 1200 mC, corresponding to 0.5, 1, 2, 4 or 8 C/cm². As per Smela (1999), these values correspond to PPy(DBS) film thicknesses of approximately 2.5, 5, 10, 20 and 40 μm , as shown below in Table 5-1.

After deposition, the beams were run through 10 rounds of stimulation in a .16 M NaDBS aqueous solution that was changed after every sample. Every round consisted of 15 cycles of ramp voltammetry stimulation. The frequency of the cycling varied along with the oxidation and reduction limits in some cases, as is shown in Table 5-2.

Table 5-1 Frequency Response Experimental Conditions

DCD	Kapton [®] type and thickness		PPy(DBS) Thickness (C/cm ² and μm)
2 mA/cm ²	HN 50	12.7 μm	.5, 1, 2, 4, 8 C/cm ² = 2.5, 5, 10, 20, 40 μm
	HN 100	25.4 μm	.5, 1, 2, 4, 8 C/cm ² = 2.5, 5, 10, 20, 40 μm
16 mA/cm ²	HN 50	12.7 μm	.5, 1, 2, 4, 8 C/cm ² = 2.5, 5, 10, 20, 40 μm
	HN 100	25.4 μm	.5, 1, 2, 4, 8 C/cm ² = 2.5, 5, 10, 20, 40 μm

Table 5-2 Stimulation Frequencies

Set	Cycling Freq (Hz)	Scanning Rate (V/s)	Cycling Range (red/ox, V)	
a	.05	0.2	-1.35*	+0.65*
b	.10	0.4	-1.35	+0.65
c	.20	0.8	-1.35	+0.65
d	.40	1.6	-1.35	+0.65
e	.80	3.2	-1.35	+0.65
f	1.60	6.4	-1.35	+0.65
g	3.20	12.8	-1.35	+0.65
h	6.40	25.6	-1.35	+0.65
i	.40	1.6	-1.35	+0.65
j	.05	0.2	-1.35*	+0.65*

*in some cases the range was -1.1 V to +0.4 V, as these parameters reduced delamination

The order in which beams were produced and then stimulated was randomized. In all, 27 samples were produced, tested and evaluated. In all stimulation conditions, cycling started and ended at the oxidation limit. Range of movement of the beam tip, charge transfer per half cycle, maximum currents, and voltages at those redox peaks, were recorded for the 14th cycle of every set. In all cases, deposition and stimulation solutions were discarded after every use.

In support of this main experiment, a second experiment was carried out as a supplement. This secondary study looked at the PPy(DBS) films under scanning electron microscopes. The intent was three-fold: to confirm expected film thicknesses, to examine

film morphology, and to reveal elemental constituents in the films, all under a variety of production and stimulation conditions.

There were 4 main conditions that were varied: DCD, deposition pyrrole concentration (DP), deposition NaDBS concentration (DN), and stimulation NaDBS concentration (SN). Samples were produced at 1, 4, 8, 16 and 28 mA/cm². At 4 mA/cm² a larger number of samples were fabricated. Eight of these were used to study the effects of varying the deposition pyrrole and NaDBS concentrations. Another 10 were used to study the effects of oxidation and reduction on the film in various stimulation NaDBS concentrations. The entire set of conditions is shown below in Table 5-3.

Table 5-3 SEM Sample Preparations

DCD (mA/cm ²)	Deposition Pyrrole (molar [])	Deposition NaDBS (molar [])	Stimulation NaDBS (molar [])
1	.08	.08	na
4	.08	.08	na
8	.08	.08	na
16	.08	.08	na
28	.08	.08	na
4	.02	.08	na
4	.32	.08	na
4	.08	.02	na
4	.08	.32	na
4	.08	.08	.02 oxidation
4	.08	.08	.02 reduction
4	.08	.08	.08 oxidation
4	.08	.08	.08 reduction
4	.08	.08	.32 oxidation
4	.08	.08	.32 reduction

In this study, the Kapton[®] HN 100 with $350 \pm 50 \text{ \AA}$ of gold (Au) was used as the deposition substrate. As with previous work, the sheets were cut into strips 1 mm wide using a sharp blade mounted on an automated Karl Süss scribing machine.

PPy was deposited galvanostatically onto a 1.0 or 1.5 cm long portion of the gold-coated surface of each strip in an aqueous NaDBS/pyrrole solution, as per the conditions listed in Table 5-3. In all cases, the charge density was 2 C/cm^2 . In other words, they were nominally all the same thickness. However, I also used some samples from the main study on frequency response to examine empirically the thicknesses under different charge density conditions.

In the case of the variable DCD and variable deposition concentration samples, the procedure was straightforward. The deposition was performed, the beam was dunk rinsed in deionized water, it was put in a storage vial, and approximately 24 hours later it was frozen in liquid nitrogen so that it could be fractured for examination of the edges of the film. The fractured piece of the beam was then put on a mount and was placed in the SEM. The samples were not coated before placement in the SEM.

In the case of the reduced or oxidized samples, the process was somewhat more involved. After deposition the samples went through 15 conditioning cycles of ramp voltammetry stimulation. The redox limits were -1.1 and $+0.4 \text{ V}$ and the cycling frequency was $.05 \text{ Hz}$. Cycling started and ended at the oxidation limit. After these conditioning cycles, the samples were stimulated with one voltage step. The step was either up to $+0.4 \text{ V}$ (oxidation) or down to -1.1 V (reduction). The hold time was approximately 20 seconds. For the oxidized samples, after returning to 0 V , the samples were quickly removed from the stimulation solution and were then prepared for the SEM

like the others. For the reduced samples, the samples were removed from solution as the voltage was being turned off. Charge, current and range of movement data were recorded during all steps.

With regard to the SEM analyses, two machines were used. One was more specialized for elemental analysis while the other was more specialized for visual analysis (although elemental analyses were also conducted with this SEM). In the case of the elemental analyses, the accelerating voltage was 20.0 keV (KV) and the takeoff angle was 30.5 degrees, although some samples were also analyzed with a takeoff angle of 75.0 degrees. The accelerating voltage implied a depth of penetration of about 8 μm . PGT bulk sample analysis scans analyzed for oxygen, sodium and sulfur content using the ZAF method of corrections. For the textural and edge analyses, an accelerating voltage of either 5 or 15 keV was used. For texture, a magnification of X100 and/or X1000 was employed, while for the edge examinations a magnification of X700-5000 (most commonly X3500) was used.

In all cases, deposition and stimulation solutions were discarded after every use (or every other use where repeating conditions were possible). The order in which beams were processed was randomized. In all, 28 samples were produced, tested and evaluated.

5.3 Results and Observations

5.3.1 Film Growth

The frequency response and SEM samples were prepared under a number of conditions. In the case of the frequency response samples, there were a set of samples for each of two DCD values (2 and 16 mA/cm²). Within each of these sets the other controlled variables were deposition duration (corresponding to PPy(DBS) film thickness) and Kapton[®] film thickness (HN 50 or HN 100). The SEM samples were prepared under a wider variety of DCD values (1, 4, 8 and 16 mA/cm²). At 4 mA/cm², there were further variations based on deposition pyrrole (DP) and deposition NaDBS (DN) concentrations.

Looking strictly at variations between DCD groups, we see once again that deposition curling tends to decrease with DCD (or shorter deposition times) and that the capacitance spike increases with DCD as do average and final deposition potentials. Comparing film thicknesses for a given DCD value, the bulk electrical properties such as capacitance spike, and average and final potential, are not very different, as one might expect. There is only a slight decrease in potentials with film thickness.

The curling behaviour during deposition was also recorded. The frequency response samples showed less curling in HN 100 samples versus HN 50 samples, and less curling in 16 mA/cm² samples versus 2 mA/cm² samples (see Figure 5-1). The SEM results, on the other hand, suggested that DP is a noticeable influence on deposition curling at .08 M NaDBS, while DN is not as important at .08 M pyrrole (see Figure 5-2). These findings were in line with similar data from the concentration effects experiment described in Chapter 3.

Figure 5-1 Deposition curling (movement of the beam tip, in cm) under different conditions of current density, and Kapton[®] and PPy(DBS) thickness. Thin Kapton[®] film results are on the left (HN 50). Thick Kapton[®] film results are on the right (HN 100). Low DCD values (2 mA/cm²) are on the top. High DCD values (16 mA/cm²) are on the bottom. Each graph shows the amount of curling half way through the deposition (Half Dep) and at the end of the deposition (Full Dep), over a range of PPy(DBS) film thicknesses (where 300 mC is approximately equivalent to 10 μm).

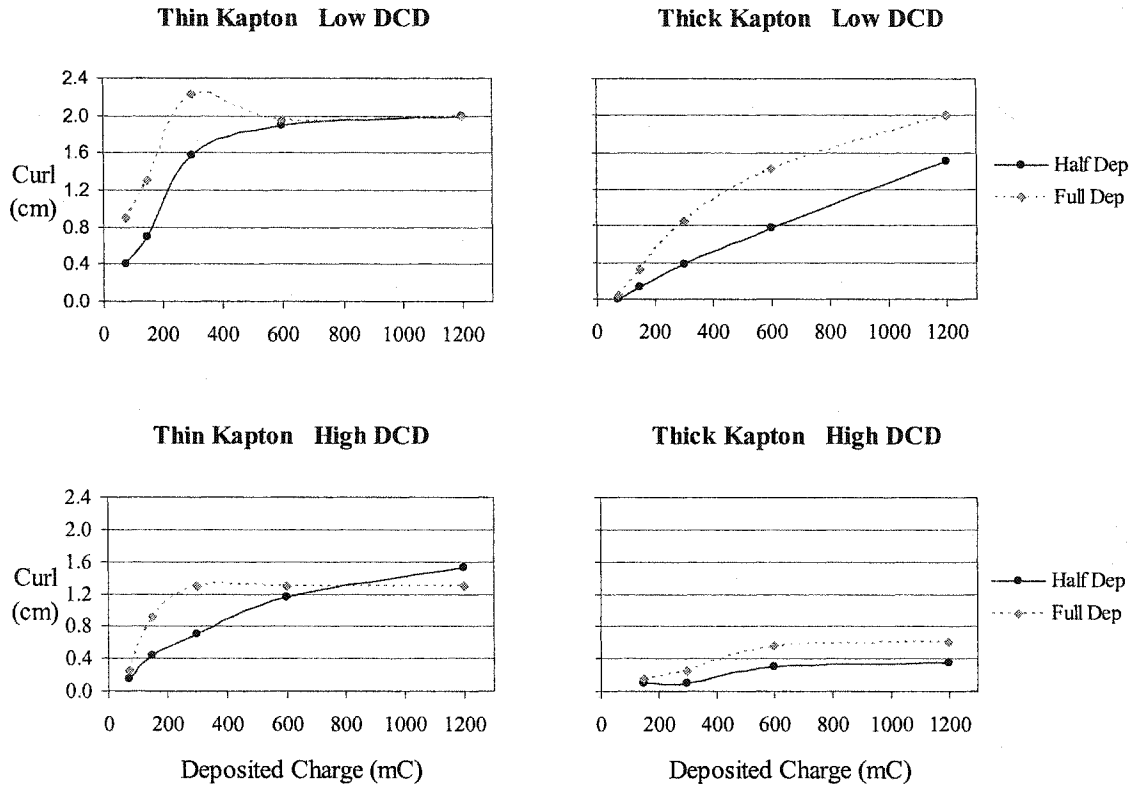
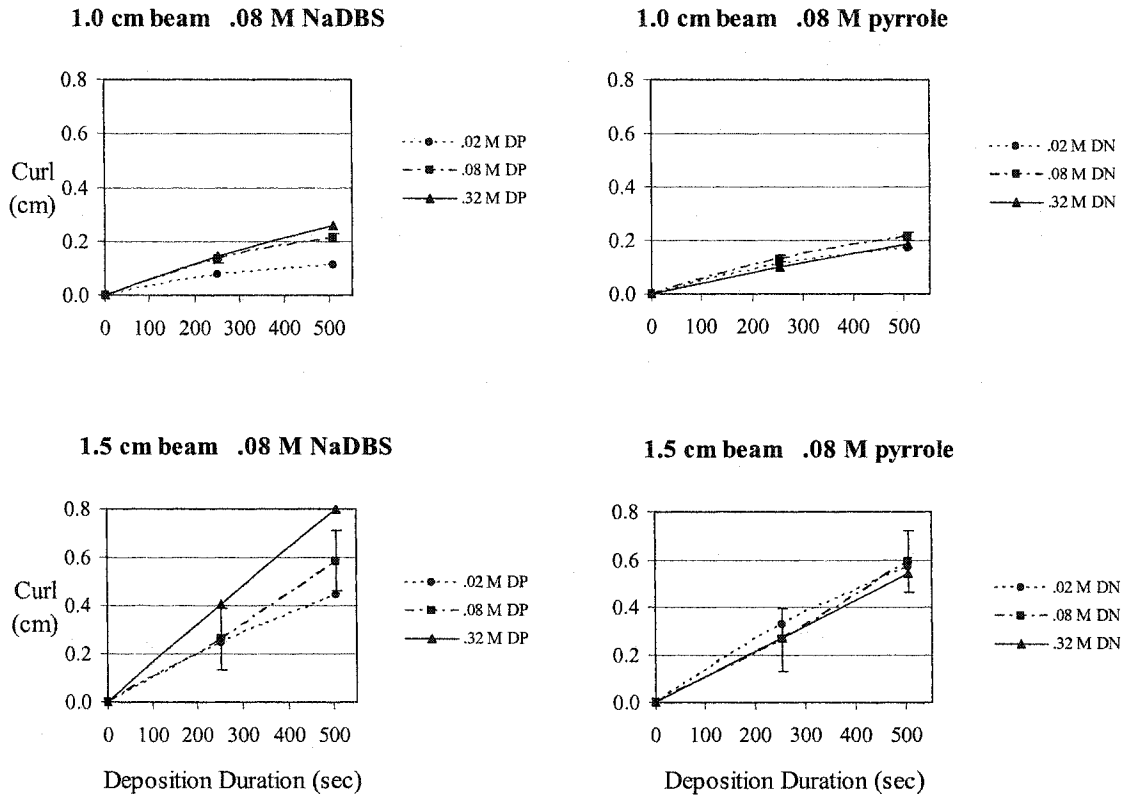


Figure 5-2 Deposition curling (movement of the beam tip, in cm) under different conditions of beam length (1.0 and 1.5 cm) and deposition concentrations (DP and DN). Constant DN results are on the left (.08 M). Constant DP results are on the right (.08 M). Short beam values (1.0 cm) are on the top. The longer beam values (1.5 cm) are on the bottom. Each graph shows the degree of curling over the deposition. In all cases, the depositions lasted about 500 seconds. The amount of curling was measured at the half-way point of the deposition and at the end of the deposition. Error bars are ± 1 standard deviation for a population of 3 for the 1.0 cm samples and of 7 for the 1.5 cm samples.



5.3.2 Conditioning Cycles

The frequency response samples did not go through any conditioning cycles. However, a subset of the SEM samples did. Of the 1 cm long samples, 2 were stimulated in .02 M NaDBS and 2 were stimulated in .32 M NaDBS. Of the 1.5 cm samples, 2 each were stimulated in .02, .08 and .32 M NaDBS.

Given my previous findings (as discussed in Chapters 2-4), there were no surprises. Higher SN concentrations brought on greater ranges of beam movement, greater levels of charge exchange, greater peak currents, and reduced peak separations. There were substantial increases in movement and charge exchange capacities from low to medium SN levels, though little difference from mid to high SN levels (.100 to .450 to .490 mm/mC, and 1.6% to 4.0% to 4.6%). Invariably, a beam would accumulate a negative charge over the 15 conditioning cycles. The magnitude of that accumulation scaled up with increasing SN, again mostly over the low-mid SN range. Also of note, the higher the SN value, the greater the tendency for the first reduction of the conditioning cycles to result in what would otherwise be considered to be an oxidative movement (curling) and the greater the charge exchange on that first cycle.

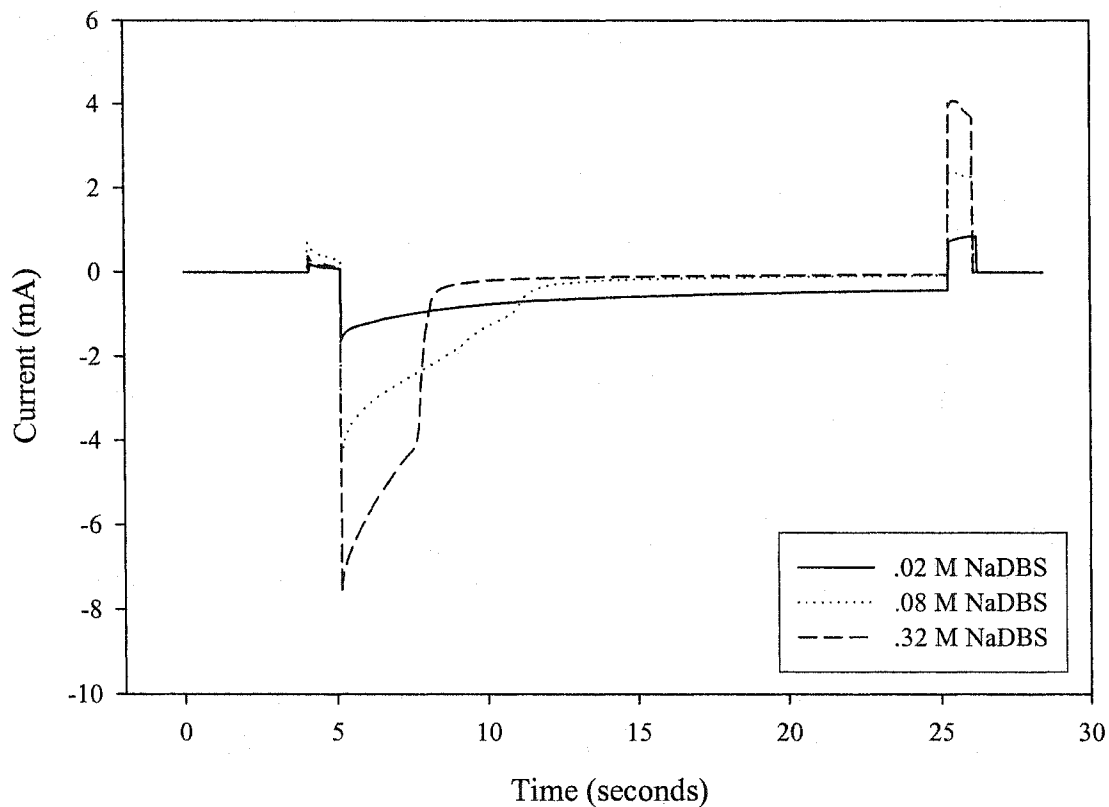
5.3.3 SEM Data

There were three noteworthy sets of SEM data. The first dealt with the voltage steps and the electrical behaviour of the beams during the steps. The second concerned the elemental makeup of the various beams, and the third focused on the surface and edge textures of the beams.

With regards to the voltage steps, there were some interesting patterns (see Figure 5-3). The reductive steps involved relatively large amounts of charge exchange, while the oxidative steps did not. For example, the maximum charge exchange during reduction was -16.8 mC while the maximum for oxidation was 3.0 mC. Similarly, after the step, some charge exchange would take place. In each case, the reduced samples accumulated some positive charge and the oxidized samples accumulated some negative charge. However, the negative accumulations were always negligible (0.0 to -0.1 mC) while the positive ones were always non-negligible (0.5 to 3.2 mC) and they scaled with the stimulation NaDBS concentration (SN). This may have been reflected in a movement pattern that occurred when the voltage step was turned off.

The nature of the movements during a step was always the same. The movement started quickly and ended slowly, holding a position at the finish. The whole movement would be smooth. However, when the voltage was turned off, the oxidized samples did not react while the reduced samples quickly jerked back towards their original position. The extent of the curling movements mirrored the corresponding electrical patterns. Curling increased with SN and reduction movements were always much greater than oxidation movements except at .02 M SN where the difference was small. Indeed, the low NaDBS oxidation step was the only condition that resulted in no measurable movement at all. Movement responsiveness and charge exchange capacity measures followed a similar pattern. Movement responsiveness values spanned the range of .000 to .294 mm/mC for oxidation and .013 to .408 mm/mC for reduction, while exchange capacity values spanned the range of .35 to 1.00% and 4.43 to 6.60%, respectively.

Figure 5-3 Reductive voltage step responses for the SEM samples stimulated in .02 M, .08 M and .32 M NaDBS. These amperograms have been sampled at 100 Hz and collected using LabVIEW software. Data analysis was performed using custom Matlab[®] routines. Note the stimulation artifacts both prior to and after the actual voltage step. They reflect the short time periods between the signal generator being on and not yet producing a signal and the signal generator power being turned on/off.



Regarding the SEM elemental analyses, the data did not always exhibit clear patterns. Assessments of oxygen (O), sodium (Na) and sulfur (S) content were made for each of several samples. These elements were chosen for a few reasons. First of all, they can be detected by the spectrometer. Second, they each reflect an important component of what should be in the films. The literature explains that sodium is the charge compensating element in this system (Pei and Inganäs 1993c). Assuming the sodium enters the film upon reduction, a relative measure of this mass transfer would be useful. Sulfur reveals the DBS molecules incorporated into the film matrix during deposition. And oxygen also reflects the presence of DBS molecules, as well as water. Over a range of seven deposition current densities, there were only hints of trends. There was a possible increase in S and a decrease in O with DCD. However, the effect was weak, and there was no discernable pattern with regards to Na. On the other hand, there was a clear pattern with respect to deposition pyrrole and NaDBS concentrations and how they influenced the makeup of the films. Figure 5-4 shows the relationships with respect to concentration. Note that the sodium percentages have all been multiplied by 5 for clarity of illustration.

The most dramatic elemental data, however, came from the reduction and oxidation steps. Figure 5-5 shows how redox reactions affected the elemental composition of the films. Note that the two sets of graphs are taken from two different takeoff angles. The elemental compositions of the films are not different, by definition, but what the spectrometers see at different takeoff angles is clearly different. In any event, it is the relative abundances that are important, not the absolute values. Other

Figure 5-4 Normalized weight percentages of the three elements oxygen, sulfur and sodium in the PPy(DBS) films produced in different concentrations of pyrrole and NaDBS. Note that low refers to .02 M, mid refers to .08 M and hi refers to .32 M. Also note that the Na percentages have all been multiplied by 5 for illustrative clarity.

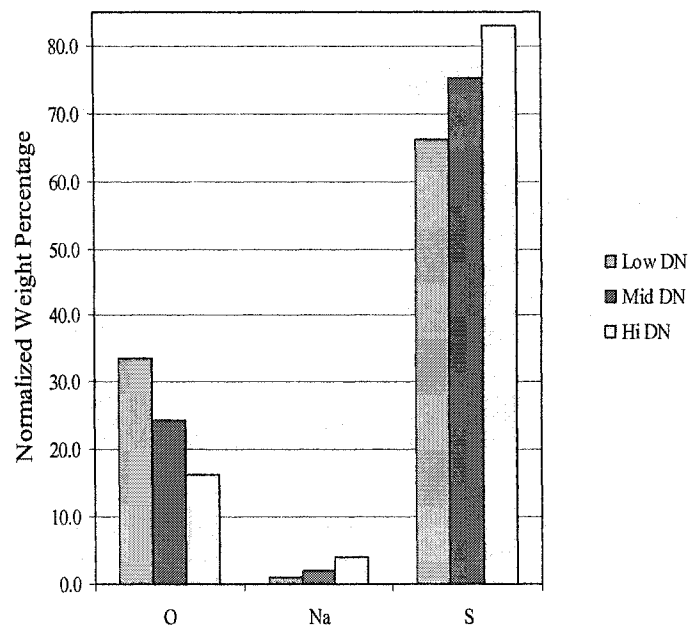
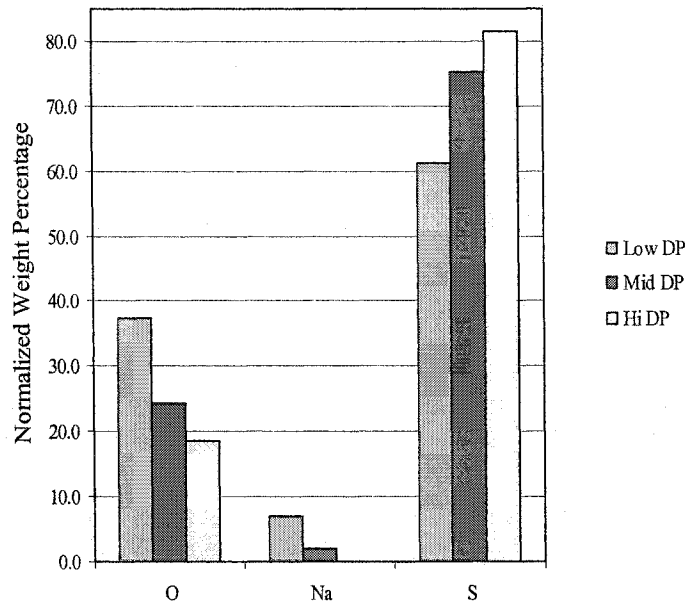
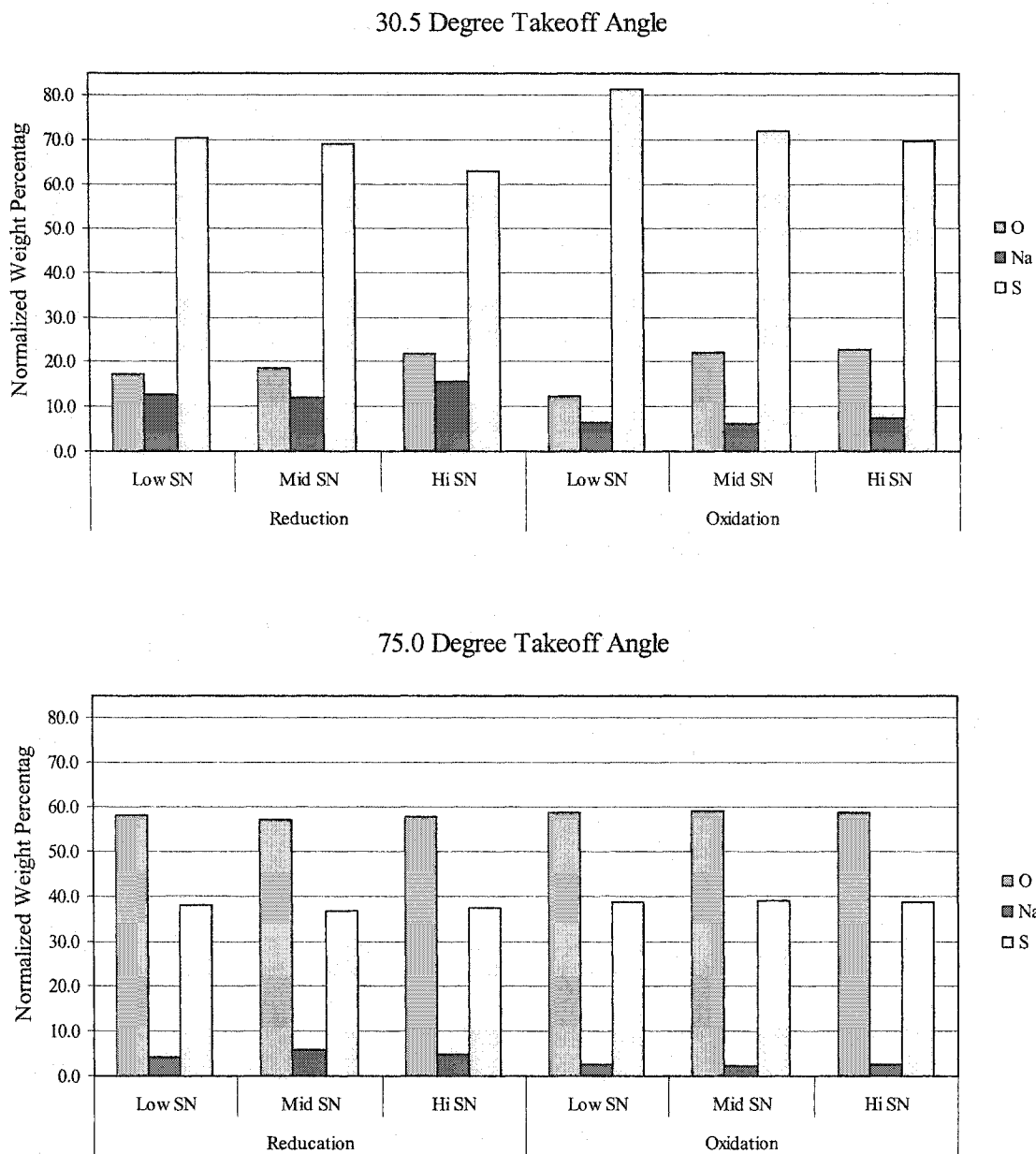


Figure 5-5 Normalized weight percentages of the three elements oxygen, sulfur and sodium in the PPy(DBS) films stimulated by reductive or oxidative voltage steps in different concentrations of stimulation NaDBS (SN). Note that low refers to .02 M, mid refers to .08 M and hi refers to .32 M NaDBS. Also note that the upper graph consists of data taken from a 30.5 degree takeoff angle, while the lower graph consists of data from the same sample set, but collected at a 75.0 degree takeoff angle.



results taken from the SEM with lower elemental precision supported these findings. Reduced samples had consistently higher levels of sodium versus oxidized samples.

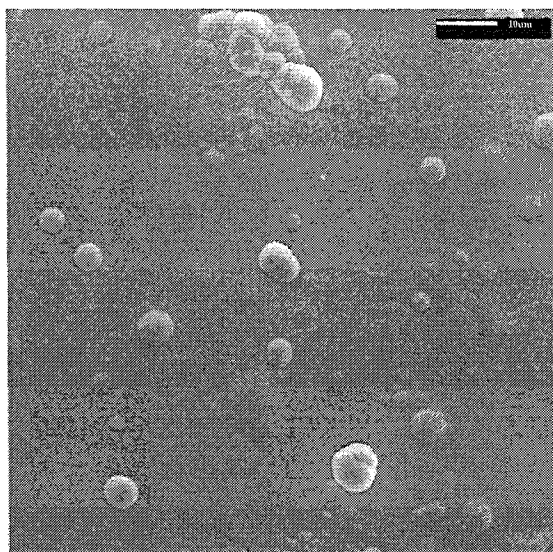
The last set of SEM data collected in this study was imagery of film textures taken from films produced and/or stimulated under different conditions. There were no consistent differences in texture among the samples varying in DCD value, or among the samples where the deposition NaDBS concentrations were varied. However, there were some marked differences among samples with varying deposition pyrrole concentrations, as shown in Figure 5-6. The degree of film surface roughness, or granularity, would appear to increase substantially with increasing pyrrole concentration.

The second aspect of the imagery was the assessment of film thicknesses. Figure 5-7 shows four examples of edge images. The examination of the edges showed a number of things. First of all, it showed that the estimation method of Smela (1999) is essentially sound, especially when employing mid-high range deposition concentrations. However, there can be significant variation along the width of the film, especially near the edges (lower left, Figure 5-7). The advantage of using SEM to assess film thickness over methods such as profilometry is that the SEM allows one to see details that may be providing otherwise misleading results. To gain these benefits, it is essential that one use freeze fracture methods though. Cutting the films with a knife, in preparation for examination in the SEM, "smudges" the edges and makes for very difficult measurement interpretations. Freeze fracturing provides much more consistent and accurate results.

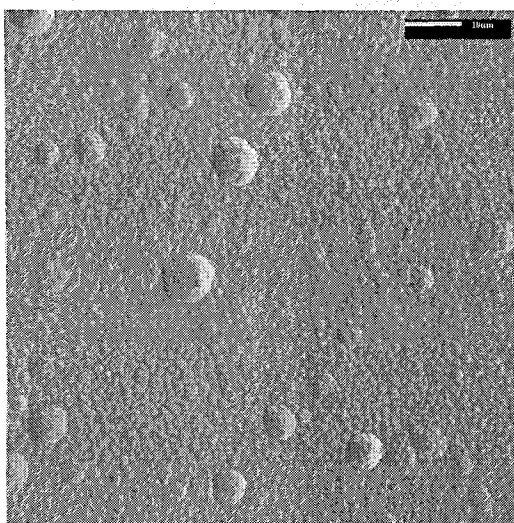
The average film thickness for the 6 samples that went through the conditioning cycles and voltage steps was 10.21 μm . The standard deviation was only .38 μm . Most

Figure 5-6 SEM images of PPy(DBS) films produced in different levels of pyrrole concentration. The top image (a) shows a film produced in .02 M pyrrole. The lower left image (b) shows a film produced in .08 M pyrrole, and the lower right image (c) shows a film produced in .32 M pyrrole. Scale bars are 10 μm . Magnification is X1000, at 5 KV.

a) .02 M pyrrole



b) .08 M pyrrole



c) .32 M pyrrole

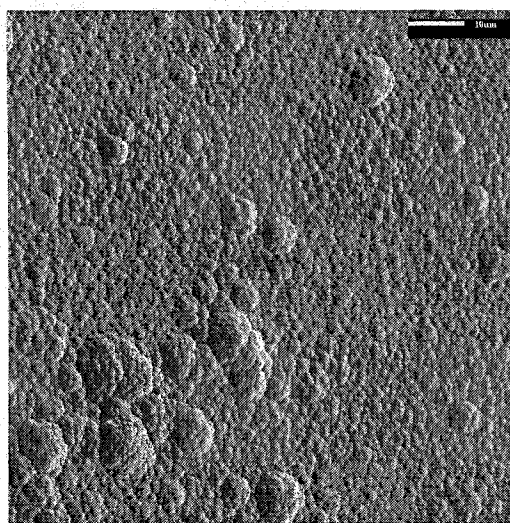
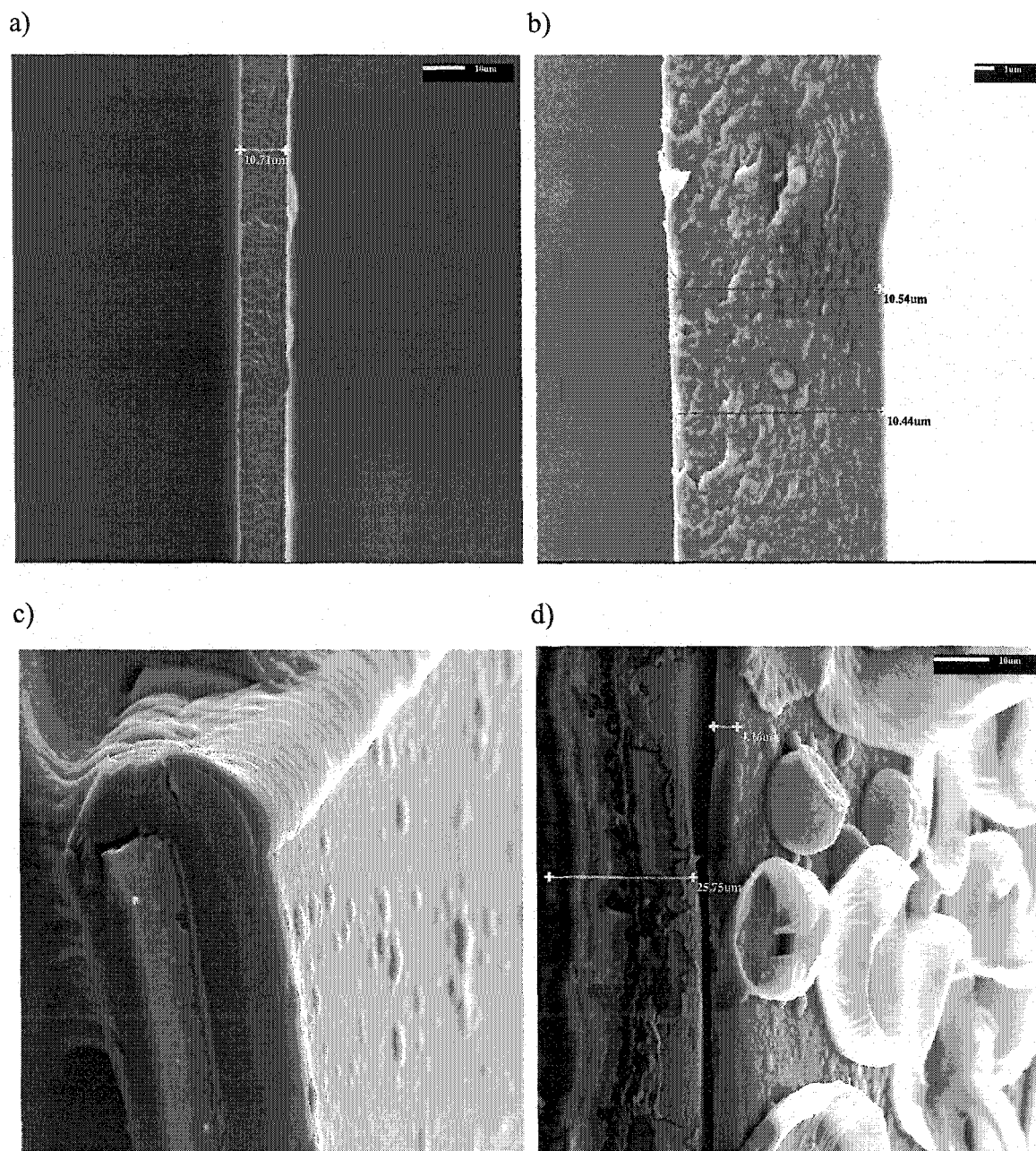


Figure 5-7 SEM images of edges of PPy(DBS) films. The top left image (a) shows the central edge of a 10 μm thick film produced in .08 M pyrrole/.08 M NaDBS at 1 mA/cm^2 . Magnification is X750 at 5 KV. The top right image (b) shows a similar sample grown at 4 mA/cm^2 (X3500, 5 KV). The lower left image (c, X750, 15 KV) shows the lateral edge of the beam shown in a) when it was still bonded to Kapton[®], illustrating the distortions that occur at the edges of the beams. The last image, lower right (d), shows the results of a difficult deposition at 28 mA/cm^2 (X1000, 15 KV).



curiously, there was a notable difference between the reduced and oxidized samples. The reduced samples, with an average edge thickness of $10.46 \mu\text{m}$ ($\text{SD} = .08 \mu\text{m}$) were consistently thicker than the oxidized samples ($9.97 \mu\text{m}$, $\text{SD} = .40 \mu\text{m}$). The differences between reduced and oxidized samples, by SN value, ranged from $.06$ to $1.14 \mu\text{m}$. The average difference was $.49 \mu\text{m}$. That's approximately 4.9% of the total film thickness.

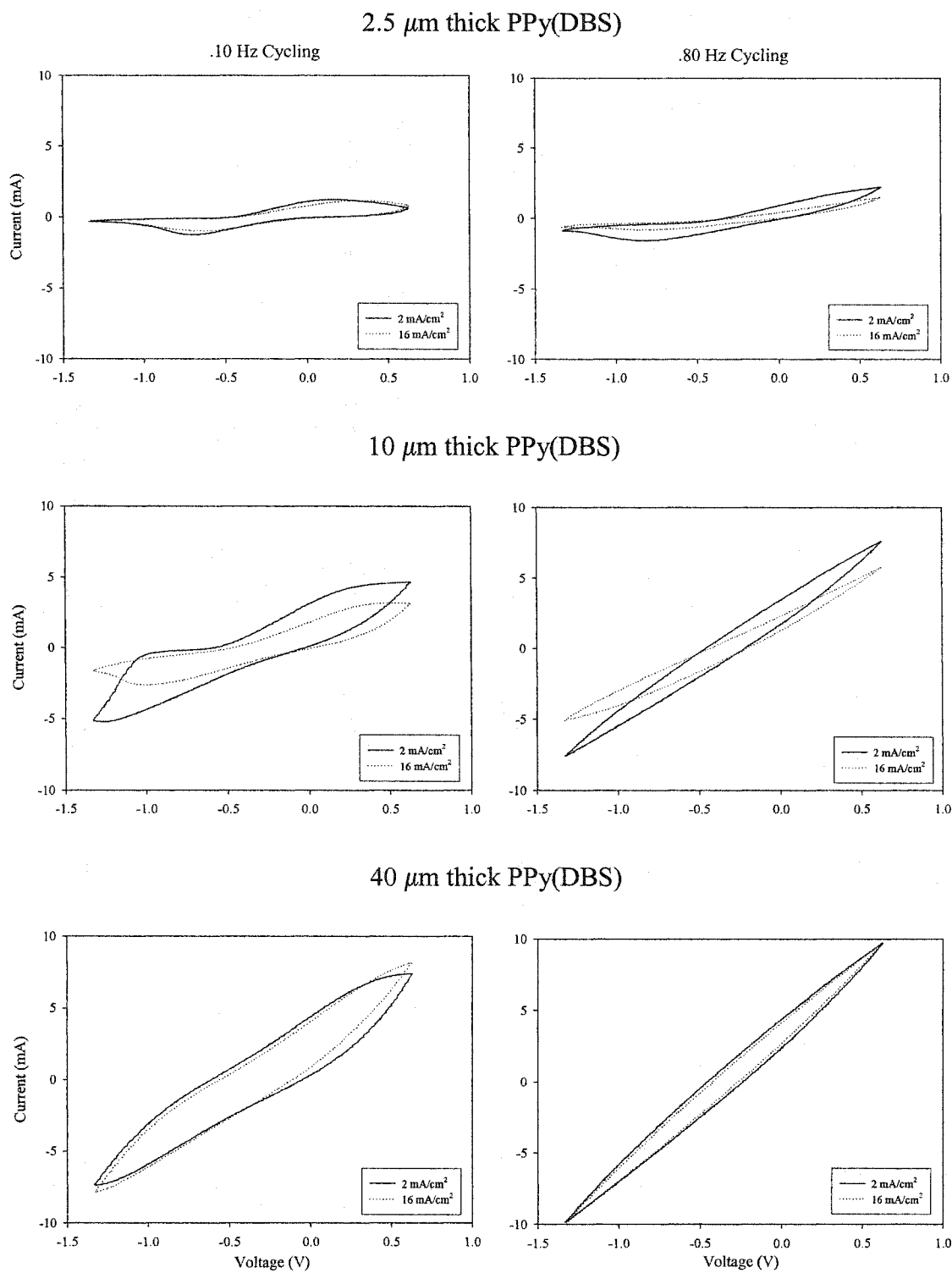
Looking at the DCD variants, there was a tendency for low DCD samples to be somewhat thicker and for high DCD samples to be noticeably thinner. Very low deposition NaDBS and pyrrole samples also appeared to be thinner than expected. Further work with more samples would be required to achieve more definitive results.

5.3.4 Frequency Response Data

Each sample in the frequency response experiment went through 10 sets of 15 cycles of ramp voltammetry, each set at a different cycling frequency (or equivalently, scan rate). As we saw in the Experimental section, there were two thicknesses of Kapton[®] film and five thicknesses of PPy(DBS) used. Also, the depositions were conducted at one of two DCD values. Figure 5-8 gives some sense of the variations in CV patterns with respect to these variables.

As such, for each beam, we could look at charge accumulation, curling, charge exchange, peak currents, peak voltages, movement responsiveness, peak separation and charge exchange to peak current ratios, all with respect to cycling frequency. We could also look at groups of beams broken out by DCD value, PPy(DBS) thickness, and Kapton[®] thickness, all with respect to cycling frequency. Indeed, I will make each of these comparisons.

Figure 5-8 Representative cyclic voltammograms for samples cycled at .10 and .80 Hz. The top row is for thin PPy(DBS) films ($2.5 \mu\text{m}$), the middle row is for medium thickness films ($10 \mu\text{m}$) and the bottom row is for thick films ($40 \mu\text{m}$). Each plot shows samples produced at 2 mA/cm^2 and at 16 mA/cm^2 .



To start with, we'll look at an example of a progression that a given beam went through. The particular example that we'll look at was a beam deposited at 2 mA/cm^2 , on HN 100 Kapton[®], to a projected thickness of $5 \text{ }\mu\text{m}$. Progressing from .05 to 6.4 Hz, charge accumulation started out negative (-6.9 mC) and gradually became more positive up to .6 mC at 6.4 Hz, where accumulated charge is the integration of the current signal from the time the data recording begins, until after the trial when the data recording is turned off. Curling fell off steadily with frequency, at .05 cm per frequency interval (Figure 5-9, top). Charge exchange did the same until .80 Hz (Figure 5-9, middle). However, it did not fall off as fast with respect to cycling frequency at higher frequencies. Peak currents generally rose with frequency but the effects were slightly different between reduction and oxidation (Figure 5-9, bottom). For reduction, there was a diminishing increase in magnitude with frequency. For oxidation, this was also true but currents peaked at 1.60 Hz and started to gradually fall after that. The charge to peak current ratio versus cycling frequency (see Figure 5-10, top) was an almost perfectly straight line with a slope of -1 on a log/log scale. As for the voltage peaks, they stayed within the cycling limits at .05 and .10 Hz, but moved outside of the limits after that. As they moved outside of the cycling limits, note that they changed the meaning of the peak current levels. No longer did the "peak current" values reflect the true redox peak currents. Now they simply reflected what maximum currents could be produced at a given cycling frequency over a cycling range that did not capture the peaks. The progression for movement responsiveness clearly showed that it increased with cycling frequency and then peaked and declined (Figure 5-10, bottom). Meanwhile, charge exchange capacity went from 8.80% to .20% and then returned to 8.06% during the last

Figure 5-9 At top, curling on the 15th cycle versus stimulation cycling frequency for a sample produced at 2 mA/cm², on HN 100 Kapton[®], to a projected thickness of 5 μm. Middle graph shows charge exchange on the 15th cycle versus stimulation cycling frequency, for the same sample. At bottom, peak currents for the same sample.

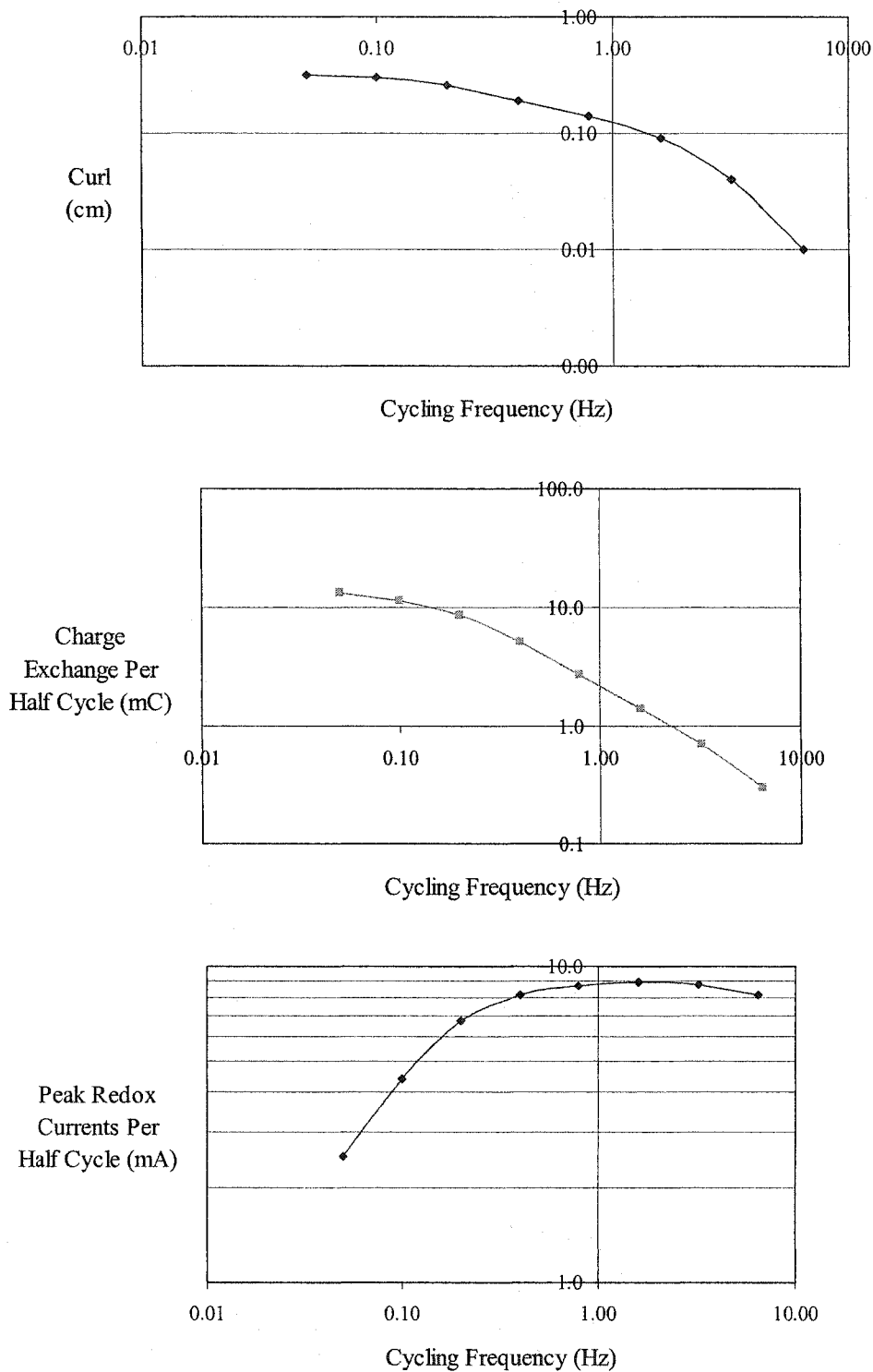
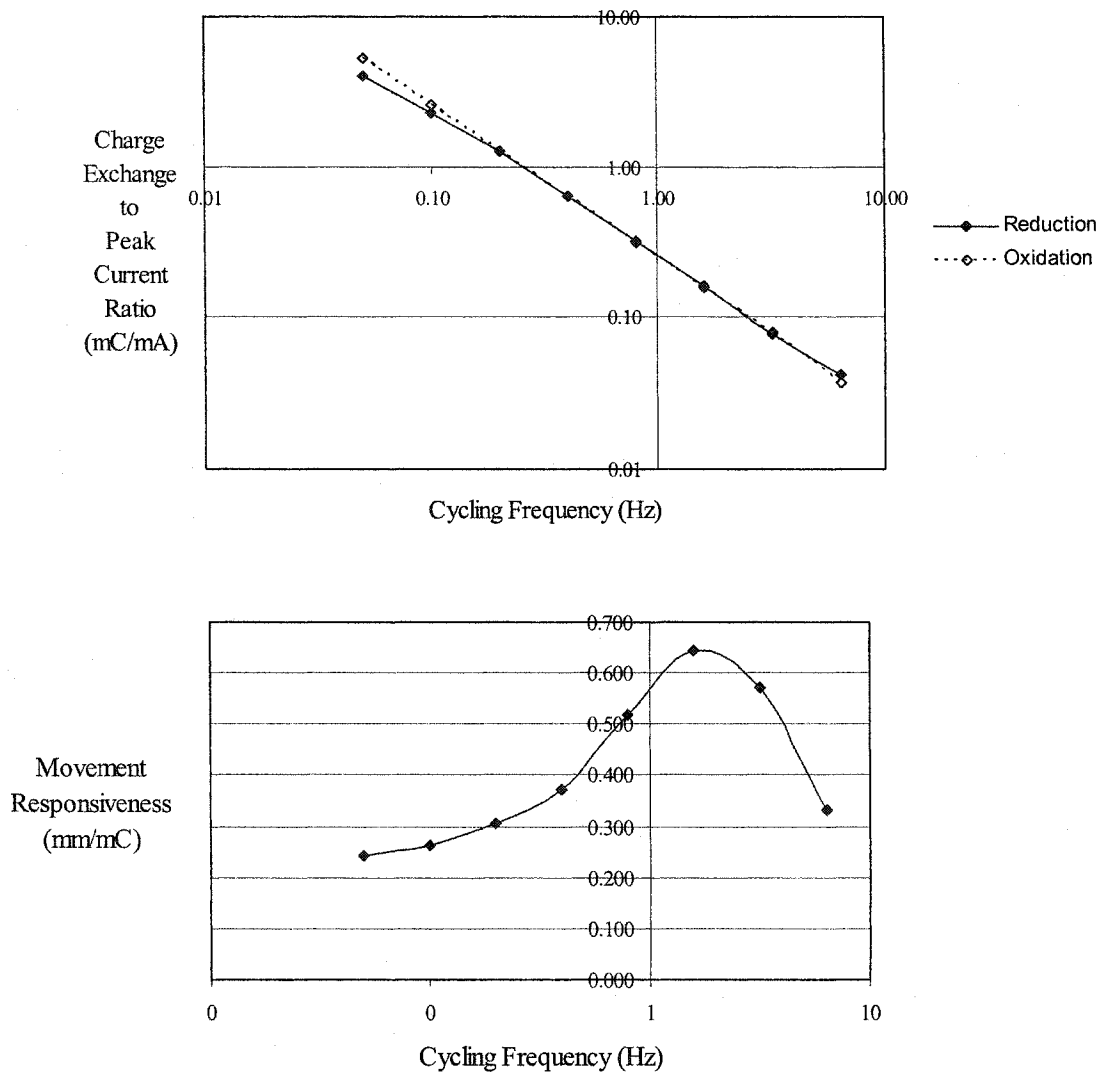


Figure 5-10 The ratio of charge exchange to peak current (top) and the ratio of curling movement to charge exchange or movement responsiveness (bottom) on the 15th cycle, versus stimulation cycling frequency, for a single sample produced at 2 mA/cm², on HN 100 Kapton[®], to a projected thickness of 5 μm.



.05 Hz cycling set. A later .20 Hz cycling set, with cycling limits of -2 V and +2 V produced a 9.66% value.

The nature of the actual beam movements changed with cycling frequency as well. In most cases, the slow movements were pendular with pauses at the limits. At higher frequencies, the pauses vanished. At still higher frequencies, the movements would no longer be considered "curls". Rather, the tips of the beams would trace out ellipses. At the highest frequencies, the movements appeared to be little more than vibrations. The situation for the rest of the samples was a variation on these themes.

Combining all samples of the same Kapton[®] thickness i.e. not accounting for within group differences in PPy(DBS) film thickness or DCD value, revealed some interesting dependencies on the beam substrate. First and least surprisingly, at every stimulation frequency the HN 50 samples out-curled the HN 100 samples. Also, at all but the highest cycling frequencies, the charge exchanges and peak currents were slightly higher for the HN 50 samples. Also at all frequencies, the peak separation was greater for the HN 50s in comparison to the HN 100s, most often due to a more cathodic reduction peak. Movement responsiveness was greater for the HN 50 samples at all but the highest PPy(DBS) film thicknesses, and charge exchange capacities were also marginally better for the HN 50 beams.

Combining all samples of the same DCD value and doing the same sort of comparisons yielded other findings. First of all, in every set except the first, the average curling of the low DCD samples exceeded that of the high DCD samples. The same was true for charge exchange and peak currents. For the peak potentials, the situation was more complex. At .05 Hz the peak separation for the low DCD samples was smaller than

for the high DCD samples because the oxidation peak was more cathodic. By .10 Hz, however, the high DCD samples had tighter peaks due to a more cathodic reduction peak for the low DCD samples. By .80 Hz, the peaks were outside of the limits for all but one (low DCD) sample and that pattern was maintained for all higher cycling frequencies. Charge exchange capacity was superior at the low DCD value, and the best DCD value for movement responsiveness depended on the cycling frequency. At lower frequencies the high DCD value performed better, while at high frequencies low DCD was preferred.

Finally, combining all samples of the same PPy(DBS) thickness yielded the clearest results. There were definite patterns in the accumulated charge with respect to PPy(DBS) film thickness and cycling frequency. Initially, at low frequencies, the negative charge accumulation would increase with film thickness. However, as cycling frequency increased, the activity with the thick films changed. The accumulation became less pronounced and eventually it became positive. Indeed, by 1.6 Hz, all of the charge accumulations were positive and the magnitude scaled with film thickness. Returning back to .05 Hz, thin films were slightly negative, medium thickness films accumulated some positive charge, and the thick films accumulated substantial negative charge. Charge exchange capacity levels tended to rise, peak and then fall at all PPy(DBS) film thicknesses, with respect to increasing cycling frequency. Movement responsiveness (curl per unit charge) tended to decrease with increasing film thickness, at most cycling frequencies.

More to the point of this thesis, the curling movements varied considerably with film thickness. Thin and thick films performed least well, and movement peaked at around 10 μm for all but the last round of cycles. In the last .05 Hz repeat round, the

peak for movement had moved slightly in the thicker PPy(DBS) film direction, somewhere between 10 and 20 μm . At the same time, charge exchange and peak currents increased substantially with respect to film thickness across all cycling frequencies. Also significant was the fact that oxidation and reduction peaks moved with film thickness. Oxidation peaks moved anodically and reduction peaks moved cathodically. This was only readily apparent at the lower cycling frequencies, however, as the peaks fell outside of the cycling limits at the higher frequencies.

Breaking the “same DCD” groups into “same Kapton[®] thickness” sub-groups, I was able to examine some of these interactions among the variables, as well as a few new subtleties. For instance, initially, there was a tendency at the lower frequencies with the high DCD samples for the optimal film thickness for curling to be slightly thicker than 10 μm . As well, by the last set of cycles (a repeat of .05 Hz), the optimal PPy(DBS) thickness for curling had moved to around 20 μm in every case. It was also made clearer that at low DCD values movement responsiveness decreased with increasing PPy(DBS) film thickness. Also, regarding the charge exchange capacity levels of high DCD samples, HN 100 samples performed notably better at higher cycling frequencies.

The main difficulty in making sense of all of these results was in trying to visualize them. One of the best ways to do this was to chart a parameter's value with respect to film thickness, with one graph for low DCD and one graph for high DCD. Furthermore, one could plot two lines on each graph, one for thin Kapton[®] and one for thick Kapton[®] if that was relevant. This strategy effectively illustrated what was happening across the cycling frequencies, taking into account all of the controlled variables. Figures 5-11 to 5-15 show some of this. Respectively, they show curling,

Figure 5-11 Curling with respect to PPy(DBS) film thickness (deposition charge density) where the data shown combines the HN 50 and HN 100 results. Left plots are for samples grown at 2 mA/cm². Right plots are for samples grown at 16 mA/cm². Plots, in descending order, are of samples stimulated at .05 Hz, .40 Hz, 3.2 Hz and then .05 Hz.

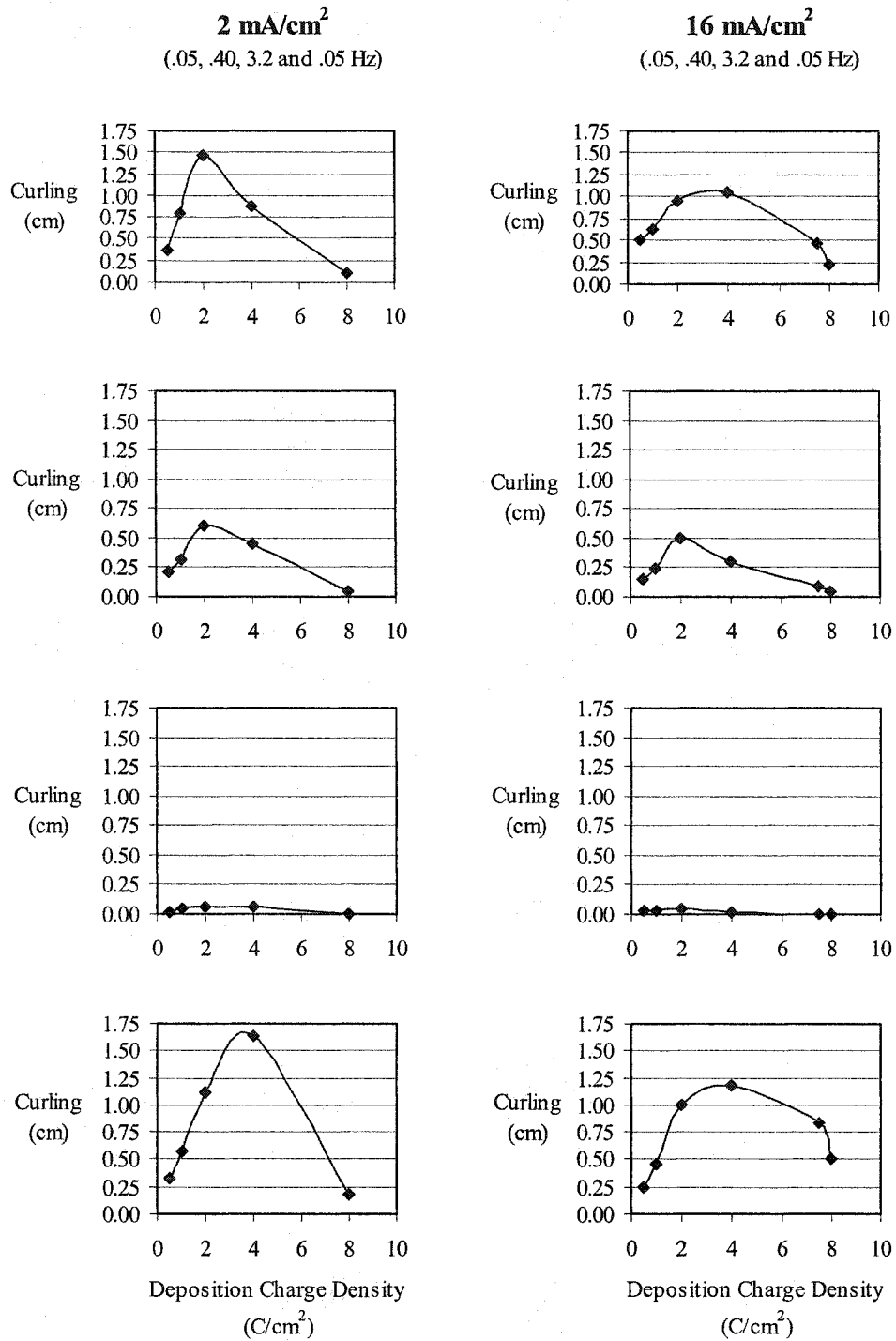


Figure 5-12 Charge exchange with respect to PPy(DBS) film thickness (deposition charge density) where the data shown combines the HN 50 and HN 100 results. Left plots are for samples grown at 2 mA/cm^2 . Right plots are for samples grown at 16 mA/cm^2 . Plots, in descending order, are of samples stimulated at .05 Hz, .40 Hz, 3.2 Hz and then .05 Hz.

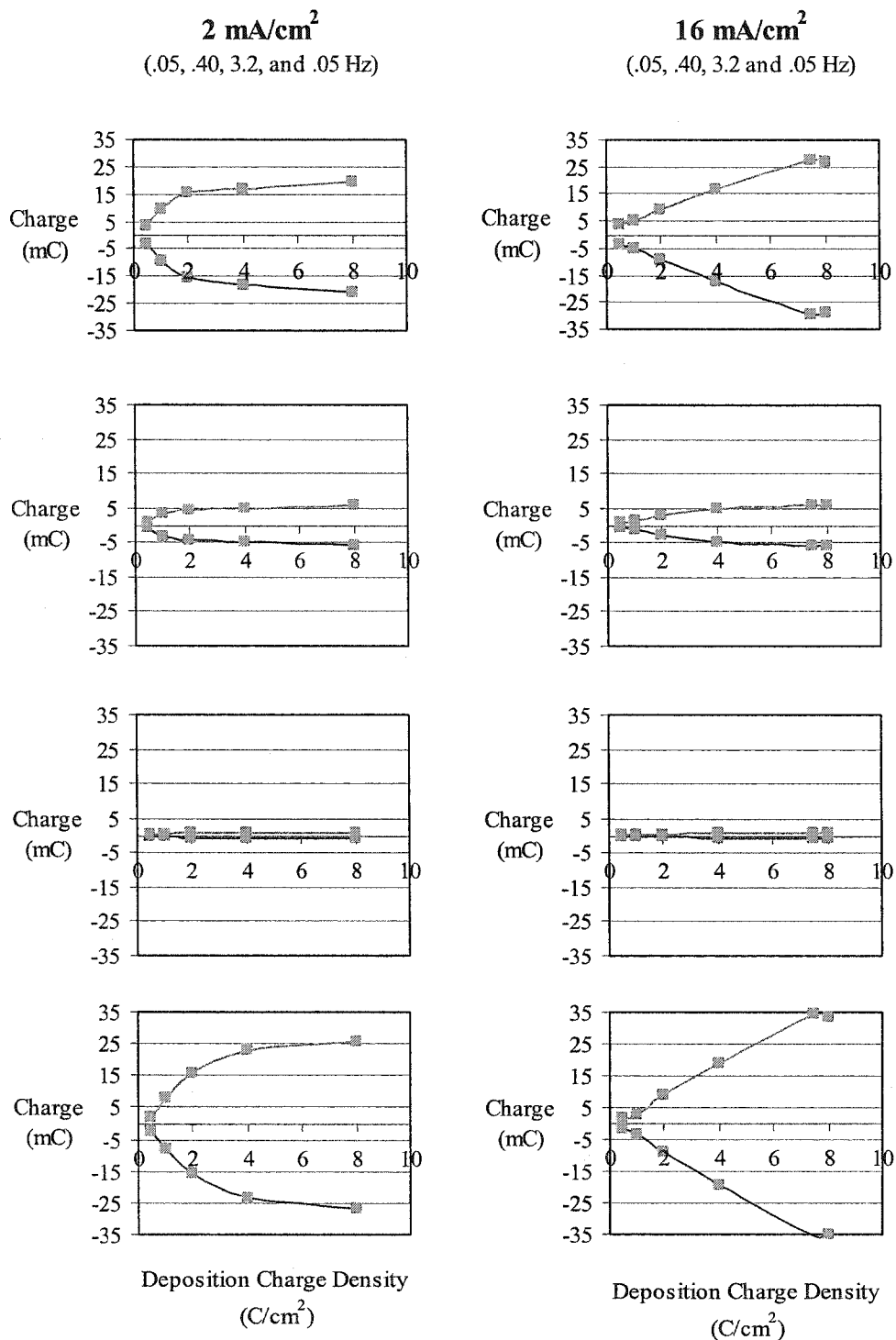


Figure 5-13 Peak currents with respect to PPy(DBS) film thickness (deposition charge density) where the data shown combines the HN 50 and HN 100 results. Left plots are for samples grown at 2 mA/cm^2 . Right plots are for samples grown at 16 mA/cm^2 . Plots, in descending order, are of samples stimulated at .05 Hz, .40 Hz, 3.2 Hz and then .05 Hz.

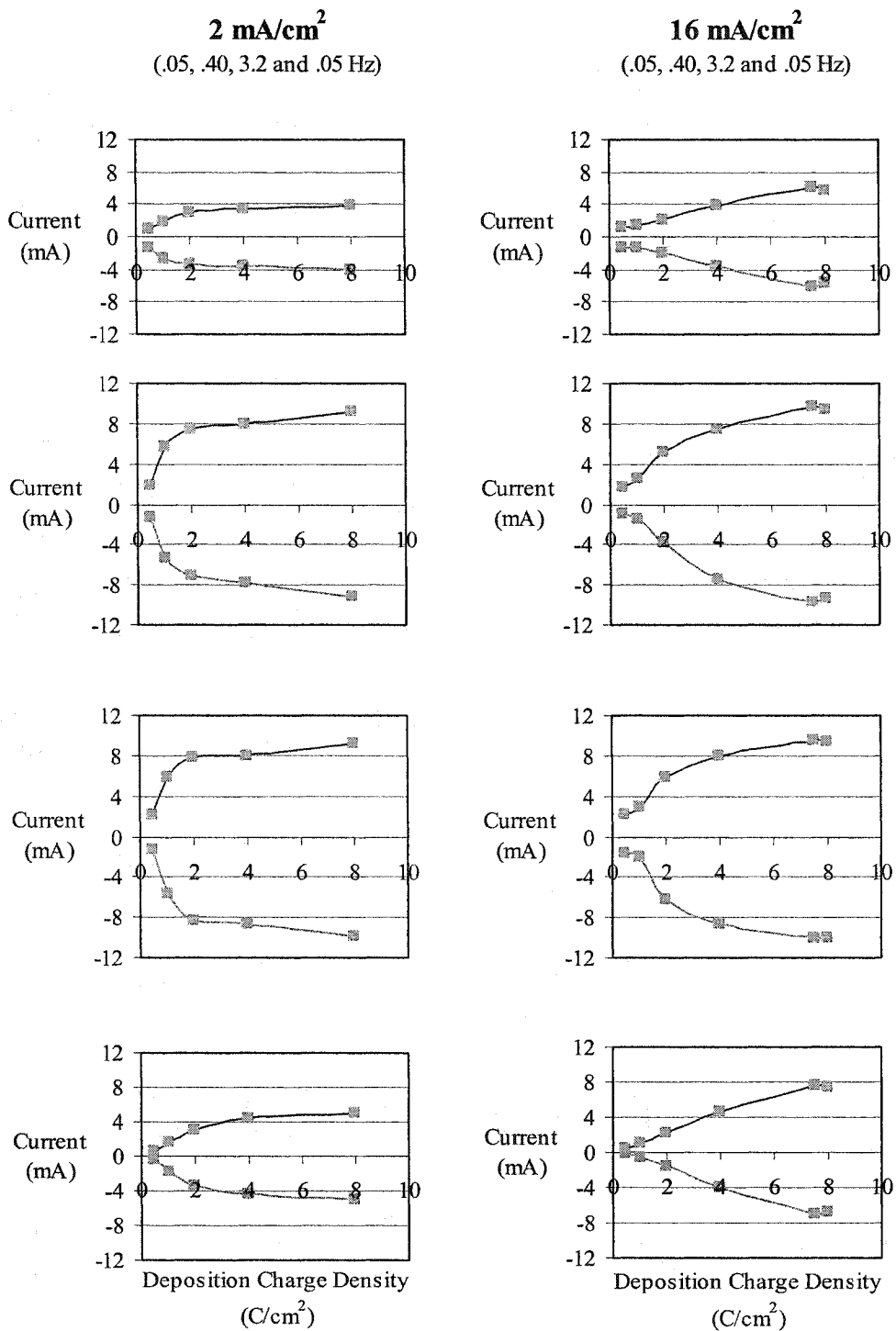


Figure 5-14 Voltage peaks with respect to PPy(DBS) film thickness (deposition charge density) where the data shown combines the HN 50 and HN 100 results. Left plots are for samples grown at 2 mA/cm². Right plots are for samples grown at 16 mA/cm². Plots, in descending order, are of samples stimulated at .05 Hz, .40 Hz, 3.2 Hz and then .05 Hz.

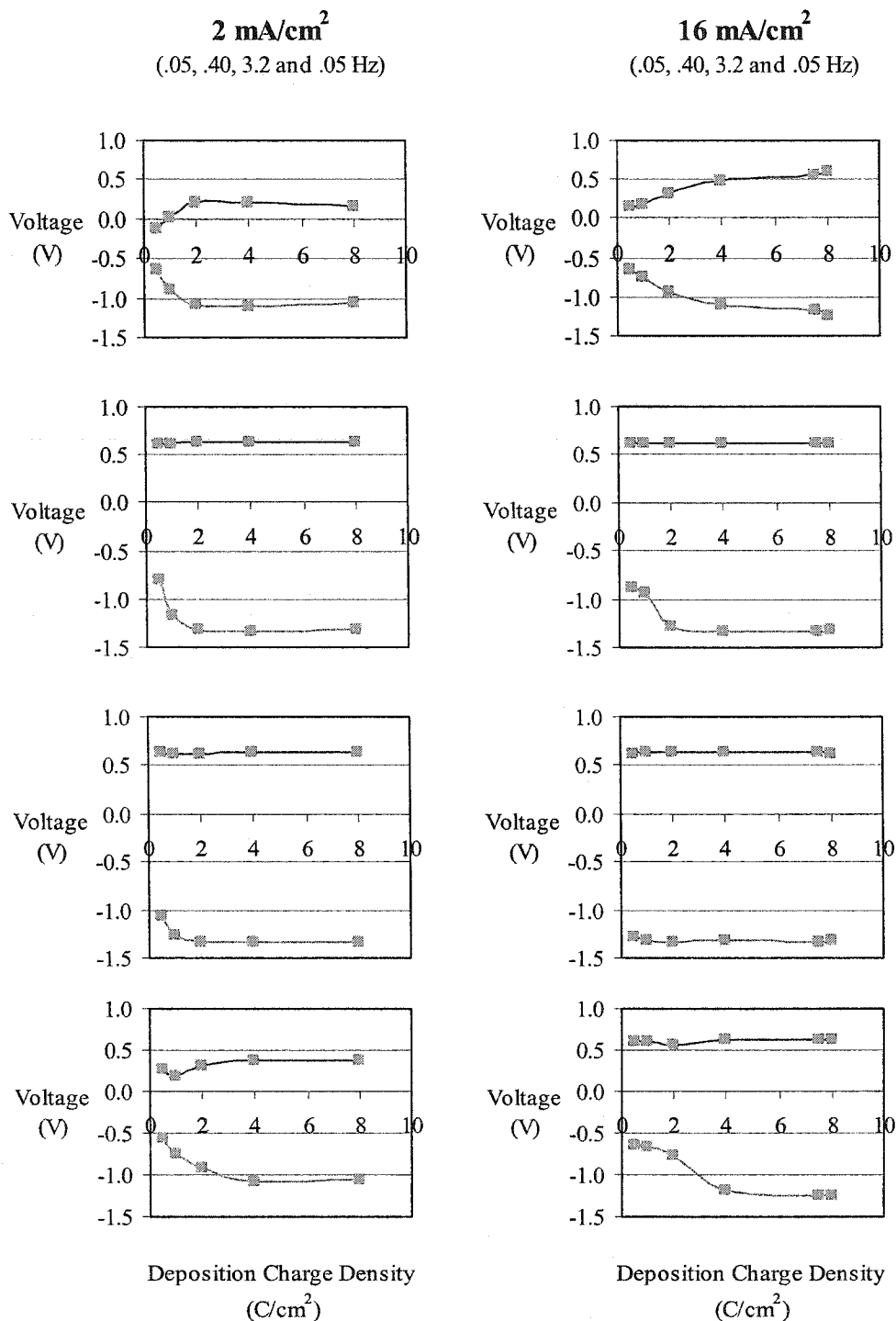
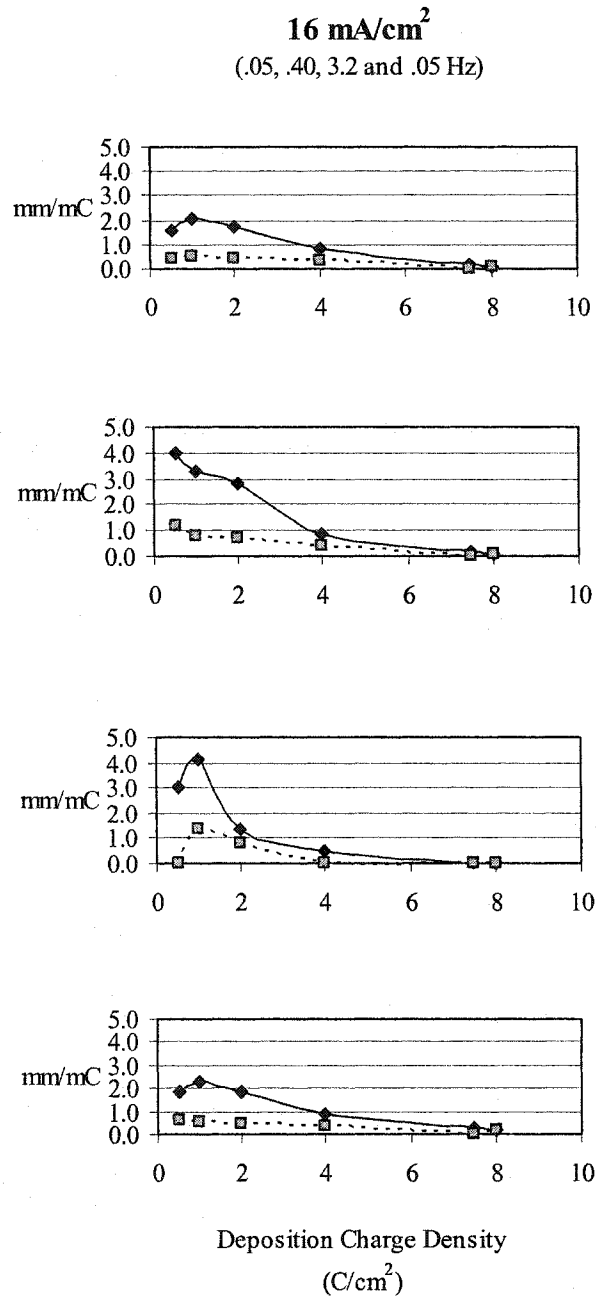


Figure 5-15 Movement responsiveness with respect to PPy(DBS) film thickness (deposition charge density) where the data shown are the 16 mA/cm² results. The lesser plots on each graph (□) are for HN 100 samples, while the more responsive plots (◇) are the HN 50 samples. Plots, in descending order, are of samples stimulated at .05 Hz, .40 Hz, 3.2 Hz and then .05 Hz again.



charge exchange, peak currents, peak voltages and movement responsiveness over a range of cycling frequencies with respect to DCD value and PPy(DBS) film thickness.

All of the results discussed so far deal with the progression of measured values from the last cycle of each set, from frequency set to frequency set and/or from film thickness to film thickness. They have shown data points from several different samples in each graph, and have been concerned with how the samples relate to each other. Of equal interest is the progression of these values within one sample over the frequency spectrum or sample group. In other words, if one looked at a single data point in Figure 5-11 and followed its evolution through the series of graphs corresponding to the frequency sets, one would see Figure 5-9 (top). We could then compare that plot with the same sort of plot for another sample (or another type of sample). Keeping in mind that we are really only looking at the same data, just from an orthogonal perspective, Figures 5-16 to 5-19 illustrate this point for curling, movement responsiveness, peak currents and charge exchange with respect to cycling frequency.

Figure 5-16 Cycling frequency versus curling range of motion (cm). Top left plot shows results for thin PPy(DBS) samples. Top right plots show results for mid-thickness PPy(DBS) samples. Bottom center plots show results for thick PPy(DBS) samples. Each plot shows results for thin and thick Kapton[®] film samples, combined with low and high DCD values.

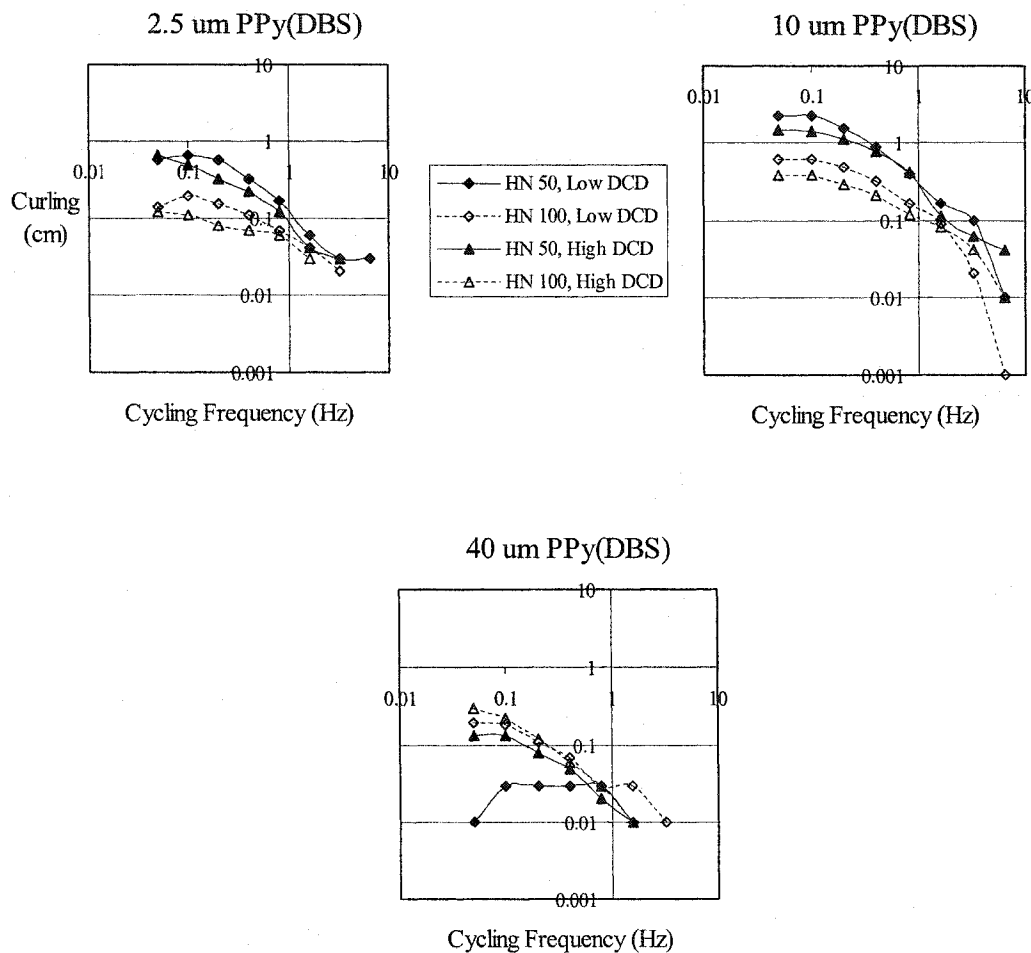


Figure 5-17 Cycling frequency versus curling responsiveness (mm/mC). Top left plot shows results for thin PPy(DBS) samples. Top right plots show results for mid-thickness PPy(DBS) samples. Bottom center plots show results for thick PPy(DBS) samples. Each plot shows results for thin and thick Kapton[®] film samples, combined with low and high DCD values.

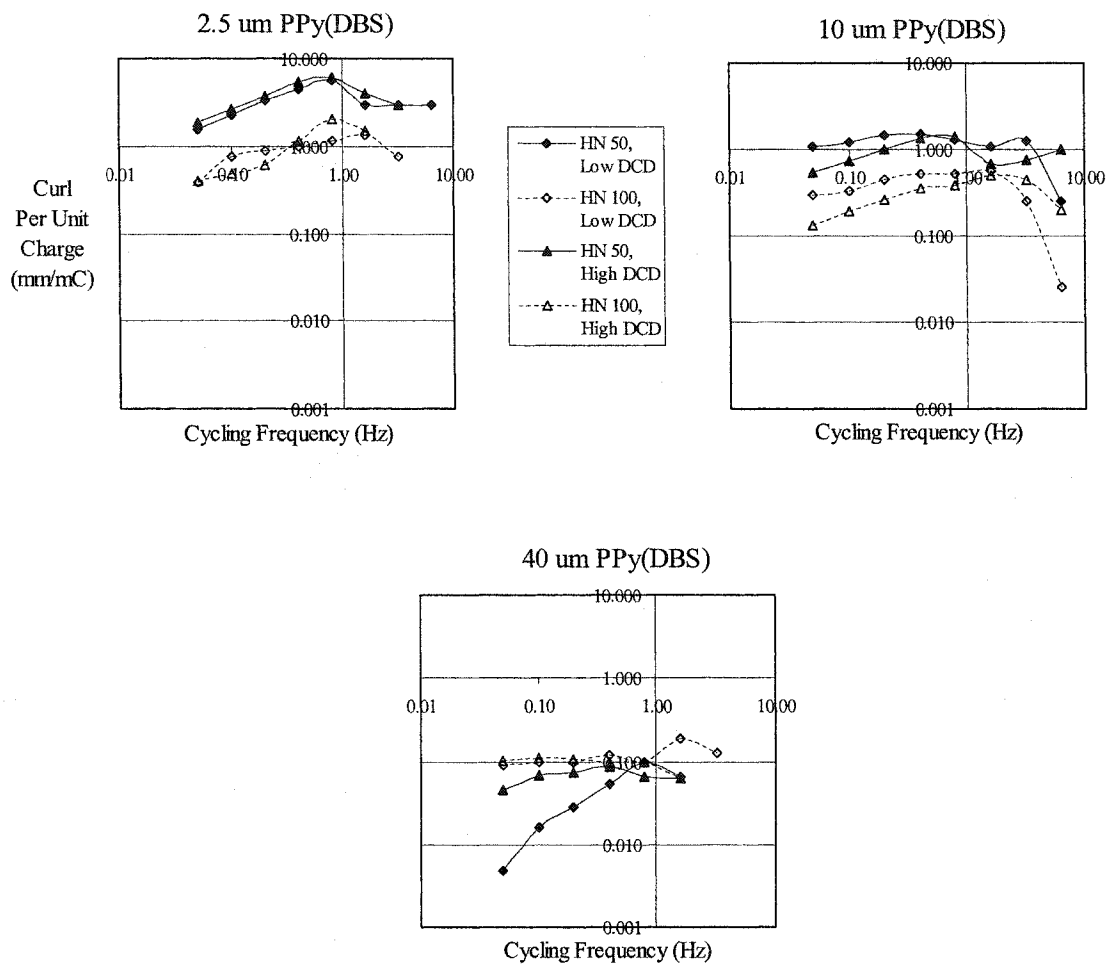


Figure 5-18 Cycling frequency versus peak redox currents (mA). Left plot shows results for thin PPy(DBS) samples. Right plots shows results for thick PPy(DBS) samples. Each plot shows results for thin and thick Kapton® film samples, combined with low and high DCD values.

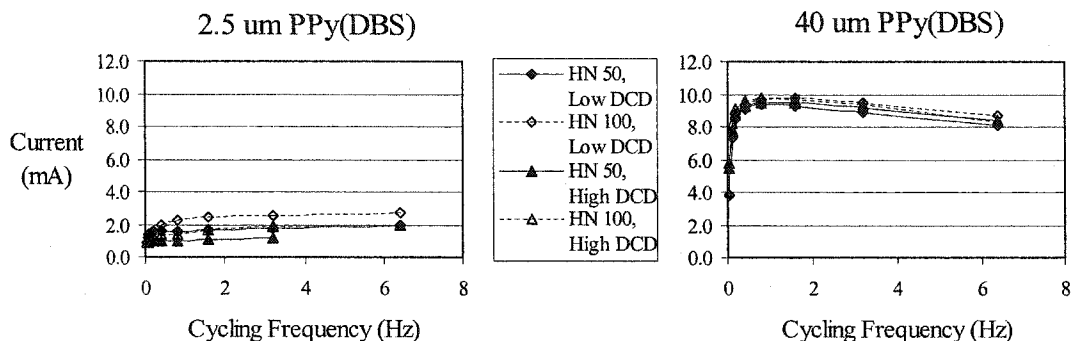
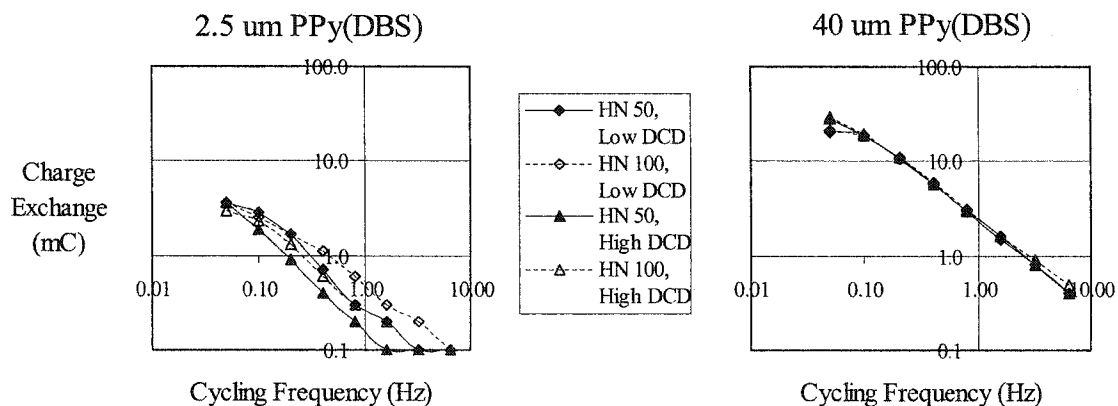


Figure 5-19 Cycling frequency versus cycle by cycle charge exchange (mC). Left plot shows results for thin PPy(DBS) samples. Right plots shows results for thick PPy(DBS) samples. Each plot shows results for thin and thick Kapton® film samples, combined with low and high DCD values.



5.4 Discussion

Many investigators have described differences in polypyrrole SEM images based on differences in electrolytes, DCD, electrode type and concentrations of monomer and dopant (Kaynak 1997, John et al. 1992, Naoi et al. 1995, An et al. 1994, Peres et al. 1989, Otero and De Larreta 1988, Ko et al. 1990, Diaz and Hall 1983, Beck et al. 1994, Kaplin and Qutubuddin 1995, Gardner and Bartlett 1995, Gandhi et al. 1995, Wallace et al. 1997, Nishizawa et al. 1991, Salmon et al. 1982, Mitchell and Geri 1987, Scrosati 1988, Stanković et al. 1994, De Paoli et al. 1992, Cheung et al. 1988). Likewise, many others have completed work to reveal details of PPy's frequency response characteristics (Kaplin and Qutubuddin 1995, Ko et al. 1990, Scrosati 1988, Cheung et al. 1988, Diaz and Bargon 1986, Ko et al. 1994, Kuwabata et al. 1984, West et al. 1992, Doblhofer and Rajeshwar 1998, Madden et al. 2000 and 2001, De Paoli et al. 1992, Ohno et al. 1994, Kaneto et al. 1995). While the specific electrolyte, dopant and solvent systems have varied, many of the findings have been fairly similar as they are often based on common principles of electrochemistry.

For instance, in general, polypyrrole has a granular or nodular cauliflower appearance at high magnification (Salmon et al. 1982, Otero and De Larreta 1988, An et al. 1994, Wallace et al. 1997, Diaz and Hall 1983, Beck et al. 1994, Gardner and Bartlett 1995). Peres et al. (1989) provide imagery of PPy(DBS) films produced in low DP, low DN, and high DCD conditions. They also examine the edges versus mid-film. Naoi et al. (1995) also look at the edges, and they vary concentrations of their electrolytes (DS and DBS). Their DBS images show film with vertically expanding columnar inclusions and nodules. John et al. (1992) mixed para-toluene sulfonate (pTS) and DS in their study.

Increases in DS concentration led to larger sized nodules. Gandhi et al. (1995) also observed these conical nodules, and noted that fractures in the films occurred around these features.

Scrosati (1988) and De Paoli et al. (1992) varied DCD and found that lower DCD values produced smoother films. My results would tend to agree with theirs. Stanković et al. (1994) also found larger nodules or grains in their high DCD films. Mitchell and Geri (1987), however, found the opposite as their high voltage depositions of PPy(pTS) were the smoothest in texture.

Nishizawa et al. (1991) and Cheung et al. (1988) showed that electrode pre-treatments can have dramatic effects on PPy(NO₃) morphology. Kaynak's (1997) PPy(pTS) films grown on steel also displayed some unusual characteristics, while Ko et al. (1990) showed imagery from both aqueous and non-aqueous systems. In Figure 5-7d, I presented an SEM image from a very high DCD deposition. The surface appears to be covered with microscopic flowers. This is not the first time this phenomenon has been seen, as shown in Kaplin and Qutubuddin (1995) under similar conditions.

In terms of the elemental analyses, there were a number of noteworthy findings. The increase in sodium content after reduction supports the idea that Na⁺ ions enter the film to bring about the volume expansion upon reduction. The apparent increase in sulfur (reflecting the DBS anions) after oxidation, would not necessarily reflect any movement of anions into the polymer. It could, instead, reflect the anticipated exodus of hydrated sodium (thus leaving the sulfur percentage relatively higher by weight). The unstimulated films showed an expected increase in sodium and sulfur content with DN.

However, the reasons for the trends in the face of increasing monomer concentration remain unclear.

The SEM thickness measurements showed us that while Smela's (1999) formula for film thickness prediction is sound, it is also subject to inaccuracies due to variances in DCD values used, and to low levels of monomer and/or electrolytes. If, as I found, the low DCD films can be up to 30% thicker than predicted and if the high DCD films can be up to 15% thinner than predicted, then some of the apparent differences between the behaviour of different DCD beams may be explained. This needs to be looked at further.

In terms of frequency response studies pertaining to polypyrrole, there are few that focus on the topic specifically. However, there are many that describe the behaviour of CVs as the scan rate is increased. In general, peak current levels increase with cycling frequency and the redox peaks move away from 0 V i.e. peak separation increases, with reduction peaks often being more mobile (West et al. 1992, Scrosati 1988, Diaz and Bargon 1986, Ko et al. 1994, Ko et al. 1990, Doblhofer and Rajeshwar 1998, De Paoli et al. 1992, Kuwabata et al. 1984). If the peak current levels are proportional to scan rate, then one can say that electron transfer is the rate limiting process. If, on the other hand, peak current levels are proportional to the square root of the scan rate, then electrolyte diffusion is the rate limiter (Kaplin and Qutubuddin 1995). For example, Ohno et al. (1994) found that peak oxidation currents with PPy(ClO₄) increased proportional to the square root (diffusion limited). However, Kaplin and Qutubuddin found them proportional to scan rate. They did find diffusion limitations in PPy(pTS), however. There, they saw peaks increase in linear proportion to the scan rate (electron transfer limited) for films produced at low deposition potentials while they increased proportional

to the square root when the films were produced at higher potentials. They also found that the peak currents were proportional to film thickness. Iseki et al. (1991) also looked closely at how film thickness influences electrochemical behaviour. They found that ion capture capacity was proportional to thickness. This is slightly different than my charge exchange capacity measurement though. Mine is a percentage of deposition charge. Theirs is an absolute charge. As such, Figure 5-12 also shows that charge exchange does increase with film thickness. However, it does so differently depending on DCD values. For the record, charge exchange capacity goes down with film thickness in most cases although it depends on cycling frequency to some extent.

Cheung et al. (1988) found further differences in the frequency response of polypyrrole films depending on what electrode surface was used, while Ko et al. (1990) found that the voltage peaks moved more in aqueous systems than in organic solvents. Kaplin and Qutubuddin (1995) noted that the relationship between scan rate and peak current levels is dependent on DCD, electrolytes and charge density (film thickness).

I did not see the proportionality between scan rate (or its square root) and peak currents. Figure 5-18 makes that quite clear. I can offer a reasonable explanation, however. For all of the half dozen or so studies that are mentioned above as having found such a relationship, the range of scan rates used to arrive at that conclusion was only 1-300 mV/s. I started my evaluations at 200 mV/s and reached a maximum of 25,600 mV/s. More importantly, I was not capturing the actual redox peaks by the 3rd set of CVs, in most cases. Thus, the basis for comparison was not present. One can certainly imagine that at relatively low scan rates, the transfer of electrons and/or the diffusion of electrolytes can keep up to increases in scan rates as per the stated

proportional relationships. However, at high enough scan rates/cycling frequencies, there must come a time when these movements of mass and charge cannot be initiated quickly enough to sustain the proportional increases in peak currents within a given cycling range. That would be reflected in the movement of the peaks outside of the cycling range, and I surely reached and exceeded that point.

While there is much to consider with the scan rate studies, there are a few papers in the literature that focus more on the frequency response of the actuators themselves. For instance, Kaneto et al. (1995) worked with polyaniline and noted that his fibers could produce vibrations up to 44 Hz. Bohon and Krause (1998), with their electrorheological fluids (ERFs), noted that they were able to produce displacements at up to 15 Hz. However, even at 1 Hz, the strain (displacement) was only about half that of the DC strain (10 μm). Similarly, Salehpoor et al.'s (1997) ionic polymeric composite films decreased their levels of deformation dramatically between .1 and .5 Hz, at a 4 V stimulation level, dropping from about .95 inches to .55 inches displacement.

If we are concerned about the frequency response of PPy exclusively, then there is really only one set of solid studies that deal with the matter. They come from the lab work of John Madden et al. (2000, 2001). In their 2000 study, bending bilayers in both aqueous solutions and air were evaluated from .1 Hz to 30 Hz. No explicit cut-off frequency was shown or noted. However, the slope of the log/log plot was about -0.4 (normalized deflection versus cycling frequency). The aqueous-based bilayers performed much better than the dry ones, reaching strain levels of 0.4% at 1 Hz and levels of 3% per second at 10 Hz. The dry bilayer, in spite of being stimulated at ± 127 mA, only reached

a maximum strain of about 0.2% at 0.1 Hz and a maximum strain rate of about 0.5% per second at 15 Hz.

Their 2001 study provided more detail. Long polypyrrole tetraethylammonium hexafluorophosphate strips were clamped at both ends in a cell. Propylene carbonate was the solvent, and the strips were prepared as per Yamaura et al. (1988). Madden developed an admittance transfer function for the strips, and determined that a linear model was suitable. At high cycling frequencies, the admittance was dominated by the electrolyte while at low frequencies a capacitive response was dominant. The intermediate behaviour was a function of the mass transport of ions in and out of the polymer. Madden pointed out that linear diffusion models describe the mass transport mechanisms, and that the capacitance has been attributed to double layer charging of pores in the film, an extension of double layer charging into the bulk of the material, and/or quasi-Nernstian behaviour.

Madden added that two time constants are important to actuator design in his model. The first is an ion diffusion time constant. It suggests that decreasing film thickness by one order of magnitude will increase the diffusion rate by two orders. He also discussed how other electrolyte ions and film morphologies might also increase the diffusion rate. The other time constant was the charging time constant, and its rate could be maximized by decreasing film thickness, and by decreasing polymer resistance and volume. He was able to achieve strains of 0.007% at 30 Hz and strain rates of 0.4% per second with these films.

I shall take up this challenge of strains and strain rates in the next chapter. For the time being, however, I can review how the performance of the bending beams in this

study fared against natural muscle. With cut-off frequencies ranging from 0.1 to about 1.0 Hz, they were often within one order of magnitude of natural muscle. However, these beams were not at all optimized. Anecdotal experience in the lab has shown that using Mylar[®] instead of Kapton[®] as a backing can increase the strain and strain rate of the PPy(DBS) enormously. That does not necessarily imply better frequency response, but it could be the case. Higher SN concentrations may also be helpful. The current findings are certainly good enough to anticipate that concerted efforts at improvement could bring about the necessary levels of performance. The variations in movement responsiveness and extent with DCD, electrolyte and monomer concentrations, cycling limit adjustments, and stimulation frequency all provide promise for fast and slow twitch varieties of artificial muscle fibers based on PPy(DBS) actuation. The LPF qualities of muscle will be harder to emulate, however. One fundamental difference between PPy and natural muscle is that natural muscle relaxes when it does not receive ongoing stimulation. PPy(DBS) does not relax, at least on the same time scale (see Pei and Inganäs 1993b-c). It needs to be actively “relaxed” or brought back to its “rest” length. This does present an interesting opportunity, though. I did not discuss in the introduction that natural muscles are always arranged in antagonistic pairs. This serves to provide fast movements of extension or flexion, and it also allows the organism to independently stiffen the joint around which the muscles lie (Hunter and Lafontaine 1992). It also allows for the dampening of ballistic movements that could otherwise cause damage to the organism. That is, as one muscle gets the limb moving, its antagonist contracts towards the end of the movement to slow down the limb. This process is characteristic of all well-programmed ballistic movements (Brooks 1983). At some future point, if conducting

polymer-based actuators were ever to be used in artificial muscle applications, it could be possible to link antagonist muscles electrochemically so that energy could be shared and/or conserved between the two muscles.

These sorts of energy, power and efficiency issues will be dealt with more explicitly in the next, and last, experimental chapter.

5.5 Conclusions

For PPy(DBS)-actuated bending beams such as those described in this chapter, curling patterns due to strains transverse to the plane of the film can reach cut-off frequencies of about 1 Hz.

Deposition curling is strongly influenced by the backing of the beams, both its thickness and its modulus. DCD also has a strong influence, and with DN at .08 M, so does DP. In the conditioning cycles, it was noted that curling increases with SN but that the increases plateau at higher SN values. Increases in SN also favour a more oxidative movement (curling) during the first reduction.

SEM elemental analyses show that relative sulfur content increases with DP, while the relative weight of sodium and oxygen decreases. Likewise, increases in DN lead to relative increases in sulfur and sodium, and to decreases in oxygen. Results were consistent with higher sodium content in reduced films, and lower sodium content in oxidized films. Increases in stimulation NaDBS led to decreases in relative sulfur content and increases in oxygen content.

SEM imagery suggests a significant change in morphology of the films as a function of DP. Increased levels of DP lead to more granular surfaces with more cauliflower textures. Low DP films are smoother. It was determined that great care is required in making beam thickness measurements with SEM. Film thicknesses vary along the width of the beam, and different edge preparations can produce misleading results. Freeze fracture methods are recommended for best results. It was found that films were somewhat thinner than expected (from Smela 1999) with high DCD, low DP

and low DN values. Reduced films were notably thicker than oxidized films, likely due to the movement of possibly hydrated Na^+ into the polymer during reduction.

With regard to the frequency response characteristics of the beams, increasing the cycling frequency reduces hysteresis in the CV, reduces the amount of strain, increases peak current levels, increases peak separation, and reduces charge exchange per cycle. There is little difference between the CVs of different DCD thick films. However, there are large differences between different DCD values with thinner films as high DCD values produce lower peak current levels. Movement responsiveness increases, peaks and then falls with respect to cycling frequency. Charge exchange capacity simply falls. However, I was able to produce exchanges of 9.7% with ± 2 V stimulation at 0.2 Hz.

The nature of the beam movements changes with increasing frequency. At lower frequencies (below 1 Hz), the beam tips trace an arc. At higher frequencies (1-3 Hz), they trace an ellipse. At the highest frequencies tested (3.2-6.4 Hz) they often just vibrated, if they moved at all. Using thin Kapton[®] always results in better movement characteristics. Low DCD values produce more curling in all sets except the first. Movement responsiveness (curl per unit charge) was best with low DCD beams at high cycling frequencies, and was best with high DCD beams at low cycling frequencies. Charge exchange capacity, and curling, rose and fell with respect to film thickness, peaking at about 10-20 μm in the system that I employed. Movement responsiveness decreased with increasing film thickness. Peak currents, peak voltage separations and charge exchanges all increased with film thickness at all frequencies.

Comparing curling (strain) in thin and thick PPy(DBS) films over the tested stimulation frequency range, thinner Kapton[®] and lower DCD worked better with thin

films while thicker Kapton[®] and higher DCD worked better with thick films. Over the full range of the tested beam conditions, the cut-off frequency varied from 0.1 to 1.0 Hz.

Movement responsiveness was optimized with thin films on thin Kapton[®] at a cycling frequency of about 1 Hz. Peak currents all increased with film thickness, and with frequency for thin films. For thin films, low DCD and/or thicker Kapton[®] peak currents were greater than those from high DCD and/or thin Kapton[®] films. For thicker films, there were no differences by condition, and the peak currents rose to peak at about 1 Hz. Charge exchange showed similar patterns.

Clearly, if a certain frequency response is desired in a PPy(DBS)-actuated bending beam, it can be designed and manufactured, within limits. The careful management and matching of film thicknesses, backing thicknesses, backing moduli, and DCD values can result in tailored frequency responses. Optimization of these variables, along with conditioning patterns and electrolyte/dopant and monomer concentrations, should enable improved frequency responses to rival those of natural muscle.

5.6 References

- An, H., Haga, Y., Yuguchi, T., and Yosomiya, R. (1994) "Synthesis of polypyrrole by electrochemical polymerization using organic anion electrolytes and its application", *Die Angewandte Makromolekulare Chemie*, Vol. 218, #3814, pg. 137-151
- Aaron, S.L. and Stein, R.B. (1976) "Comparison of an EMG-controlled prosthesis and the normal human biceps brachii muscle", *Am. J. Phys. Med.*, Vol. 55, #1, pg. 1-14
- Bawa, P., Mannard, A., and Stein, R.B. (1976) "Effects of elastic loads on the contractions of cat muscles", *Biol. Cybernetics*, Vol. 22, pg. 129-137
- Beck, F., Michaelis, R., Schloten, F., and Zinger, B. (1994) "Filmforming electropolymerization of pyrrole on iron in aqueous oxalic acid", *Electrochimica Acta*, Vol. 39, #2, pg. 229-234
- Bohon, K. and Krause, S. (1998) "An electrorheological fluid and siloxane gel based electromechanical actuator: working toward an artificial muscle", *J. Poly. Sci. B. Polym. Phys.*, pg. 1091-94
- Brooks, V.B. (1983) "Motor control: how posture and movements are governed", *Phys. Ther.*, Vol. 63, pg. 664-673
- Cheung, K.M., Bloor, D., and Stevens, G.C. (1988) "Characterization of polypyrrole electropolymerized on different electrodes", *Polymer*, Vol. 29, September, pg. 1709-17
- De Paoli, M.-A., Peres, R.C.D., Panero, S., and Scrosati, B. (1992) "Properties of electrochemically synthesized polymer electrodes – X. Study of polypyrrole/dodecylbenzene sulfonate", *Electrochimica Acta*, Vol. 37, pg. 1173-82

Diaz, A.F. and Hall, B. (1983) "Mechanical properties of electrochemically prepared polypyrrole films", *IBM J. Res. Develop.*, Vol. 27, #4, July, pg. 342-347

Diaz, A.F. and Bargon, J. (1986) "Chapter 3 – Electrochemical Synthesis of Conducting Polymers", In: **Handbook of Conducting Polymers Vol. 1**, Skotheim [ed.], Marcel Dekker Inc, NY, pg. 81-115

Doblhofer, K. and Rajeshwar, K. (1998) "Chapter 20 – Electrochemistry of Conducting Polymers", In: **Handbook of Conducting Polymers 2nd Ed.**, T.A. Skotheim, R.L. Elsenbaumer and J.R. Reynolds [eds], Marcel Dekker Inc, NY, pg. 531-588

Gandhi, M., Spinks, G.M., Burford, R.P., and Wallace, G.G. (1995) "Film substructure and mechanical properties of electrochemically prepared polypyrrole", *Polymer*, Vol. 36, #25, pg. 4761-4765

Gardner, J.W. and Bartlett, P.N. (1995) "Application of conducting polymer technology to microsystems", *Sensors and Actuators A*, Vol. 51, pg. 57-66

Hunter, I.W. and Lafontaine, S. (1992) "A comparison of muscle with artificial actuators", *IEEE Solid-State Sensors and Actuators Workshop Technical Digest*, June 21-25, Hilton Head Island, USA, pg. 178-85

Iseki, M., Kuhara, K., and Mizukami, A. (1991) "Study on electrically plastic devices made with electropolymerized films", *Jap. J. App. Phys.*, Vol. 30, #5, May, pg. 1117-121

John, R., John, M.J., Wallace, G.G., and Zhao, H. (1992) "Use of surfactants in the oxidative synthesis of conductive, electroactive polymers", In: **Electrochemistry in Colloids and Dispersions**, R.A. Mackay and J. Texter [eds], VCR Publishers, NY, pg. 225-34

Kaneto, K., Kaneko, M., Min, Y., and MacDiarmid, A.G. (1995) "Artificial muscle: electromechanical actuators using polyaniline films", *Synthetic Metals*, Vol. 71, pg. 2211-2212

Kaplin, D.A. and Qutubuddin, S. (1995) "Electrochemically synthesized polypyrrole films: effects of polymerization potential and electrolyte type", *Polymer*, Vol. 36, #6, pg. 1275-1286

Kaynak, A. (1997) "Effect of synthesis parameters on the surface morphology of conducting polypyrrole films", *Mat. Research. Bull.*, Vol. 32, #3, pg. 271-85

Ko, J.M., Rhee, H.W., Park, S.-M., and Kim, C.Y. (1990) "Morphology and electrochemical properties of polypyrrole films prepared in aqueous and nonaqueous solvents", *J. Electrochem. Soc.*, Vol. 137, #3, March, pg. 905-909

Ko, J.M., Kim, S., Kim, K.M., and Chung, I.J. (1994) "Electrochemical properties of dodecylsulfate-doped polypyrrole films in aqueous solution containing NH_4Cl and ZnCl_2 ", *Synthetic Metals*, Vol. 64, pg. 9-15

Kuwabata, S., Yoneyama, H., and Tamura, H. (1984) "Redox behavior and electrochromic properties of polypyrrole films in aqueous solutions", *Bulletin of the Chemical Society of Japan*, Vol. 57, pg. 2247-2253

Madden, J.D., Cush, R.A., Kanigan, T.S., Brenan, C.J., and Hunter, I.W. (2000) "Fast contracting polypyrrole actuators", *Synthetic Metals*, Vol. 113, pg. 185-92

Madden, J.D.W., Madden, P.G.A., and Hunter, I.W. (2001) "Polypyrrole actuators: modeling and performance", *SPIE 8th Ann. Int. Symp. Smart Struct. Mat. Proc.*, March 5

Mannard, A. and Stein, R.B. (1973) "Determination of the frequency response of isometric soleus muscle in the cat using random nerve stimulation", *J. Physiol. (London)*, Vol. 229, pg. 275-296

Maw, S., Smela, E., Yoshida, K., Sommer-Larsen, P., and Stein, R.B. (2001) "The effects of varying deposition current density on bending behaviour in PPy(DBS)-actuated bending beams", *Sensors and Actuators A*, Vol. 89, pg. 175-184

Mitchell, G.R. and Geri, A. (1987) "Molecular organisation of electrochemically prepared conducting polypyrrole films", *J. Phys. D: Appl. Phys.*, Vol. 20, pg. 1346-1353

Naoi, K., Oura, Y., Maeda, M., and Nakamura, S. (1995) "Electrochemistry of surfactant-doped polypyrrole film (I): Formation of columnar structure by electropolymerization", *J. Electrochem. Soc.*, Vol. 142, #2, February, pg. 417-422

Nishizawa, M., Shibuya, M., Sawaguchi, T., Matsue, T., and Uchida, I. (1991) "Electrochemical preparation of ultrathin polypyrrole film at microarray electrodes", *J. Phys. Chem.*, Vol. 95, pg. 9042-9044

Ogasawara, M., Funahashi, K., Demura, T., Hagiwara, T., and Iwata, K. (1986) "Enhancement of electrical conductivity of polypyrrole by stretching", *Synthetic Metals*, Vol. 14, pg. 61-69

Ohno, H., Yoshida, H., and Ohtsuka, Y. (1994) "Effect of salt species on the electrochemical p-doping of poly(pyrrole) films in poly(ethylene oxide) oligomers", *Solid State Ionics*, Vol. 68, pg. 125-131

Otero, T.F. and De Larreta, E. (1988) "Electrochemical control of the morphology, adherence, appearance and growth of polypyrrole films", *Synthetic Metals*, Vol. 26, pg. 79-88

Partridge, L.D. (1966) "Signal-handling characteristics of load-moving skeletal muscle", *Am. J. Physiol.*, Vol. 210, pg. 1178-1191

Pei, Q. and Inganäs, O. (1992) "Electrochemical applications of the bending beam method. 1. Mass transport and volume changes in polypyrrole during redox", *J. Phys. Chem.*, Vol. 96, #25, pg. 10507-514

Pei, Q. and Inganäs, O. (1993a) "Electrochemical muscles: bending strips built from conjugated polymers", *Synthetic Metals*, Vol. 55-57, pg. 3718-23

Pei, Q. and Inganäs, O. (1993b) "Electrochemical applications of the bending beam method; a novel way to study ion transport in electroactive polymers," *Sol. State Ion.*, Vol. 60, pg. 161-66

Pei, Q. and Inganäs, O. (1993c) "Electrochemical applications of the bending beam method. 2. Electroshrinking and slow relaxation in polypyrrole," *J. Phys. Chem.*, Vol. 97, pg. 6034-41

Peres, R.C.D., Pernaut, J.M., and DePaoli, M.A. (1989) "Properties of poly(pyrrole) films electrochemically synthesized in the presence of surfactants", *Synthetic Metals*, Vol. 28, pg. C59-C64

Salehpoor, K., Shahinpoor, M., and Mojarrad, M. (1997) "Linear and platform type robotic actuators made from ion-exchange membrane-metal composites", *SPIE*, Vol. 3040, pg. 192-198

Salmon, M., Diaz, A.F., Logan, A.J., Krounbi, M., and Bargon, J. (1982) "Chemical modification of conducting polypyrrole films", *Mol. Cryst. Liq. Cryst.*, Vol. 83, pg. 265-276

Scrosati, B. (1988) "Electrochemical properties of conducting polymers", *Prog. Solid St. Chem.*, Vol. 18, pg. 1-77

Smela, E., Inganäs, O., and Lundström, I. (1995) "Controlled folding of micrometer-size structures", *Science*, Vol. 268, June 23, pg. 1735-38

Smela, E. (1999) "Microfabrication of PPy microactuators and other conjugated polymer devices", *J. Micromech. Microeng.*, Vol. 9, pg. 1-18

Smela, E. and Gadegaard, N. (1999) "Surprising volume change in PPy(DBS): an atomic force microscopy study", *Adv. Mat.*, Vol. 11, #11, pg. 953-57

Stanković, R., Pavlovic, O., Vojnovic, M., and Jovanovic, S. (1994) "The effects of preparation conditions on the properties of electrochemically synthesized thick films of polypyrrole", *Eur. Polym. J.*, Vol. 30, #3, pg. 385-393

Wallace, G.G., Spinks, G.M., and Teasdale, P.R. (1997) **Conductive Electroactive Polymers: Intelligent Materials Systems**, Technomic Publishing, USA, pg.1-106

West, K., Zachau-Christiansen, B., Jacobsen, T., and Skaarup, S. (1992) "Electrochemical characterization of conducting polymers: polypyrrole", *Materials Science and Engineering*, Vol. B13, pg. 229-33

Yamaura, M., Hagiwara, T., and Iwata, K. (1988) "Enhancement of electrical conductivity of polypyrrole film by stretching: counter ion effect", *Synthetic Metals*, Vol. 26, pg. 209-224

6. Power, Efficiency, Endurance and Other Functional Characteristics of PPy(DBS)-Actuated Bending Beams

6.1 Introduction

If one seeks to create an artificial muscle fiber (AMF) that mimics the behavioural characteristics of natural muscle fibers, then some of the most important performance parameters that must be duplicated include strength, strain, power, work, efficiency, endurance and response/reaction time. These parameters establish the functionality and practical value of any AMF and it should be noted that poor performance on any one of them is usually enough to render them unusable or infeasible for anything more than laboratory studies. This chapter looks at how PPy(DBS)-actuated bending beams (Pei and Inganäs 1992, 1993a-c, Maw et al. 2001) behave with respect to these measures.

Natural muscle exhibits a truly unique combination of these qualities, and that combination has proven difficult to match along all of the dimensions simultaneously. For example, isolated muscle fibers can contract by over 50% when stimulated, and by over 10% within the context of actual limb movements. They are about 50 μm in diameter in adult humans. The peak static stress developed by vertebrate skeletal muscle is about 350 kPa, although the maximum sustainable stress level is about 100 kPa. Power per unit mass varies between 50 and 200 W/kg in humans, and efficiency levels can exceed 35%. Power (load force \times velocity) is maximized in the intermediate load range of any given muscle, as the force and velocity tend to vary inversely with each other (McComas 1996). In terms of cycling endurance, a useful benchmark is the number of times a heart beats over an average person's life. That figure is approximately 3×10^9 assuming a 75 year life and an average heart rate of 75 beats per minute.

Hunter and Lafontaine (1992) discuss all of these findings, as well as others such as the importance of stiffness in natural muscle, in their comparative study of natural muscle versus various actuator technologies. They also add to the list of specifications by noting that muscle's maximum strain rate is on the order of 300% per second.

Most studies of polypyrrole do not concern themselves with these issues because they are not concerned with the volume-changing characteristics of the material. Instead, they usually focus on electrical conductivity. Nevertheless, there are a number of researchers who concentrate on the electromechanical workings of these films for the purpose of developing actuators, or artificial muscle fiber (AMF) systems (Smela et al. 1995, Smela 1999, Smela et al. 1993, Madden et al. 2000 and 2001, Otero and Sansiñena 1995 and 1996, Lewis et al. 1997, Pei and Inganäs 1992 and 1993a-c, Pei et al. 1993, Maw et al. 2001, Della Santa et al. 1997, Chiarelli et al. 1995, Iseki et al. 1991, De Rossi et al. 1986, Gandhi et al. 1995, Otero and Santamaria 1993, Otero and Rodríguez 1993, Jager et al. 2000). Collectively, these researchers have looked at work, power, efficiency, speed, response time, strength, strain, and endurance. I will compare my results in this study to theirs wherever it is possible and appropriate.

As noted, the bulk of this chapter examines work, power and efficiency issues with respect to PPy(DBS)-actuated bending beams (Maw et al. 2001). A series of 8 bending beams were produced, each of them unique in the values of three parameters that were varied among them. Over the 8 samples, there were 4 each with two different Kapton[®] film thickness backings, two different PPy(DBS) film thicknesses, and two different deposition current density levels. As well, every beam was cycled through 4 sets of cyclic voltammetry, each set cycled at a different frequency. The beams swung

back and forth (or curled and then uncurled) cyclically in response to the stimulation. The movement of the beams was modeled for a work and energy analysis, and this was the basis for the work, power and efficiency measurements that were made.

In addition, data was gathered on the phase lag of the beams in following the ramp voltammetry signal, as well as on the ability of the beams to cycle for long periods of time. Altogether, they provided a picture that described how suitable PPy(DBS) might be in the AMF-actuation role.

6.2 Experimental

This chapter details the findings from two experiments, one focusing on endurance and the other focusing on power and efficiency. The general methods and equipment for production and stimulation of the fibers used in this study were once again identical to those described in Chapter 2. However, as in Chapters 3 to 5, the protocols differed from the earlier work and these are reviewed below. As well, the analysis of the results was more involved, and the techniques used will be detailed in a separate section.

In terms of production, for both experiments, Kapton[®] HN 50 and Kapton[®] HN 100 sheets from Dupont, .5 mil (12.7 μm) and 1 mil (25.4 μm) thick respectively, were coated on one side with $450 \pm 50 \text{ \AA}$ and $500 \pm 50 \text{ \AA}$ of gold (Au) respectively, both by vacuum evaporation. The sheets were then cut into strips 1 mm wide using a sharp blade mounted on an automated Karl Süss scribing machine. In both cases, PPy(DBS) was deposited galvanostatically on a 1.5 cm long portion of the gold-coated surface of each strip in an aqueous .16 M NaDBS / .16 M pyrrole solution, and ramp voltammetry stimulation took place in a .16 M NaDBS solution.

For the endurance experiment, 3 samples were prepared and tested. The goal was simple: try to get the cycling beam to cycle as long as possible. All samples were deposited at 4 mA/cm^2 on 1.5 cm long portions of the beam. The thickness of the PPy(DBS) film on the first two samples was approximately 5 μm as per Smela (1999), while the thickness of the film on the 3rd sample was approximately 20 μm . Kapton[®] HN 100 film was used in all three cases. The beams were cycled at .20 Hz, and their status was monitored every 6-12 hours (or more frequently at the start of each run). First, however, they underwent 15 cycles of conditioning ramp voltammetry to ensure that they

were viable samples. After the conditioning cycles, the upper and lower cycling limits were altered at each status check to try and capture the redox peaks in the CV without going much beyond the peaks. Indeed, the first sample failed relatively early because this task was not performed adequately enough. Cycling at voltages well beyond the peaks definitely led to delamination problems. Also at each status check, the reference electrode was refreshed and the stimulation solution was replaced. As well, data from a few cycles was recorded to gather information on charge transfer, peak currents, the voltages at which those currents were achieved, and the range of motion of the beam tips. Changes in the upper and lower limits were also recorded for later analysis.

The second “power and efficiency” experiment was similar to the frequency response experiment of Chapter 5. However, it was much shorter, and it only involved 9 samples. The protocol involved a nominal 8 samples (one was repeated) where four were deposited at 2 mA/cm² and four were deposited at 16 mA/cm². Similarly, four beams used Kapton[®] HN 50 for backing while four used Kapton[®] HN 100. Finally, the PPy(DBS) was 5 μm thick in four samples while it was 20 μm thick in the others. With three variables each having two values, all 8 permutations were produced as is shown below in Table 6-1.

Each of the power and efficiency samples went through four sets of 15 cycles of ramp voltammetry stimulation, cycling between -1.1 V and +0.4 V. The cycling frequency was .05 Hz during the first set, .10 Hz during the second set, .20 Hz during the third set and .40 Hz during the fourth and final set. As with the frequency response experiment of Chapter 5, data was collected on the 14th cycle of each set since the beam had settled into consistent behaviour by that point. What made this study unique was the

subsequent data analysis, which will be described shortly. This data analysis involved precise measures of the beam position, velocity and curvature over (cycling) time. To gather the data, video footage was digitized and then analyzed using the siliconCOACH software package. While used primarily for golf and other similar sports, it proved entirely adequate to the task of analyzing the details of the movement of the beams.

Table 6-1 Power Sample Preparations

DCD (mA/cm ²)	Kapton [®] HN	PPy(DBS) Thickness (μm)
2	50	5
	50	20
	100	5
	100	20
16	50	5
	50	20
	100	5
	100	20

6.3 Methods of Analysis

The main purpose of the power and efficiency study was to determine the efficiency of the PPy(DBS) in performing mechanical work through its beam bending action. The mechanical work, in turn, was brought about by electrical stimulation. The efficiency of the whole system was evaluated using the ratio of work out (mechanical) to work in (electrical) on the 14th of 15 cycles performed per stimulation frequency per sample. The issues involved in the calculation of these work terms will be addressed sequentially in this section.

6.3.1 Mechanical Work

In general, mechanical work can be defined as the product of a force applied over a distance, or mathematically as

$$W = F \times d \quad (1)$$

However, since there are many types of forces and distance measures, there are many types of mechanical work. Four of these types of mechanical work were evaluated in analyzing the work done by the PPy(DBS) films during stimulation. The first type was work due to gravity (and buoyancy). The beams were waving back and forth in an aqueous solution, alternately curling up to the right and then down to the left. The mass of the bending beams was therefore moving up and down with respect to gravity. More specifically in this situation,

$$F_G = m \times g \quad (2) \quad \text{and} \quad d = \Delta h \quad (3)$$

$$\text{giving } W_G = m \times g \times \Delta h \quad (4)$$

where F_G is the force of gravity, m is mass, g is acceleration due to gravity, d is distance, Δh is height, and W_G is mechanical work with respect to gravity.

Approximately 1.3 to 1.4 cm of the bending beams were immersed in the stimulation solution. For the purposes of these analyses, each beam was divided into 2-3 beam elements (top, mid and end). The points at which the beams were divided varied from beam to beam. The choices were made so as to select regions of beam where the bending activity was relatively uniform within elements and different between elements. Thus, the work calculations were performed on each of the beam elements for each time step in the analysis. Video data was collected at a frame rate of 29.97 Hz, or once every .03337 seconds. The time steps for the data analysis varied by stimulation frequency but were proportionally very similar, as is shown in Table 6-2 below.

Table 6-2 Video Analysis Time Steps versus Stimulation Frequency

Stimulation Frequency (Hz)	Cycle Duration (sec)	Video Frames per Time Step	Time Step (sec)	Steps per Cycle
0.10	10.0	15	0.500	19.98
0.20	5.0	8	0.267	18.73
0.40	2.5	4	0.133	18.73

Thus, for each time interval and for each beam element, the location of the center of gravity of the beam element was determined. This measurement was taken twice, and the two values were averaged. This averaged data was then smoothed with a running 3-point average. The displacement from one time interval to the next was then determined

from this smoothed average data, providing the Δh of equations (3) and (4) to a precision of about .01 mm.

The mass term of equations (2) and (4) deserves some mention, as it is not the actual mass of the beam element but rather the apparent mass of the element, given its submersion in a buoyant medium. Using the specified thicknesses of the Kapton[®] and gold, along with the expected thicknesses of the PPy(DBS) as per Smela (1999), the actual mass of each beam element was determined using densities of 1.42 g/cc (Dupont 2002) and 1.4 g/cc (Sato et al. 1986, Buckley et al. 1987, Rane and Beaucage 1999) for the Kapton[®] and PPy(DBS) respectively. Then the mass of the displaced aqueous electrolyte was subtracted, using an approximated density value of 1 g/cc.

Being a conservative force, the work performed due to gravity netted to almost zero over the course of each cycle. By the 14th cycle in each set, the movements were highly similar from cycle to cycle such that any positive work (raising a mass against gravity) was cyclically offset by “negative” work (a mass descending with gravity). That is, when the beams were moving down and to the left during PPy(DBS) expansion, which took place during reduction, the work was negative due to the negative Δh term of equations (3) and (4).

The second form of work that was evaluated was that of viscous drag. The bending beams were moving back and forth in an aqueous solution. Therefore, the beam encountered a drag force as it moved. Using the same ideas of calculating work by beam element (top, mid and end) and by time interval, the position and velocity of the end of each beam element was determined.

The drag was then modeled as that of a flat plate moving through a fluid, where the flat plate was the beam element. In this situation,

$$F_D = C_D \times A \times \rho \times (v^2/2) \quad (5)$$

$$\text{giving } W_D = C_D \times A \times \rho \times (v^2/2) \times \Delta x \quad (6)$$

where C_D is the coefficient of drag, A is the projected area of the plate, ρ is the density of the fluid (again 1 g/cc) and v is the velocity of the beam as it moves through the fluid. The Δx represents the distance that the beam moves through the fluid from one time interval to the next. The coefficient of (pressure) drag for a flat plate oriented into the flow varies according to Reynolds number at low Reynolds numbers, which is the flow regime in our situation ($0.1 < Re < 100$). At Reynolds numbers greater than 10^3 , the drag coefficient is well known to be about 1.2 (National Aeronautics and Space Administration 2002). At lower ranges, it is not as well documented. Nevertheless, there is some literature that suggests the absolute values of the Re/C_D relationship, as well as the rate of change of the relationship (Hoerner 1965, Fay 1994). The following equations were derived to model these findings over the $.005 < Re < 10$ range (see Figure 6-1).

$$C_D = \text{EXP} \left(- (\ln Re) / (.55 \times (1 - Re - .2 \times (1 - Re^2)) + .6 \times (1 - Re^{(.17 \times (Re - .6)(Re - .6) + .06)})) \right) \\ \text{for } .005 < Re < .99 \quad (7)$$

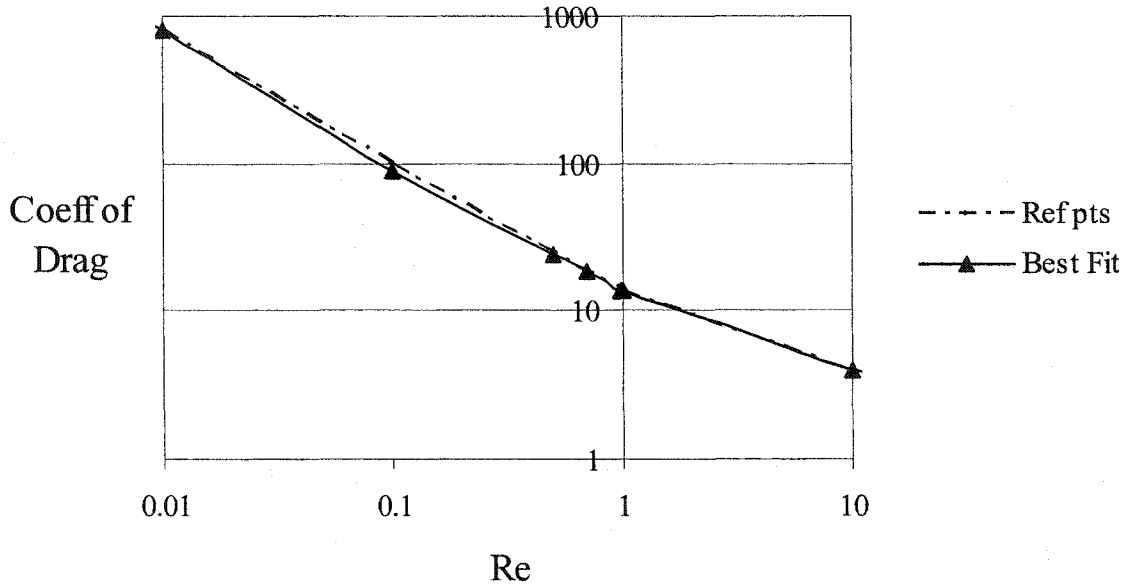
$$C_D = 13.8 - 8.5 \times ((\log(10 \times Re)) - 1) - .13 \times Re \quad \text{for } 1.01 < Re < 10 \quad (8)$$

The Reynolds number itself comes from the following equation,

$$Re = (v \times d) / \nu \quad (9)$$

where v is velocity of the beam element, d is the width of the body facing the flow, and ν is the kinematic viscosity of the fluid. In my case, the velocity was garnered from the video footage of the cycling movements using the velocity of each beam element's center

Figure 6-1 Plot of the equations used to relate Reynolds number to coefficient of drag (C_D). From .005 to .99, the equation used is $C_D = \text{EXP}(-(\ln \text{Re}) / (.55 \times (1 - \text{Re} - .2 \times (1 - \text{Re}^2)) + .6 \times (1 - \text{Re}^{(.17 \times (\text{Re}^{-.6}) (\text{Re}^{-.6}) + .06)})))$. From 1.01 to 10, the equation is $C_D = 13.8 - 8.5 \times ((\log(10 \times \text{Re})) - 1) - .13 \times \text{Re}$. These two equations covered the range of Reynolds numbers that arose during the analysis.



of gravity. These velocity values were found by averaging the velocity values at each end of each element, assuming a velocity of zero for the top of the top element. The d value was simply the width of the beams (1 mm). For the kinematic viscosity, I used a value of $.014 \text{ cm}^2/\text{s}$, which was empirically determined by performing a standard drop test in a column of the electrolyte solution (Douglas et al. 1995).

The third work component that was evaluated in this analysis was inertial work. Almost all of the time, each beam element was either accelerating or decelerating. Since

$$F = m \times a \quad (10)$$

where m is the actual mass of the beam element being evaluated, we get a work term of

$$W_I = m \times a \times \Delta x \quad (11)$$

that accounts for this inertial work. This term was evaluated in the same way as the previous work components with respect to beam elements and time intervals.

The fourth and last mechanical work component was handled very differently. This was the work performed by bending the beam. In other words, it was the work required to bend a spring, which in this case was the elastic beam. For this term, I considered that as a beam bends, some portions are in compression and some are in tension. The small strains that allow for such bending are a function of the stress/strain relationships of the materials making up the beam. Indeed, a bent beam has a particular internal elastic energy as the beam will inherently seek to return to a state of no strain (or balanced stress). The amount of this internal elastic energy can be calculated such that differences in it from time interval to time interval can be taken as the work performed during a given time interval. More specifically, if we take σ to be the stress acting on a tiny section of the beam at time T , then the force acting is

$$F = \sigma \, dy \, dz \quad (12)$$

$$\text{such that } dU = \sigma \, dy \, dz \times \epsilon_x \, dx = \sigma \times \epsilon_x \, dV \quad (13)$$

where dU is the internal elastic energy of the infinitesimally small element. Since we know that

$$\epsilon_x = \sigma / E \quad (14)$$

we can substitute equation (14) into (13) in the elastic range to give us

$$U = \int_{\text{vol}} (\sigma^2 / E) \, dV \quad (15)$$

However, we also know that

$$\sigma = - (M \times y) / I \quad (16) \quad \text{and} \quad dV = dx \, dA \quad (17)$$

Substituting (16) and (17) into (15), and then simplifying, we get

$$U = \int_{\text{vol}} (M^2 \times y^2) / (E \times I^2) \, dx \, dA \quad (18)$$

$$U = \int_{\text{beam length}} M^2 / (E \times I^2) \, dx \int_{\text{area}} y^2 \, dA \quad (19)$$

$$U = \int_{\text{beam length}} M^2 / (E \times I) \, dx \quad (20)$$

$$U = (L \times M^2) / (E \times I) \quad (21)$$

This gives us the internal strain energy of the beam element at time T . To get the work performed in bending the beam, we simply take the difference ΔU between time intervals. There are still a few loose ends, though. We do not know M or I at this stage. To get M , we need to measure the radius of curvature of the beam element that we are analyzing. For that, we use the equation

$$\rho = (L^2/4 + x^2) / 2x \quad (22)$$

where ρ is the radius of curvature (roc), L is the straight-line distance from one end of a curled beam element to the other end, and x is the maximum distance between the L line and the arc of the beam element. Then, we substitute ρ into

$$M = (E \times I) / \rho \quad (23)$$

That leaves the I term, the moment of inertia (MOI) of the beam. The MOI term is actually fairly complicated, as the modulus of the PPy(DBS) is assumed to change over the course of the cycling i.e. $E_{\text{red}} < E_{\text{ox}}$. Values of .15 and .45 GPa were adopted as the presumed E_{red} and E_{ox} (Bay et al. 2001). The modulus was assumed to vary linearly from one limit to the other during cycling, in phase with the cycling. Thus, each time interval featured an average modulus for the PPy(DBS) and that average value was assumed to be constant over the time interval for the purposes of calculations.

Even if the modulus of the PPy(DBS) did not change over time, a composite beam flexure analysis still would have been necessary. I assumed three layers in the composite beam: the Kapton[®] backing, the gold interlayer and the active PPy(DBS) layer. The gold layer was taken to be 45 nm thick, with a modulus of 83 GPa. The Kapton[®] backing was either 12.7 μm or 25 μm thick. Its modulus is 2.5 GPa (Dupont 2002). To find the composite beam's moment of inertia, I needed to convert two of the layers into layers mechanically equivalent to the third. After the beam of 3 materials is reduced to an equivalent of one, the usual elastic flexure formulas apply. In this case, the Kapton[®] layer was used as the reference layer, as its qualities are the best characterized. As such, the apparent width of the other layers was altered according to the ratio of their moduli as compared to that of Kapton[®], so as to create a virtual beam constructed out of Kapton[®] exclusively. Now, for the purposes of the calculations, the Au and PPy(DBS) layers would not be considered to be 1 mm wide anymore, reflecting the tradeoff in changing their moduli. As a result, a standard formulation was followed for calculating the MOI of a beam consisting of more than one geometric component or part. In other words,

$$I = (w/12 \cdot h_K^3 + w h_K (y - h_K/2)^2) + (w n_1 / 12 \cdot h_G^3 + w n_1 h_G (y - (h_G/2 + h_K))^2) + (w n_2 / 12 \cdot h_P^3 + w n_2 h_P (y - (h_P/2 + h_G + h_K))^2) \quad (24)$$

where $w = 1\text{mm}$, h_K , h_G and h_P are the heights of the Kapton[®], gold and PPy(DBS) layers respectively, $n_1 = E_G/E_K$, $n_2 = E_P(T)/E_K$, and $y = \sum yA / \sum A$ is the vertical location of the neutral axis (NA) of the composite beam. The y values are taken from the bottom of the beam (bottom of the Kapton[®] layer).

Having calculated each of the types of mechanical work for each of the beam elements at each of the time intervals in the cycle, the work terms were totaled by beam element, by time interval and by cycle. Also, the moment equation (23) offered the opportunity to examine the maximum stresses in the PPy(DBS) films, as

$$\sigma_{K_{\max}} = (M \times c_K) / I \quad (25)$$

where $\sigma_{K_{\max}}$ is the maximum stress in the Kapton[®] and c_K is the largest moment arm (y) value in the Kapton[®] film. The maximum stress in the PPy(DBS) is found in a similar manner. It is

$$\sigma_{P_{\max}} = (n_2 \times M \times c_P) / I \quad (26)$$

Finally, if we know the maximum stresses in the films, and their moduli of elasticity, then we also know their strains by equation (14).

6.3.2 Electrical Work, Efficiency and Power

Having determined the work output of the system, all that remained was to calculate the work input to the system. This was the electrical driving energy. In deriving this term, we know that the power is

$$P(t) = I(t) V(t) \quad (27)$$

$$\text{thus } W = \int I(t) V(t) dt \quad (28)$$

Having collected the V and I signals from the cell during the experiment (see Experimental Methods), data points from these signals were multiplied directly to give instantaneous power levels (see Figure 6-2) and then they were numerically integrated with respect to time using a Matlab[®] trapezoidal integration function. Positive and negative electrical work totals were kept track of separately. Totals were derived for the entire cycle, as well as for each time interval within the cycle (to match the mechanical work data).

This is not the entire story though. Intuitively, one could consider the electrical work to be the area inside of a cyclic voltammogram (I x V over time). However, this is not what equation (28) calculates. Equation (28) calculates much more than that i.e. the vertically striped areas of Figure 6-3 *plus* the darkly shaded sections. This is the true electrical work input into the system, and it includes work that is directed towards non-electromechanical transduction such as heating the electrolyte solution and/or oxidizing water. Note in Figure 6-3 the difference between the slow scan CV (top) and the fast scan CV (bottom). The slow scan involves much more hysteresis. This strongly suggests possible changes in efficiency with cycling rate. Figure 6-3 also shows how negative electrical work can play a role in the behaviour of the beams. Most of the CV areas fall within the upper right and lower left quadrants of the IV plot where the IV product is positive. However, there are areas of the CV that fall within the other two quadrants (lightly shaded) and in these two quadrants the IV product is negative. In other words, there is negative work taking place at the times during which the IV values fall within those lightly shaded quadrants.

Figure 6-2 Instantaneous current, voltage and power for the 14th cycle of one of the power and efficiency samples, at .05 Hz and at .40 Hz. The driving ramp voltage signal is the same in both cases. However, the current response is quite different in quality and magnitude, resulting in a substantially different power signal between the two cases.

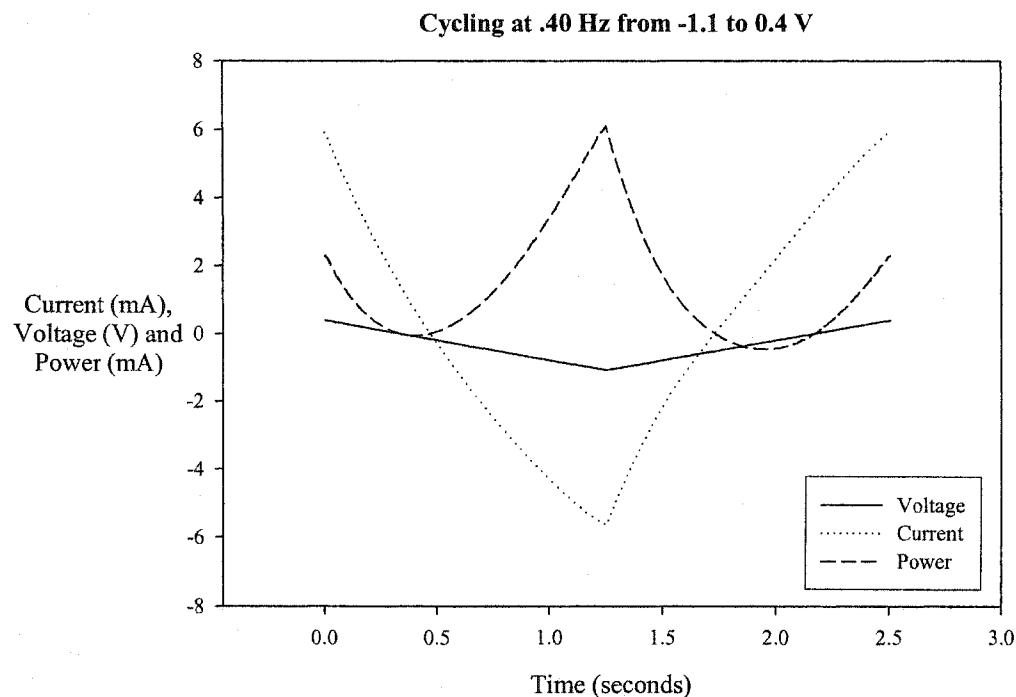
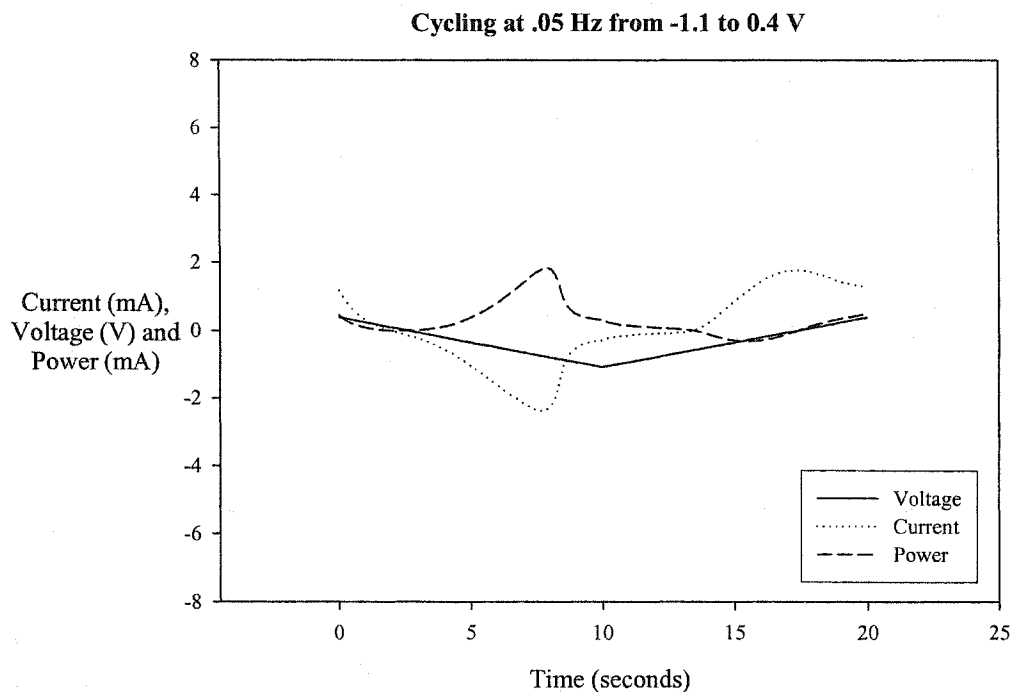
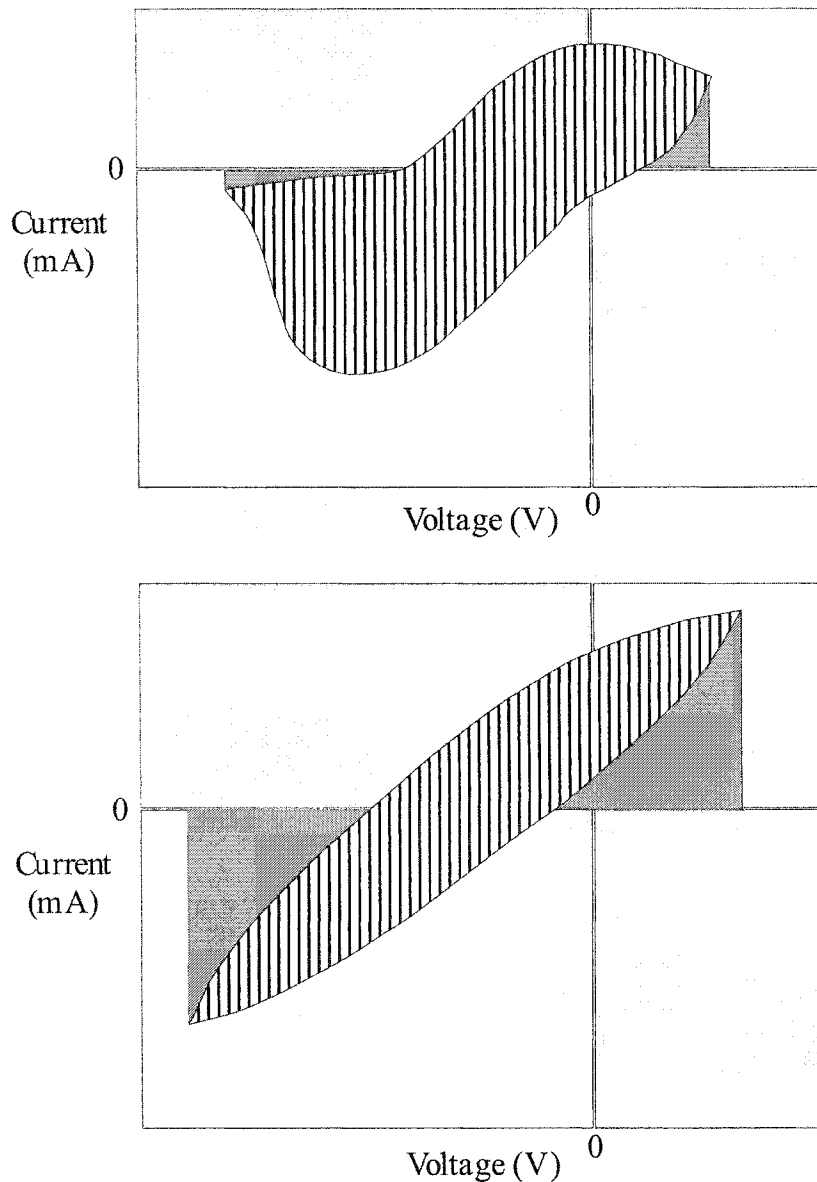


Figure 6-3 Simulated CVs illustrating issues of electrical work and efficiency. In both diagrams, the vertically striped areas represent the work accounted for within the CV. The darkly shaded areas represent electrical work that is also consumed during stimulation. The lightly shaded quadrants represent those areas where the electrical work is actually negative since the IV product contains one negative term. Finally, note that the upper diagram shows a relatively slow cycling frequency while the bottom diagram shows a CV taken at a relatively higher cycling frequency.



This all begs the question, what values should be compared when making a fair efficiency calculation? On the mechanical side of the balance, we could look at the total work per cycle. This has questionable validity though, since 3 of the 4 types of work are cyclical. In other words, they should net out to approximately zero each cycle. Drag is the only factor that is positive all of the time. So we could just look at drag. However, positive work is being done with respect to gravity, inertia and especially torque ... just not all of the time during a given cycle. So we could look at the net mechanical work per time interval and then assess the efficiency of work performed during those intervals when net positive mechanical work was being carried out. That would still not be quite right. There would potentially be negative work components mixing with positive work components. One term that we could look at is the total work performed during time intervals when only positive work is being carried out. As it turns out, there are several time intervals per cycle when that happens. The other term we could look at is simply the total amount of positive mechanical work per cycle. This is what we will use.

That's not the end of the dilemma though. Now we must reconsider what aspect of the electrical work is used in the efficiency calculation. As with the mechanical work, it comes in positive and negative varieties. As such, we could look at the total positive mechanical work per cycle over the total positive electrical work per cycle. We call this the fair efficiency as it includes the darkly shaded areas of Figure 6-3.

While it was not necessary since the efficiency calculations were cycle by cycle and not time interval by time interval, it was deemed desirable to properly synchronize the mechanical work calculations and the electrical work calculations. To do this, an audio signal proportional to voltage was recorded over the video signal on some of the

power and efficiency samples. Afterwards, the time at which the peak of a ramp cycle was reached was noted on the digitized version of the video footage to an accuracy of a few tenths of a second. Electrical work calculations were then performed at the same time (and therefore time intervals) as the mechanical work calculations to within that level of accuracy. Any offset error in the synchronization would not have an effect on a cycle by cycle analysis, since the capture of a full cycle of either mechanical or electrical work would obviate the importance of the starting point in the cycle. However, for an understanding of the dynamics of the electrical and mechanical work interactions, proper synchronization was quite important.

6.4 Results and Observations

6.4.1 Film Growth

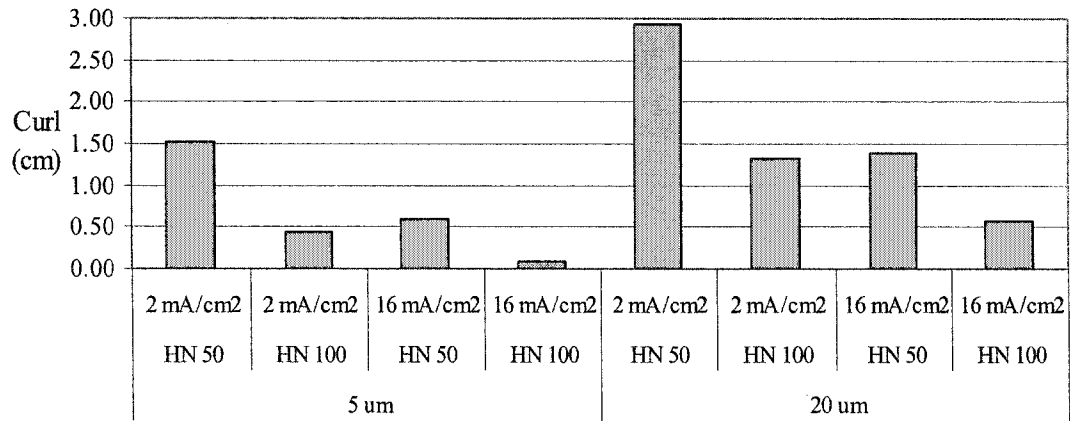
The endurance samples differed only in their PPy(DBS) film thicknesses. As such, their deposition statistics were very similar to those of the frequency response depositions (see Chapter 5). The DCD was $3.90 \pm .06$ mA/cm² and the deposition durations were $252.7 \pm .1$ and 1012.0 seconds for the 5 and 20 μ m thick film samples, respectively.

On the other hand, the power and efficiency samples differed on the basis of 3 variables: Kapton[®] thickness, PPy(DBS) thickness, and DCD. The two deposition currents that were used were .295 and 2.368 mA. The charge densities were $1.003 \pm .03$ and $4.004 \pm .03$ C/cm² for the 5 and 20 μ m thick film samples, respectively. The capacitance spike, and the average and final deposition potentials were higher for the high DCD samples, while the curling was greater for the HN 50, thicker PPy(DBS) and low DCD samples (see Figure 6-4).

6.4.2 Conditioning Cycles

The power and efficiency samples did not go through any conditioning cycles. However, the three endurance samples did. The first two samples were produced under the same conditions, and behaved very much like one another. The third sample differed by virtue of the fact that its PPy(DBS) film thickness was 20 μ m, versus the 5 μ m film thicknesses of the other samples. That difference brought about several changes in behaviour similar to those noted in Chapter 5.

Figure 6-4 Deposition curling (movement of the beam tip, in cm) under conditions of different Kapton® thicknesses (HN 50 = 12.7 μm and HN 100 = 25.4 μm), different PPy(DBS) thicknesses (5 μm and 20 μm), and different DCD values (2 mA/cm² and 16 mA/cm²).



For instance, the 3rd sample's range of movement was about twice as great as that of the first two samples. Its charge exchange and peak currents were also about twice as great. Its charge accumulation was about 4 times that of the thinner samples, and its voltage peaks were spaced farther apart than those of the first two samples.

6.4.3 Cycling Endurance

Given the small number of samples, the results from the endurance study were largely qualitative. However, the intent was simply to see how long the beams would curl back and forth, and the target was 100,000 cycles. This target was achieved.

The first sample performed least well. It was "dead" within 12 hours, meaning that it exhibited no movement when stimulated at that point. When this first trial was terminated, peak current and charge exchange levels were negligible and peak separation had been dramatically reduced ($V_{\text{red}} = .02$, $V_{\text{ox}} = .65$ V). The beam had apparently "oxidized to death". It had started out at with a charge exchange capacity of 5.9%.

The second sample ran for 104,400 cycles without any sign of stopping. At .20 Hz, this equates to a running time of 145 hours. Compared to the first sample, this second sample was monitored much more closely for the first 8 hours, which seemed to be critical. Leaving the upper and lower limits fixed probably led to the degradation of the first sample. Starting with the second sample, the limits were adjusted at each status check so that the peaks were captured just within the CV. The sample started at -1.25 V to +0.5 V and finished at -1.00 V to +0.75 V. The peaks were always kept just inside the limits. The movement of the peaks was slow and steady over the 145 hours. Meanwhile, the peak currents fell gradually. The charge exchange was relatively constant over the

duration and charge exchange capacity went from 4.7 to 4.0%. As such, the charge exchange to peak current ratio increased slightly with time, and most clearly on the reduction side.

The amount of curling increased from .23 cm to .28 cm in the first several hours. It then fell to .18-.22 cm for about 45 hours and then stayed at .14-.16 cm for the rest of the evaluation. There was no relationship found between the amount of curling and the scan range. However, the beam did curl more in the early going when the peaks were both more cathodic. Also in the early going, the peak currents were greater and the charge exchange was highest. The movement responsiveness decreased over time from .437 mm/mC to .211 mm/mC.

The third sample was similar to the second except that its PPy(DBS) film was four times as thick. Like the second sample, this sample did not stop functioning. Rather it was terminated after 13,320 cycles (or 18.5 hours). With the overall endurance goal already achieved, the intent with the third sample was to note any differences/similarities in the progression of the various parameters. The range of movement fell by about a third over the 18 hours, and with the current and charge exchange staying fairly steady, the movement responsiveness fell with time (.417 to .266 mm/mC). Charge exchange capacity was somewhat more stable, starting at 1.57% and ending at 1.60% (although it hit as high as 1.8% and as low as 1.1%). There were no other remarkable features that contradicted the findings of the second sample.

6.4.4 Power and Efficiency

There are three ways to look at the power and efficiency (PE) data that was collected. The first is to focus on the actual work, power and efficiency measures. However, seeing as how these measures were only made in the last step of the analyses for the PE results, we can also look at the cycling using the same sort of parameters that have been employed previously, such as charge exchange, peak currents and voltages, etc (see Maw et al. 2001, Chapters 3-5). Not only can we look at these basic measures, but we can also look at those measures in the context of changing cycling frequency, similar to the studies detailed in Chapter 5. The important differences here are the different DN and DP levels, and the reduced numbers of samples.

While the number of samples was limited, there were only two variations in Kapton[®] thickness, PPy(DBS) thickness and DCD value. With 8 samples in total, there were 4 samples with the same value of each variable, and 8 different combinations of the 3 variables. As well, none of the values of these variables were in a difficult range for film production. With frequency changes being an additional variation on top of this, it provided an interesting opportunity to build on the results of Chapters 3-5 before examining the overall power and efficiency issues.

In fact, the data patterns that were produced were generally very clear and informative. Looking first at the features of the CVs at .05 Hz cycling, the patterns reinforced the findings of earlier chapters. For charge exchange and peak current levels, thicker PPy(DBS) films produced higher levels, as did low DCD values versus high DCD values. In at least 3 of every 4 possible comparisons, the charge exchange and peak current levels of the thin Kapton[®] beams were somewhat greater than those of the HN

100 beams. Curling behaviour showed these same patterns, although the differences between the HN 50 and HN 100 beams were very large. More complex were the patterns of the peak voltages, the magnitude of which were always greater for the thicker PPy(DBS) films. While there were no apparent differences between the two Kapton[®] thicknesses, both peaks of the CVs were shifted cathodically at low DCD levels relative to higher ones. Charge accumulation during cycling was much greater for the thicker PPy(DBS) films, and tended to be greater for high DCD and low Kapton[®] thickness values. Movement responsiveness was also sensitive to the controlled variables, with greater efficiencies arising from thinner films (PPy(DBS) and Kapton[®]) and lower DCD values. The ratio of charge exchange to initial charge deposition, a measure of efficiency with respect to theoretical charge exchange limitations was also affected in a very clear way. The higher the DCD value and the thicker the PPy(DBS), the worse the performance.

The situation for the .10 Hz cycling was largely similar, except that now the higher DCD value samples produced better movement responsiveness results. Likewise, for .20 Hz, the patterns were mostly the same. However, the peak voltages were now all at or beyond cycling limits except for the thin PPy(DBS) film/high DCD reduction peaks, and curling was not favoured by one PPy(DBS) film thickness over the other. Charge accumulation was now greatest for the thin PPy(DBS) in combination with the low DCD value, and otherwise, HN 50 samples had greater accumulations than HN 100 samples. On movement responsiveness, the better DCD value was not clear. Finally, for the .40 Hz cycling, all peak voltages were at or beyond limits. Thin, high DCD beams accumulated more charge while thin, low DCD films curled the most. At this frequency

there was little difference in charge exchange across conditions, although thick PPy(DBS)/low DCD films still produced higher peak currents. Figures 6-5 to 6-7 show all of these results quantitatively, by cycling frequency.

Figures 6-8 to 6-12 show the same data, but with respect to how the parameter values evolved over changes in cycling frequency. From this perspective, it was clear that the charge accumulation during cycling was only substantial at .05 Hz, although the nature of the patterns remained intriguing at higher frequencies. The cut-off frequency for the curling of the beams was higher for high DCD samples versus low DCD samples, and the thicker PPy(DBS) beams had a steeper fall-off in performance with respect to increasing frequency. Regarding charge exchange, the low DCD and/or thick PPy(DBS) films started with more exchange, but progressed to the same low levels as the other fibers by .40 Hz. The same was true of the peak currents. Peak separation increased with cycling frequency in all cases, but started at the lowest value with the thin PPy(DBS) film samples and first reached a maximum with the thick PPy(DBS) film samples. The charge exchange to peak current ratio remained remarkably similar under all conditions, and decreased with frequency while the charge exchange capacity fell in a linear fashion on a semi-log plot in all conditions. However, it started at higher values at lower frequencies with low DCD and thin PPy(DBS) films. In terms of movement responsiveness, there were a variety of patterns. The movement responsiveness of thin PPy(DBS) film beams increased with frequency while those with thick films either stayed relatively constant or fell slightly. Thin Kapton[®] tended to favour the increase with cycling frequency, while thick Kapton[®] tended to favour the decrease with frequency.

Figure 6-5 Curling (top) and oxidative half cycle charge exchange (bottom) in the power and efficiency experiment, under all 8 experimental conditions and all 4 stimulation frequencies. Note the relationships between corresponding PPy(DBS) film thicknesses (150 mC and 600 mC), Kapton® thicknesses (HN 50 and HN 100) and DCD values (2 mA/cm² and 16 mA/cm²).

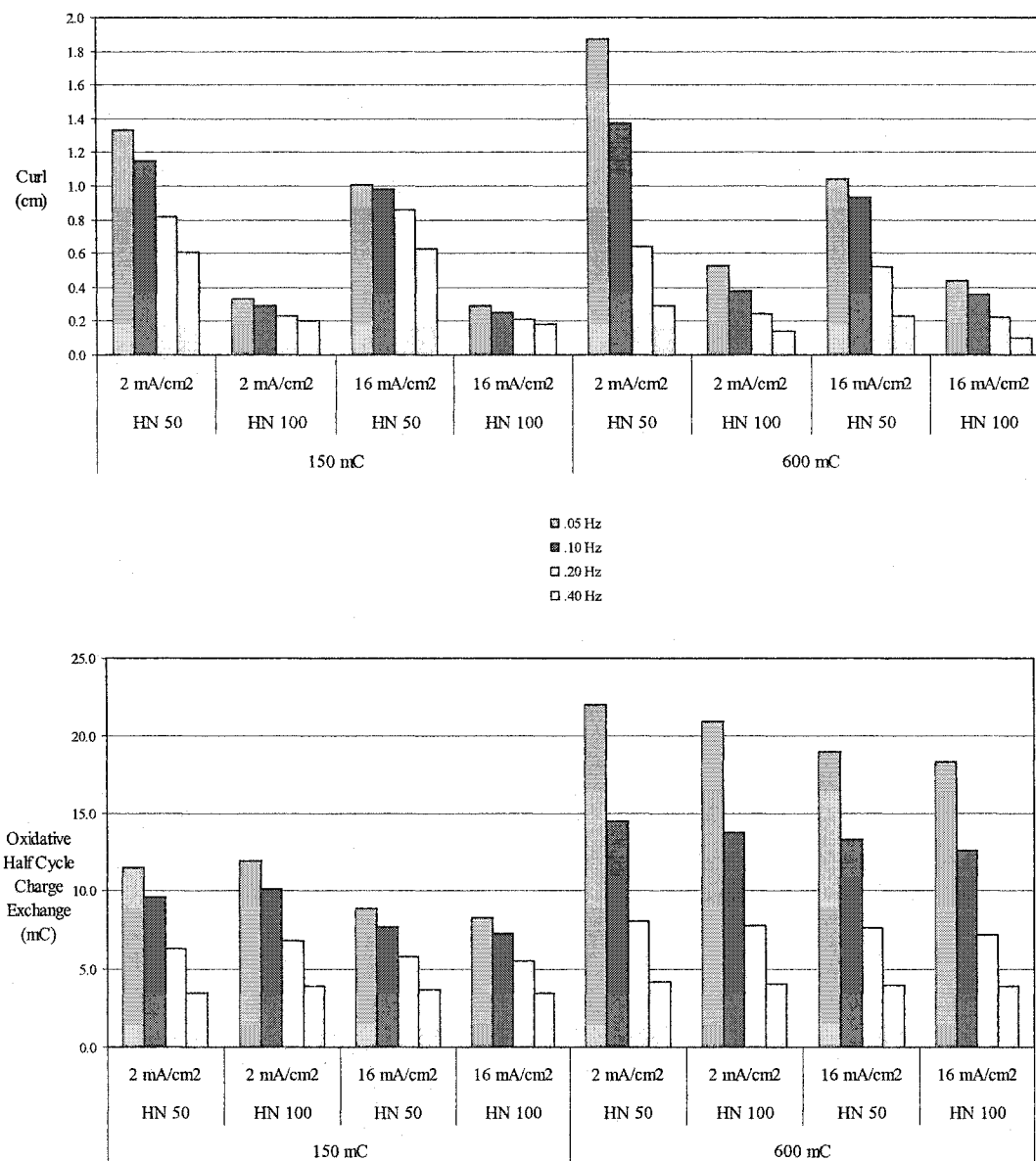
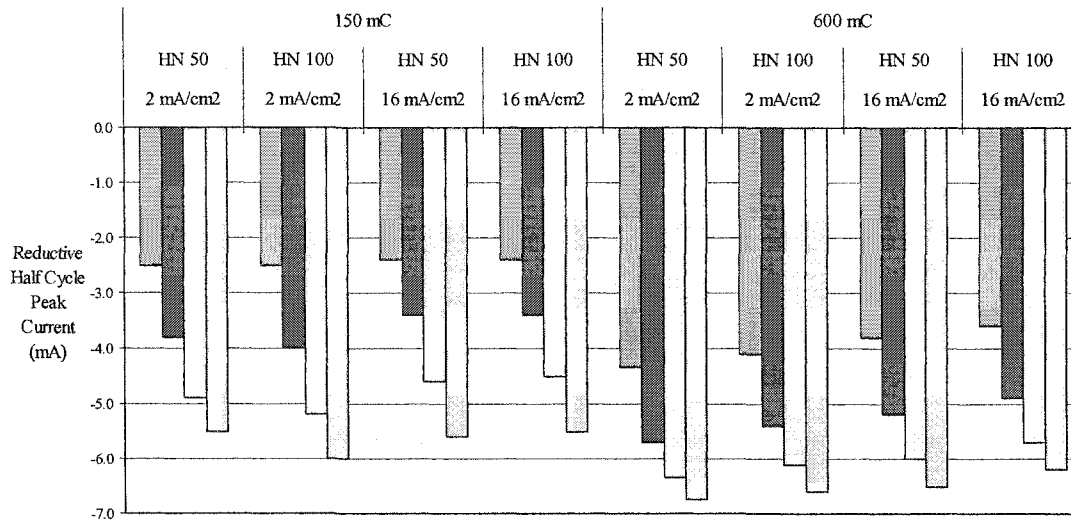


Figure 6-6 Reductive half cycle peak currents (top) and reductive half cycle peak voltages (bottom) in the power and efficiency experiment, under all 8 experimental conditions and all 4 stimulation frequencies. Note the relationships between corresponding PPy(DBS) film thicknesses (150 mC and 600 mC), Kapton® thicknesses (HN 50 and HN 100) and DCD values (2 mA/cm² and 16 mA/cm²).



- 0.05 Hz
- 0.10 Hz
- 0.20 Hz
- 0.40 Hz

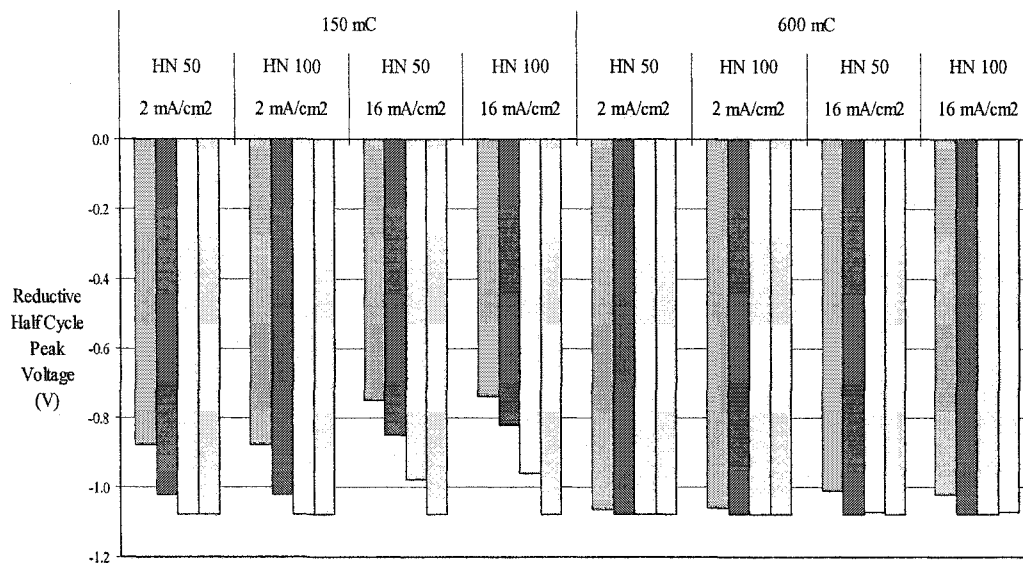


Figure 6-7 Movement responsiveness, or curling per unit charge exchange (top) and charge exchange capacity, or ratio of charge exchange during cycling to initial doping charge deposited during polymerization (bottom) in the power and efficiency experiment, under all 8 experimental conditions and all 4 stimulation frequencies. Note the relationships between corresponding PPy(DBS) film thicknesses (150 mC and 600 mC), Kapton® thicknesses (HN 50 and HN 100) and DCD values (2 mA/cm² and 16 mA/cm²).

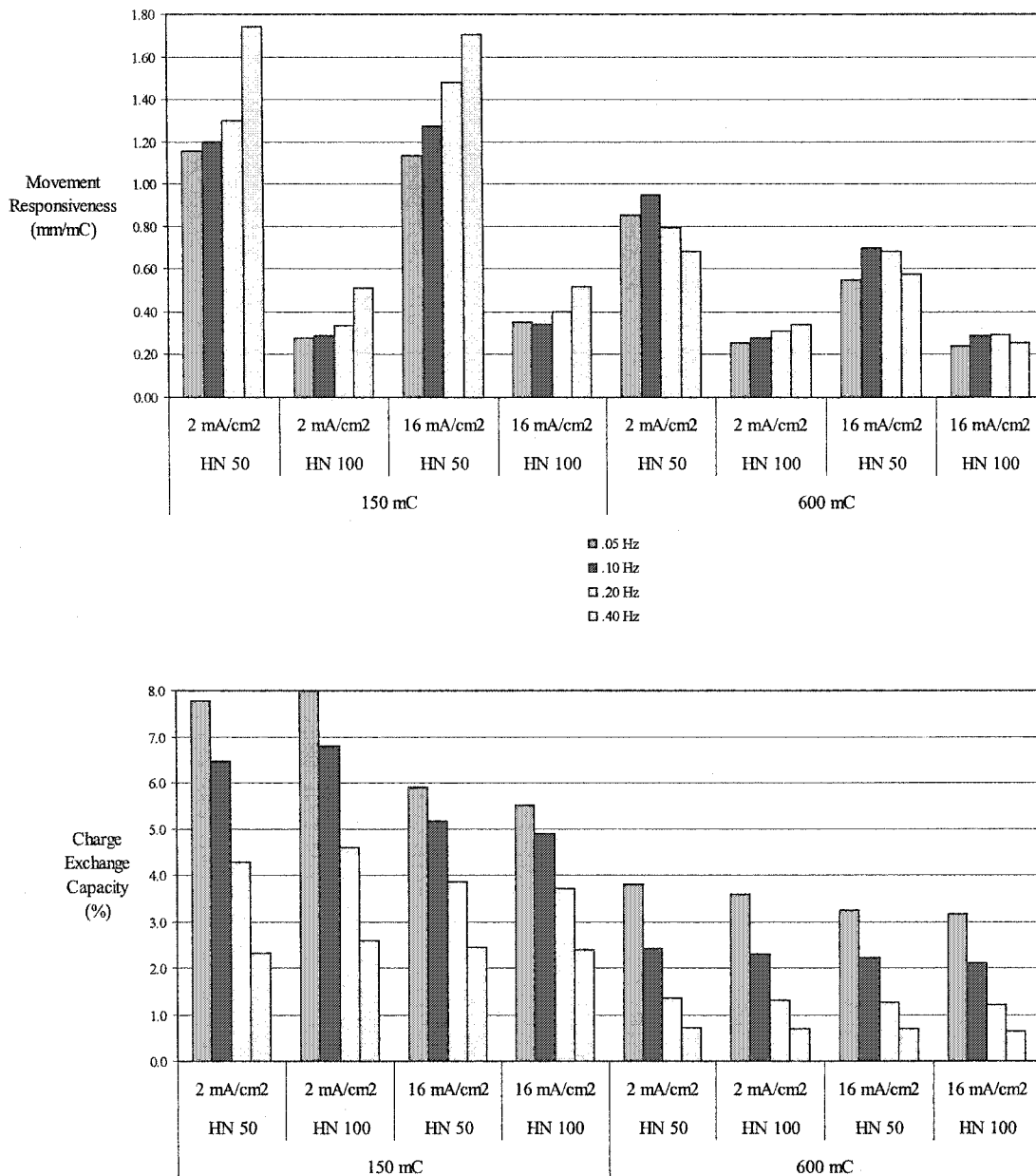


Figure 6-8 Power and efficiency experimental data, shown relative to cycling frequency. Top graph shows curling of thin Kapton® samples. Bottom graph shows curling of thick Kapton® samples. Each graph shows the samples varying in DCD (2 mA/cm² or 16 mA/cm²) and PPy(DBS) film thickness (5 μm or 20 μm). Note the relationships between samples differing in one variable, as well as the interaction effects.

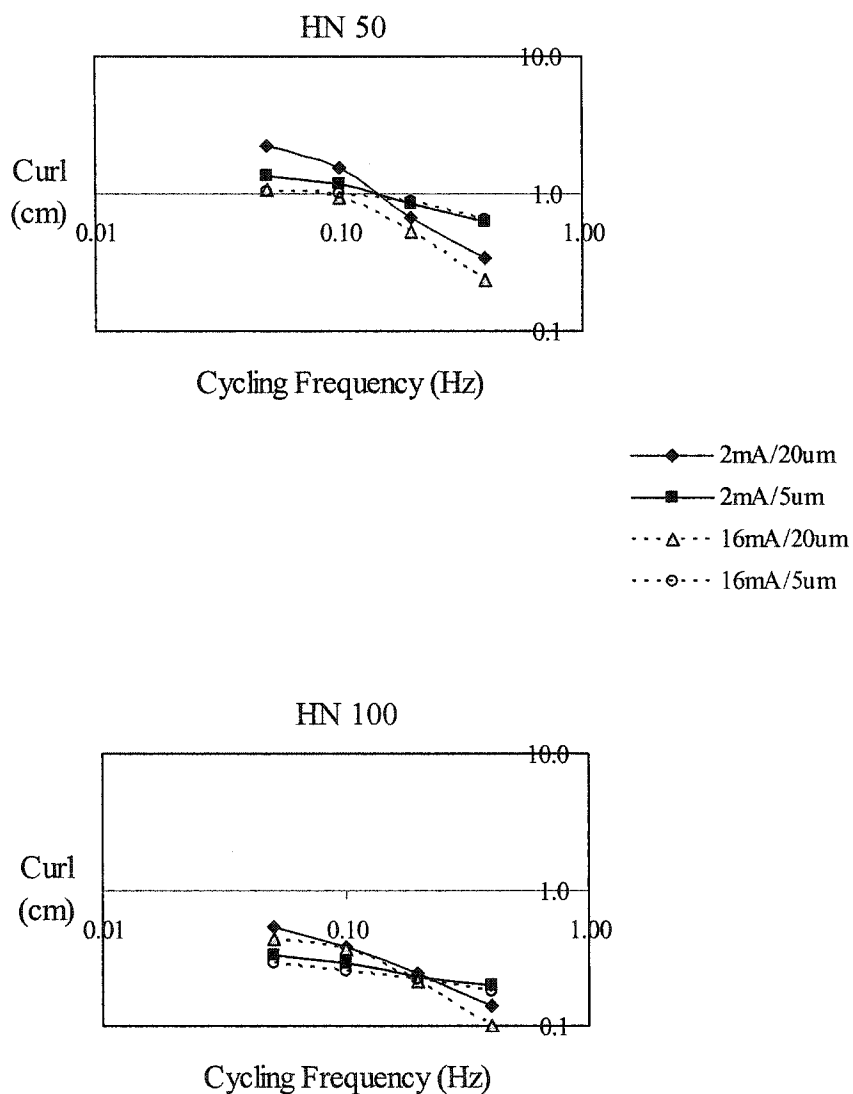


Figure 6-9 Power and efficiency experimental data, shown relative to cycling frequency. Top graph shows the peak currents of thin Kapton® samples. Bottom graph shows the peak currents of thick Kapton® samples. Each graph shows the samples varying in DCD (2 mA/cm² or 16 mA/cm²) and PPy(DBS) film thickness (5 μm or 20 μm). Note the relationships between samples differing in one variable, as well as the interaction effects.

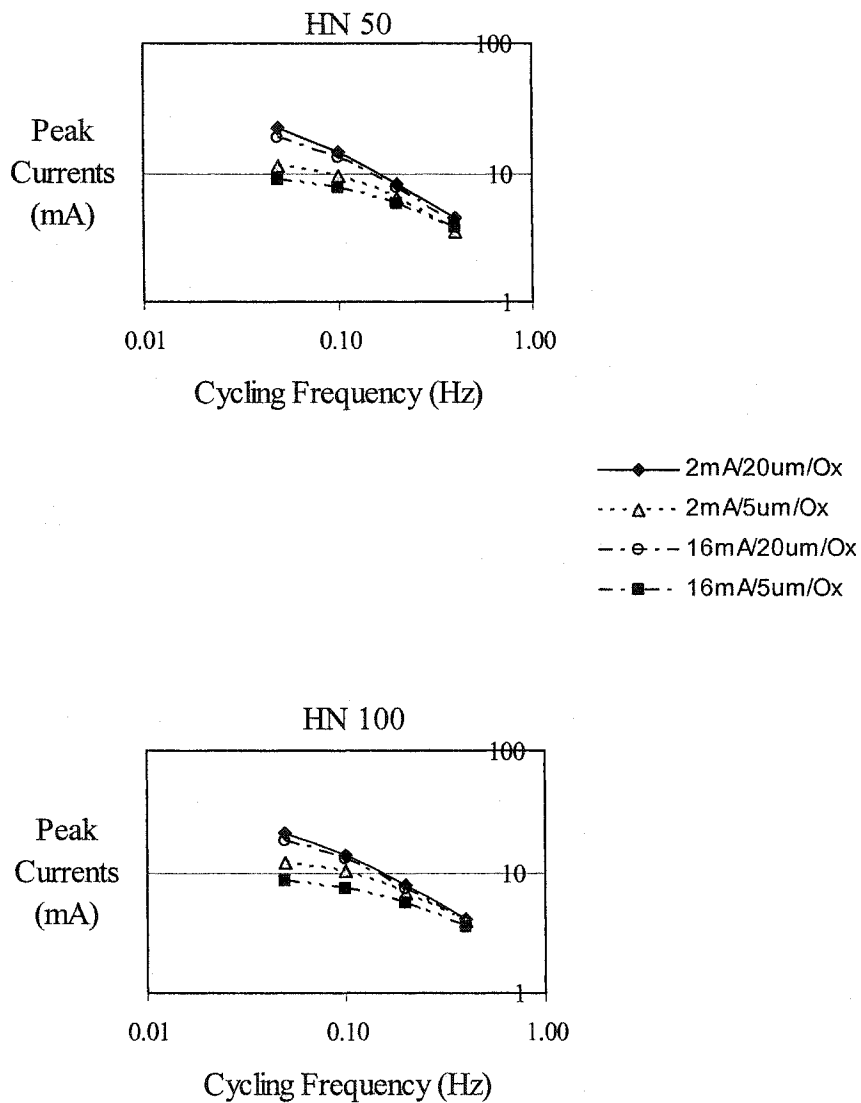


Figure 6-10 Power and efficiency experimental data, shown relative to cycling frequency. Top graph shows the peak voltages of thin Kapton® samples. Bottom graph shows the peak voltages of thick Kapton® samples. Each graph shows the samples varying in DCD (2 mA/cm² or 16 mA/cm²) and PPy(DBS) film thickness (5 μm or 20 μm). Note the relationships between samples differing in one variable, as well as the interaction effects.

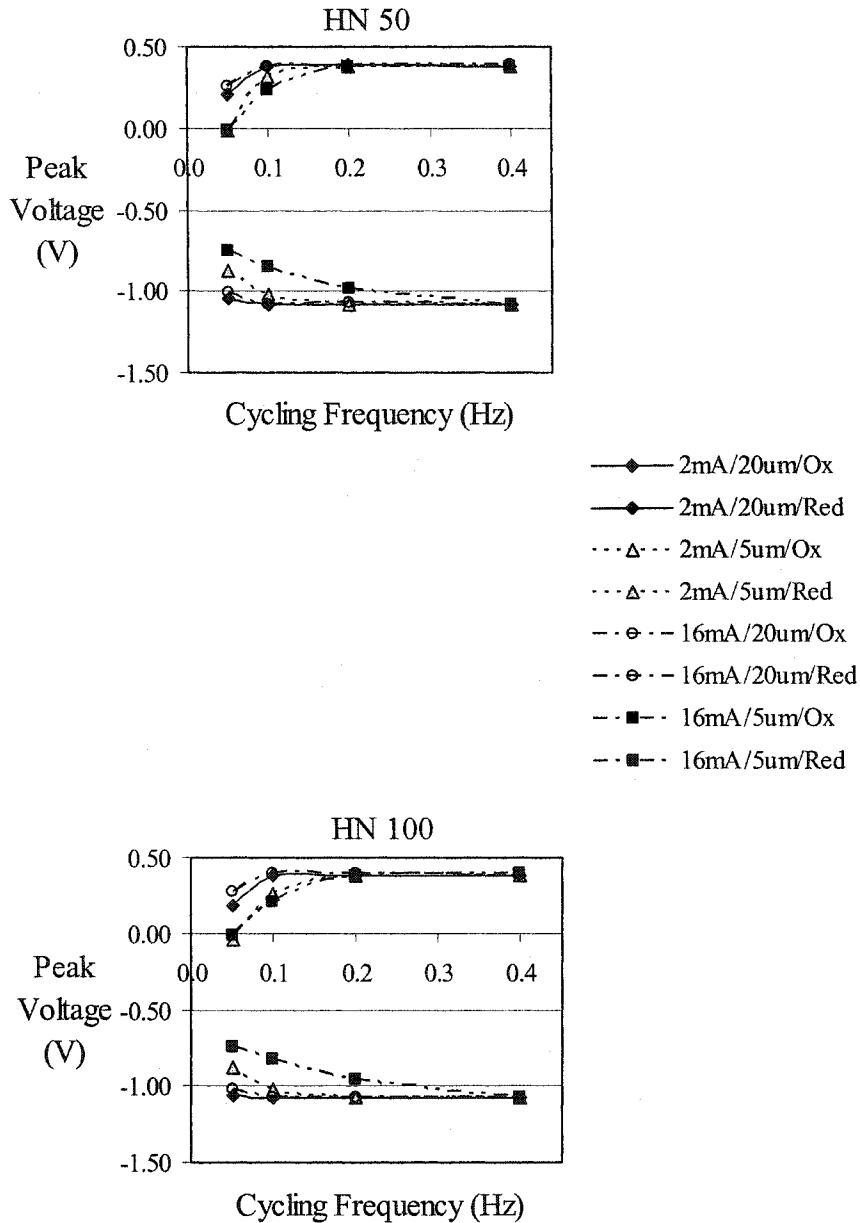


Figure 6-11 Power and efficiency experimental data, shown relative to cycling frequency. Top graph shows the movement responsiveness of thin Kapton® samples, where the efficiency measure is the ratio of beam curling to charge exchange bringing about the beam curling. Bottom graph shows the movement responsiveness of thick Kapton® samples. Each graph shows the samples varying in DCD (2 mA/cm² or 16 mA/cm²) and PPy(DBS) film thickness (5 μm or 20 μm). Note the relationships between samples differing in one variable, as well as the interaction effects.

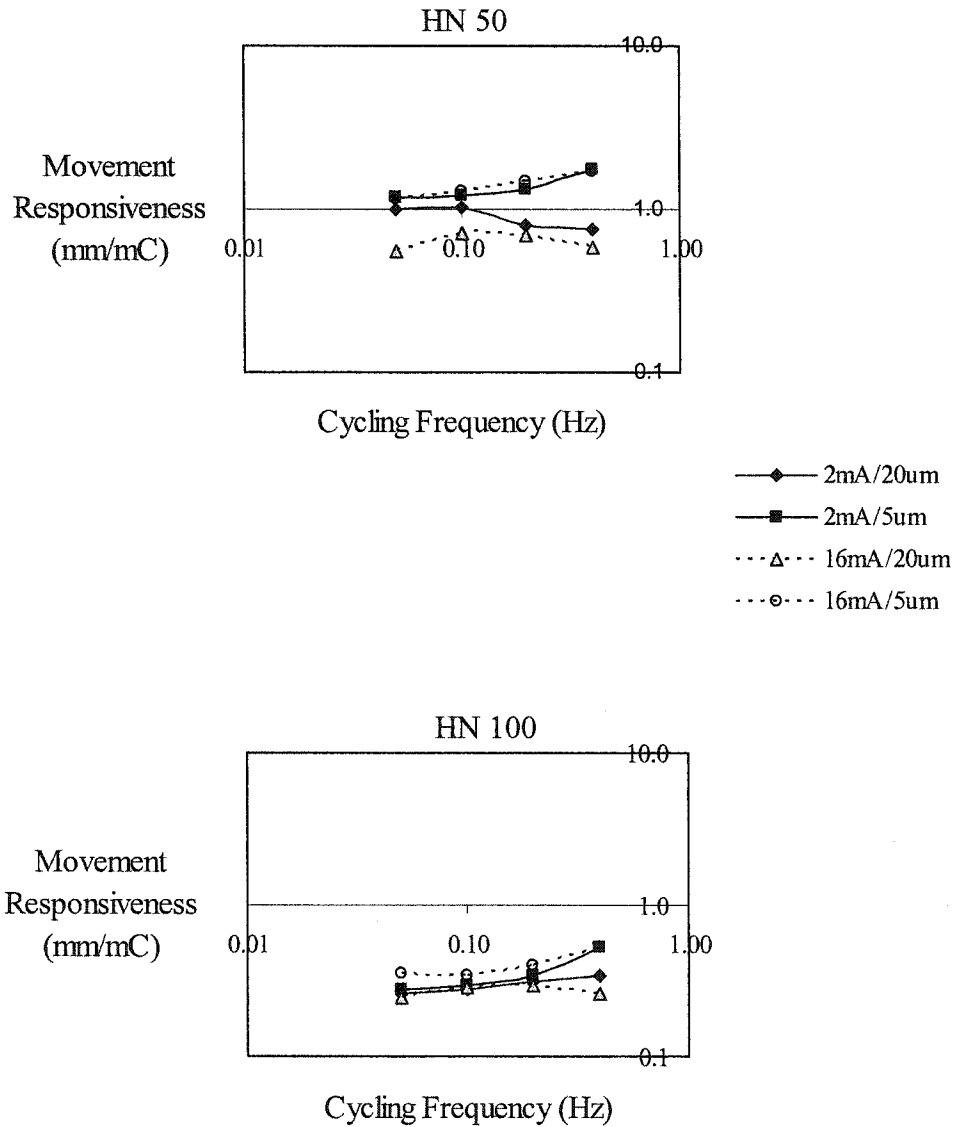
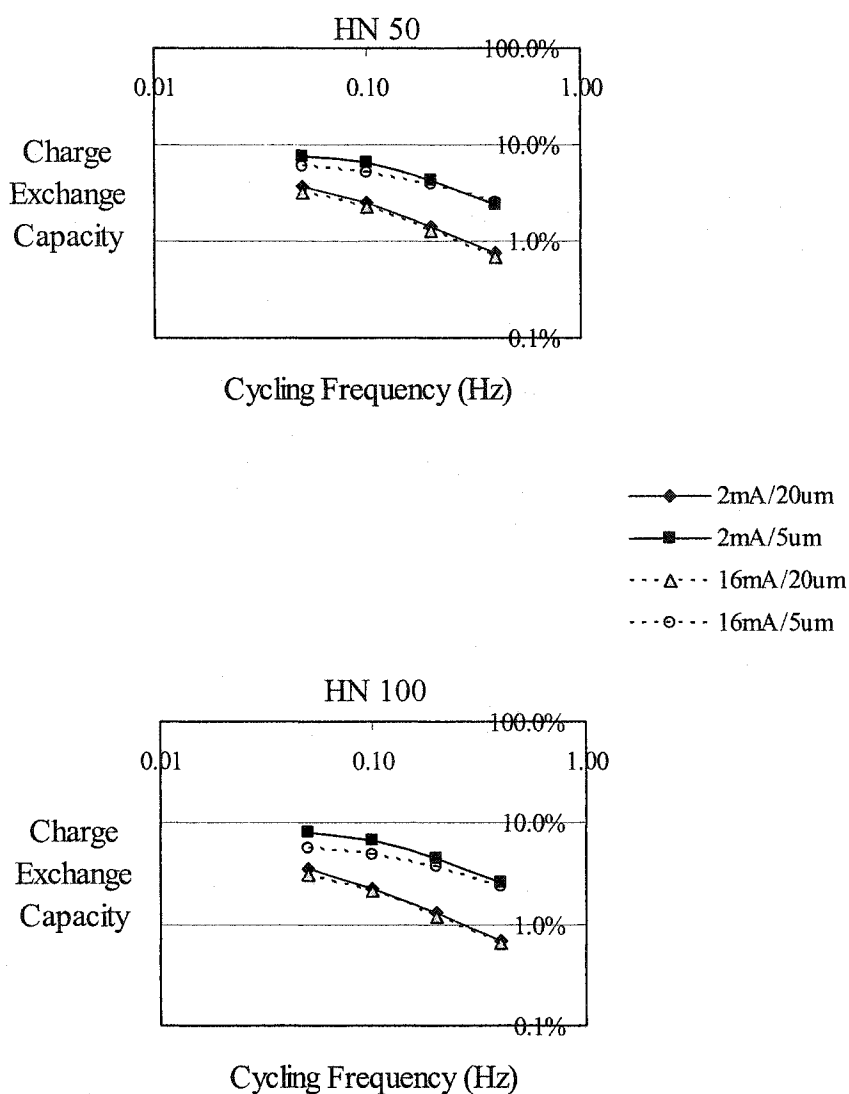


Figure 6-12 Power and efficiency experimental data, shown relative to cycling frequency. Top graph shows the charge exchange capacity of thin Kapton[®] samples, where the efficiency measure is the ratio of charge exchange during cycling to the doping charge deposited on the beam during polymerization. Bottom graph shows the charge exchange capacities of thick Kapton[®] samples. Each graph shows the samples varying in DCD (2 mA/cm² or 16 mA/cm²) and PPy(DBS) film thickness (5 μm or 20 μm). Note the relationships between samples differing in one variable, as well as the interaction effects.



The last set of data that was gathered in this experiment pertained to the overall efficiency of the beams in terms of performing work. Figures 6-13 and 6-14 show some examples of the plots that were used to visualize some of the work calculations.

A wide variety of measures were taken for each of the samples at .20 and .40 Hz, with respect to the various mechanical and electrical characteristics of the beams. These measures were then compared with respect to Kapton[®] thickness, PPy(DBS) thickness, beam thickness and DCD value. From the electrical perspective, I looked at charge exchange, peak currents, charge exchange capacity, and negative and positive electrical work. All of these measures were strongly influenced by the PPy(DBS) film thickness. Charge exchange capacity was much higher for the thin PPy(DBS) films than for the thick (2.6% versus 0.8% at .40 Hz, 4.5% versus 1.4% at .20 Hz). The DCD value also had a noticeable effect on the amount of negative work performed which ranged from 3.3% to 6.8% of the total work performed.

On the mechanical side, differences in work due to gravity, drag and inertia were all primarily influenced by the Kapton[®] thickness, and less so by the PPy(DBS) film thickness. Details concerning the elastic beam energy (torque work) followed this trend as well, although the PPy(DBS) thickness was also important. Indeed, the maximum positive work per time interval and the total positive work per cycle were both influenced most by the PPy(DBS) film thickness, as were the maximum stresses and strains in the PPy(DBS). Stresses ranged from 0.42 to 1.97 MPa, and strains varied from .10% to .46%. Overall, the percentage contribution of the various mechanical work elements to the total mechanical work depended mostly on the Kapton[®] but also on the PPy(DBS). The DCD value played a minor role. On average, the mechanical work contributions by

Figure 6-13 Plots used to visualize the power and efficiency calculations of the gravitational, drag and inertial work components of the first sample (2 mA/cm^2 , HN 50, $5 \mu\text{m PPy(DBS)}$). The two lines on each graph correspond to the position, velocity or work of the two beam elements that the beam was divided into for the analysis.

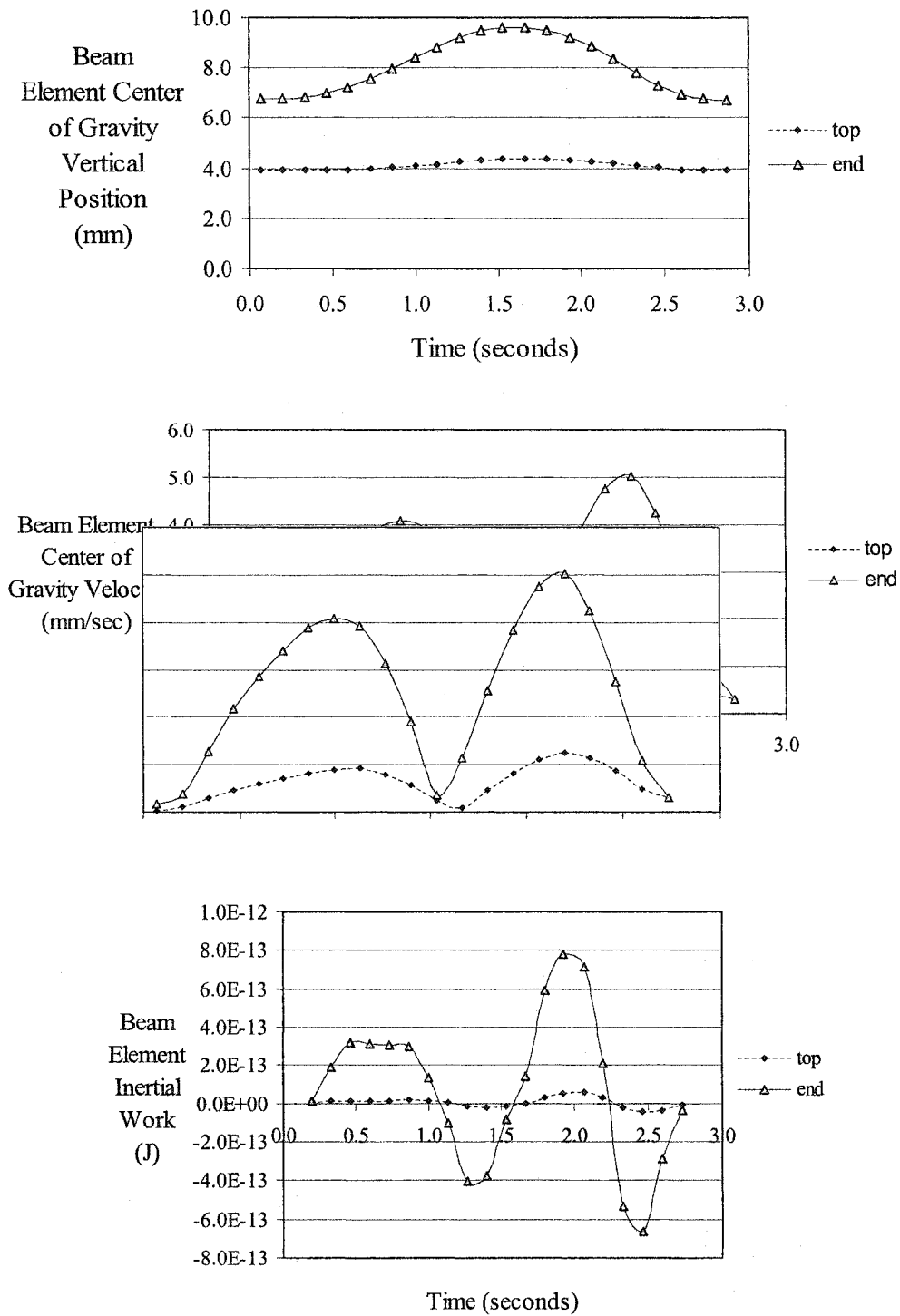
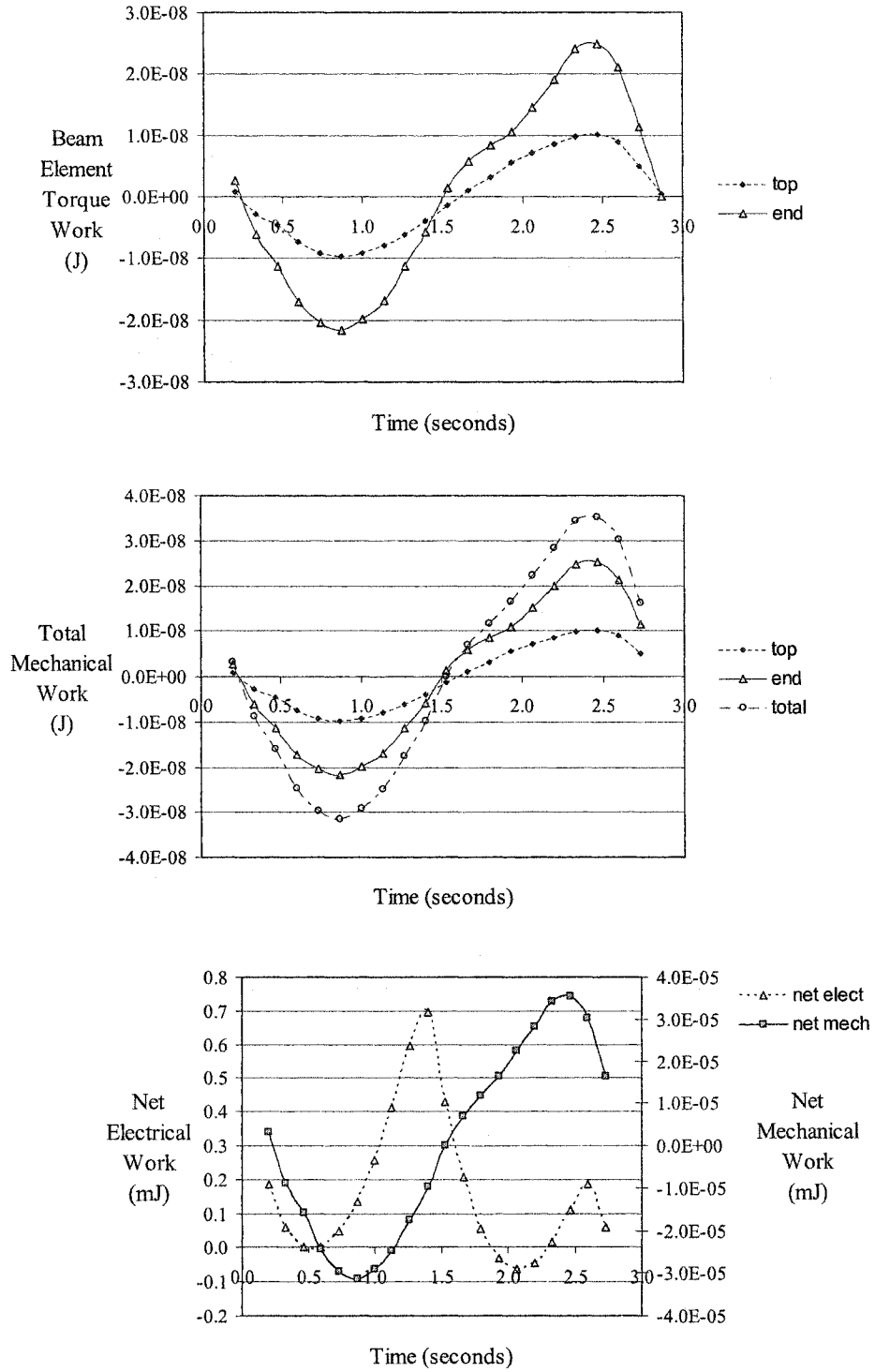


Figure 6-14 Plots used to visualize the power and efficiency calculations of the torque (elastic energy), total mechanical, and total electrical work of the first sample (2 mA/cm², HN 50, 5 μm PPy(DBS)). The “top” and “end” lines on the upper two graphs correspond to the work of the two beam elements that the beam was divided into for the analysis.



the various mechanical elements were 0.0% for inertia, 0.5% for gravity, 0-6% for drag, and 92-99% for elastic beam energy (torque work). The total positive electrical work was 3.3 to 4.1 mJ at .40 Hz, and 4.9 to 7.7 mJ at .20 Hz.

Overall, the fair work efficiency ratio was most dependent on the PPy(DBS) film thickness. The fair ratio ranged from .002 to .019% for the .40 Hz data, and from .001 to .013% for the .20 Hz data. Tables 6-3 and 6-4 present much of this data in tabular form. The 5th sample's poor .20 Hz efficiency score masks the fact that its movement was qualitatively different than that of the others. It was the only sample to swing right through the vertically hanging position. In so doing, it changed the synchronization of the various electrical and mechanical work components substantially.

In terms of peak power, the peak electrical power draws ranged from 4.0 to 6.2 mW at .20 Hz and from 5.1 to 6.7 mW at .40 Hz. The corresponding positive mechanical power production levels were 0.6 to 5.8 and 1.0 to 9.0 x 10⁻⁴ mW. The thicker PPy(DBS) films produced the higher values, and thicker Kapton[®] helped enhance the mechanical power numbers. Low DCD values also tended to favour higher electrical power values.

The other relevant perspective on the PE data was the rate at which the PE data changed with frequency, with respect to the thickness and DCD variables. For many of the electrical and mechanical measures, the PPy(DBS) film thickness was the only strong influence. Many of the electrical and mechanical measures fell faster from .20 to .40 Hz in the thicker PPy(DBS) films than in the thinner films, for instance. However, Kapton[®] thickness also had an influence on those values related to the beam's elastic energy (torque work) and the fair efficiency ratio. The work done by thin PPy(DBS)/thick Kapton[®] beams falls off faster with frequency than with other beams. The fair

Table 6-3 .20 Hz Power and Efficiency Data

	Beam1	Beam2	Beam3	Beam4	Beam5	Beam6	Beam7	Beam8
DCD (mA/cm ²)	2	2	16	16	2	2	16	16
Kapton [®] thickness (μm)	12.7	25.4	25.4	12.7	12.7	25.4	25.4	12.7
PPy thickness (μm)	5	5	20	20	20	20	5	5
Total Thickness (μm)	17.7	30.4	45.4	32.7	32.7	45.4	30.4	17.7
.20 Hz Cycling								
Total +ve Work/ Inertia (10 ⁻¹²)	2.3	0.3	0.3	1.8	3.6	0.4	0.3	2.9
Inertia (%)	0.00%	0.00%	0.00%	0.00%	0.00%	0.00%	0.00%	0.00%
Total +ve Work/ Gravity (10 ⁻⁹)	2.6	1.1	1.2	2.4	0.7	0.9	0.9	0.7
Gravity (%)	0.71%	0.65%	0.36%	0.73%	0.88%	0.33%	0.62%	0.87%
Total +ve Work/ Drag (10 ⁻⁹)	2.7	0.1	0.1	0.8	2.0	0.1	0.1	3.0
Drag (%)	0.66%	0.08%	0.03%	0.25%	2.51%	0.04%	0.08%	3.58%
Total +ve Work/ Torque (10 ⁻⁷)	2.9	1.9	3.8	2.9	0.8	3.0	1.4	0.7
Torque (%)	98.63%	99.28%	99.62%	99.01%	96.61%	99.64%	99.31%	95.55%
Total +ve Mech Work (10 ⁻⁴ mJ)	3.0	1.9	3.8	3.0	0.9	3.0	1.4	0.7
Charge Exchange (mC)	6.4	6.8	7.2	7.6	8.3	7.8	5.5	5.8
Exchange Capac (%)	4.3%	4.5%	1.2%	1.3%	1.4%	1.3%	3.7%	3.9%
Curling Range of Movement (cm)	0.82	0.23	0.21	0.52	0.66	0.24	0.22	0.86
Movement Responsiveness (mm/mC)	1.281	0.338	0.292	0.684	0.795	0.308	0.400	1.483
Max Stress in Polypyrrole (MPa)	1.01	0.57	1.00	0.98	0.50	0.84	0.50	0.46
Max Strain in Polypyrrole (%)	0.23%	0.13%	0.24%	0.23%	0.12%	0.22%	0.11%	0.10%
Total +ve Electrical Work (mJ)	5.89	6.35	7.05	7.41	7.71	7.20	4.66	4.93
Negative Electrical Work (%)	6.42%	6.80%	3.66%	3.64%	4.54%	4.41%	4.90%	5.56%
Peak Mech Power (10 ⁻⁴ mW)	1.93	1.05	2.22	1.8	0.86	1.92	0.82	0.61
Peak Elect Power (mW)	4.55	4.88	5.42	5.68	6.16	5.79	4.04	4.14
Peak Current (mA)	4.8	5.2	5.7	6.0	6.5	6.1	4.5	4.7
Fair Effic (%)	0.004%	0.003%	0.005%	0.003%	0.001%	0.004%	0.003%	0.001%

Table 6-4 .40 Hz Power and Efficiency Data

	Beam1	Beam2	Beam3	Beam4	Beam5	Beam6	Beam7	Beam8
DCD (mA/cm ²)	2	2	16	16	2	2	16	16
Kapton [®] thickness (μm)	12.7	25.4	25.4	12.7	12.7	25.4	25.4	12.7
PPy thickness (μm)	5	5	20	20	20	20	5	5
Total Thickness (μm)	17.7	30.4	45.4	32.7	32.7	45.4	30.4	17.7
.40 Hz Cycling								
Total +ve Work/ Inertia (10 ⁻¹²)	4.3	0.8	0.4	1.5	3.4	0.6	0.8	5.6
Inertia (%)	0.00%	0.00%	0.00%	0.00%	0.01%	0.00%	0.00%	0.01%
Total +ve Work/ Gravity (10 ⁻⁹)	1.7	0.8	0.5	1.0	0.6	0.5	0.6	0.6
Gravity (%)	0.70%	0.76%	0.43%	0.45%	0.84%	0.25%	0.87%	0.93%
Total +ve Work/ Drag (10 ⁻⁹)	2.9	0.2	0.1	0.3	1.0	0.1	0.2	4.3
Drag (%)	1.03%	0.21%	0.05%	0.13%	1.45%	0.05%	0.28%	6.19%
Total +ve Work/ Torque (10 ⁻⁷)	2.0	1.2	2.4	2.1	0.8	1.8	0.9	0.6
Torque (%)	98.27%	99.04%	99.52%	99.41%	97.70%	99.70%	98.85%	92.87%
Total +ve Mech Work (10 ⁻⁴ mJ)	2.1	1.2	2.4	2.2	0.8	1.8	0.9	0.6
Charge Exchange (mC)	3.5	3.9	3.9	4.1	4.5	4.2	3.6	3.7
Exchange Capac (%)	2.3%	2.6%	0.7%	0.7%	0.8%	0.7%	2.4%	2.5%
Curling Range of Movement (cm)	0.61	0.20	0.10	0.23	0.33	0.14	0.18	0.63
Movement Responsiveness (mm/mC)	1.743	0.513	0.256	0.561	0.733	0.333	0.500	1.703
Max Stress in Polypyrrole (MPa)	1.03	0.53	1.01	1.10	0.55	0.82	0.50	0.42
Max Strain in Polypyrrole (%)	0.24%	0.12%	0.23%	0.25%	0.13%	0.19%	0.11%	0.10%
Total +ve Electrical Work (mJ)	3.27	3.65	3.62	3.87	4.11	3.84	3.43	3.37
Negative Electrical Work (%)	4.51%	4.79%	3.56%	3.34%	3.77%	3.76%	3.82%	4.04%
Peak Mech Power (10 ⁻⁴ mW)	2.64	1.19	2.87	2.74	1.29	2.16	1.27	1.04
Peak Elect Power (mW)	5.24	5.72	5.93	6.14	6.68	6.29	5.1	5.35
Peak Current (mA)	5.5	6.1	6.2	6.5	7.1	6.6	5.7	5.7
Fair Effic (%)	0.006%	0.003%	0.007%	0.006%	0.002%	0.005%	0.003%	0.002%

efficiencies increased from .20 to .40 Hz in all conditions.

Incidental to the power calculations was the synchronization of the time steps for the mechanical analyses and the electrical power calculations. In carrying out this task, it became very clear that the movements of the thin PPy(DBS) film samples followed the ramp voltammetry very closely to within the estimated accuracy of the measurement procedure, or a couple of tenths of a second. On the other hand, the thick film samples were clearly slower, lagging behind the driving voltage signal. The phase delay was estimated to be approximately one time interval for the .20 and .40 Hz analyses i.e. .267 and .133 seconds, respectively. While these estimates are not precise, they do suggest a good reaction time to stimuli, especially for the thin samples and as compared to other types of polymer actuators (Caldwell and Taylor 1990).

In terms of other relevant performance parameters that are sometimes found in the literature, the highest bending energy exhibited by any of the beams was about .001 mJ. That corresponds to an energy density of 4.9 kJ/m^3 , a figure well beyond the 0.8 kJ/m^3 of human muscle (Hunter and Lafontaine 1992). Charge density was found to be as high as $.18 \text{ C/mm}^3$. The maximum PPy(DBS) film stress was 1.97 MPa, while the maximum observed strain was .46% and the maximum strain rate was about 0.15% per second (at .40 Hz). The peak mechanical power density was 2.8 W/kg. However, the peak electrical power density was an amazing 19.4 kW/kg. Overall, the best efficiency measure was 0.02%.

6.5 Discussion

I was able to collect measurements on a wide variety of functional parameters for the bending beams that were examined in this study. Likewise, other researchers have gathered data on polymer actuator strength (force density), strain and strain rate, power, work, energy, efficiency, speed, endurance and response/reaction time.

Cycling endurance has the benchmark of human cardiac muscle which beats approximately 3×10^9 times in a person's life (Hunter and Lafontaine 1992). Often times, researchers have been happy to demonstrate anywhere from 20 to 100 cycles of contraction (Sussman and Katchalsky 1970, Lewis et al. 1997, Otero and Rodríguez 1993). Others have reached the hundreds or thousands before delamination (Otero 1997, Smela et al. 1993, Jager et al. 2000), including Gazard (1986) who ran films for 20,000 cycles at 100 ms switching times. While I did well at over 100,000 cycles, Lee et al. (1994) have run 500,000 cycles at 1.2 Hz. To further the efforts to keep electroactive polymers changing volume, Shahinpoor et al. (1998) has noted that overpotentials degrade the films. Baughman (1996) has also recommended keeping stimulation voltages low to enhance durability. Chiarelli et al. (1995) observed the charge exchange capacity idea that I have worked with, and added that exceeding it will lead to rapid deterioration of the fibers. I would concur. Kuwabata et al. (1984) completed 10,000 cycles of CVs with PPy(ClO₄) in KCl. Peak magnitudes decreased with time and both peaks shifted anodically. I found the same sort of behaviours.

Recently, Madden et al. (1999, 2000, 2001) have broken new ground with their encapsulated fibers. However, endurance has yet to be optimized, as they dry out in a matter of hours and lose their strain capabilities over a few cycles. They have run

aqueous-based fibers for 120,000 cycles, however, at 3 Hz, ± 7 V stimulation, producing strains in excess of .25% and strain rates of 1.5% per second, without any obvious signs of deterioration.

Regarding the speed of actuation, there are many examples in the literature and many suggestions for improvements. Kuhn et al. (1950) started things off with his pH activated fibers. However, they were quite slow, reacting over several seconds and minutes. Since then, others have achieved very fast response times, such as Bohon and Krause (1998) whose ERFs respond within 1 ms to electric fields. In combination with siloxane gels they still maintain responses of less than 100 ms. However, they require field strengths of 3-20 kV/cm to achieve this. I have cycled at 6.4 Hz with my beams, only to see small vibrations at the best of times.

Iseki et al. (1991) looked at ionic conductivity and saw faster reaction times with higher concentration electrolytes. Otero and Sansiñena (1996) noted something similar when they observed that higher electrolyte levels reduced the time necessary to make set movements at given voltage or current levels. Several researchers have noted that strain rate is proportional to current density such as Otero and Sansiñena (1995), Sansiñena et al. (1997) and us (Maw et al. 2001). A few researchers, including this author, have noted that oxidation movements tend to be slightly faster than reduction movements (Smela et al. 1993, Otero and Santamaria 1993), and that thicker films are slower than thin (Iseki et al. 1991, Otero and Santamaria 1993).

Curling speeds for bending beams have been recorded in many papers, and they vary considerably e.g. 4.5 sec to bend 90° (Otero and Sansiñena 1995), 1-2 seconds to bend “fully” (Smela et al. 1993), 5.4 sec to bend 90° (Sansiñena et al. 1997), 0.5 sec to

curl 180° (Smela et al. 1995), and 0.5 mm per second for the beam tip (Pei and Inganäs 1993b). Pei et al. (1993) did better with PANi fibers, getting them to move at a peak speed of 8 mm per second. Shahinpoor et al. (1998) has been able to move 1.2 g at 0.5 Hz using stimulation levels of 3 V and 40 mA. My maximum beam tip speeds of 10 mm per second compare quite favourably with these results.

Contraction strength is another key parameter of any muscle, natural or otherwise, and many researchers have touched upon this subject. Hunter and Lafontaine (1992) noted that natural muscle exhibits a peak stress level of about 350 kPa static, and about 100 kPa sustainable. Meanwhile, SMAs can sustain 200 MPa while polyaniline spans the range of 180-450 MPa. Piezoelectric and electrostatic actuators were reported to produce approximately 35 kPa, while piezoelectric polymers were reported to sustain values of 3 MPa. Sussman and Katchalsky (1970) derived a figure of 100 kg/cm² (10 MPa) with their collagen in LiBr. De Rossi et al.'s (1986) PVA/PAA copolymers produced 200-300 kPa. Caldwell and Taylor's (1990) PVA/PAA samples achieved similar values, and exhibited the force/velocity relationships described by Hill (1938).

Closer to my current work, Pei et al. (1993) recorded a maximum stress of 6.8 MN/m in their bending beams, and that compares favourably with my maximum value of about 2 MPa. Madden et al. (1999) also found a maximum of about 2 MPa, or 0.5 MPa if all of the encapsulation materials were included in their dry fiber formulation. Their (2001) work produced actuators that could produce discernable changes in force at up to 30 Hz, and Lee et al. (1994) have been able to reach levels of 50 MPa.

Changes in polymer volume, strain and strain rate have been the focus of many studies, primarily because these factors are so critical to the actuator application. Also,

conducting polymers have had mixed success in this regard, and there has, at times, been some confusion as to what has actually been achieved. Steinberg et al. (1966) established a 50% strain with unloaded collagen. Caldwell and Taylor (1990) did well with their PVA/PAA copolymers, producing up to 40% reversible length changes at a maximum rate of about 10% per second. However, they took several seconds to get moving. Shahinpoor et al.'s (1998) IPMCs were able to follow AC signals up to 35 Hz, producing reversible strains of 8mm at 0.5 Hz (± 2 V stimulation). With their polymer gels, deflection was a function of the square of the stimulation voltage. In comparison, Bohon and Krause (1998) were only able to produce 0.1 mm strains with high voltage ERFs.

Hunter and Lafontaine (1992) have pointed out that SMAs can achieve strain rates of 300% per second, similar to fast twitch natural muscle. Electrostatic actuators, on the other hand, can achieve the 100% per second rates of slow twitch muscle in combination with strains of more than 10%. Magnetostrictives can attain 0.2% strains but only at 100 kA/m stimulation levels. They suggest that piezoelectric actuators and polymers can only achieve strains of up to 0.1%. De Rossi and Chiarelli (1994) add that piezopolymers can achieve length changes on the order of 1 μm under 2 kV stimulation. However, they also add that PVDF strips can cycle over 13 μm at 300 V.

With polypyrrole systems, there have been quite a variety of findings. To begin with, many researchers point out that they can make their bending beams bend 90° or 180° reversibly (Lewis et al. 1997, Smela et al. 1995, Sansiñena et al. 1997, Otero and Sansiñena 1995 and 1996). I have easily done the same. However, without more information, it is not possible to directly determine the strains involved. Chiarelli et al.

(1995) worked with long free standing PPy strips, so he was able to directly measure strain and found values of about 0.35%. (0.3 mm change in length over 9 cm strips).

Smela and Gadegaard (1999) recently found some of the most interesting findings in this area in years. They discovered that the out-of-plane volume changes of the PPy(DBS) film were vastly different than the in-plane volume changes. They noted 35% volume changes vertically, and a maximum rate of change of 4.5% per second. The first reduction was even more interesting, as the typical large first reduction current appeared to result in a volume change of 125% out-of-plane while the in-plane change was around 0% (Shimoda and Smela 1998). In other words, it would appear that PPy(DBS) may be extremely anisotropic. They also noted that oxidative volume changes were faster than reductive changes.

With regard to bending beams, most of the strain data has come from Pei and Inganäs (1992, 1993a-b) and Pei et al. (1993). They calculated the curvature of their beams using a geometric formula. These radius of curvature (roc) values were then used to infer a certain volume change and linear strain by another set of formulas based on Timoshenko's beam theory (Timoshenko 1925). The strains that they calculated over their studies vary from .45% to 3.4%.

The gold standard for calculating the strain for any given bending beam is to determine the radius of curvature of the beam, as well as the constituent thicknesses of the beam layers, and the location of the neutral axis in the beam. Then it is simply a matter of comparing the circumferences of the circles that would be made by the neutral axis and the outer (PPy(DBS)) edge of the beam. On a percentage basis, this yields a very accurate strain value. Pei and Inganäs' values are over-estimates as a result of a few

assumptions made or broken. First of all, Timoshenko's formulation assumes uniform "heating" of the metal bilayers. It also assumes small bends and thin beams (in width). In addition, Timoshenko's coefficient of thermal expansion was a material property of the metals in question, not a function of how much bending was occurring. The modulus of the metals was also expected to be constant.

The PPy(DBS) in this model is supposed to be one of the uniformly heated metals in the bilayer. The stresses applied to it are not uniformly distributed over time or space, however. Madden et al. (2000) give a good example of this when they note how free standing films first curl and then straighten, revealing a wave of strain that moves through the film with time. If all of the film is not subjected to the same stressors, the model breaks down. Also, the formulation was not meant to deal with deflections on the scale that I see with my beams e.g. 90° or more. Furthermore, the modulus changes with time and reduction/oxidation (Chiarelli et al. 1995). More to the point, for a 3.4% volume change with a beam 155 μm thick (with the neutral axis somewhere near the middle), the radius of curvature of a 2.2 cm long beam would be 2.2 mm versus the 0.3 cm^{-1} (3.3 cm roc) reported. By describing the 3.4% figure as a volume change, the reader is led to believe that this is strain. As Smela and Gadegaard (1999) have shown, this could well be out-of-plane volume expansion. However, the erstwhile "coefficient of thermal expansion" is the better indicator of strain, and it is only about one third of the volume change (or 1.1% in this case). Using this figure instead, one would get a 7 mm roc. That would still be an almost 180° curl of the 2.2 cm long beam.

In contrast, I have done these calculations for my beams and I have compared the values found with my derived strain values. They agree very well, often to two significant digits.

Most recently, there have been Madden et al.'s (1999, 2000, 2001) fast contracting beams and encapsulated beams. The encapsulated "dry" beams have shown length changes of 2% at .03% per second with ± 20 mA stimulation. However, performance decays over just a few cycles. With wet beams, they were able to achieve levels of 0.4% strain at 1 Hz, and more than 3% per second at 20 Hz. The most recent work has achieved 2.4% strain at frequencies less than .01 Hz, and .007% strain at 30 Hz (0.4% per second).

Regarding work and energy measures, Sussman and Katchalsky (1970) recorded maximum work values of 7.85×10^6 erg/g for their fibers. Otero and Sansiñena (1996) noted that the same movement required the same amount of work with voltage stimulation. One could increase the voltage to complete the movement faster, but the total work and charge exchange would remain the same. Nevertheless, they contended that the amount of electrical work consumed would decrease if electrolyte levels were increased. Pei et al. (1993) found a bending energy of .011 mJ for their beams, which translates into 4.0 kJ/m^3 . My figure (4.9 kJ/m^3) is comparable and both exceed that of human muscle (0.8 kJ/m^3).

The rate at which work is performed is power, and power levels and densities have also been a popular way to compare different devices and polymer actuator formulations. Sussman and Katchalsky (1970) calculated an ideal maximum power output of 70 mW for their collagen machine. They produced 30 mW, making for a 40%

efficiency level. Likewise, Steinberg et al. (1966) achieved levels of 30 mW/g with collagen, which is approximately the value for the frog sartorius muscle. Shahinpoor et al. (1998) noted that power increases with voltage geometrically for their polymer-based device. Madden et al. (2001) also noted that increases in voltage lead to increases in power. Madden et al. (2000) produced films that exhibited 39 W/kg. My respective figure was about 3 W/kg. Caldwell and Taylor (1990) were able to reach levels of 5.8 W/kg. Hunter and Lafontaine (1992) noted that electrostatic actuators can achieve 17 W/kg while SMAs can attain 50 kW/kg. Baughman (1996) also noted an electrostatic macroactuator that produced 15 W/kg. However, it also required an 800 V driving signal. Pei et al. (1993) achieved levels of 400 W/m³ or 0.3 W/kg.

With regard to overall efficiency, 1% seems to be the magic number. Sussman and Katchalsky (1970) estimated their free energy conversion efficiency with their collagen system at about 1% and no one has done much better since then. Pei et al. (1993) arrived at a value of 1% for their PANi fibers, Jager et al. (2000) estimated 0.2% for their polypyrrole-based weight lifters, and Otero (1997) suggests that efficiencies of conducting polymers are always below 1%. Pei et al. (1993) noted that most of the energy in their films went into bending their beams, and into the thermal energy of the electrolyte solution. Madden et al. (2001) also found efficiency values of about 0.1%. However, he developed models that suggested ways in which to improve upon efficiency. Specifically, he suggests that increases in loads and strain to charge ratios, and reductions in the stimulating voltages used will help. He also feels that very small strains could be produced much more efficiently. My findings suggest this might be possible too, as small variations in voltage in the oxidized regions did exhibit transiently high efficiency

readings. However, this was in the context of full redox cycling so it may not be reasonable to assume that those levels could be produced on an ongoing basis without full cycling. Otero and Rodríguez (1993) noted that in general, the same movement requires the same exchange of charge no matter the current levels that deliver the charge. However, at very high voltages, there would be extra charge losses for other reactions such as water oxidation and that would lower the efficiency.

Finally, it is worth noting that Pei et al. (1993) did a very similar analysis to ours, regarding the work and efficiency formulation. There were some differences, however, and they are worth reviewing. First of all, they used a standard loaded beam model which depends on a minimal beam deflection and a parallel loading force. Neither of these assumptions is valid, as deflections of beams often reach 90° or more, and the loading force was directed radially due to it originating from within the PPy(DBS) film. They undertook the same type of analysis as I did, but they did not include drag (which was often a very reasonable decision). They did not include gravity, but then again, they did their curling parallel to the ground. For simplicity, they also assumed a uniform beam in terms of modulus, which I could not do since the moduli of Kapton® and PPy(DBS) are so different. This necessitated a composite beam analysis for me.

The “gold standard” method mentioned earlier provided some evidence that my internal elastic beam energy calculations were sound. It also provided an easy way to speak confidently about some anecdotal findings from past work in my lab. I have done work of the nature described in this chapter, with beams backed by Mylar® instead of Kapton®. Mylar® has a much lower modulus (about 140 MPa). I have observed on several occasions that such beams curl up into tiny balls rapidly (within 1-2 seconds).

The diameter of the curls is approximately 1 mm. One can say quite confidently then, that the maximum strains in those situations are on the order of 10%, with strain rates of as high as 5% per second. This compares very favourably with the highest strain levels found in any other polypyrrole experiment in the literature.

This also highlights the point that we should not read too much, or too little, into the poor strain results in the current experiment. The Kapton[®] is relatively rigid, and most of the PPy(DBS) film's productive mechanical work goes into bending it. Since the degree of bending was limited, as it needed to be to control factors that were important for allowing accurate measurements of other variables, we should not be surprised at the low values. Nor should anyone believe that the films cannot do better under different arrangements with more pliable backings.

With regard to the mechanical work analyses that I conducted, they were all based on models of the physical system. As such, a number of assumptions and simplifications were made to keep the models tractable. The models were found to be sensitive to the nature and values of these assumptions and simplifications to varying degrees. I will go through each of them to examine the critical issues.

Overall, there were two general parameters of potential concern. The first was the choice of the number of beam elements per beam. In almost all cases, the choice was two (top and end). However, one sample was also analyzed with three beam elements (top, mid, and end). The difference in a wide array of measures (absolute values of work terms, relative percentages, etc) was about 3-8%. Given the much greater variation between samples, this was taken to be negligible. Indeed, it was generally easier to collect more accurate data from the siliconCOACH system using two beam elements as

opposed to three, such that any gains in accuracy from finer quantization of the beam elements could easily have been lost in the accuracy of the measurements made for each element individually.

The other general parameter of potential concern was the identity of the cycle that was being analyzed. Was there great variation between cycles? Again, one sample's 13th cycle was analyzed after its 14th cycle had been analyzed. There was even less difference in measurements (about 3% on average), with the biggest differences showing up on the least significant terms e.g. inertia.

Also, as a general point, the reader should be aware that the more extensive and/or faster the movement, the easier it was to analyze in terms of marking the digitized video each time interval. More specifically, the accuracy of the measurements for fast and extensive movements was likely better than those of slower, less extensive movements. Also, the smoothing that was performed on the raw data would, of course, blunt peaks in velocity and position just as they would eliminate noise. For the drag term, for instance, in a worst case scenario, eliminating all of the smoothing would alter the total drag work by as much as 30%. However, in practice, the average effect was much smaller, since the 30% value came from the sample that moved the most/fastest by quite a margin.

With regards to the gravity term, there was also a potential for problems if the beam elements curled enough that their orientation to gravity was not monotonic increasing or decreasing. However, this was noted and prevented early on. More significant were the assumptions regarding film thicknesses, densities and masses. Looking at total positive work as an indicator of parametric sensitivity, the Kapton[®] thickness was increased/decreased by 5 μm , the Kapton[®] density was increased/decreased

by 0.1 g/cc, the density of the electrolyte solution was increased by 0.1, the gold thickness was doubled, the gold density was increased/decreased by 2 g/cc, the PPy(DBS) film thickness was doubled and halved, and the PPy(DBS) density was increased/decreased by 0.2 g/cc. Variations in the density of the solution and in the density of Kapton[®] had the largest effects, but even so, they only produced changes of about 20% in the gravity term. Given the relative unimportance of gravity as compared to the beam elastic energy, this was a relatively insignificant effect overall.

With regard to the drag calculations, it should be noted that the data points for this term were the easiest to collect accurately, using siliconCOACH. As with gravity, there were potential problems if the beam elements were not chosen such that a given beam element's orientation was monotonic increasing or decreasing. However, that problem was anticipated and prevented. The main issues with the drag calculations were the choice of kinematic viscosity, and the determination of the relationship between the Reynolds number and the coefficient of drag (C_D). For the kinematic viscosity term, a drop column experiment was performed and the value that came out of that experiment was .014 cm²/s, expectedly close to that of water. Even with a 100% error, the effect would not even double the drag work in most cases. And the drag effect, while noticeable, is not that significant overall.

The relationship between Re and C_D was a more important issue. There is not much data in the literature, even for flat plates facing flow, at these Reynolds numbers. However, there is a significant amount of data on other shapes such as cylinders and spheres. They certainly support the general relationship of the two values that I used, but it would be prudent to examine the effects of being off by a factor of 10 or more in one

direction or the other. In most cases, the effect of an increase is again negligible. In most cases, the drag contribution is less than 1% of the total mechanical work. However, for the thinnest samples, which generally move faster and more extensively, there could be as much as a doubling of the total work if the drag coefficient was off by a factor of ten. Still, that would only approach a doubling of the overall efficiency, which was quite low to begin with.

Inertia, whose contribution to the overall mechanical work was always very small, would suffer from the same potential pitfalls as the gravity work data in terms of the dimensions and densities of the beam. The raw data for the velocity and acceleration came from the drag data, so it would be relatively more accurate, although the smoothing would have some attenuating effect.

The main contributor to the mechanical work in the system was the work done to bend the beams. While this component also involves some of the larger assumptions and simplifications, it is nevertheless relatively insensitive to realistic changes or errors in these parameter values. To begin with, the original measurement of the data for deriving the radius of curvature was challenging. Nevertheless, for relatively rigid beams, the computations for top and end elements often showed very similar radii of curvature, suggesting that the smoothed data was consistent in terms of data gathering quality. In a sense, the measures for the top and end elements were independent measures of the same variable, and the fact that they always ended up being very close in value supported the consistency of the data gathering techniques. Also, the largest elastic energy terms from time interval to time interval were found in the most highly bent regions, which were also the easiest to measure. One of the main uncertainties arose from the moduli of the beam

materials, and especially that of the PPy(DBS) film. Still, the final results were not very sensitive to these values. The results scaled with the Kapton[®] and PPy(DBS) moduli, where a doubling of the Kapton[®] would increase the work by about 50%. Doubling the PPy(DBS) modulus had a slightly greater effect.

Another potential concern was that of the materials' compressive moduli. All of the three moduli used in the model were tensile, and yet the various layers and elements of the beam are as often in compression as they are in tension, especially the PPy(DBS). The elastic energy calculation is also quite sensitive to the thicknesses of the various layers in the beam. Increasing either the Kapton[®] thickness or the PPy(DBS) thickness by 50% would almost double the work performed. Still, keeping this in context, even a doubling or tripling of efficiency assuming several unlikely errors in parameter values would still leave the overall efficiency levels at fairly low values.

The integration of all of these work components both spatially and temporally left one more possibility for error. That was with the synchronization of the mechanical and electrical work values, time interval by time interval. As was noted earlier, on a cycle by cycle basis, this issue is irrelevant. However, if one wanted to look at the relative mechanical and electrical work (energy) levels within a cycle, then it is very important. My approach in the current study used eye-hand coordination and timing. While the author is well practiced in this skill (from being a coach), it is nevertheless inaccurate. Within the range of potential error though, the net changes on efficiency would be minimal.

6.6 Conclusions

In determining the values of a number of functional measures for the bending beams in this study, I was able to conclude that bending beams such as those used in this study can be cycled for at least 100,000 cycles at .20 Hz. There does tend to be some moderate degradation in strain characteristics, however. In terms of the beam bending, it is the actual bending of the beam that constitutes most of the mechanical work that is performed. Drag can have a non-negligible contribution, and work against gravity can also play a very minor role. It is not necessary to consider the inertial work. The strains in these samples were relatively small and were at the low end of what has been observed in other studies. However, given what I have observed in other situations with Mylar[®] backings, strains of up to 10% and strain rates of as much as 5% per second are likely very possible. Most importantly, the efficiency of these beams is very low in absolute terms, and very low in comparison to other systems (including natural muscle). It is not clear how and if the efficiency values can be increased by a few orders of magnitude.

From a fabrication perspective, I showed that if a bending beam is to be produced for the purposes of optimizing some aspect of its electromechanical performance (strength, power, strain, strain rate, endurance, efficiency) then the AMF designer must consider the deposition current density, monomer and electrolyte concentration levels, film conditioning, film backing modulus, backing thickness, film thickness, and stimulation mode and intensity, if they wish to achieve particular performance goals.

6.7 References

- Baughman, R.H. (1996) "Conducting polymer artificial muscles", *Synthetic Metals*, Vol. 78, pg. 339-53
- Bay, L., Jacobsen, T., Skaarup, S., and West, K. (2001) "Mechanism of actuation in conducting polymers: osmotic expansion", *J. Phys. Chem. B.*, Vol. 105, pg. 8492-497
- Bohon, K. and Krause, S. (1998) "An electrorheological fluid and siloxane gel based electromechanical actuator: working toward an artificial muscle", *J. Poly. Sci. B. Polym. Phys.*, pg. 1091-94
- Buckley, L.J., Roylance, D.K., and Wnek, G.E. (1987) "Influence of dopant ion and synthesis variables on mechanical properties of polypyrrole films", *Journal of Polymer Science B: Polymer Physics*, Vol. 25, pg. 2179-2188
- Caldwell, D.G. and Taylor, P.M. (1990) "Chemically stimulated pseudo-muscular actuation", *Int. J. Engng. Sci.*, Vol. 28, #8, pg. 797-808
- Chiarelli, P., Della Santa, A., De Rossi, D., and Mazzoldi, A. (1995) "Actuation properties of electrochemically driven polypyrrole free-standing films", *J. Intell. Mater. Syst. Struct.*, Vol. 6, January, pg. 352-360
- De Rossi, D.E., Chiarelli, P., Buzzigoli, G., Domenici, C., and Lazzeri, L. (1986) "Contractile behaviour of electrically activated Mechanochemical polymer actuators", *Vol. XXXII Trans. Am. Soc. Artif. Intern. Organs*, pg. 157-162
- De Rossi, D. and Chiarelli, P. (1994) "Chapter 40 – Biomimetic Macromolecular Actuators", In: **Macro-Ion Characterization**, K.S. Schmitz [ed], ACS Symposium Series, American Chemical Society, Vol. 548, Washington, pg. 517-530

Della Santa, A., De Rossi, D., and Mazzoldi, A. (1997) "Characterization and modeling of a conducting polymer muscle-like linear actuator", *Smart Mater. Struct.*, Vol. 6, pg. 23-24

Douglas, J.F., Gasiorek, J.M., and Swaffield, J.A. (1995) **Fluid Mechanics**, 3rd Ed., Longman Group Limited, pg. 367-368

Dupont (2002) *General Specifications for Kapton®*, <http://www.kapton-dupont.com/daten2.htm>

Fay, James A. (1994) **Introduction to Fluid Mechanics**, MIT Press, Cambridge, MA, USA, pg. 473-477

Gandhi, M.R., Murray, P., Spinks, G.M., and Wallace, G.G. (1995) "Mechanism of electromechanical actuation in polypyrrole", *Synthetic Metals*, Vol. 73, pg. 247-256

Gazard, M. (1986) In: **Handbook of Conducting Polymers, Vol. 1**, T.A. Skotheim [ed], Marcel Dekker, NY, pg. 673

Hill, A.V. (1938) "The heat of shortening and the dynamic constants of muscle", *Proc. Roy. Soc. (London)*, Vol. B126, pg. 136-195

Hoerner, F. Sighard (1965) **Fluid-Dynamic Drag: Practical Information on Aerodynamic Drag and Hydrodynamic Resistance**, published by the author, pg. 3-14 to 3-15

Hunter, I.W. and Lafontaine, S. (1992) "A comparison of muscle with artificial actuators", *IEEE Solid-State Sensors and Actuators Workshop Technical Digest*, June 21-25, Hilton Head Island, USA, pg. 178-85

Iseki, M., Kuhara, K., and Mizukami, A. (1991) "Study on electrically plastic devices made with electropolymerized films", *Japanese Journal of Applied Physics*, Vol. 30, #5, May, pg. 1117-1121

Jager, W.H., Smela, E., and Inganäs, O. (2000) "Microfabrication: conjugated polymer actuators", *Science*, Vol. 290, #5496, November, pg. 1540-1545

Kuhn, W., Hargitay, B., Katchalsky, A., and Eisenberg, H. (1950) "Reversible dilation and contraction by changing the state of ionization of high-polymer acid networks", *Nature*, Vol. 165, #4196, April 1, pg. 514-16

Kuwabata, S., Yoneyama, H., and Tamura, H. (1984) "Redox behavior and electrochromic properties of polypyrrole films in aqueous solutions", *Bulletin of the Chemical Society of Japan*, Vol. 57, pg. 2247-2253

Lee, A.P., Hong, K.C., Trevino, J., and Northrop, M.A. (1994) **Dynamic Systems and Control**, ASME Publications, DSC 55-2, ASME, NY, pg. 725

Lewis, T.W., Spinks, G.M., and Wallace, G.G. (1997) "Development of an all polymer electromechanical actuator", *Polym. Prep.*, Vol. 38, pg. 520-521

Madden, J.D., Cush, R.A., Kanigan, T.S., Brenan, C.J., and Hunter, I.W. (1999) "Encapsulated polypyrrole actuators", *Synthetic Metals*, Vol. 105, pg. 61-64

Madden, J.D., Cush, R.A., Kanigan, T.S., and Hunter, I.W. (2000) "Fast contracting polypyrrole actuators", *Synthetic Metals*, Vol. 113, pg. 185-92

Madden, J.D.W., Madden, P.G.A., and Hunter, I.W. (2001) "Polypyrrole actuators: modeling and performance", *SPIE 8th Ann. Int. Symp. Smart Struct. Mat. Proc.*, March 5

Maw, S., Smela, E., Yoshida, K., Sommer-Larsen, P., and Stein, R.B. (2001) "The effects of varying deposition current density on bending behaviour in PPy(DBS)-actuated bending beams", *Sensors and Actuators A*, Vol. 89, pg. 175-184

McComas, A.J. (1996) **Skeletal Muscle: Form and Function**, Human Kinetics, USA

National Aeronautics and Space Administration, Glenn Research Center (2002) *Shape Effects on Drag*, <http://www.grc.nasa.gov/WWW/K-12/airplain/shaped.html>, USA

Otero, T.F. and Rodríguez, J., (1993) "Electrochemomechanical and Electrochemopositioning Devices: Artificial Muscles", In: **Intrinsically Conducting Polymers: An Emerging Technology**, M. Aldissi [ed], Kluwer Academic Publishers, pg. 179-190

Otero, T.F. and Santamaria, C. (1993) "Redox behaviour of thin polypyrrole films. Optimization of response times", *Solid State Ionics*, Vol. 63-65, pg. 810-815

Otero, T.F. and Sansiñena, J.M. (1995) "Artificial muscles based on conducting polymers", *Bioelectrochemistry and Bioenergetics*, Vol. 38, pg. 411-414

Otero, T.F. and Sansiñena, J.M. (1996) "Artificial muscles: influence of electrolyte concentration on bilayer movement", *3rd ICIM/ECSSM '96 Proceedings*, pg. 365-370

Otero, T.F. (1997) "Chapter 10 - Artificial Muscles, Electrodeposition and Redox Processes in Conducting Polymers", In: **Handbook of Organic Conductive Molecules and Polymers, Vol. 14. Conductive Polymers: Transport, Photophysics and Applications**, H.S. Nalwa [ed], John Wiley & Sons Ltd.

Pei, Q. and Inganäs, O. (1992) "Electrochemical applications of the bending beam method. 1. Mass transport and volume changes in polypyrrole during redox", *J. Phys. Chem.*, Vol. 96, #25, pg. 10507-514

Pei, Q. and Inganäs, O. (1993a) "Electrochemical muscles: bending strips built from conjugated polymers", *Synthetic Metals*, Vol. 55-57, pg. 3718-23

Pei, Q. and Inganäs, O. (1993b) "Electrochemical applications of the bending beam method; a novel way to study ion transport in electroactive polymers," *Sol. State Ion.*, Vol. 60, pg. 161-66

Pei, Q. and Inganäs, O. (1993c) "Electrochemical applications of the bending beam method. 2. Electroshrinking and slow relaxation in polypyrrole," *J. Phys. Chem.*, Vol. 97, pg. 6034-41

Pei, Q., Inganäs, O., and Lundström, I. (1993) "Bending bilayer strips built from polyaniline for artificial electrochemical muscles", *Smart Mater. Struct.*, Vol. 2, pg. 1-6

Popov, E.P. (1976) **Mechanics of Materials**, 2nd Ed., Prentice-Hall, pg. 144-47, 525-29

Rane, S. and Beaucage, G. (1999) "Polypyrrole", In: **Polymer Data Handbook**, Oxford University Press, pg. 810-813

Sansiñena, J.M., Olazabal, V., Otero, T.F., Polo da Fonseca, C.N., and De Paoli, M.A. (1997) "A solid state artificial muscle based on polypyrrole and a solid polymeric electrolyte working in air", *Chem. Commun.*, pg. 2217-18

Satoh, M., Kaneto, K., and Yoshino, K. (1986) "Dependences of electrical and mechanical properties of conducting polypyrrole films on conditions of electrochemical polymerization in an aqueous medium", *Synthetic Metals*, Vol. 14, pg. 289-296

Shahinpoor, M., Bar-Cohen, Y., Simpson, J.O., and Smith, J. (1998) "Ionic Polymer-Metal Composites (IPMC) as biomimetic sensors, actuators & artificial muscles – a review", *Smart Mater. Struct.*, Vol. 7, pg. R15-30

Shimoda, S. and Smela, E. (1998) "The effect of pH on polymerization and volume change in PPy(DBS)," *Electrochim. Acta*, Vol. 44, #2-3, pg. 219-38

Smela, E., Inganäs, O., and Lundström, I. (1993) "Conducting polymers as artificial muscles: challenges and possibilities", *J. Micromech. Microeng.*, Vol. 3, pg. 203-205

Smela, E., Inganäs, O., and Lundström, I. (1995) "Controlled folding of micrometer-size structures", *Science*, Vol. 268, June 23, pg. 1735-38

Smela, E. (1999) "Microfabrication of PPy microactuators and other conjugated polymer devices", *J. Micromech. Microeng.*, Vol. 9, pg. 1-18

Smela, E. and Gadegaard, N. (1999) "Surprising volume change in PPy(DBS): an atomic force microscopy study", *Advanced Materials*, Vol. 11, pg. 953-57

Steinberg, I.Z., Oplatka, A., and Katchalsky, A. (1966) "Mechanochemical engines", *Nature*, Vol. 210, #5036, May 7, pg. 568-71

Sussman, M.V. and Katchalsky, A. (1970) "Mechanochemical turbine: a new power cycle", *Science*, Vol. 167, January 2, pg. 45-47

Timoshenko, S. (1925) "Analysis of bi-metal thermostats", *J. Opt. Soc. Am.*, Vol. 11, pg. 233-256

7. General Discussion

7.1 A Model to Fit the Observations

Over the course of the last five chapters, I have accumulated a large number of findings regarding the behaviour of PPy(DBS) under a wide variety of conditions. Much like a giant jigsaw puzzle, I have been able to bring out of the box a great many pieces. I have many of the important pieces, the ones that tell us about PPy(DBS)'s suitability for use in AMFs. However, without putting the pieces together, I might be missing the big picture.

That's what this section is all about, putting the pieces together into a qualitative model that provides a reasonable way in which to view all of this data as a coherent whole. To do this, we must identify the "important" phenomena that were observed and we must account for them convincingly without being distracted by other features that were less reflective of key processes occurring in the films during deposition or redox cycling. Some of these important observations include:

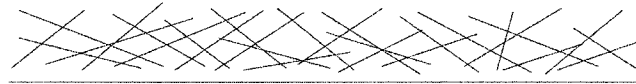
- the beams bend during depositions
- the first reduction does not result in much bending unless SN is high, and then the beams curl in the oxidation direction
- beams contract during oxidation and backcurl during reduction
- higher DCD values result in less curling, tighter redox peaks and less charge exchange
- movement extent is proportional to charge exchange, and movement speed is proportional to current
- films have a maximum cycling capacity, and exceeding that capacity leads to electromechanical failure of the film
- low DCD beams move faster and farther

- increased DP levels result in lower deposition voltages (for a given DCD) and increased peak separation
- increased SN values lead to higher peak currents, charge exchanges and curl, along with decreased peak separation
- it is primarily DP that sets the charge carrying/exchange capacity of a film
- symmetric increases in cycling range result in more curl, and lasting effects
- at broader cycling ranges, the fall-off in curling with frequency is reduced
- increases in cycling frequency result in less CV hysteresis, curl and charge exchange, as well as greater peak currents and peak separation
- low DCD films curl less during high frequency cycling, and curl more during low frequency cycling, compared to high DCD films
- SEM analyses show relatively more sulfur and less sodium and oxygen with increases in DP, more sulfur and sodium and less oxygen with increases in DN, more sodium with reduction, more sulfur with oxidation, and less sulfur and more oxygen with increases in SN
- higher levels of DP result in a grainier film surface morphologies
- reduced films are thicker than oxidized films
- charge exchange capacity increases with cycling range
- oxidation movements are somewhat faster than reduction movements
- high DCD, low DP, low DN films are thinner than average
- curling, peak currents and charge exchange increase with cycling time

The following model is offered as a way to view these phenomena. Not all elements of the model are original. However, the total picture would appear to be unique.

The model is based on two major points and a number of nuances. First, at low deposition current densities (and voltages), longer polymer chain growth can take place. While these chains may be oriented more-or-less planar to the electrode, they are not entirely planar. As a result, one can visualize them as a series of developing pikes angled up into the electrolyte solution off of the electrode surface (see Figure 7-1). These pikes

Figure 7-1 Proposed differences in the nature of the polymer growth in relatively favourable (top) and relatively poor (bottom) growing conditions. Better growth conditions would result in lower bulk density due to the reduced space filling of longer chains, and more electrostatic interactions pushing chains away from each other away due to improved polaron and bipolaron formation would create more deposition stresses leading to more deposition strain i.e. bending.



eventually start pushing against each other, creating a pressure that results in the bending of the beam backwards. On the other hand, high current densities (and voltages) result in shorter chains due to an increased level of chain termination reactions. One could visualize them as being very short pikes that develop relatively little leverage (electrostatic or otherwise) against each other, causing less beam bending. The often noted inverted conical (nodular) features in PPy films (e.g. Wallace et al. 1997) would then be a function of these pikes starting growth together in a localized area and pushing each other away as they grow out into solution. The films made of the shorter “pikes” would appear as a more ordered film, and that feature has indeed been seen in X-ray scattering studies of PPy(pTS) (Mitchell and Geri 1987).

The second major idea is that hydrated sodium ions go into the polymer matrix during reduction, and leave during oxidation. They enter and leave the polymer through molecular channels, much like paths through dense brush in a forest. These paths appear during reduction, and are compressed considerably during oxidation. They appear in the same places each cycle. The drive to compress and expand comes from a combination of the electrostatic effects resulting from the charging and discharging of the polarons and bipolarons of the polymer chains, in conjunction with the fact that negative DBS anions get trapped in the polymer during polymerization. Sodium ions act as charge compensators when the chains are neutralized, but leave quickly when the chains are oxidized, or charged.

The model accommodates the stated “important” phenomena in the following ways. Beam bending during depositions is accounted for by the pressure of the “pikes” as they grow against each other. As thicker Kapton[®] backings require more bending

force, they therefore bend less. Higher DP levels create a more conducive environment for long chain growth and charge carrying capacity. Longer intertwined chains result in a grainier film appearance compared to those of the short chains, and more anions can be stored in the film. This would be (and is) apparent in both the SEM elemental analysis and in the charge carrying capacity of the film. Increased levels of DN, all other things being equal, create more opportunities for NaDBS salts to enter the polymer film during polymerization. High DCD, low DP and low DN films would be particularly lacking in chain length, charge capacity, and anion and salt content. As a result, films made under these conditions could be expected to be thinner than other deposition conditions.

Looking at the stimulation situation, as a film is being oxidized, the cations file out of the matrix and it collapses. Upon reduction, it takes longer to get the cation intake process going, as the initial cations have to wedge their way into opening the pathways. Indeed, they would act as wedges in the polymer, helping to create the forces necessary to create the bending in the bending beams. As such, it would be entirely reasonable to expect proportionality between charge exchange and strain, and if low DCD films had more charge capacity, then it would follow that they would have a greater strain capacity. That would not necessarily imply a greater strain rate, but such is the case. It may be that for a given stimulation voltage, more charge sites are activated, creating a proportionally greater driving force for the cations to enter/exit i.e. reflected in current.

It would also be quite possible to expand the network of pathways and their current capacity by “stressing” (internally) the films. The stressors would include higher stimulation voltages and currents, and equivalently, expansion of the cycling range. These conditions would drive the ions through the films with greater energy, potentially

opening up new parts of the polymer previously left inaccessible. If the stresses were excessive however, it would mean that we would be asking the films to transfer more charge than they could, and that would potentially lead to damaging electrochemical reactions that would destroy charging sites on the chains, reducing the electromechanical activity in future cycles.

The lack of charge capacity in high DCD films would limit cation flux in those films, and that in turn would limit the drive for volume change. However, it would be less difficult to drive the lower number of ions in and out of such films, and that would be apparent in reduced peak separation. Indeed, “harder” ion diffusion processes would tend to spread the peaks while “easier” processes would tend to bring them together. Take SN concentration for example. Increases in SN lead to reduced peak separation because they make it easier for the film to “find” the cations needed to invade the matrix in a timely manner. Conversely, increasing the cycling frequency shifts the redox peaks in the CVs away from zero as the peaks simply never have the time to be attained. They never allow a peaking of ion flow. The ion flow in and out of the polymer at high cycling frequencies is relatively superficial, resulting in less charge transfer and less curling. However, what little charge transfer there is happens quickly, resulting in high peak currents. Also, the speed of the processes means that the pathways don’t have time to open and close as much as they would normally, and that means that the difference in the difficulty of entering or exiting the polymer is reduced. That, in turn, means less CV hysteresis as the currents remain mostly faradaic. High DP values, on the other hand, would spread the peaks because they would create films with greater charge capacities that would take longer to charge and discharge. In a sense, since the peaks reflect faradaic (redox)

currents, their positions express the ease with which charge is exchanged in and out of the films. When the peaks are close together (in terms of voltage) it implies that it doesn't take much to get the charges exchanged. That can be a function of there not being much charge to move, or in having plenty of time to move them. When the peaks are spread apart, it means that it takes more time to get the charges exchanged than is conveniently available. This is why at broader cycling ranges the fall-off in curling versus cycling frequency is reduced. As frequency increases, the peaks move apart. But if the range is large, then the peaks will at least stay within the cycling limits, ensuring that the movements will continue to be significant and robust.

While the model potentially explains all of these observations, the first reduction still poses a dilemma. However, it is not difficult to imagine that during the first reduction, which would normally involve just the flow of cations into the polymer, more superficial salts built into the polymer during the deposition would get an opportunity to leave. Alternatively, or at the same time, the first reduction could bring in cations that would expand the film out-of-plane, straightening the pikes as it were, and setting them up (literally and figuratively) for the expansion and compression cycles that would follow with any further cycling. They would be more properly aligned to have their charges interact in such a way as to either compress the film or to allow cations to move into it from there on in. The curling that happens during the first reduction in high SN solutions would still be challenging to explain. However, as this oxidative curling only takes place in high SN solutions, the curling may well be an osmotic effect, as any salt draining would bring out more water with it than normally would be the case.

The model also offers some predictive value. It suggests that the densities of high DCD films should be greater than those of low DCD films, and that the X-ray diffraction patterns should be different on the basis of different chain lengths. As well, with high enough magnification, the model would predict that the ion exchange channels should be visible. In addition, the films should appear significantly different under X-ray diffraction between their “just deposited” state and their post-first reduction state. As well, it would be interesting to try adding a small amount of a small cation into the stimulation solution to see if the small cation could act as a “door opener” for the larger sodium cations during reduction. The expected effect would be a faster reduction response (more anodic reduction peak) at the potential cost of reduced bending due to the smaller cations offering less bending leverage inside the polymer matrix.

Where does this leave the voltage steps, then? The voltage steps could be seen as shock therapy for the film, driving the ions hard and fast in and out of the films, the result being clearer and deeper pathways for the ions in and out of the films. This would potentially open up access to more of the charge in the film. This would not have as much effect on the low DCD samples, however, as they would already be relatively open and accessible due to their more favourable growth processes and lower density. For high DCD samples, however, it would help in penetrating deeper, denser regions of film.

Last but not least, in terms of the phenomena observed during the DCD work, was the increase in curling with cycling in spite of the fact that the charge exchange was not growing very much. Clearly, the movement efficiency was improving, but what was the reason? If the volume expansion in the films occurs closer to the gold layer, the expansion can create greater strain in the beam since the leverage is closer to the neutral

axis of the beam. Bending strength should be greatest for volume changes at the outer edges of the film, but bending extent (per charge) should be greater for volume changes occurring closer to the electrode surface. If the cations are able to penetrate farther into the film with time, then they should have a greater effect on strain per unit charge. That would also explain why the effect is so muted in high DCD films. If their lower reaches are relatively inaccessible, then the cations simply can't get down far enough to develop the strain to the extent that happens in the low DCD samples.

The purpose in outlining this model was to provide context for the various findings in the thesis, many of which did not always seem to be related or relevant. It was also meant to serve as a contextual basis for further work some of which will be described shortly.

7.2 Assessing PPy(DBS) Against the Performance Criteria

The main goal of this thesis was to evaluate PPy(DBS) as an actuating agent for use in artificial muscle fibers. To measure how well I was doing in reaching this goal, I had laid out a number of performance criteria in Table 1-1 of the first chapter. At this stage, it is worth reviewing how the PPy(DBS) fared against these criteria and/or how it may be expected to fare with more research, time and effort. This will also give us an opportunity to highlight any major strengths and weaknesses that the material may have.

In terms of physical characteristics, and keeping in mind that the bending beam model will likely not be the way in which PPy(DBS) will be used in a practical actuator, it is likely that the films will fare well in terms of manufacturability for shape, sound and smell. PPy(DBS) can be polymerized in many ways and forms, and it does not inherently involve any noise-producing processes during operation. As well, once polymerized, it does not smell and the NaDBS is not particularly aromatic. In terms of density, PPy(DBS) is about as dense as we would want. However, in combination with supporting electrolyte fluids and/or gels, it should be possible to stay under 1500 kg/m^3 .

While I did not evaluate reaction time directly, I am confident that thin films especially, can produce strain within a couple of tenths of a second. One potential problem for the future, however, is that the responsiveness that I did see is likely dependent on the gold interlayer in our beams. If a free standing film was produced, and then peeled off of its conductive metal substrate, issues of conduction velocity would become more relevant.

I did investigate functional durability directly though, and while I only tested to 10^5 cycles, it looks like the films should be able to perform longer. Certainly, there

would be plenty of room for optimization on that front. Likewise, I tested 3 stimulation modes, and PPy(DBS) can operate on pulsatile electrical control using either currents or voltages as control signals. Current control offers the attraction of managing charge exchange more effectively. Voltage feedback could be used to monitor the health of the films during cycling.

The issue of twitch and tetanus tension is not something that I was able to explore directly with this model. However, if a free standing film was used, one could anticipate stimulating it with sub-maximal levels of current (charge) to produce tension, keeping in mind that the film would have to be actively relaxed afterwards as well. To simulate increasing levels of activation, one would simply stimulate with increasing levels of current, keeping in mind that the PPy(DBS) would not be commanded to fully “relax” at some critical stimulating frequency and that tension would begin to summate at that point. In this way, twitch and tetanus could at least be simulated.

As well, PPy(DBS) does seem to offer the hope of functional variability in strength, speed, and strain capacity. By altering deposition current densities, backing thicknesses, PPy(DBS) film thicknesses, and electrolyte and monomer concentrations, I was able to create a variety of contractile qualities and characteristics.

In terms of the contractile strength parameter, PPy(DBS) fared quite well. Levels of at least 2 MPa were attained, and while this would be diluted in a full system that included supporting electrolyte fluids or gels, it offers realistic hope of achieving natural muscle’s 50-400 kPa levels. Frequency response was also fairly good, at about 1 Hz. If it can be doubled or tripled in magnitude, then it will be entirely adequate as well.

While fatigue is a complex process in natural muscle, it would also appear to be a complex process in PPy(DBS). I saw some functional degradation with time, but the films seemed to hold up well if they were not excessively stimulated. However, much more work is needed before this factor can be well characterized. In natural muscle, one recovers from fatigue. It is not yet clear whether that is possible with PPy(DBS) i.e. is the functional degradation from long-term activity temporary or permanent?

One of PPy(DBS)'s main strengths would be biocompatibility. Necessary current and voltage stimulation levels are low. The polymer is not toxic, and it can be used in aqueous systems. Indeed, it is now a potential scaffolding material for nerve regeneration (Rivers et al. 2002).

Manufacturability would also appear to be a manageable issue. As we have seen, PPy(DBS) is very sensitive to environmental conditions. However, when those conditions are controlled, so are the qualities of the polymer. Micro-scale actuators do require more elaborate and expensive infrastructure. As such, manufacturing costs could become a problem. However, the techniques themselves are relatively well developed (e.g. Smela 1999).

It would also appear that PPy(DBS) is trainable, although much more work is required to specify exactly how. I certainly noted changes in behaviour with time and with stimulation condition. There is a lot of unexplored potential in this area.

Energy density was another strong point of the PPy(DBS). It exceeded that of natural muscle by a factor of five. However, translating that into power and strain production was a problem. Indeed, the major concerns with the PPy(DBS) films were strain, strain rate, power density and efficiency. Strain levels were under 1%, although I

have seen cases in the lab where strains of around 10% were occurring. While not ideal, this is within an order of magnitude of natural muscle. In addition, Smela and Gadegaard's (1999) findings of 35% volume changes in the out-of-plane direction do offer some promise. Strain rate is a similar concern, being almost two orders of magnitude poorer than that of natural muscle (Madden et al. 2000, Hunter and Lafontaine 1992). If both of these factors were improved significantly, then the relatively poor power density levels would also likely rise. The critical challenge, for which no obvious solution is apparent, is the poor efficiency. I found overall efficiency to be generally less than 0.01%, and that is somewhat lower than others (e.g. Jager et al. 2000, Madden et al. 2000). In any event, even at 1% this is grossly inadequate if a practical and portable artificial muscle is ever to be made with PPy(DBS). Improving efficiency is a must.

Finally, I did not undertake free standing film studies on stiffness or contractile behaviour under shortening or lengthening conditions. Nor did I do any studies on thermal output and endurance. Nevertheless, these could be challenging issues too and they should be investigated in subsequent studies.

Overall, PPy(DBS) fared well against the naturally inspired performance criteria. There are certainly critical shortcomings, most notably efficiency. However, there are several strengths as well, and few other insurmountable challenges. The stage is clearly set for a number of future experiments but we should review the significance of what has been achieved thus far, first.

7.3 Significance of the Findings

In this section I consider the value of the findings presented in this thesis. To conduct this evaluation fairly, however, we need to identify who it is that may find value in the work. There are at least three groups of academics that could have an interest.

Neuromuscular physiologists could be interested in learning about the natural muscle system as a result of attempts at its physical simulation. Indeed, this was one of the primary motivators for doing this thesis in the first place. Unfortunately, the work did not progress far enough and fast enough to be of much value to this group. However, even at this very preliminary stage, there may still be some value in following the discussions regarding the factors affecting polymer interactions and changes in conformation and volume. PPy(DBS) films and natural muscle both rely on changes in cation concentrations to bring about changes in polymer chain conformation. Beyond that, PPy(DBS) uses the cations in a brute force “wedging” approach while natural muscle leverages the conformational changes with ATP to bring about the power strokes of the sliding filament theory. As electrochemists gradually determine how various classes of electroactive polymers work in more detail, we may be able to design our polymers at a finer level of detail to help leverage the activity of the cations in much the same way natural muscle does. As this process develops, which is already happening with the advent of nanotechnology, electrochemists will gradually be able to offer neuromuscular biologists more and more assistance in determining the importance of various electrochemical processes that take place in muscle cells.

The second group that could make use of the findings in this thesis would be the electrochemists. While the thesis was not written for them, there is certainly much here

that may be of interest to them. The volume-changing behaviour of certain electroactive polymers may not be their primary concern, but the electrochemical processes which produce it and accompany it are important to this group. That was one of the main reasons that details on redox peak movement, peak currents, deposition voltages, charge carrying capacities and charge exchanges were documented so exhaustively. They are phenomena that should be able to be explained by a sound electrochemical model that describes the system well. These findings may also be useful in questioning the validity of existing models, as we saw on a few occasions.

The third group that could make use of these findings would be those individuals interested in actuation, and more specifically PPy(DBS)-based actuation. Certainly the findings will be of most interest to researchers involved in PPy-based actuators. Researchers should be able to improve the performance of their actuators based on the results of this thesis. However, the methods and approaches can be used with other PPy and other polymer-based systems too. The conclusions may also be of use to researchers pursuing other technologies such as piezoelectrics or magnetostrictives, for comparative purposes.

The tracking of parameter values such as peak separation may also be of interest to some members of this group, since the goals of those interested in actuation are as varied as the technical approaches they take. Everyone has different priorities and constraints in this field. Some are perfectly happy to work with hundreds of volts, or with high powered devices. Others require efficiency or speed or durability. The vast array of requirements requires either a flexible approach or a focused approach. I have shown that many variables affect the properties of PPy(DBS) films and that if one wants

certain qualities, one can often get them by manipulating some of the variables. For example, if one is willing to forgo the best strain levels possible, one may be able to use stimulation protocols that require less voltage or current. These may make certain applications more attractive, or even feasible, for use in biological systems, for instance.

Certainly the curling (strain) behaviour of the PPy(DBS) bending beams will be of primary interest to this group. I have shown how several different factors affect the strain levels in this polymer, and that will help researchers decide if PPy(DBS) is useful to them in their work, and how it may be best used. What the actuation field currently lacks is a systematic approach to the evaluation of different polymer systems. This is understandable, since it may reveal in rather dramatic fashion, the inadequacies of one polymer system over another. However, if progress is to occur, each approach must be assessed by common performance measures and this thesis was all about whether PPy(DBS) is worth pursuing for the artificial muscle application. By defining the relevant effects of varying a wide array of variables that do have an effect on the strain behaviour of PPy(DBS), I was able to put this material up for scrutiny in a fair and balanced way. Part of this process involves debunking other results that don't seem to measure up, and I was able to do some of this as well.

To conclude, I believe that the findings in this thesis are significant, though primarily to researchers interested in actuation. The findings characterize performance over a range of values for each of a number of variables. Several metrics are put forward as useful comparative measures of performance, and a clearer and more accurate assessment of mechanical work in bending beams was provided as well.

7.4 Future Work

There are three general classes of future work that I will recommend in this section. The first deals with matters closely related to the experiments documented in this thesis. The second class includes logical extensions of the thesis work, and the third class will include more speculative suggestions years removed in research time from the current research activities.

Before touching upon any specific future work, however, it would be worth reviewing recommendations for methodological changes that will facilitate any future plans. In general, the protocols that were developed for the thesis work produced good results. Still, there were several areas where improvements could be made. The major one would be in productivity. Data gathered with LabVIEW software was saved in Matlab[®] format for later analysis. Some was analyzed and plotted in Matlab[®]. Other data was transcribed into Excel and SigmaPlot[®] along with the beam bending measurements. Later familiarity with Matlab[®] provided the necessary import/export commands. However, developing a wider array of data analysis routines for Matlab[®] would save time and energy. It would also allow an analysis of all cycles just as easily as a subset of them. Even more importantly would be the automation of the image processing of the beam movements. This was done by hand for the thesis and it was a very long and tedious process, with potential for error. LabVIEW image processing tools now exist that could be used to gather the required data, providing a hassle-free synchronization of the beam bending and electrical data, not to mention an automated gathering of the beam bending data. This would allow for a whole new set of studies

related to frequency response, reaction time, efficiency and phase lag for beams of various qualities.

Other desirable methodology changes would include greater attention to sample sizes for statistical significance calculations. As well, it would be good to have the ability to monitor and/or control solution pH and temperature, again tied into LabVIEW equipment and software. It would also be worth investigating whether a switch to thick Mylar[®] would offer an improvement over relatively thinner Kapton[®]. The Kapton[®] worked well, all things being equal, and I did have lots of problems with thin Mylar[®] in the early days. However, thick Mylar[®] would have the advantages of Kapton[®]'s stability without its rigidity which limited the range of movement of the fibers. Similarly, it would be worth investigating different metallic interlayers for better adhesion. For example, Smela (1999) has mentioned that titanium may be superior. Altogether, these changes would create an environment with better experimental controls, more accurate and much faster data gathering, and more flexibility.

With such an improved system, the following enhancements on the thesis studies would be both possible and desirable. Regarding the DCD work, improved data capture would allow for a more in-depth study of deposition bending. The importance of this lies in revealing what is really going on structurally during the depositions. Similarly, it would be worthwhile to vary the deposition concentrations with respect to the various DCD values. Including a greater variety of sizes of current steps would also provide clearer information on the significance of DCD in current controlled stimulation.

The concentration effects experiment could be repeated with more samples per condition, and over a greater range of DCD values (say 1, 4 and 16 mA/cm²). Spreading

the concentration levels (e.g. .01, .05, .15, .25 and .35 M) would also offer a clearer picture of what is going on.

With respect to the history experiment, it would be worth repeating the same experiment but over a much longer time period (e.g. 100-1000 cycles), looking especially closely at the current stimulation data. There would be value in trying the same procedures on different film thicknesses and deposition concentration values. Regarding range expansion, one could again try running more cycles, and over greater cycling ranges. Different film thicknesses and DCD values could also be employed, as well as a wider frequency range.

For endurance, the natural thing to do would be to try and go longer. However, it would probably be more valuable to go for a standard number of cycles (say 100,000) at different film thicknesses, electrolyte concentrations, DCD values, cycling frequencies, and over different cycling ranges, at least at first. It would be important to complete the enhanced adhesion strategy before doing this work. It would also be worth looking at responses to "standard" stimulation protocols (say 15 CVs with limits of -1.1 and +0.4 V) after having run for such a long time. Natural muscle does recover from fatigue. It would be important to know if, and under what conditions, the "fatigue" that I saw in the PPy(DBS) would be reversible.

SEM analyses should also be worked into all experiments such that the thickness of every beam used is evaluated. Conversely, it would also be worthwhile to ensure that beams were of the desired thickness in all situations i.e. even in low deposition concentrations or high DCD values. This would require abandoning the requirement for constant deposition charge densities in some situations. However, it is of more inherent

value to compare beams with films of a set thickness than depositions of set charge densities. Parallel sets of beams could also be evaluated for elemental composition at various points in various experiments e.g. after deposition, after conditioning, after current steps, etc.

With the frequency response experiment, it would be worth cycling more slowly to get data points clearly before the cut-off frequency in all cases. As well, automated data collection would also hopefully improve resolution of the differences between conditions. Different backings, such as the Mylar[®], could facilitate greater ranges of motion and effects to assist in this. It would also be interesting/valuable to run parallel sets of fibers through the frequency response protocols, one in order of ascending frequency, the other stimulated in a random order, to see if stimulation frequency history was indeed important or not.

Finally, for the efficiency experiment, it would be worth varying the conditions more than was done. For instance, a wider variety of DCD is called for (say .5, 2, 8, 32 mA/cm²). Different deposition and stimulation concentrations could be tried, and the apparatus could be rotated to work parallel to gravity instead of perpendicular to it. That would simplify some of the later data analysis. Also, if the equipment was available, it would be worth measuring film density and modulus values empirically, and the efficiency calculations could be performed over a greater range of cycling frequencies and ranges.

Such changes would contribute incrementally to the understanding developed in this thesis of the effects of these variables on PPy(DBS)-actuated bending beams. There are several more ambitious projects to attempt, however. One would be to experiment

with mixes of different electrolytes. This would serve to possibly enhance the performance of the beams in bending as well as helping to clarify what mechanisms were at work in causing the volume changes. Another pair of important studies would be to vary pH and temperature to see the effects that they would have on the electromechanical behaviour. This work could also present an opportunity to study thermal cycling. A fourth line of research would be to examine the anisotropic volume changes in the PPy(DBS) films as noted by Smela and Gadegaard (1999). That effect demands attention for its potential benefits. Another line of investigation could be directed towards the way in which the fibers would be stimulated. One of the clearest effects over all of my work has been that the CV reflects the movement of the beams. That is, movement is proportional to charge and movement speed is proportional to current. To a first approximation under relatively normal conditions, a CV can tell you very accurately how a given beam is moving in terms of speed, direction, timing and extent. Given that, and given the various other findings that have been shown in this thesis, we can fairly easily create a CV that reflects the types of beam motion that we want. For instance, we could create a skewed sinusoidal current signal to create a rapid movement followed by a slow “relaxation”. In addition, it would be interesting to try growing the PPy(DBS) on beams held taut, and at different orientations with respect to gravity. Any changes in subsequent curling behaviour could be used to refute or support the model put forward in the earlier modeling section. If gravity did influence morphology, it would then be desirable to try growing PPy(DBS) in microgravity.

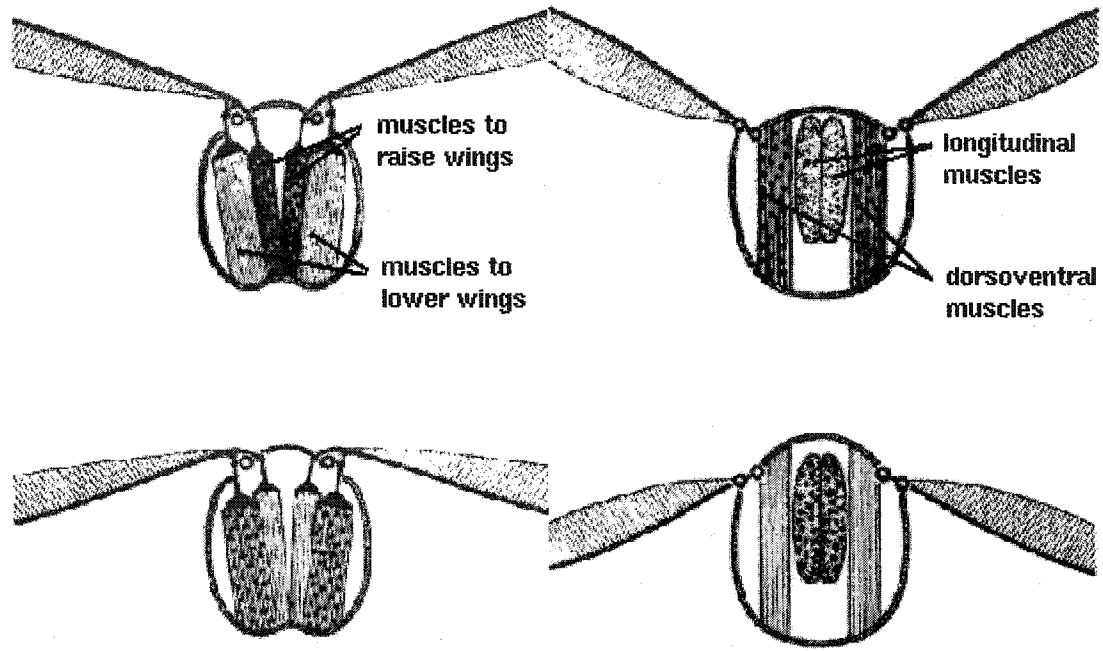
A natural accompaniment to this work would be to expand the modeling of the system to a quantitative level. That would greatly enhance the predictive value of the research work, and therefore its practical value.

To conclude, we can also discuss more distant goals. These would be long-term projects with greater developmental lead times and higher risk. There would be four that I would recommend. The first would be to shrink, simplify and/or eliminate the reference electrode, similar to what Madden et al. (1999, 2000) have done. This would provide much greater operational flexibility for any otherwise useful devices that would be created. The second would be to develop a thin, high molarity gel with the electrolyte inside of it i.e. a large and crude sarcoplasmic reticulum. The third would be to develop a small, portable system (in conjunction with the reference electrode improvements). This would facilitate trying different small mechanisms in trial applications. And that would be the last point: develop new mechanical models that use the PPy(DBS) in such a way that the work performed goes towards a functional task as opposed to just bending a beam. The bending beam is an effective model for studying the effects of parameter variations on the behaviour of the PPy(DBS) films. With the metallic interlayer, it also provides a fast way to distribute changes in current and voltage. However, practical devices need to be smaller and they need to do productive work instead of spending all their energy on bending their support structure. Part of this project would include studies on free standing films to determine stiffness, and isotonic and isometric strength responses under different conditions. This would shore up most of the remaining evaluation criteria for AMF performance against natural muscle standards. Ideas of potential mechanisms to explore would include a multi-decker "sandwich" of PPy(DBS)

that could take advantage of the out-of-plane volume changes noted by Smela and Gadegaard (1999), or a micro-scale “crawling” device that would have various sets of paddles that would “row” much the same way that myosin heads are expected to behave in the power stroke. Smela et al. (1995) have already demonstrated the feasibility of such paddles at the micron-scale.

Altogether, this collection of “future work” could keep a busy lab occupied for many years. The outcome of such efforts would likely be quite gratifying, and could facilitate the use of the PPy(DBS) films in AMF applications such as the one shown in Figure 7-2. Such biorobotic insects could become feasible for use in any number of entertainment, exploratory or reconnaissance applications.

Figure 7-2 Schematics of various muscle biomechanics for insect flight (<http://hannover.park.org/Canada/Museum/insects/evolution>). AMFs could function in such an arrangement to facilitate the development of biorobotic insects for use in exploration, remote sensing, intelligence gathering, and entertainment.



7.5 Conclusions and Recommendations

PPy(DBS) does have legitimate potential as an actuating agent in artificial muscle fibers. Across a wide array of performance criteria it either matches or exceeds natural muscle, or it clearly has the potential to. The only major exception to this generalization is efficiency. PPy(DBS)'s work efficiency is currently poor, and this is supported by other researchers (e.g. Madden et al. 2001). If this major challenge can be overcome, meeting the other challenges will likely be no more than a matter of time and effort.

As such, it is my primary recommendation that research into PPy(DBS)-actuators be continued, with the major focus being on efficiency. If efficiency cannot be substantially improved by at least two orders of magnitude, the volume-changing behaviour of the material will have limited practical applicability. There will still be considerable academic/electrochemical interest in the behaviour of the material, but the usefulness of it in an actuation role will be limited.

In any event, I have demonstrated in this thesis that any potential developers of PPy(DBS)-actuated devices would do well to consider deposition current density, electrolyte and monomer concentration levels, cycling range, cycling mode, film thickness and cycling frequency in their work. Each of these factors is critical in determining the performance of PPy(DBS) in an actuation role, as are other factors such as temperature (e.g. Yamaura et al. 1988), electrolytes/dopants (e.g. Warren and Anderson 1987) and pH (e.g. Shimoda and Smela 1998).

Furthermore, while I have shown that millimeter-scale beams, such as the ones that I have worked with, are suitable for parametric studies such as the ones discussed in this thesis, micron-scale devices will be where the improved efficiencies lie, if they can

be achieved at all. The diffusion rate limitations of the volume-changing agents (cations) simply require this and that is the strength of natural systems. They have highly optimized systems for managing the diffusion of muscle metabolites.

Finally, the bending beam model (e.g. Pei and Inganäs 1993a) is an excellent platform for evaluating the effects of various influences on the volume-changing behaviour of PPy(DBS) films in-plane. It is not, however, effective at revealing what is happening out-of-plane, which may be a direction that offers new opportunities in stress, strain and efficiency (Smela and Gadegaard 1999). The geometry of the model also ends up applying most of the useful work performed by the films to the bending of the beams. As such, I would also recommend that efforts be directed towards developing mechanical actuation models and systems that maximize the abilities of the PPy(DBS) to do useful work, such as what Smela et al. (1995) demonstrated several years ago, where PPy(DBS) films were integrated into a system optimized to carry out a particular mechanical function (move relatively large paddles).

Natural muscle is an amazing machine, well designed and well made. Much of the work with polymer-based AMFs is a primitive engineering exercise in comparison. However, if we are ever to build similar machines, we will do well to study nature's design, understand how it is made and how it works, and then construct our own using potentially similar parts and concepts. From the neuromuscular physiology perspective, the design of natural muscle has been well studied, although critical aspects such as the sliding filament theory's power stroke are still debated (Pollack 1990). As we learn more about how the volume-changing polymers work at the molecular level, we may be able to contribute to the understanding of muscle physiology by revealing similar principles at

work in both systems. By trying to imitate something, we learn more about that thing. My intent with this research, where the thesis was but the first step, was to advance the understanding of neuromuscular physiology by trying to imitate it. I was clearly over-optimistic as to how far I would get in this pursuit. I have barely contributed to any carry-over understanding of how contraction cycling in natural muscle may work, and on what it depends. Indeed, it is now clearer than ever how different natural muscle is from the various contractile polymers currently under study. With our PPy(DBS) system, for example, the movement of cations causes the mechanical stresses. In natural muscle, the movement of cations acts as part of the control signal cascade, while the hydrolysis of ATP is the actual power source for mechanical work. Nevertheless, I think this research and other research like it has the potential to enrich our understanding of natural systems with time. When that happens, I will have achieved my goal i.e. to learn about natural systems through the process of trying to imitate them. Additionally, when that has been achieved we will have acquired as a by-product the knowledge necessary to allow us to further heal the sick and infirm, and to create many new and wonderful biorobotic devices that will hopefully be able to enrich the lives of all of us someday.

7.6 References

Hunter, I.W. and Lafontaine, S. (1992) "A comparison of muscle with artificial actuators", *IEEE Solid-State Sensors and Actuators Workshop Technical Digest*, June 21-25, Hilton Head Island, USA, pg. 178-85

Jager, W.H., Smela, E., and Inganäs, O. (2000) "Microfabrication: conjugated polymer actuators", *Science*, Vol. 290, #5496, November, pg. 1540-1545

Madden, J.D., Cush, R.A., Kanigan, T.S., Brennan, C.J., and Hunter, I.W. (1999) "Encapsulated polypyrrole actuators", *Synthetic Metals*, Vol. 105, pg. 61-64

Madden, J.D., Cush, R.A., Kanigan, T.S., and Hunter, I.W. (2000) "Fast contracting polypyrrole actuators", *Synthetic Metals*, Vol. 113, pg. 185-92

Madden, J.D.W., Madden, P.G.A., and Hunter, I.W. (2001) "Polypyrrole actuators: modeling and performance", *SPIE 8th Ann. Int. Symp. Smart Struct. Mat. Proc.*, March 5

Mitchell, G.R. and Geri, A. (1987) "Molecular organisation of electrochemically prepared conducting polypyrrole films", *J. Phys. D: Appl. Phys.*, Vol. 20, pg. 1346-1353

Pei, Q. and Inganäs, O. (1993a) "Electrochemical muscles: bending strips built from conjugated polymers", *Synthetic Metals*, Vol. 55-57, pg. 3718-23

Pollack, G.H. (1990) **Muscles and Molecules: Uncovering the Principles of Biological Motion**, Ebner and Sons, Seattle, WA, USA

Rivers, T.J., Hudson, T.W., and Schmidt, C.E. (2002) "Synthesis of a novel, biodegradable electrically conducting polymer for biomedical applications", *Advanced Functional Materials*, Vol. 12, pg. 33-37

Shimoda, S. and Smela, E. (1998) "The effect of pH on polymerization and volume change in PPy(DBS)," *Electrochim. Acta*, Vol. 44, #2-3, pg. 219-38

Smela, E., Inganäs, O., and Lundström, I. (1995) "Controlled folding of micrometer-size structures", *Science*, Vol. 268, June 23, pg. 1735-38

Smela, E. (1999) "Microfabrication of PPy microactuators and other conjugated polymer devices", *J. Micromech. Microeng.*, Vol. 9, pg. 1-18

Smela, E. and Gadegaard, N. (1999) "Surprising volume change in PPy(DBS): an atomic force microscopy study", *Advanced Materials*, Vol. 11, pg. 953-57

Wallace, G.G., Spinks, G.M., and Teasdale, P.R. (1997) **Conductive Electroactive Polymers: Intelligent Materials Systems**, Technomic Publishing, USA, pg.1-106

Warren, L.F. and Anderson, D.P. (1987) "Polypyrrole films from aqueous electrolytes", *Journal of the Electrochemical Society: Electrochemical Science and Technology*, Vol. 134, #1, January, pg. 101-105

Yamaura, M., Hagiwara, T., and Iwata, K. (1988) "Enhancement of electrical conductivity of polypyrrole film by stretching: counter ion effect", *Synthetic Metals*, Vol. 26, pg. 209-224